The potential of satellite-based data to detect weather extremes and crop yield variation for hedging agricultural weather risks in Central Asia and Mongolia: Three essays

Dissertation
zur Erlangung des
Doktorgrades der Agrarwissenschaften (Dr. agr.)

der

Naturwissenschaftlichen Fakultät III
Agrar- und Ernährungswissenschaften,
Geowissenschaften und Informatik

der Martin-Luther-Universität Halle-Wittenberg

vorgelegt von
Herrn Sarvarbek Eltazarov

Gutachter:
Prof. Dr. Dr. h.c. mult. Thomas Glauben
Prof. Dr. Martin Odening
Prof. Dr. Christopher Conrad

Tag der Verteidigung:
11.12.2023

Betreuer:
Prof. Dr. Dr. h.c. mult. Thomas Glauben

SUMMARY

Index insurance has been introduced as a solution to tackle several challenges that prevail in the agricultural insurance sector of developing countries. One of the major implementation challenges in these countries is the need for more reliable weather data for index insurance development and implementation. The increasing availability of satellite-based data could ease the constraints of data access. However, the suitability of various satellite products for detecting weather extremes and crop yield variations across world regions must be thoroughly assessed.

Therefore, the main subject of this dissertation centers on the potential of satellite-based index insurance to mitigate climate risks in agricultural lands in the arid and semi-arid zones of Central Asia and Mongolia. The overall objective of the dissertation is to investigate the feasibility and performance of various satellite and reanalysis-based weather and vegetation data to design index insurance products for agricultural producers.

The dissertation consists of five chapters: The first chapter provides the general background of the dissertation and outlines its main research objectives. The following chapters 2, 3 and 4 represent three peer-reviewed and published articles. The second chapter provides a comprehensive literature review on the potentials and limitations of index insurance development in the study areas. Moreover, the second chapter illustrates the empirical findings on the relationship between weather data retrieved from satellite sources and weather stations. Additionally, this chapter investigates the ability of satellite-based weather data to detect extreme events for the design and implementation of weather-based index insurance in arid and semi-arid climatic zones of Central Asia. The third chapter delivers empirical evidence on the applicability and performance of various satellite-based vegetation data to detect wheat yield variation. Moreover, this chapter studies the potential benefits of considering land use/cover classification in index insurance design in rainfed, mixed and irrigated land in the study area. The fourth chapter provides empirical evidence on the potential benefits of machine learning-based downscaling of gridded climate data to improve risk reduction of index insurance products in Kazakhstan and Mongolia. Lastly, the fifth chapter concludes the findings presented in the dissertation.

The findings of this dissertation are manifold. Those in the second chapter demonstrate that there are interests, ongoing initiatives and support from local governments and international organizations to pilot and implement index insurance products in the region. However, there are significant limitations regarding in-situ weather and crop yield data to design and operate index insurance products. Findings from this chapter illustrate the significant agreement between in-situ and satellite-based weather data that enable their applicability for index insurance design and operation. Moreover, there is evidence that the performance of satellite-based weather data improves in semi-arid climatic zones during wet and rainy seasons as well as when higher temporal aggregation has been applied. The results of the third chapter show that less prominent satellite-based vegetation data in the insurance industry has a higher precision for detecting wheat yield variations than well-known alternatives (e.g., NDVI). Moreover, there is evidence that designing indices based on land use/cover information noticeably increases the performance of indices for detecting wheat yield

variation in rainfed and mixed lands. The findings of the fourth chapter indicate that designing index insurance products based on spatially downscaled (machine learning-based) climate data significantly improves their risk reduction potential. Among other climate data, there are more improvements in risk reduction potential when the index insurance design is based on downscaled temperature and precipitation data.

The fifth chapter summarizes the research findings, highlights the contribution of this dissertation to the scientific literature and presents general concluding statements. Based on the findings of the abovementioned chapters, it can be concluded that the studied satellite-based weather and vegetation data could serve as a good source to establish and implement index insurance products in the region. However, careful assessment and selection of index, temporal aggregation, and land use/cover classification remain essential. Additionally, as part of this dissertation, three open-source web applications and one statistical package in R have been developed. They assist and ease the process of obtaining satellite-based weather and vegetation data and analyzing the performance of index insurance products.

ZUSAMMENFASSUNG

Indexversicherungen wurden als Lösung für verschiedene Herausforderungen im Agrarversicherungssektor von Entwicklungsländern eingeführt. Eine seiner größten Implementierungsherausforderungen in diesen Ländern ist der Bedarf an zuverlässigeren Wetterdaten für die Entwicklung und Umsetzung von Indexversicherungen. Die zunehmende Verfügbarkeit satellitengestützter Daten könnte die Beschränkungen des Datenzugangs lockern. Allerdings muss die Eignung verschiedener Satellitenprodukte für die Erkennung von Wetterextremen und Ernteertragsschwankungen in verschiedenen Regionen der Welt gründlich geprüft werden.

Daher konzentriert sich das Hauptthema dieser Dissertation auf das Potenzial satellitengestützter Indexversicherungen zur Minderung von Klimarisiken in landwirtschaftlichen Gebieten in den ariden und semiariden Zonen Zentralasiens und der Mongolei. Das übergeordnete Ziel der Dissertation ist es, die Machbarkeit und Leistungsfähigkeit verschiedener Wetter- und Vegetationsdaten auf der Grundlage von Satelliten und Reanalyse zu untersuchen, um Indexversicherungsprodukte für landwirtschaftliche Erzeuger zu entwickeln.

Die Dissertation besteht aus fünf Kapiteln: Das erste Kapitel liefert den allgemeinen Hintergrund der Dissertation und umreißt ihre wichtigsten Forschungsziele. In den darauffolgenden Kapitel 2, 3 und 4 werden drei begutachtete und veröffentlichte Manuskripte vorgestellt. Das zweite Kapitel enthält eine umfassende Literaturübersicht über die Möglichkeiten und Grenzen der Entwicklung von Indexversicherungen in den Untersuchungsgebieten. Darüber hinaus veranschaulicht das zweite Kapitel die empirischen Erkenntnisse der Beziehung zwischen Wetterdaten, die aus Satellitenquellen und Wetterstationen gewonnen werden. Des Weiteren untersucht dieses Kapitel die Fähigkeit satellitengestützter Wetterdaten, Extremereignisse zu erkennen, um wetterbasierte Indexversicherungen in ariden und semiariden Klimazonen Zentralasiens zu konzipieren und zu implementieren. Das dritte Kapitel liefert empirische Evidenz für die Anwendbarkeit und Leistungsfähigkeit verschiedener satellitengestützter Vegetationsdaten zur Erkennung von Ertragsschwankungen bei Weizen. Dieses Kapitel untersucht den potenziellen Nutzen, wenn die Klassifizierung der Landnutzung/Bodenbedeckung bei der Gestaltung von Indexversicherungen für unbewässerte, gemischte und bewässerte Flächen im Untersuchungsgebiet berücksichtigt wird. Das vierte Kapitel liefert empirische Evidenz für den potenziellen Nutzen der auf maschinellem Lernen basierten Herunterskalierung von gerasterten Klimadaten zur Verbesserung der Risikominderung von Indexversicherungsprodukten in Kasachstan und der Mongolei. Das fünfte Kapitel fasst schließlich die Ergebnisse aus der zugrundeliegenden Dissertation zusammen.

Die Erkenntnisse aus dieser Dissertation sind vielfältig. Die Ergebnisse des zweiten Kapitels zeigen, dass es Interesse, laufende Initiativen und Unterstützung von lokalen Regierungen und internationalen Organisationen gibt, um Indexversicherungsprodukte in der Region zu erproben und umzusetzen. Allerdings gibt es erhebliche Einschränkungen in Bezug auf Wetter- und Ernteertragsdaten vor Ort (in-situ) für die Entwicklung und den Betrieb von Indexversicherungsprodukten. Die Ergebnisse dieses Kapitels verdeutlichen die signifikante Übereinstimmung zwischen in-situ- und satelli-

tengestützten Wetterdaten, die ihre Anwendbarkeit für die Gestaltung und den Betrieb von Indexversicherungen ermöglichen. Darüber hinaus gibt es Beweise dafür, dass sich die Leistung satellitengestützter Wetterdaten in semiariden Klimazonen während der nassen und regnerischen Zeiten sowie bei höherer zeitlicher Aggregation verbessert. Die Ergebnisse des dritten Kapitels zeigen, dass weniger verbreitete satellitengestützte Vegetationsdaten in der Versicherungswirtschaft eine höhere Genauigkeit bei der Erkennung von Weizenertragsschwankungen aufweisen als bekannte Alternativen (z. B. NDVI). Es gibt auch Anhaltspunkte dafür, dass die Entwicklung von Indizes auf der Grundlage von Informationen zur Landnutzung/Bodenbedeckung die Leistung von Indizes zur Erkennung von Weizenertragsschwankungen in Regen- und Mischgebieten deutlich erhöht. Die Ergebnisse des vierten Kapitels deuten darauf hin, dass die Entwicklung von Indexversicherungsprodukten auf der Grundlage von räumlich herunterskalierten Klimadaten (Ansatz des maschinellen Lernens) deren Risikominderungspotenzial deutlich verbessert. Neben anderen Klimadaten ist das Risikominderungspotenzial höher, wenn die Indexversicherung auf der Grundlage von herunterskalierten Temperatur- und Niederschlagsdaten konzipiert wird.

Das fünfte Kapitel fasst die Forschungsergebnisse zusammen, hebt den Beitrag dieser Dissertation zur wissenschaftlichen Literatur hervor und gibt allgemeine Schlusserklärungen ab. Auf der Grundlage der Ergebnisse des oben genannten Kapitels kann man insgesamt zu dem Schluss kommen, dass die untersuchten satellitengestützten Wetter- und Vegetationsdaten eine gute Quelle für die Einführung und Umsetzung von Indexversicherungsprodukten in der Region darstellen könnten. Eine sorgfältige Bewertung und Auswahl des Indexes, der zeitlichen Aggregation und der Klassifizierung der Landnutzung/Bodenbedeckung ist jedoch weiterhin unerlässlich. Zusätzlich wurden im Rahmen dieser Dissertation drei Open-Source-Webanwendungen und ein Statistikpaket in R entwickelt. Diese unterstützen und erleichtern den Prozess der Beschaffung von satellitengestützten Wetter- und Vegetationsdaten und die Analyse der Leistung von Indexversicherungsprodukten.

Table of Contents

List of Tables

List of Figures

1. General introduction

1.1. Problem statement and motivation

During the last decades, climate change has increased the frequency of weather extremes such as floods and droughts (WMO, 2021). Climate change is thus putting agricultural production at risk and leads to the use of modern tools for an early detection of weather extremes in order to reduce and enable coping with climate change-related consequences (FAO, 2015; Hellmuth et al., 2009; IPCC, 2022). It is clear that a variable and unpredictable climate significantly restricts the options of agricultural producers, thus limiting their development (Niles et al., 2015; Rao, 2011), since they avoid taking a risk when there is a possibility of weather shocks (Benami et al., 2021). Moreover, creditors are also hesitant to lend if extreme events may happen, causing widespread defaults if the agricultural producers are not insured (Hellmuth et al., 2009). Agricultural producers who don't have access to credit are also critically limited when it comes to agricultural inputs and technologies, and even if a drought or flood only happens once every five or six years, the threat of the phenomenon is sufficient to slow down economic development and wealth growth over all years (Hellmuth et al., 2009). Moreover, these limitations may be an obstacle to meeting the current and future demand for crop production (Ray et al., 2015), which would significantly affect food security in many regions of the world where agriculture is a main source of food and income (FAO, 2015).

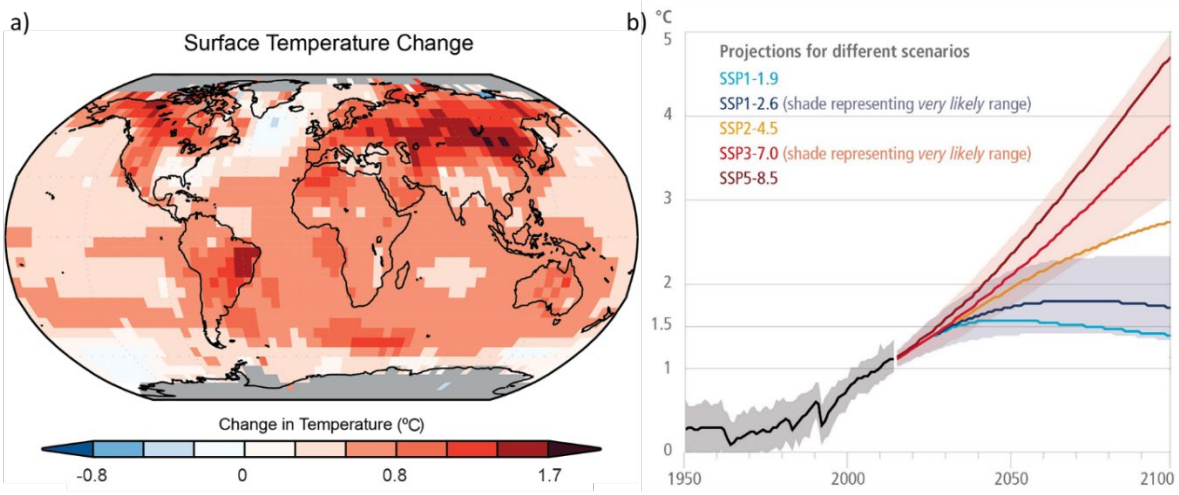

Figure 1.1: (a) Current global surface temperature change (period 1986-2016 relative to 1901-1960) and (b) global surface temperature change (increase relative to the period 1850-1900)

Source: Retrieved and adjusted from (a) USGCRP (2017) and (b) IPCC (2022).

Central Asia and Mongolia are located in one of the regions of the world where the effect of climate change is more severe than the global average (de Beurs et al., 2018; FAO and UNICEF, 2023; Haag et al., 2019). Agricultural production has a substantial contribution to the economy in this region, and between 20-50% of the population are employed in this sector (Bobojonov et al., 2019; Hamidov et al., 2016; ILO, 2022). Meanwhile, due to climate change, systematic drought has become more

frequent and is putting agricultural production at risk (Hamidov et al., 2016; Zhang et al., 2019). Drought events during the critical period of crop growth have had a great effect on crop production and the socio-economy of Central Asia and Mongolia during the last decades. The most recent widespread drought in Central Asia during the early growing season in 2021 caused dramatic water shortages, in turn causing a mass decrease in the agricultural sector (Jiang and Zhou, 2023). Moreover, the most prolonged and widespread drought in Central Asia occurred in 2001 and led to below-average drops of 40-60% for rainfall levels and 35-40% for river flows. This drought event resulted in an income loss of 80% of rural households, which in turn led to increased poverty rates and negative impacts on food security and public health (Patrick, 2017). The loss of agricultural production in that year was estimated at US$800 million for the entire region, which was a significant cost for all countries (World Bank, 2005). According to the literature, drought events in 2000-2001, 2008 and 2011 had a significant effect on agricultural production in Uzbekistan, and damages cost US$130 million in 2000 and 2001 (Christmann et al., 2009; Rakhmatova et al., 2021; Tolipov and Solokov, 2022). In the case of Kazakhstan, more than 50% of the country area were affected by droughts of various severity in the years 2000, 2008, 2010, 2011, 2012 and 2014; the most severe events were observed in 2012 and 2014, significantly decreasing agricultural production (Dubovyk et al., 2019). In the case of Tajikistan, drought events were experienced in the years 2000-2001, 2003, 2008 and 2011, and the total damage to the agricultural sector was estimated at US$63 million in 2001 and 2011, impacting around 2.5 million people (Patrick, 2017; World Bank, 2023). In the case of Kyrgyzstan, the gross agricultural output significantly decreased in 2009 and 2014 due to droughts in the preceding years that caused extreme climatic conditions and a deterioration of the economic situation (Iliasov and Yakimov, 2009; Logistics Cluster, 2021). In the case of Mongolia, the most extended droughts during 2000 and 2010 caused major social and environmental changes like migration of population, drying-up of grasslands and lakes, and die-off of crops and livestock (Hessl et al., 2018). All of these implications indicate a need for effective strategies and financial instruments for risk-sharing and mitigating the effects of climate change and extreme events.

To reduce climate-related risks for agricultural producers, insurance could be an efficient tool that transfers agricultural production risks from farmers to insurance companies (Bobojonov et al., 2019; Giné et al., 2010). Nevertheless, in developing countries, conventional agricultural insurance, known as 'named-peril' and 'multi-peril' crop insurance, can't effectively assist and mitigate all of the risks of agricultural producers, with the main obstacles and reasons being high costs of premiums, moral hazards and the adverse selection for the successful implementation of conventional crop insurance (Coleman et al., 2018). To overcome the challenges of conventional insurance in transition economies and developing countries, index-based agricultural insurance (the term "index insurance" will be used from here onwards) has been developed and suggested as a potential solution by various organizations and scholars (Coleman et al., 2018; Dick et al., 2011; World Bank, 2011). In index insurance, payoffs are contingent on the value of a pre-determined index (average yield of a unit, temperature, rainfall, soil moisture, vegetation, etc.), with one of the main requirements and advantages of index insurance being that the index cannot be affected by agricultural producers, nor is it vulnerable to manipulation from third parties (Barnett et al., 2008). This approach is aimed at

reducing adverse selection and problems of moral hazard, which are frequent issues with conventional agricultural insurance (Miranda and Gonzalez-Vega, 2011). Moreover, index insurance does not require a ground verification of the reported crop yield losses, thus significantly reducing administrative costs and consequently lowering the premium costs (Benami et al., 2021).

Regarding the potential for implementation of index insurance in Central Asia, the governments of Tajikistan and Kyrgyzstan have already initiated and developed a law regarding the use of index insurance in the agricultural sector. Despite their aim to partially finance the insurance premiums, these initiatives are not being taken up, due to little interest from local insurance companies and farmers, as well as a lack of weather data for designing the index insurance. (Broka et al., 2016a, 2016b). In Uzbekistan and Kazakhstan, governments support the implementation of traditional insurances with the help of various mechanisms, but there are no orders or initiatives at the state level for the implementation of index insurance. However, big challenges in the implementation of traditional insurances create a bottleneck for the development of an insurance market in these countries (Bobojonov et al., 2019; Broka et al., 2016c; Muradullayev et al., 2015). To solve existing challenges in the traditional insurance markets, several international organizations have recommended the use of index insurance in the agricultural sector of Kazakhstan and Uzbekistan (Broka et al., 2016c; Sutton et al., 2013), and some feasibility studies and small-scale piloting activities have started to emerge in recent years (Bobojonov et al., 2019; Bokusheva et al., 2016; Conradt et al., 2015).

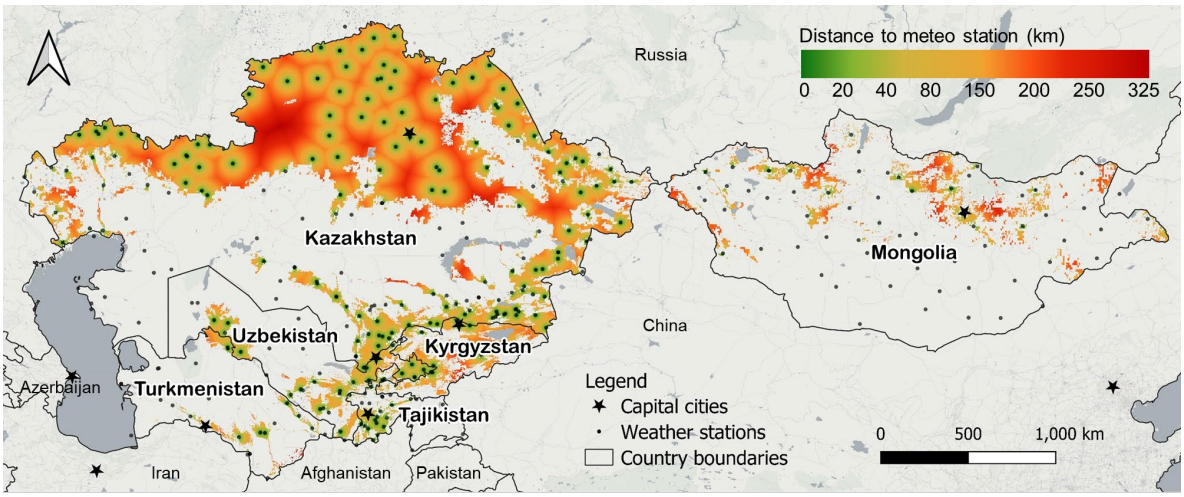

Figure 1.2: Geographical distribution of meteorological stations in the croplands of Central Asia and Mongolia

Source: Own presentation based on data from Teluguntla et al. (2015) and NCEI (2019)

It should be noted that index insurance is considered a potential solution, however, it is also not a panacea, as there are some issues regarding systematic risks, information asymmetry, financial literacy of farmers, and quality and availability of crop yield data (Fisher et al., 2019; Greatrex et al., 2015; World Bank, 2015). More importantly, index insurance requires sufficient correlation between

crop yields and the selected index in order to minimize the amount of basis risks (Norton et al., 2015). Usually, data obtained from weather stations is used for index insurance design. Numerous studies have investigated the feasibility and financial efficiency of weather station-based index insurances, which have typically been low precipitation or drought indices for agricultural producers (Bobojonov et al., 2014; Bokusheva and Breustedt, 2012; Conradt et al., 2015; Kath et al., 2019). However, this approach is strongly dependent on weather stations, which are rarely available in developing countries (Barnett and Mahul, 2007). In the case of Central Asia and Mongolia, specifically, according to the spatial analysis presented in Figure 1.2, the vast majority of croplands are located beyond a distance of 20 km from the nearest station. The figure demonstrates the low level of density and insufficiency of weather stations for designing index insurance, with the sparsely distributed weather stations often failing to capture the wide spatial crop losses and showing an inclination to geographical basis risk (Makaudze and Miranda, 2010). Moreover, weather data from weather stations rarely correlates with crop yields due to a high basis risk (Smith and Watts, 2009). Setting up new weather stations has been promoted as a potential solution; however, the installation and maintenance of new weather stations every 10-20 km (as suggested by Hazell et al. (2010)) would be costly and significantly increase the prices of the insurance products, which is not the aim of the index insurance concept. Furthermore, the nonexistence of historical weather records also halts the development of adequate and accurate insurance products (Norton et al., 2012).

As a potential solution to overcome the issues regarding weather data limitations, the use of satellite-based weather and vegetation data has been tested and suggested for index insurance design and implementation (Coleman et al., 2018; Osgood et al., 2018; Tarnavsky et al., 2018). Satellite-based weather and vegetation data is provided almost in real time and is available free of charge for most locations worldwide (CHC, 2015; Didan, 2015). Numerous studies have investigated the potential and applicability of satellite-based data for index insurance design and implementation in developing and emerging economies (Black et al., 2016a; Brahm et al., 2019; Collier et al., 2009; M Enenkel et al., 2018; Osgood et al., 2018; Tarnavsky et al., 2018).

1.2. Problem statement and research objectives

A literature review within the framework of this dissertation (chapters 2.1 and 2.2) has demonstrated that existing studies have not yet tested the applicability of satellite-based weather data for index insurance development in Central Asia, even though the vast majority of it is publicly available and might be particularly suitable for developing and transformation countries. Moreover, none of the existing studies have tested the accuracy of satellite-based precipitation and temperature estimates and their ability to detect weather extremes for index insurance development or other datasets for the Central Asian region. This study aimed to fill this gap by setting the following objective and conducting a study:

- To analyze the performance of satellite-based weather data and its ability to detect weather extremes for index insurance development in arid and semi-arid zones in Central Asia

This study contributes to the literature by analyzing the performance of satellite-based weather data, employing 14 statistical accuracy metrics and seven ground-based weather stations in arid and semi-arid zones of Central Asia. The specific satellite-based weather products have been chosen after a comprehensive review of existing satellite-based weather products in terms of their spatial and temporal coverage and resolution. Additionally, one of the novelties of this study was the application of the quantile regression method to analyze the relationship between ground- and satellite-based weather information. Furthermore, the ability of satellite-based weather data to detect weather extremes was analyzed using agronomically suitable Meteorological Drought Indices (MDI) during the vegetation and harvesting period of rainfed crops in the region.

Moreover, a review of the existing literature (chapter 3.1) has identified the following gaps that need further investigation: Not all wheat-producing regions worldwide are purely rainfed, but at least partially irrigated or fully irrigated. More specifically, around 35% of global wheat is produced in irrigated lands (Wang et al., 2021). However, no literature has focused on investigating the potential of satellite-based data for index insurance development for wheat producers in irrigated and mixed lands. In real life, these regions also suffer from high variations in weather parameters, as climate change affects not only water availability but also the demand of crops for water. In addition, based on the literature review, the research and industry spheres are using administrative boundaries of units to estimate regional index values for insurance design that omit the effects of crop rotation, diversity, allocation and land cover/use change. However, in regions with diverse land use/cover patterns, calculating a regional index value based on all pixels located within the administrative boundaries may not have a good power for detection of crop yield variation and index insurance design. Overall, the literature review outlines a need for comprehensive and comparative analyses of the applicability of more satellite-based vegetation data for index insurance development among various farming types and land cover/use classifications. This study aimed to fill this gap by setting the following objective and conducting a study:

- To analyze and compare the performance of well- and less-known satellite-based vegetation data to detect variation of wheat yield, taking the land use/cover information in rainfed, irrigation and mixed farming systems allocated in arid and semi-arid zones of Central Asia and Mongolia into account

This study provides two critical contributions to the literature. Firstly, according to the literature review, this study is the first attempt to explore the effect of using land cover classification (e.g., croplands and wheat-cultivated lands) in addition to administrative boundaries for data sampling and index insurance development. Second, within this study, the applicability of satellite-based vegetation indices, such as an Enhanced Vegetation Index (EVI), Green Chlorophyll Index (GCI) and Leaf Area Index (LAI), as well as a well-known Normalized Difference Vegetation Index (NDVI) and Land Surface Temperature (LST) are compared for index insurance development in rainfed, irrigated and mixed lands.

Furthermore, it should be noted that index insurance development and design require climate data with long historical records, global geographical coverage and fine spatial resolution simultaneously,

which is nearly impossible to satisfy, especially with open-access satellite-based data. According to the literature review (chapter 4.1), most satellite-based weather data with fine resolution is only available for limited land areas or time periods, which significantly limits its applicability for index development and design. Overall, in order to effectively measure climate risks and design robust index insurance products, there is a need for long historical climate records with fine spatial resolution covering the entire earth. For index insurance design, there is some potential re-analysis-based climate data that is produced by combining models with ground- and satellite-based observations, such as ERA5-based climate data from the European Centre for Medium-Range Weather Forecasts (ECMWF) (Hersbach et al., 2020). Likewise, satellite-based climate data from the European Space Agency (ESA) Climate Change Initiative (CCI)-based soil moisture data (Dorigo et al., 2017) covers the entire earth and provides data from the 1980s until near real-time. However, the spatial resolution of these climate products is very low, around 25–30 kilometers, which limits their potential for index insurance design and implementation. Particularly, designing index insurance based on such coarse-resolution climate data may lead to an increase in basis risk, specifically geographical basis risk. A potential solution, but still an under-researched method to deal with the issue of spatial resolution, could be to spatially downscale this climate data using statistical methods. Several studies have investigated and validated the capacity and precision of downscaling the spatial resolution of climate data sources using regression and machine learning (Bai et al., 2019; Hu et al., 2020; Im et al., 2016; Liu et al., 2020; Zhang et al., 2021; Zhu et al., 2017). However, possible advantages of spatially downscaling such coarse-resolution climate data for index insurance design have not yet been investigated. This study aimed to fill this gap by setting the following objective and conducting a study:

- To analyze the effect of index insurance products based on downscaled climate data (using satellite-based data in finer spatial resolution and a machine learning algorithm) for hedging crop yield in arid and semi-arid zones of Kazakhstan and Mongolia

This study provides two main key contributions to the literature. Firstly, based on the literature review, this study is the first attempt to systematically evaluate and compare index insurance products with a design based on original coarse resolution and spatially downscaled climate data to reduce farmers' financial downside risk exposure. The spatial downscaling of long-term and coarse-resolution soil moisture, precipitation and temperature data has been done using a machine learning algorithm. Secondly, the best source of climate data for index insurance products has been identified for each county to maximize the climate risk reduction capacity.

1.3. Structure and research contributions

This dissertation contains three main, independent and non-consecutive chapters (chapters 2, 3 and 4) representing three peer-reviewed and published articles. Table 1.1 lists the details of all research contributions. The second chapter offers empirical evidence on the accuracy and applicability of satellite-based weather data to measure precipitation and temperature, and to detect extreme weather events for index insurance development. The third chapter analyzes potential accuracy

gains from land-use classification that allow for the design of reginal indices specifically for croplands and wheatlands. It also investigates the potential benefits of employing less-known indices for detecting the variation of crop yield and index insurance design. The fourth chapter empirically investigates the effect of index insurance contracts based on spatially downscaled climate data for hedging crop yield. Overall, all chapters focus on testing the applicability and performance of various satellite-based data for index insurance design and operation in arid and semi-arid zones of Central Asia and Mongolia.

Table 1.1: List of research contributions

Chapter	Authors	Title	Publication outlet
2	Eltazarov, S., Bobojonov, I., Kuhn, L. and Glauben, T.	Mapping weather risk – A multi-indicator analysis of satellite-based weather data for agricultural index insurance development in semi-arid and arid zones of Central Asia	Climate Services, 23, 100251 (2021)
3	Eltazarov, S., Bobojonov, I., Kuhn, L. and Glauben, T.	The role of crop classification in detecting wheat yield variation for index-based agricultural insurance in arid and semiarid environments	Environmental and Sustainability Indicators 18, 100250 (2023)
4	Eltazarov, S., Bobojonov, I., Kuhn, L. and Glauben, T.	Improving risk reduction potential of weather index insurance by spatially downscaling gridded climate data - a machine learning approach	Big Earth Data (2023)

2. Mapping weather risk: A multi-indicator analysis of satellite-based weather data for agricultural index insurance development in semi-arid and arid zones of Central Asia[1]

2.1. Introduction

Agricultural insurance is a risk management tool that can assist with coping with climate risks in agricultural areas by protecting assets, opening access to credits, mitigating risk, maintaining the resilience of farmers, and supporting food security. However, because of high costs, moral hazard and adverse selection, traditional agricultural insurance, known as "loss-indemnifying" insurance has not yet effectively assisted and mitigated all of the risks for farmers in developing countries. Index-based insurance has been proposed and recommended as a solution by various organizations and scholars as a means for developing countries to overcome the challenges of traditional insurance (Bobojonov et al., 2014; Coleman et al., 2018; World Bank, 2011). The most common and widely used form of index insurance is weather index insurance, which makes use of the typically high correlation between weather data and crop yields (Bobojonov et al., 2014; Chantarat et al., 2007; Coleman et al., 2018; World Bank, 2011). For the case of index-based insurance, indemnity payments are determined by an index that is neither affected by farm-individual production decisions nor vulnerable to manipulation by third parties. This approach is aimed at reducing adverse selection and problems of moral hazard, which are frequent issues in traditional agricultural insurances (Fisher et al., 2019; World Bank, 2015).

Meanwhile, there are several challenges in the implementation of index insurance under real-life conditions. One of the largest challenges is the availability of historical weather data for implementing such an insurance (Barnett et al., 2008; Kath et al., 2019). In many developing and transition economies, a complete lack or the poor quality of long-term daily climate data with all the necessary parameters hinders large scale dissemination (Barnett and Mahul, 2007; Collier et al., 2009). Moreover, requesting and obtaining weather data from data holders might be challenging, time consuming and costly; in many developing countries, high-quality data has been commercialized.

Additionally, an insufficient density of meteorological stations (the term "station" will be used from here onwards) in agricultural areas significantly affects the reliability of insurance products. Because of micro-climatic factors, weather parameters may differ even between locations in close proximity (Tadesse et al., 2015). Existing studies have shown that using station data for index insurance leads to a very high basis risk (i.e., the correlation between index and yields is very low) when the station is located more than 20-25 kms away (Gommes and Göbel, 2013; Osgood et al., 2007). Consequently, Hazell et al. (2010) have suggested keeping a distance of 10-20 km between the station and farms in order to decrease basis risk.

[1] This chapter was published as the following open-access article: Eltazarov, S., Bobojonov, I., Kuhn, L., Glauben, T. (2021): Mapping weather risk – A multi-indicator analysis of satellite-based weather data for agricultural index insurance development in semi-arid and arid zones of Central Asia. Climate Service, 23, 100251. https://doi.org/10.1016/j.cliser.2021.100251; This chapter benefitted from the comments by the anonymous referees of Climate Services

Figure 2.1 illustrates the challenge of sufficient station density for the case of Central Asia. Here, stations are installed and regulated by governmental agencies, but also recognized by the World Meteorological Organization (WMO) and included in the dataset of the Global Historical Climatology Network (GHCN) (NCEI, 2019). As presented by the spatial analysis in Figure 2.1, more than 94% of farmland in Central Asia is located beyond a distance of 20 km from the nearest station. Only 6% of the region's cropland (highlighted in dark green) is situated close enough to a weather station to allow for reliable yield estimation along the weather station data. Any area that is not classified as cropland is shown as a transparent area (see also in Appendix 1.1).

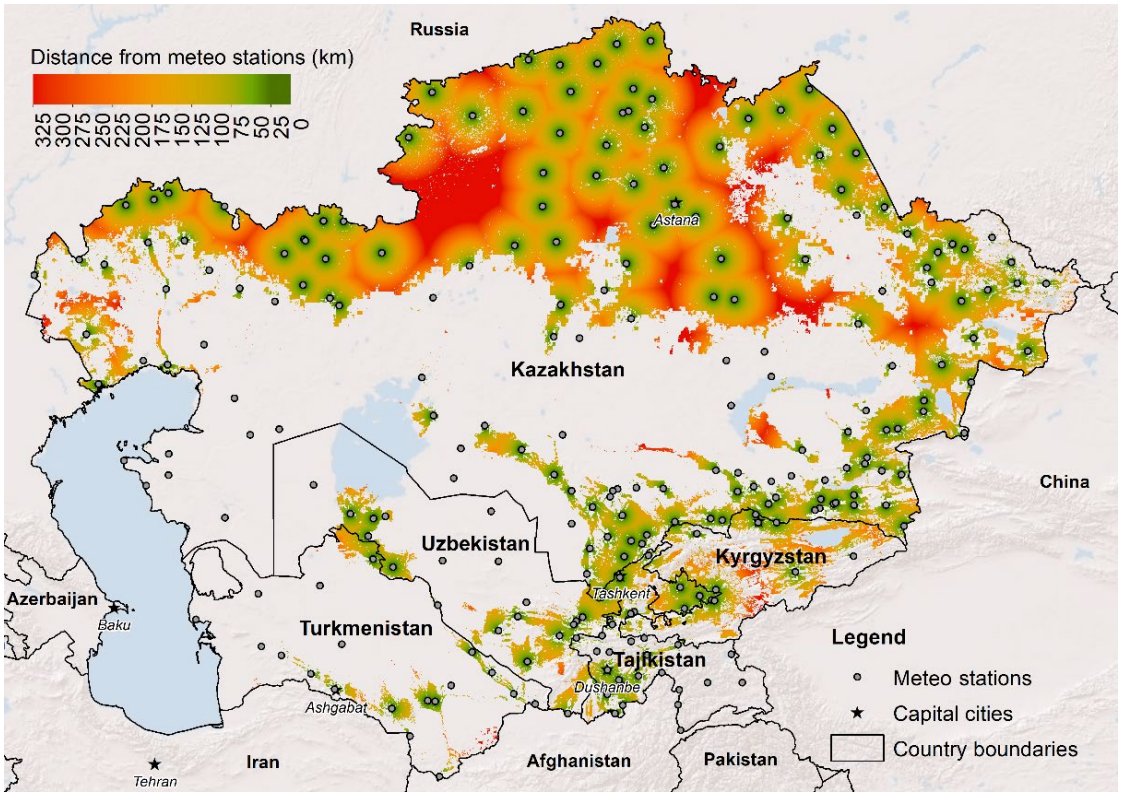

Figure 2.1: Geographical distribution of meteorological stations in the croplands of Central Asia

Source: Own presentation based on data from Teluguntla et al. (2015) and NCEI (2019).

Retrieved from the published open-access article: Eltazarov, S., Bobojonov, I., Kuhn, L., Glauben, T. (2021): Mapping weather risk – A multi-indicator analysis of satellite-based weather data for agricultural index insurance development in semi-arid and arid zones of Central Asia. Climate Service, 23, 100251.

In many high-income countries, the installation of new weather stations at the farm level is promoted as a potential solution. However, starting from the above conclusion that accurate data for weather indices requires a density of one station every 10-20 km, both the installation and maintenance of these stations would considerably increase the price of products relying on this data, which

is a problem for extensive or low-yield production. Furthermore, the lack of historical records for these new stations will pose an additional problem for product design.

Under these conditions, satellite remote sensing data (the term "satellite data" will be used from here onwards) is increasingly used for designing and operating index insurance programs. Numerous recent studies have investigated and proposed the use of agronomically suitable Meteorological Drought Indices (MDI) that do not require yield data for designing and implementing index-based insurance, as yield data is often inaccurate or difficult to obtain at sufficient resolution (Bezdan et al., 2019; Bobojonov et al., 2014; Ghamghami et al., 2017; Okpara et al., 2017; Tarnavsky et al., 2018). Many studies have found a significant correlation between MDIs and crop yields (Elhag and Zhang, 2018; Gunst et al., 2015; Salehnia et al., 2018; Todisco et al., 2008; Vicente-Serrano et al., 2012). Moreover, Musshoff et al. (2011) and Odening et al. (2007), found a higher risk reduction potential of index insurance based on MDIs rather than cumulative rainfall.

Meanwhile, each of the available satellites differs in terms of resolution, coverage, quality and frequency of data collection. Therefore, one can expect differences in accuracy of the produced data for measuring weather parameters for each particular region. However, the question of how accurate the various satellite products actually are has not been studied to a sufficient extent in the region. Our study therefore provides two distinct contributions to the literature: First, the accuracy of two important satellite-based weather products, as Global Satellite Mapping of Precipitation (GSMaP) and Global Land Data Assimilation System (GLDAS)[2] have never been scientifically tested in the context of index insurance. This study undertakes the investigation of the accuracy of these, along with CHIRPS data, for various classification, quantitative and agreement statistic metrics. Secondly, this is the first attempt at undertaking an accuracy assessment of selected satellite-based temperature and precipitation data and calculation of MDIs based on satellite-based weather products for Central Asia. While region-specific climate challenges need to be taken into account, the results of this case study may also provide insights relevant for arid and semi-arid agricultural regions elsewhere in the world.

This paper is structured as follows: The second chapter provides a review of the literature on the application of satellite data on index insurance in various countries. The third chapter discusses opportunities for establishing index insurance in Central Asia, while the fourth chapter describes the process of in-situ and satellite-based data selection and acquisition. We report on methods selected for the accurate assessment of satellite-based weather data and selected MDIs that examine the ability of satellite-based weather data to detect droughts and floods. Chapter five provides the results from our analyses followed by a comprehensive discussion. We conclude with an outlook on opportunities and limitations of satellite-based data in the detection of drought and flood events.

[2] Details about the selected satellite-based weather products will be discussed in the following chapters.

2.2. Literature review of the application of Satellite Remote Sensing data to index insurance

A number of studies in developing countries have investigated and proven significant accuracy, applicability and the potential of satellite data for index insurance in the agricultural sector at various temporal and spatial scales. De Leeuw et al. (2014) conducted a systematic search of the available literature to review the potential and uptake of remote sensing in the insurance industry, concluding that there is particular scope for the application of remote sensing by the index insurance industry. They have also concluded that satellite-based indices can be applied when there is a significant correlation with what is insured, as such indices serve to lower the cost of the insurance product and create new insurance markets and services[3]. Therefore, this literature review focuses on research papers published after De Leeuw et al. (2014).

Many existing research articles provide evidence of the suitability of satellite indices, such as the Normalized Difference Vegetation Index (NDVI); the Vegetation Condition Index (VCI); the Temperature Condition Index (TCI); and the Vegetation Health Index (VHI) (see Appendix 1.2 for detailed information) or Satellite-based Precipitation Estimates (SPE), in selected countries and under various agro-climatic conditions (Coleman et al., 2018; World Bank, 2015, 2011). Some studies have focused on assessing the accuracy of single indices: For example, Black et al. (2016a, 2016b) analyzed the applicability of the Tropical Application of Meteorology Using Satellite Data (TAMSAT) SPE to develop an index insurance for cotton fields in Zambia. They found a significant relationship between rainfall and soil moisture, and a strong association between cotton production losses and rainfall on a national scale. Enenkel et al. (2018) investigated the efficiency of using Climate Hazards Group InfraRed Precipitation with Station (CHIRPS) SPE for detecting drought and developing an advanced index insurance design in Ethiopia, Senegal and Zambia. By comparing drought years reported by farmers, they identified a high ''hit rate'', albeit with some limitations when it came to detecting moderate drought events.

Other studies have conducted comparative analyses of two or more indices: Coleman et al. (2018) investigated the suitability of NOAA-based African Rainfall Climatology Version 2 (ARC2) and TAMSAT SPE to detect drought events and develop a village-scale index insurance for groundnut, millet and maize in Senegal. Tarnavsky et al. (2018) tested three different SPE products, namely ARC2, CHIRPS and TAMSAT SPEs to monitor country-level maize production in Tanzania, and analyzed their applicability for designing an index insurance. They discovered a higher correlation between SPE and maize when CHIRPS SPE was employed and suggest that CHIRPS SPE is more suitable for the application of index insurance. Osgood et al. (2018) tested the link between village-level drought years in Ethiopia as reported by farmers and drought years detected by SPE products ARC2 and CHIRPS; they found evidence that events reported by farmers are independently reflected in satellite datasets. Brahm et al. (2019) conducted cross-correlation analyses with Climate Hazards Group Infra-

[3] A more detailed review of literature before 2014 can be found in DeLeeuw et al. 2014.

Red Precipitation (CHIRP), CHIRPS, Tropical Rainfall Measuring Mission (TRMM), Multisatellite Precipitation Analysis (TMPA) and MODIS-NDVI to test the accuracy of the newly released data source Historical Database for Gridded Daily Precipitation Dataset over Latin America (LatAmPrec). They also used a logistic regression approach with aggregated farmer-reported data to check the ability of the LatAmPrec to detect drought events across regions in Latin America. Their results show that LatAmPrec performs better than other satellite data sources in Latin America and is able to satisfactorily identify those yield losses that are relevant to insurances.

As can be seen in this summary, existing studies have not yet tested the applicability of the GSMaP and GLDAS datasets, both of which might be particularly suitable for developing and transformation countries, as their data is publicly available and free of charge. Moreover, none of the existing studies have tested the accuracy of precipitation estimates and the applicability of these to index insurance or other datasets for the Central Asian region.

2.3. Development of index insurance in Central Asia

Agricultural production has a substantial contribution to the economy and GDP of Central Asian countries. Between 20-50% of the population is employed in the agricultural sector (Bobojonov et al., 2019; Hamidov et al., 2016). In the meantime, systematic extreme weather events due to climate change in Central Asia have become more frequent, putting agricultural production at risk (Hamidov et al., 2016; Zhang et al., 2019). Based on information provided in Christmann et al. (2009), Bobojonov and Aw-Hassan (2014) reported that drought events during the critical period of rainfed crop growth in 2001 and 2008 had a great effect on crop production and the socio-economy of Central Asia, particularly in Tajikistan where more than a third of the cropping area was damaged, costing US$63 million (Patrick, 2017). In the case of Kyrgyzstan, the gross agricultural output significantly decreased in 2009 due to droughts in preceding years that caused extreme climatic conditions and a deterioration of the economic situation. Generally, in Central Asia, the drought of 2001 was the most prolonged and widespread drought, resulting in below-average drops of 40-60% for rainfall levels and 35-40% for river flows. This drought event contributed to a loss of 80% of rural households' income, resulting in consequences of increased poverty rates and negative impacts on food security and public health (Patrick, 2017). In that year, the loss of agricultural production was estimated at US$800 million for the whole region, which was a significant cost for all countries (World Bank, 2005). All of these implications indicate a need for improving risk management strategies and especially agricultural insurance.

Concerning the potential for the implementation of index insurance in Central Asia, the governments of Tajikistan and Kyrgyzstan have already initiated and developed a law regarding the use of index insurance in the agricultural sector. However, because of little interest from insurance companies and farmers, and a lack of weather data for designing the index insurance, these initiatives are not being taken up by local insurance industries even though both states aim to partially finance the insurance premiums (Broka et al., 2016a, 2016b). In Uzbekistan and Kazakhstan, there are no orders or initiatives at the state level for the implementation of index insurance, while both states

support the implementation of traditional insurances with the help of various mechanisms. However, big challenges in the implementation of traditional insurances create a bottleneck for the development of an insurance market in these countries (Bobojonov et al., 2019; Broka et al., 2016c; Muradullayev et al., 2015). Several international organizations have recommended the use of index insurance in the agricultural sector of Kazakhstan and Uzbekistan to solve existing challenges in the traditional insurance markets (Broka et al., 2016c; Sutton et al., 2013), and some feasibility studies and small scale piloting activities have started to emerge in recent years. For example, Bokusheva & Breustedt (2012) have proved the suitability of drought indices based on station data, while Bokusheva et al. (2016) have extended this analysis to the applicability of VCI and TCI in index insurance for wheat production in northern Kazakhstan. For the same location, Conradt et al. (2015) investigated the applicability of station-based cumulative rainfall data for designing an index insurance. Bobojonov et al. (2019) reported on the suitability of cumulative precipitation based on weather station data and MODIS-based NDVI to identify shortfalls in wheat yields and index design in the Gallaral district, Uzbekistan.

A number of international organizations and projects in cooperation with local governmental agencies are attempting to implement satellite-based index insurance in Kazakhstan, Uzbekistan and Kyrgyzstan. For example, the United Nations Development Programme (UNDP) and the Ministry of Agriculture of Kazakhstan (MAK) are introducing an NDVI-based index insurance for croplands and livestock in Kazakhstan (UNDP, 2016). Swiss insurance company SwissRE and Dutch company Vandersat, in cooperation with MAK, have been working on introducing a satellite soil-moisture-based index insurance since 2018 (Allinsurance, 2018). Moreover, the Leibniz Institute of Agricultural Development in Transition Economies (IAMO), together with local and international insurance companies, has been developing and piloting a satellite NDVI and precipitation-based index insurance for croplands in Uzbekistan and Kyrgyzstan since 2018 (Bobojonov et al., 2019).

The above-mentioned studies and projects have not explored the accuracy of satellite-based weather data for index development in Central Asia. Since farming systems are heterogeneous and risks are diverse, weather data could be important for measuring various climate-related risks (a review on the need for satellite weather data usage in the region can be found in Appendix 1.3).

2.4. Methods and materials

2.4.1. Data sources

2.4.1.1. Meteorological Data

Whenever station proximity, historical records and general data quality are provided, weather station data remains the most accurate source of information for the design of weather indices. Therefore, we chose the daily precipitation and temperature data of six meteorological stations located in Uzbekistan as a benchmark for our accuracy assessment. The selected weather stations provide information on a time period from January 1st, 2000 to December 31st, 2017, which is a sufficient

time horizon for comparison. Furthermore, we only compared data from a satellite that was in direct proximity[4] to the selected stations.

The meteorological data was provided by the Centre of Hydro-meteorological Service at the Ministry of Emergency Situations of the Republic of Uzbekistan (Uzhydromet), which is responsible for all national hydro-meteorological network stations (Uzhydromet, 2008). The Djizzakh, Gallaral and Lalmikor stations are located in the Djizzakh province. The Samarkand station is located in the Samarkand province, and the Karshi station in situated in the Kashkadarya province of Uzbekistan (Figure 2.2) (see Appendix 1.4 for detailed information). Among the selected stations, only Djizzakh, Samarkand and Karshi stations were used during the calibration of all selected satellite-based weather products (CHC, 2021; Ji et al., 2015; Mega et al., 2019; NCEI, 2019).

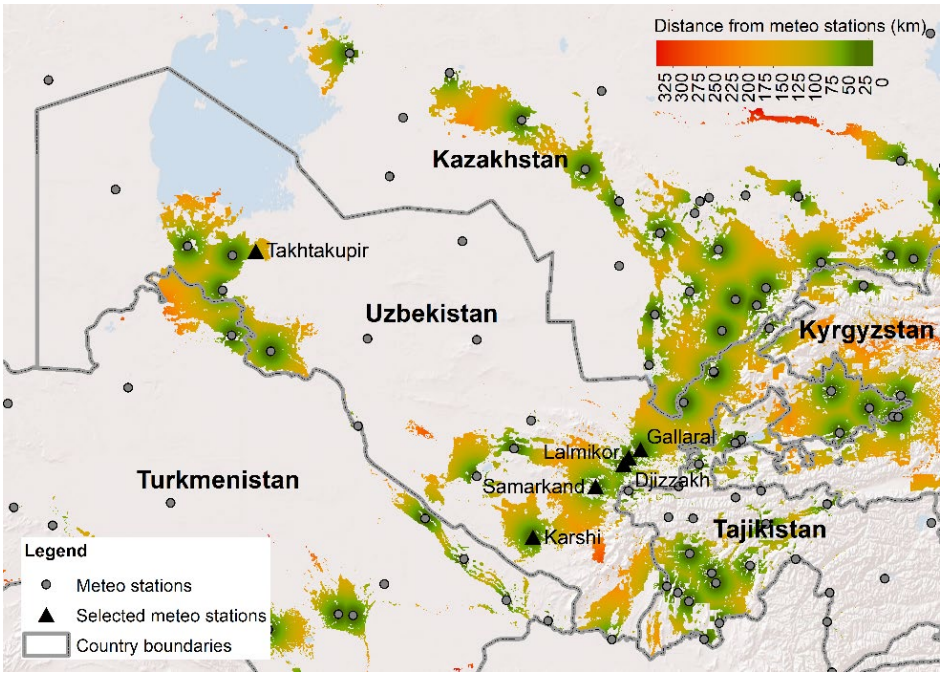

Figure 2.2: Selected meteorological stations

Source: Own presentation based on data from Teluguntla et al. (2015) and NCEI (2019).

Retrieved from the published open-access article: Eltazarov, S., Bobojonov, I., Kuhn, L., Glauben, T. (2021): Mapping weather risk – A multi-indicator analysis of satellite-based weather data for agricultural index insurance development in semi-arid and arid zones of Central Asia. Climate Service, 23, 100251.

2.4.1.2. Satellite Remote Sensing precipitation and temperature data

After a systematic review of available satellite-based weather products (see Appendix 1.5 for a detailed review), we selected three satellite weather products for this study: Firstly CHIRPS, secondly GSMaP, and finally the satellite temperature product GLDAS. The selection was made based on the

[4] Details about the spatial resolution of the selected satellite-based weather products will be discussed in following chapters

coverage area of the case study region, spatial and temporal performances in terms of suitability for index insurance development (e.g., extreme large resolution may not be suitable due to high basis risk), as well as data accessibility, which would also be relevant for the sustainable application to insurance products.

CHIRPS[5] is a semi-global precipitation product, covering latitudes 50°S-50°N and all longitudes. The product is designed for drought monitoring and environmental analyses (Funk et al., 2015). CHIRPS data is available starting from 1981 to the near present, and the dataset consist of daily, pentadal, decadal and monthly temporal resolution data, which were completed and made available to the public in February 2015 by the Climate Hazards Group (CHC, 2015). CHIRPS integrates a 0.05° x 0.05° spatial resolution of satellite images and data from stations to produce a gridded precipitation time series. A detailed description of the CHIRPS dataset has been published in Funk et al. (2015).

GSMaP is a semi-global precipitation product with 0.1°x 0.1° spatial resolution and 1-hour temporal resolution that uses multi-band passive microwave and infrared radiometers from the GPM Core Observatory satellite and, with the assistance of a constellation of other satellites, covering latitudes 60°S-60°N and all longitudes. The product is designed for flood monitoring, meteorology and climatology analyses. GSMaP data is available starting from 2000 to the near present, and the dataset consist of hourly and daily data, which is available through the JAXA G-Portal (2019). This study uses a gauge-data (GG) band, which has adjusted precipitation rate to rain gauge. The dataset is processed using a GSMaP algorithm version 6 (product version 3).

GLDAS is a global 3-hourly climate product created by combining satellite and ground-based observation datasets, which apply multiple advanced land surface modelling and data assimilation methods to generate optimal fields of land surface states and fluxes (Rodell et al., 2004). For this study, we used the Tair_f_inst (air temperature) band from 2.1 version of the GLDAS. GLDAS 2.1 is analogous to previous versions with upgraded models, which integrate GDAS, GPCP and AGRMET datasets. Data from the GLDAS 2.1 is available for the period from early 2000 to the near present. The spatial resolution of the product is 0.25° x 0.25° (Chen et al., 2013). The GLDAS data is archived and freely available through GSFC DISC (2019).

In order to obtain daily updates on CHIRPS, GSMaP and GLDAS data, we developed an algorithm and programmed an automatic web platform (see Appendix 1.6 for details and information on the free data platform), which allows easy access to the related datasets. This web platform for data acquisition can be found under the following link: https://www.klimalez.org/srs-export. A large number of existing studies that have assessed the accuracy of satellite products are characterized by decadal, monthly, seasonal and annual scales (e.g., Darand and Khandu (2020); Peng et al. (2020); Rivera et al. (2018); Yu et al. (2020)), especially studies in the field of index insurance design (e.g. Bobojonov et al. (2014); Odening et al. (2007); Osgood et al. (2007); Westerhold et al. (2018); Xu et al. (2008)).

[5] Climate Hazards Group Infrared Precipitation (CHIRP) was not considered for this study since we already included CHIRPS, which is the improved version of CHIRP, providing higher accuracy than its predecessor, as pointed out by (Dinku et al., 2018; Funk et al., 2015; Shen et al., 2020)

To comprehend the pattern of the satellite precipitation and temperature measurements at different time scales and locations, this study assessed the satellite data in decadal and monthly aggregation. The aggregation of hourly, 3-hourly and daily data into decadal and monthly values cancels out errors observable in short-term data, as mentioned for instance by Usman & Nichol (2020). Coleman et al. (2018) have stated that aggregated SPEs are more accurate than daily ones, as there is significant uncertainty in an individual precipitation measurement either by the satellite or the station.

2.4.2. Accuracy measures

To evaluate the accuracy of the GSMaP, CHIRPS and GLDAS data, we used a number of classification metrics, which are based on existing indices or adaptions of such as used in the existing research literature (Hu et al., 2013; C. Yu et al., 2020):

Frequency Bias (BIAS), Critical Success Index (CSI), also known as Threat Score, Probability of Detection (POD) and False Alarm Ratio (FAR) were used to demonstrate the ability of remote sensing to precisely measure decadal and monthly precipitation and temperature (Schaefer, 1990; Stephenson, 2000). BIAS measures the tendency of a satellite to underestimate or overestimate events. POD measures the probability of a satellite to detect precipitation events. FAR indicates the probability of a satellite-based precipitation event being detected by mistake. CSI represents the overall accuracy of a satellite in classifying precipitation events. CSI, POD and FAR are recommended and extensively used by the US National Weather Service to verify various weather events (Gerapetritis and Pelissier, 2004). The details of these statistics can be found in Table 2.1, where a represents correctly detected precipitation events by a satellite, b stands for precipitation events that are detected by the satellite but not confirmed by station data, and c denotes precipitation events that are not detected by satellite data but are observed by station data.

Furthermore, we employed a number of quantitative metrics. In detail, these are 1) Percentage Bias (PBIAS), which measures the average tendency of satellite estimates to be larger or smaller than the benchmark; 2) Mean Bias Error (MBE), which measures the average satellite estimate error; 3) Mean Absolute Error (MAE), which measures the average magnitude of a satellite's estimate; 4) Root Mean Square Error (RMSE), which measures the same as MBE but puts greater weight on higher errors than MBE.

We also applied some agreement metrics such as 1) Spearman's Rank-order Correlation Coefficient (SC), which measures the strength of a monotonic relationship between estimations and observations; 2) Pearson's Correlation Coefficient (PC), which measures the linear correlation between estimations and observations; 3) Determination Coefficient (R^2), which measures how well data points fit in a regression line, as well as the predictability level of the observation data from satellite data; 4) Index of Agreement (d), which solves certain problems associated with PC and R^2 and measures the degree to which satellite estimation is free of error; it also measures how well a satellite estimate simulates station data (Willmott, 1981); 5) Linear Error in Probability Space (LEPS), which measures the mean absolute difference between the estimated cumulative distribution value and the observation (Potts et al., 1996); 6) Nash-Sutcliffe Efficiency (NSE), which was first proposed by

Nash & Sutcliffe (1970) and originally used for assessing the predictive power of hydrological models, but was later widely used for quantity accuracy assessment of various models. However, NSE is highly sensitive for data that has a high temporal volatility. Therefore, NSE has been used only for accuracy assessment of the temperature data. The details of these statistical indices can be found in Table 2.1, where E_i and O_i are satellite and station observations, respectively, at a specific time i; $\bar{O}$ is the average of the observed precipitation/temperature.

Table 2.1: Details of accuracy measures

Statistics	Formula	Range	Unit	Perfect Value
Frequency Bias	$BIAS = \frac{a+b}{a+c}$	0 to ∞	None	1
Critical Success Index	$CSI = \frac{a}{a+b+c}$	0 to 1	None	1
Probability of Detection	$POD = \frac{a}{a+c}$	0 to 1	None	1
False Alarm Ratio	$FAR = \frac{b}{a+b}$	0 to 1	None	0
Percentage Bias	$PBIAS = \frac{\sum_{i=1}^{n}(E_i - O_i)}{\sum_{i=1}^{n}(O_i)} \times 100\%$	–∞ to ∞	%	0
Mean Bias Error	$MBE = \sum_{i=1}^{n}(E_i - O_i)$	–∞ to ∞	mm or C°	0
Mean Absolute Error	$MAE = \frac{1}{n}\sum_{i=1}^{n}\lvert E_i - O_i\rvert$	0 to ∞	mm or C°	0
Root Mean Square Error	$RMSE = \sqrt{\frac{1}{n}\sum_{i=1}^{n}(E_i - O_i)^2}$	0 to ∞	mm or C°	0
Linear Error in Probability Space	$LEPS = \frac{1}{n}\sum_{i=1}^{n}\lvert CDF_O(E_i) - CDF_O(O_i)\rvert$	0 to 1	None	0
Spearman's Correlation	$SC = \frac{\frac{1}{n}\sum_{i=1}^{n}(O_i - \overline{O})(E_i - \overline{E})}{\sqrt{\frac{1}{n}\sum_{i=1}^{n}(O_i - \overline{O})^2}\sqrt{\frac{1}{n}\sum_{i=1}^{n}(E_i - \overline{E})^2}}$	–1 to 1	None	1
Pearson's Correlation	$PC = \frac{\sum_{i=1}^{n}(O_i - \overline{O})(E_i - \overline{E})}{\sqrt{\sum_{i=1}^{n}(O_i - \overline{O})^2}\sqrt{\sum_{i=1}^{n}(E_i - \overline{E})^2}}$	–1 to 1	None	1
Determination Coefficient	$R^2 = 1 - \frac{\sum_{i=1}^{n}(E_i - \overline{O})^2}{\sum_{i=1}^{n}(O_i - \overline{O})^2}$	–1 to 1	None	1
Index of Agreement	$d = 1 - \frac{\sum_{i=1}^{n}(O_i - E_i)^2}{\sum_{i=1}^{n}(\lvert E_i - \overline{O}\rvert + \lvert O_i - \overline{O}\rvert)^2}$	0 to 1	None	1
Nash-Sutcliffe Efficiency	$NSE = 1 - \frac{\sum_{i=1}^{n}(O_i - E_i)^2}{\sum_{i=1}^{n}(O_i - \overline{O})^2}$	–∞ to 1	None	1

Source: compiled by the authors.

Retrieved from the published open-access article: Eltazarov, S., Bobojonov, I., Kuhn, L., Glauben, T. (2021): Mapping weather risk – A multi-indicator analysis of satellite-based weather data for agricultural index insurance development in semi-arid and arid zones of Central Asia. Climate Service, 23, 100251.

Additionally, we used Ordinary Least Squares (OLS) regression and Quantile Regression (QR) to measure the relationship between decadal and monthly weather measurements by station and satellite. QR was used to assess the satellite decadal and monthly weather data in various quantiles of the station precipitation measurements, which is not possible in traditional regression methods. QR

has a number of advantages for measuring the relationship between variables compared to traditional regression methods. QR measures the relationship between minimum and maximum response and provides a more detailed overview of the relationship (Cade and Noon, 2003). QR minimizes the sum of absolute residuals and is robust to outliers (Li, 2014). In our study, we focused on all lower, median and upper tile quantiles .05, .1, .25, .5, .75, .9, .95 to check the ability of SPE during drought/flood periods. All statistical calculations and figures were developed using the R project (R Development Core Team, 2018) and just the results of the QR analysis were generated with STATA 15 (StataCorp, 2019).

2.4.3. Meteorological drought indices and anomaly detection

In order to check the ability of satellite-based MDIs to detect weather shocks during the vegetation period of rainfed crops (March-May) and irrigated crops (May, September, October), we calculated MDIs using both in-situ weather and satellite data and applied correlation analyses. For the analyses, we selected two drought indices, namely the Standardized Precipitation Index (SPI) and the Standardized Precipitation-Evapotranspiration Index (SPEI). According to Wanders et al. (2017), the SPI and SPEI are among the most frequently used drought indices worldwide. Ghamghami et al. (2017) and Okpara et al. (2017) have found the SPI well-suited for index insurance purposes. SPI is based on the conversion of precipitation data into probabilities using gamma distribution. The negative output value of SPI represents drought intensity, with the following categories: > 0 is no drought, 0 to -0.99 is mild drought, -1.00 to -1.49 is moderate drought, -1.50 to -1.99 is severe drought and ≤ -2.00 is extreme drought (McKee et al., 1993). The main advantages of the SPI are a simple calculation that uses only precipitation data and its multi-temporal character. Meanwhile, the SPI measures only the water supply and does not take into account any temperature changes over the given period, thus ignoring the problem of evapotranspiration. In this regard, SPEI is an improvement of SPI, by taking into account both precipitation and Potential Evapotranspiration (PET) in defining drought (Vicente-Serrano et al., 2010). Bezdan et al. (2019) have proposed the use of SPEI in decision-making at both national and regional levels and in the agricultural insurance sector. In our calculations, the PET have been calculated according to the Hargreaves & Samani (1982) method, which has an option of calculating the PET using only Tmax and Tmin data. Categories of output values are similar to the SPI. A detailed explanation of the SPI index calculation can be found in McKee et al. (1993), and for SPEI calculation in Vicente-Serrano et al. (2010). SPI and SPIE were calculated using the R package developed by Beguería & Maintainer (2017), who are the authors of SPEI itself.

Additionally, we tested the ability of SPEs to detect the extreme weather events by using the percentiles as a threshold for anomaly detection. We applied <10th and <20th percentiles for drought (March, April and May) and >80th and >90th percentiles for flood events (May, September, October) detection. Classification accuracy measures listed in Table 2.1 were applied to examine the performance of products.

2.5. Results

2.5.1. Accuracy of satellite precipitation data

Figure 2.3 provides a comparison of decadal and monthly precipitation levels as measured by satellites at the Djizzakh station in the period of March-December 2017. A similar visualization for the remaining five stations can be found in Figure A.1.7.1 and 1.7.2. While both satellites did record the local precipitation events, we noticed that monthly precipitation, in comparison with our benchmark stations, was overestimated by CHIRPS, while it was underestimated by GSMaP.

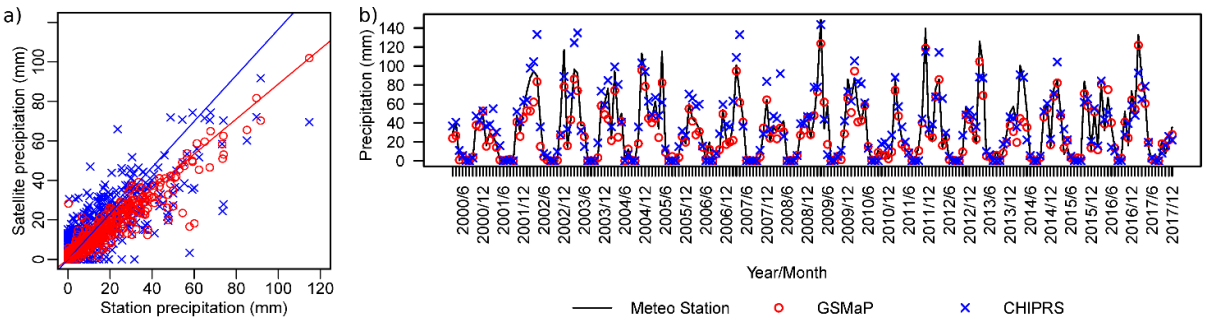

Figure 2.3: Decadal (a) and monthly (b) precipitation by stations, GSMaP and CHIRPS at the Djizzakh station

Source: compiled by the authors.

Retrieved from the published open-access article: Eltazarov, S., Bobojonov, I., Kuhn, L., Glauben, T. (2021): Mapping weather risk – A multi-indicator analysis of satellite-based weather data for agricultural index insurance development in semi-arid and arid zones of Central Asia. Climate Service, 23, 100251.

Table 2.2: Accuracy assessment of continuous monthly precipitation in selected locations (March 2000-December 2017)

	Djizzakh		Gallaral		Lalmikor		Samarkand		Karshi		Takhtakupir		Average	
	GSMaP	CHIPRS	GSMaP	CHIPRS	GSMaP	CHIPRS	GSMaP	CHIPRS	GSMaP	CHIPRS	GSMaP	CHIPRS	GSMaP	CHIPRS
BIAS	1.09	0.89	1.11	0.90	1.08	0.88	1.10	0.87	1.28	1.02	1.08	0.91	1.12	0.91
CSI	0.91	0.89	0.90	0.86	0.91	0.86	0.91	0.86	0.78	0.91	0.89	0.82	0.88	0.87
POD	0.99	0.89	1.00	0.88	0.99	0.87	1.00	0.87	1.00	0.97	0.98	0.86	0.99	0.89
FAR	0.08	0.00	0.10	0.02	0.08	0.01	0.09	0.01	0.22	0.05	0.09	0.05	0.11	0.02
PBIA	-14.20	10.60	-9.10	18.00	-18.90	4.00	-12.90	4.90	-6.80	28.50	-13.90	9.50	-12.63	12.58
MBE	-4.68	3.50	-2.79	5.52	-6.48	1.37	-3.81	1.46	-1.22	5.11	-1.41	0.96	-3.40	2.99
MAE	6.45	10.37	7.77	11.74	9.25	10.93	6.27	8.33	3.69	6.97	4.15	4.86	6.26	8.87
RMS	11.13	15.76	12.37	16.98	14.11	15.71	10.64	12.77	6.59	11.57	7.58	7.26	10.40	13.34
SC	0.97	0.92	0.94	0.91	0.95	0.91	0.98	0.94	0.96	0.95	0.84	0.84	0.94	0.91
PC	0.96	0.90	0.93	0.88	0.93	0.89	0.95	0.92	0.96	0.91	0.79	0.80	0.92	0.88
R^2	0.93	0.81	0.86	0.78	0.87	0.79	0.91	0.84	0.92	0.84	0.63	0.65	0.85	0.79
p	0.00	0.00	0.00	0.00	0.00	0.00	0.00	0.00	0.00	0.00	0.00	0.00	0.00	0.00
d	0.97	0.94	0.96	0.93	0.95	0.94	0.97	0.96	0.97	0.94	0.88	0.88	0.95	0.93
LEPS	0.05	0.08	0.06	0.09	0.07	0.09	0.04	0.07	0.04	0.06	0.10	0.13	0.06	0.09

Source: compiled by the authors.

Retrieved from the published open-access article: Eltazarov, S., Bobojonov, I., Kuhn, L., Glauben, T. (2021): Mapping weather risk – A multi-indicator analysis of satellite-based weather data for agricultural index insurance development in semi-arid and arid zones of Central Asia. Climate Service, 23, 100251.

To quantify this difference in precipitation data, Table 2.2 and Table A.1.8.1 provide the results of classification, quantitative and agreement statistics of continuous decadal and monthly precipitation for all six stations. The results obtained from BIAS show that GSMaP slightly overestimate the precipitation events while CHIRPS underestimates; mean values are equal to 1.12 and 0.91 for monthly scale and 1.24 and 0.91 for decadal scale, respectively. According to POD, GSMaP has almost perfect values and significantly better probability to detect precipitation events than CHIRPS. Meanwhile, based on FAR results, CHIRPS has a lower probability of false positives in terms of precipitation events than GSMaP. The values of CSI, which measures comprehensive detection probability of satellite to precipitation events, vary from 0.78 to 0.91 on a monthly scale and from 0.71 and 0.86 on a decadal scale for GSMaP; and from 0.82 to 0.89 on a monthly scale and from 0.82 to 0.98 for CHIRPS.

According to results from PBIAS and MBE in both temporal aggregations, GSMaP underestimates precipitation in all locations while CHIRPS overestimates. MBE and RMSE shows that GSMaP has a lower difference from benchmark measurements and a higher accuracy compared to CHIRPS in all locations. Results of SC, PC, R^2, d and LEPS for GSMaP are close to perfect values in all locations, except for the Takhtakupir station, which is located in an arid zone. Meanwhile, these agreement metrics are also high for CHIRPS but slightly lower than GSMaP. As shown in Table 2.2 and Table A.1.8.1, the results of all statistical metrics for the Takhtakupir station are slightly lower in both SPEs. Overall, the results of all statistical metrics for all stations are on a satisfactorily accurate level. GSMaP showed a stronger ability to measure precipitation variance than CHIRPS in terms of most statistical metrics.

Table 2.3: Quantile regression results of satellite-based monthly precipitation estimates for the Djizzakh station (n = 214)

		OLS	QR0.5	QR 0.1	QR 0.25	QR 0.5	QR 0.75	QR 0.9	QR 0.95
	Coef.	1.150***	0.914***	0.940***	1.039***	1.126***	1.249***	1.480***	1.640***
Djizzakh-GSMaP	**SE**	0.022	0.054	0.022	0.022	0.013	0.029	0.066	0.159
	R^2/pR^2	0.925	0.605	0.6708	0.7529	0.8046	0.7897	0.7531	0.711
	Coef.	0.876***	0.558***	0.535***	0.681***	0.900***	1.044***	1.168***	1.137***
Djizzakh-CHIRPS	**SE**	0.029	0.048	0.033	0.034	0.026	0.034	0.077	0.106
	R^2/pR^2	0.807	0.3273	0.4044	0.5469	0.6408	0.6534	0.6123	0.5873

Coef. = Coefficient; SE = standard error; R^2 = R-square for OLS; pR^2 = pseudo R-square for quantiles; * p<0.05, ** p<0.01, *** p<0.001

Note: A similar table for the remaining five stations can be found in Table A.1.9.2 and for decadal scale in Table A.1.9.4.

Source: compiled by the authors.

Retrieved from the published open-access article: Eltazarov, S., Bobojonov, I., Kuhn, L., Glauben, T. (2021): Mapping weather risk – A multi-indicator analysis of satellite-based weather data for agricultural index insurance development in semi-arid and arid zones of Central Asia. Climate Service, 23, 100251.

In both SPE products for the decadal and monthly scales, the quantile coefficients and their 95% confidence intervals do not lie within the 95% confidence interval (Figure 2.4, Figure A.1.9.3 and A.1.9.5); furthermore, there is a significant difference between coefficients in the upper and lower quantiles compared to OLS (Table 2.3, Table A.1.9.2 and A.1.9.4). This indicates a different relationship between precipitation by station and SPE along the quantiles, showing that the OLS regression slope is not sufficient to describe this relationship. Both Figure 2.4 and Table 2.3 show that the magnitude of coefficients is increasing as they approach the upper quantiles of the distribution of station precipitation. Coefficients of GSMaP in the lowest quantiles (low precipitation decades and months) are below one, as opposed to the quarter quantiles coefficients, which exceed one. Correspondingly, GSMaP overestimates the precipitation in lower quantiles, but starts underestimating after quarter quantiles. Structurally, the results for CHIRPS are similar; however, CHIRPS overestimates the precipitation until about the median, after which it starts underestimating precipitation. Overall, both SPE products have a significant correlation with station precipitation measures, according to both OLS and quantile regression.

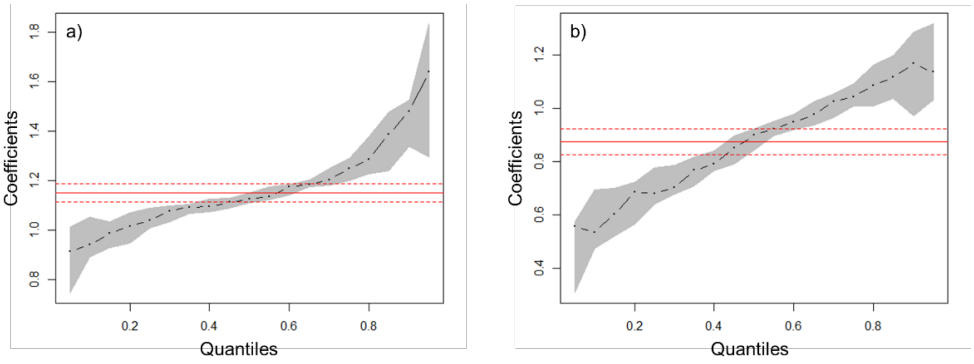

Figure 2.4: Estimated results of quantile regressions for monthly scale precipitation by (a) GSMaP and (b) CHIRPS in Djizzakh station

Note: A similar visualization for the remaining five stations can be found in Figure A.1.9.1 and for decadal scale in Figure A.1.9.3

Source: compiled by the authors.

Retrieved from the published open-access article: Eltazarov, S., Bobojonov, I., Kuhn, L., Glauben, T. (2021): Mapping weather risk – A multi-indicator analysis of satellite-based weather data for agricultural index insurance development in semi-arid and arid zones of Central Asia. Climate Service, 23, 100251.

Figure A.1.8.3 and Figure 2.5 illustrate the average results from all six stations for classification, quantitative and agreement accuracy metrics of the decadal and monthly precipitation records for each period from March 2000 to December 2017. This means that each month offers 18 periodic precipitation observations for analysis, except January to March, for which there are 17 periodic precipitation observations. According to the averaged results, GSMaP shows a significantly higher

accuracy than CHIRPS in most decades and months in all accuracy metrics. The values of classification accuracy metrics (BIAS, CSI, POD and FAR) for GSMaP are close to a perfect value in all months excluding the dry season (June to September), which indicates a higher classification accuracy for GSMaP in wet seasons (winter, spring and fall). Meanwhile, the classification accuracy metrics for CHIRPS are lower than GSMaP, while CHIRPS also has a significantly lower classification accuracy in the summer season, as compared to other seasons. Based on these results, the average values of PBIAS and MBE confirm that GSMaP underestimated precipitation levels in the vast majority of decades and months; meanwhile, CHIRPS overestimated the amount of precipitation in decades and months from January to May and from October to December, even though for both satellite products, the MAE and RMSE in summer season are significantly lower than in other seasons. GSMaP has higher and moderately close to perfect values in SC, PC, R^2, d and LEPS than CHIRPS provides in all months, and a decrease of quantitative and agreement accuracy can be observed during the summer season for both products. Overall, GSMaP has a significantly higher accuracy in terms of all statistics than CHIRPS, which can be observed from both continuous decadal and monthly precipitation analyses and analyses for each decades' and months' precipitation.

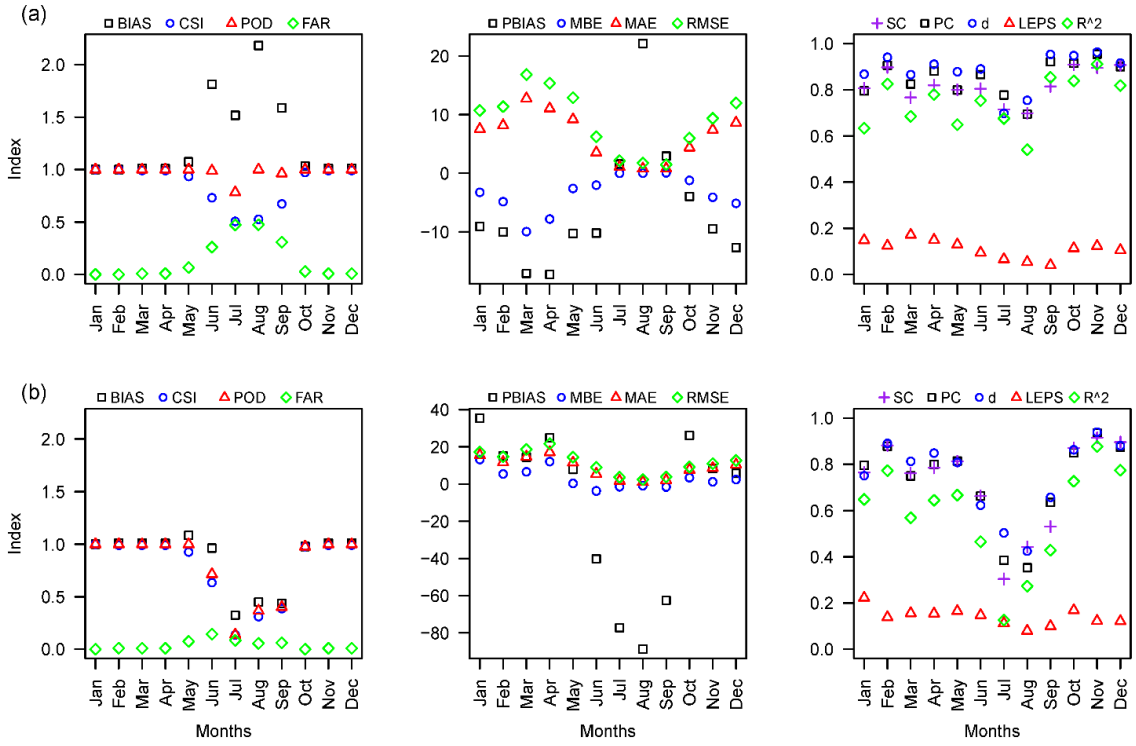

Figure 2.5: Average results of classification, quantitative and agreement accuracy metrics of monthly precipitation for all stations, by (a) GSMaP and (b) CHIRPS

Note: A similar visualization of results for decadal scale can be found in Figure A.1.8.3.

Source: compiled by the authors.

Retrieved from the published open-access article: Eltazarov, S., Bobojonov, I., Kuhn, L., Glauben, T. (2021): Mapping weather risk – A multi-indicator analysis of satellite-based weather data for agricultural index insurance development in semi-arid and arid zones of Central Asia. Climate Service, 23, 100251.

2.5.2. Accuracy of satellite temperature data

Using the Djizzakh station as an example, Figure 2.6 demonstrates the decadal and monthly average Tmax and Tmin estimates by GLDAS and the stations between January 2000 and December 2017. A similar visualization for the remaining five stations can be found in Figure A.1.7.3 and A.1.7.4. According to results, GLDAS has a high ability to detect average Tmax and Tmin, and performs extremely accurate measurements at the 1% level in both temporal aggregation for all periods and all locations.

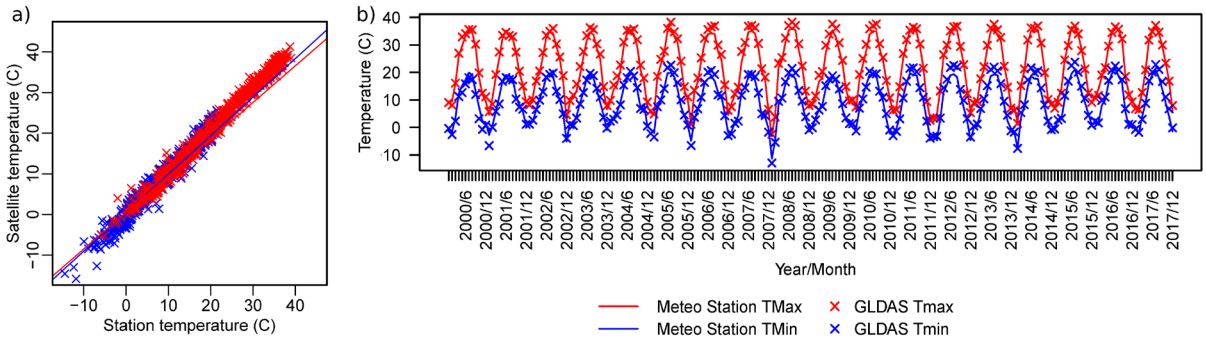

Figure 2.6: Decadal (a) and monthly (b) average Tmax and Tmin by stations and GLDAS for the Djizzakh station

Source: compiled by the authors.

Retrieved from the published open-access article: Eltazarov, S., Bobojonov, I., Kuhn, L., Glauben, T. (2021): Mapping weather risk – A multi-indicator analysis of satellite-based weather data for agricultural index insurance development in semi-arid and arid zones of Central Asia. Climate Service, 23, 100251.

Table 2.4: Accuracy assessment of continuous monthly average temperature in selected locations (January 2000-December 2017)

	Djizzakh		Gallaral		Lalmikor		Samar-kand		Karshi		Takhtakupir		Average	
	Tmax	Tmin	Tmax	Tmin	Tmax	Tmin	Tmax	Tmin	Tmax	Tmin	Tmax	Tmin	Tmax	Tmin
BIAS	1.00	1.00	1.00	1.00	1.00	1.00	1.00	1.00	1.00	1.00	1.00	1.00	1.00	1.00
CSI	1.00	1.00	1.00	1.00	1.00	1.00	1.00	1.00	1.00	1.00	1.00	1.00	1.00	1.00
POD	1.00	1.00	1.00	1.00	1.00	1.00	1.00	1.00	1.00	1.00	1.00	1.00	1.00	1.00
FAR	0.00	0.00	0.00	0.00	0.00	0.00	0.00	0.00	0.00	0.00	0.00	0.00	0.00	0.00
PBIA	3.40	4.60	2.80	28.60	1.30	-11.60	-3.70	2.30	0.10	11.60	-0.70	58.80	0.53	15.72
MBE	0.73	0.43	0.58	1.86	0.25	-1.03	-0.81	0.21	0.03	1.21	-0.13	3.39	0.11	1.01
MAE	1.11	1.13	0.95	2.14	0.89	1.42	1.34	1.02	0.88	1.95	0.72	3.40	0.98	1.84
RMS	1.36	1.42	1.20	2.68	1.16	1.87	1.72	1.35	1.14	2.31	0.95	3.88	1.26	2.25
SC	0.99	0.99	0.99	0.97	0.99	0.98	0.99	0.99	0.99	0.97	1.00	0.98	0.99	0.98
PC	1.00	0.99	1.00	0.97	0.99	0.98	0.99	0.99	1.00	0.98	1.00	0.98	1.00	0.98
R^2	0.99	0.98	0.99	0.95	0.99	0.96	0.98	0.98	0.99	0.95	0.99	0.97	0.99	0.97
p	0.00	0.00	0.00	0.00	0.00	0.00	0.00	0.00	0.00	0.00	0.00	0.00	0.00	0.00
d	1.00	0.99	1.00	0.97	1.00	0.99	0.99	0.99	1.00	0.98	1.00	0.97	1.00	0.98
LEPS	0.04	0.05	0.03	0.07	0.03	0.06	0.05	0.04	0.03	0.07	0.02	0.09	0.03	0.06
NSE	0.98	0.97	0.99	0.88	0.99	0.95	0.97	0.97	0.99	0.92	0.99	0.86	0.99	0.93

Note: A similar table for the decadal scale analyses can be found in Table A.1.8.1.

Source: compiled by the authors.

Retrieved from the published open-access article: Eltazarov, S., Bobojonov, I., Kuhn, L., Glauben, T. (2021): Mapping weather risk – A multi-indicator analysis of satellite-based weather data for agricultural index insurance development in semi-arid and arid zones of Central Asia. Climate Service, 23, 100251.

Table A.1.8.1 and Table 2.4 illustrate the results of classification, quantitative and agreement statistics of continuous decadal and monthly Tmax and Tmin in all six station locations between January 2000 and December 2017, all in all 642 decades and 214 months. According to this data, GLDAS has perfect classification accuracy in all indices, which means that GLDAS captured Tmax and Tmin in all decades and months of the study period in selected locations.

The obtained results from the quantitative statistic metrics demonstrate a satisfactory accuracy of both Tmax and Tmin measurements by GLDAS in both temporal aggregations according to Yu et al. (2020). According to PBIAS and MBE values, GLDAS slightly overestimated Tmax in four locations and underestimated in two locations. Similarly, GLDAS overestimated Tmin in five locations and underestimated in one location. Meanwhile, the results of MAE and RMSE values show that these over-/underestimations, as well as the difference between station and GLDAS measurements, can be disregarded. Overall, results of SC, PC, R^2, d, LEPS and NSE for Tmax and Tmin are near to the perfect value of zero or one, respectively, which indicates the strong ability of GLDAS to measure variance of decadal and monthly mean Tmax and Tmin, even though agreement statistical metrics of Tmax are slightly and insignificantly higher than Tmin.

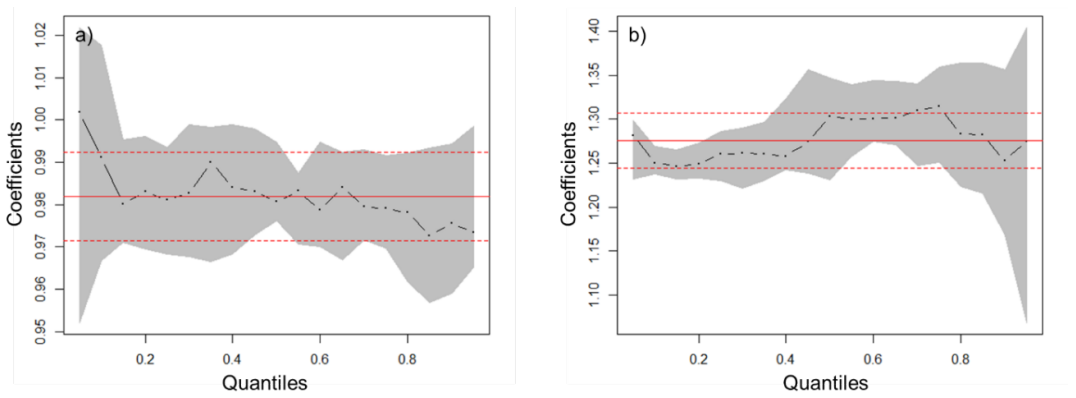

Figure 2.7: Estimated results of quantile regressions for (a) GLDAS Tmax and (b) GLDAS Tmin in Djizzakh station

Note: A similar visualization for the remaining five stations can be found in Figure A.1.9.1 and for decadal scale in Figure A.1.9.3.

Source: compiled by the authors.

Retrieved from the published open-access article: Eltazarov, S., Bobojonov, I., Kuhn, L., Glauben, T. (2021): Mapping weather risk – A multi-indicator analysis of satellite-based weather data for agricultural index insurance development in semi-arid and arid zones of Central Asia. Climate Service, 23, 100251.

Table 2.5: Estimated results of OLS regressions for monthly GLDAS Tmax and GLDAS Tmin in all locations

	Djizzakh		Gallaral		Lalmikor		Samarkand		Karshi		Takhtakupir	
	GLDAS Tmax	GLDAS Tmin	GLDAS Tmax	GLDAS Tmin	GLDAS Tmax	GLDAS Tmin	GLDAS Tmax	GLDAS Tmin	GLDAS Tmax	GLDAS Tmin	GLDAS Tmax	GLDAS Tmin
Coef.	0.947***	1.255***	0.982***	1.276***	0.979***	1.253***	0.934***	1.188***	0.945***	1.155***	1.016***	1.249***
SE	0.006	0.014	0.006	0.019	0.007	0.019	0.009	0.015	0.006	0.017	0.005	0.015
R-sq	0.991	0.973	0.991	0.953	0.989	0.954	0.981	0.967	0.992	0.954	0.995	0.972

Note: A similar table for the remaining five stations can be found in 9.2 and for decadal scale in Table A.1.9.4.

Coef. = Coefficient; SE = standard error; R-square; * p<0.05, ** p<0.01, *** p<0.001

Source: compiled by the authors.

Retrieved from the published open-access article: Eltazarov, S., Bobojonov, I., Kuhn, L., Glauben, T. (2021): Mapping weather risk – A multi-indicator analysis of satellite-based weather data for agricultural index insurance development in semi-arid and arid zones of Central Asia. Climate Service, 23, 100251.

Figure A.1.9.3 and Figure 2.7 show that OLS is sufficient to describe the relationship between temperature (decadal and monthly) measurements by satellite and station. The quantile slope estimates are not statistically different from the OLS estimate. Therefore, we conducted only OLS regression for satellite temperature data. The average R^2 of Tmax is 0.99, ranging from 0.98 to 0.99, and Tmin varies from 0.95 to 0.98, with a mean of 0.97. P-values in all locations are below 0.001, which means the results are statistically significant at the 1 % level. Coefficients of GLDAS Tmax in all locations are less than one, as opposed to GLDAS Tmin, which reach higher than one. Correspondingly, GLDAS slightly overestimates the decadal and monthly mean Tmax and underestimates the Tmin. Overall, both GLDAS Tmax and Tmin in all locations have a significant correlation with station temperature measurements according to both OLSs.

Figure A.1.8.4 and Figure 2.8 illustrate the average results (from six stations) of classification, quantitative and agreement accuracy metrics of decadal and monthly temperature records for each period between January 2000 and December 2017, which means each month has 18 periodic temperature data measurements. Both Tmax and Tmin have perfect values for all classification accuracy metrics in all decades and months, which means that GLDAS is capturing all decadal and monthly temperature events and there is no data missing in any of the locations. In quantitative and agreement accuracy metrics, Tmax has a slightly higher accuracy than Tmin in most periods. PBIASs of Tmax and Tmin are significantly higher during the winter season, as average Tmax and Tmin during the winter season are very close to zero, and a slight difference between measurements might cause high PBIAS values. The PBIAS values are 107.55% in January and -7.75% in February for Tmax. The PBIAS values of Tmin are 19.06%, 102.85%, 45.6%, 14.43%, 35.83% and -203.85% in January, February, March, September, October and December, respectively. Despite this, the MBE, MAE and RMSE values of Tmax and Tmin during the winter season are lower than in other seasons, which demonstrates the low relevance of high PBIAS values to the overall quantitative and agreement accuracy. As shown in the figure, Tmax has higher and closer to perfect values in SC, PC, R^2, d and LEPS than

Tmin in the majority of decades and months. Even though the SC, PC, d, LEPS and R^2 values are lower in summer seasons, those do not significantly affect the MBE, MAE and RMSE. Overall, both Tmax and Tmin have significant classification, quantitative and agreement accuracy, which can be observed from both continuous decadal and monthly temperature analyses and analyses for each decades' and months' temperature. Additionally, accuracy comparisons were performed over the seasonal scale for the Djizzakh station only and results can be found in Appendix 1.10.

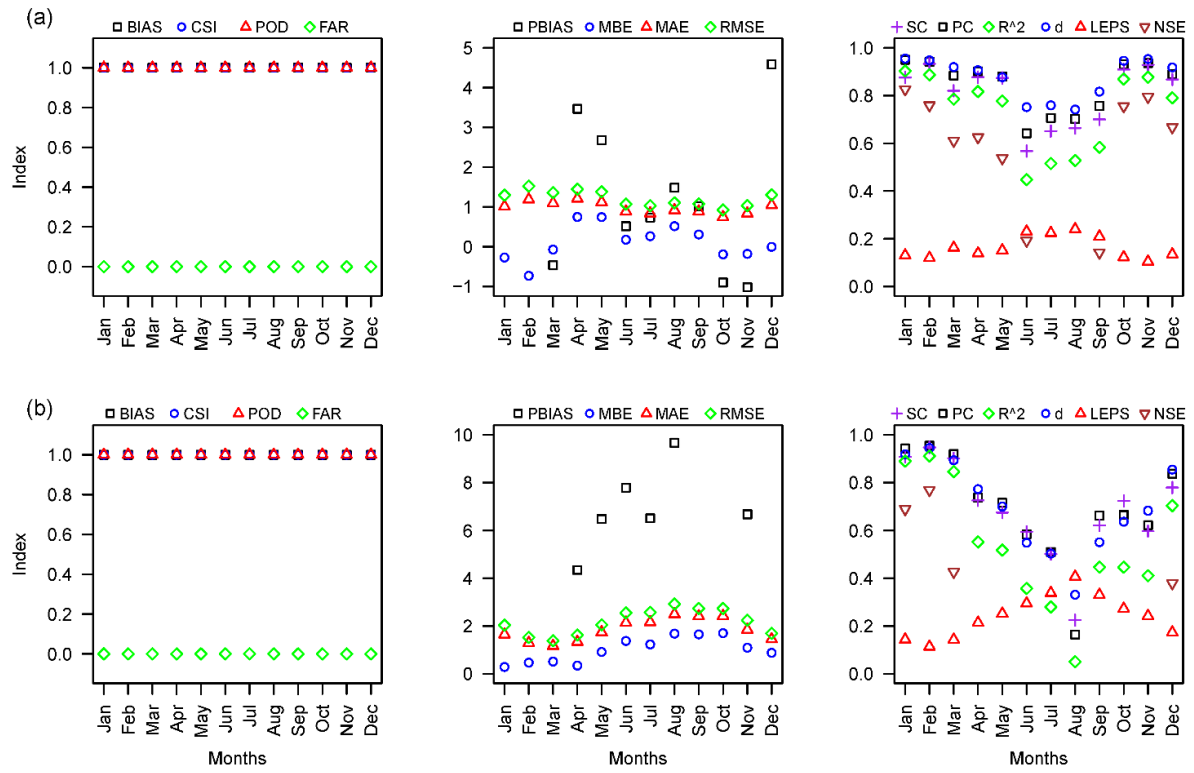

Figure 2.8: Average results of classification, quantitative and agreement accuracy metrics of monthly precipitation for all stations, for (a) GLDAS Tmax and (b) GLDAS Tmin

Note: A similar visualization of results for the decadal scale can be found in Figure A.1.8.4

Source: compiled by the authors.

Retrieved from the published open-access article: Eltazarov, S., Bobojonov, I., Kuhn, L., Glauben, T. (2021): Mapping weather risk – A multi-indicator analysis of satellite-based weather data for agricultural index insurance development in semi-arid and arid zones of Central Asia. Climate Service, 23, 100251.

2.5.3. Meteorological drought indices and anomaly detection

In the previous two sections, we have assessed the accuracy of satellite-based weather data. Our findings indicate the occurrence of considerable over- and underestimations. The following analysis illustrates the impact of these deficiencies on drought indices, as they might find application in index-based insurance products. In this chapter we focused on drought during the vegetation period of rainfed crops (March-May), on flood during the seeding of irrigated crops (May) and on flood

during the harvesting of irrigated crops (September-October). Figure 2.9 compares the SPI values during March, April, May, September and October based on precipitation data from stations, GSMaP and CHIRPS for the Djizzakh station (a similar visualization for the remaining five stations can be found in Figure A.1.11.1). In general, SPI values from both SPEs are able to detect drought and flood, and performed reasonably accurate measurements in most locations. The PC between GSMaP-SPI and station-SPI is slightly higher than CHIRPS-SPI in all cases. Another finding is that the agreement between SPIs located in the semi-arid agro-climatic zone was higher than in the arid agro-climatic zone.

Moreover, Figure 2.9 illustrates the calculated SPEI values based on the data combinations station & station (M & M), GSMaP & GLDAS (G & G) and CHIRPS & GLDAS (C & G) for the months of March, April, May, September and October for the Djizzakh station (a similar visualization for the remaining five stations can be found in Figure A.1.11.2). Generally, SPEI values from satellite precipitation and temperature products are able to detect drought and gave reasonably accurate measurements in most locations. This was confirmed by the SPEI results. The weather data combination involving GSMaP has a slightly higher agreement than the C&G combination. In addition, the PC of SPEIs located in the semi-arid agro-climatic zone was higher than that in the arid agro-climatic zone, in line with SPI results.

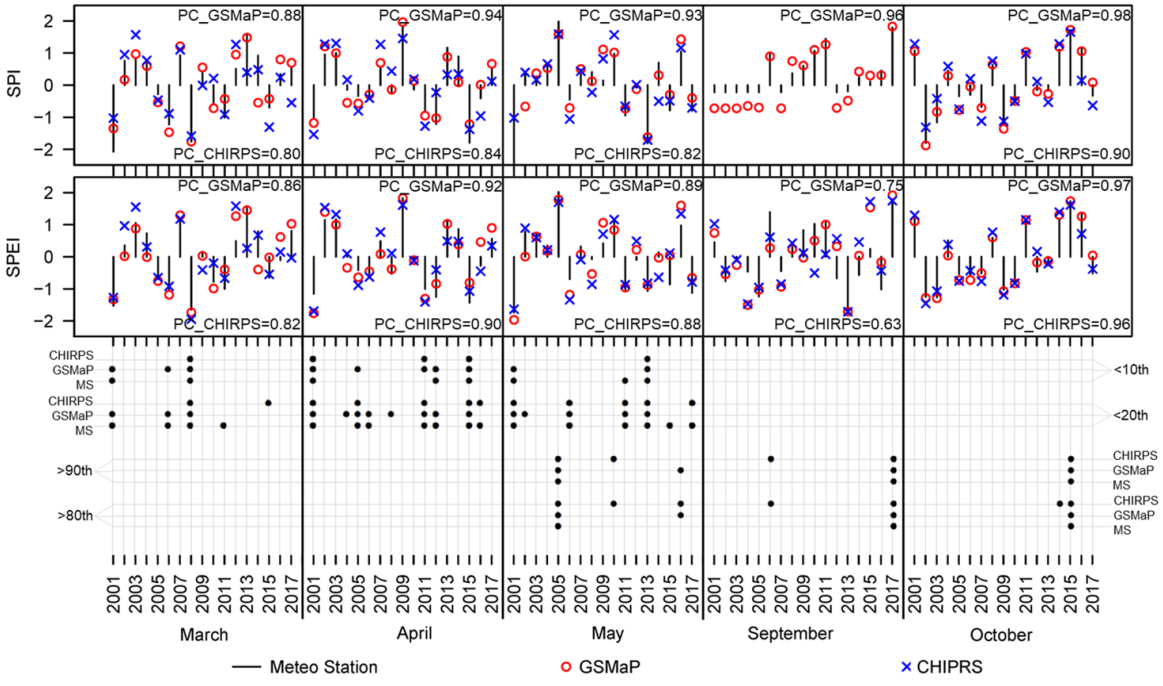

Figure 2.9: Monthly values of Standardized Precipitation Index (SPI), Standardized Precipitation-Evapotranspiration Index (SPEI) and detected anomalies at 10th and 20th (March, April and May) percentiles for drought and 80th and 90th (May, September, October) percentiles for flood by stations, GSMaP and CHIRPS at the Djizzakh station

Note: CHIRPS-SPI for September was not calculated due to a lack of measurements in this month

Source: compiled by the authors.

In addition, Figure 2.9, Table A.1.11.3 and Table A.1.11.4 illustrate the capacity of GSMaP and CHIRPS to detect precipitation anomalies at <10th and <20th (March, April and May) percentiles for droughts as well as >80th and >90th (May, September, October) percentiles for floods. The results show that in the vast majority cases, SPEs detected the anomalies correctly, but there are minor false alarms and gaps that exist in both products. The capacity of SPEs to detect drought is slightly better than flood detection. In both types of extreme events and temporal aggregations, the GSMaP showed slightly better performance than CHIRPS, which is clearly evident from Figure 2.9 and Table 2.6. Regarding the accuracy of the applied temporal scales, we obtained ambiguous results since the classification accuracy varies across months and percentiles.

Overall, both satellite-based MDIs and detected anomalies align with the station-based estimates, and have the potential to some extent to detect the drought and flood events in focused periods. However, MDIs provide a more clear picture of drought and flood events with its strength, which is not possible with an anomaly detection approach based on percentiles. It was reported that drought events during the critical period of rainfed crop growth in 2001 and 2008 had a significant effect on crop production and the socio-economy of the region (Bobojonov and Aw-Hassan, 2014). These drought events were also precisely detected by both station and satellite-based MDIs, as well as anomaly detection. GSMAP itself, and in combination with GLDAS as MDIs, performed slightly better than CHIRPS in detecting these events. According to Figure 2.9, in 2001, drought was moderate in March and followed by more severe drought in April and May, while in 2008 severe drought in March was followed by mild drought in April and May. Also, we can see some months with drought in other years, but these drought events were not prolonged that mitigate the effect of them, which are not reported as extreme drought years in any publications.

2.6. Discussion and conclusion

The main aim of the study was to investigate the suitability of freely available satellite temperature and precipitation data for designing and implementing an index insurance in Central Asia by analyzing the satellites products' accuracy and ability to detect droughts or floods using MDIs. For this assessment, the study used weather data acquired from six stations located in arid and semi-arid agro-climatic zones between 2000 and 2017. An accuracy analysis was conducted for those locations in pixel scale. Fourteen classification, quantitative and agreement statistical metrics were used to evaluate the accuracy and applicability of the satellite products in decadal and monthly time-series as well as on a per-decade and per-month scale. Additionally, we investigated the ability of these satellite-based weather products to detect drought and flood using SPI and SPEI.

Our assessments of decadal and monthly precipitation data by GSMaP indicate a better accuracy for the selected locations than CHIRPS can offer. Additionally, GSMaP spatially covers the full region of

Central Asia. Nevertheless, we found a number of limitations, such as underestimation of precipitation during wet/rainy seasons and overestimation in the dry season, which have also been investigated by Trinh-Tuan et al. (2019) in Vietnam, Reddy et al. (2019) in India and Fatkhuroyan & TrinahWati (2018) in Indonesia. Additionally, we observed a slight overestimation of precipitation events by GSMaP, caused by minor GSMaP precipitation records during the summer period that do not exist in station observations. Moreover, we found that GSMaP performs better SPE during wet/rainy seasons compared to the dry season, which is in line with Hu et al. (2013), Fu et al. (2011) and Thiemig et al. (2012). Nevertheless, in the region observed by us, GSMaP performs better measurements in the dry season compared to CHIRPS. A novel quantile regression analysis checking the relationship between SPE products and in-situ weather data in various tiles confirms that both SPE products overestimate precipitation during low precipitation periods and underestimate it during high precipitation periods. GLDAS was in significant agreement with in-situ temperature data in both time series and per period scale in all locations. Similar to GSMaP and CHIRPS, we found lower accuracy results during the dry season for GLDAS temperature estimates, which have also been investigated by Wang et al. (2016) in China. Lower quantitative and agreement accuracy metrics for Tmax and Tmin by GLDAS during the summer season can be explained by a low diversity of average decadal and monthly Tmax and Tmin in the summer season. Overall, all three satellite products have shown slightly better accuracy in measuring weather parameters in the semi-arid zones than in the arid zones. Additionally, we observed similar accuracy and performance for each climatic zone despite the fact that not all studied stations were used during the development of selected satellite-based weather products.

After calculating various classifications, quantitative and agreement statistical metrics to test the accuracy of satellite-based weather data, we found this combination of metrics to be useful and worth testing. Some of them, however, we found more useful than others and sufficient to assess the accuracy of satellite-based weather data: these are BIAS, POD and FAR for classification metrics; MBE and RMSE for quantitative metrics; SC, PC and d for agreement metrics. This combination of metrics allows an assessment of the accuracy of event classification, bias and variation between station and satellite-based weather data. In addition, for the first time, we could show the potential of using QR to access the accuracy of satellite-based weather data: By applying QR we were able to observe the relationship between station and satellite-based weather data among various quantiles, which cannot be achieved by using OLS.

Over- and underestimations of SPEs observed from accuracy and QR analyses are likely to lead to missing triggers. Consequently, it introduces basis risk, which is when the developed index estimations do not match with actual losses of insured farmers. However, these limitations might be mitigated or eliminated by the application of bias correction methods. As Yeh et al. (2020) for GSMaP particularly and Kimani et al. (2018) for CHIRPS demonstrated, significant improvements of SPE measures can be obtained after the application of bias correction methods.

In general, the years with extreme events reported by publications and detected by satellite products are matching, where the frequency is around once in eight years. As long as moderate frequency of risk serves to lower prices and premiums, making it affordable for farmers (Hazell et al.,

2010), it may ease introducing index insurance in the region. Despite some limitations, GSMaP itself, and in a combination with GLDAS as MDIs and anomaly detection, performed better than CHIRPS not only in detecting drought but also in detecting floods during the vegetation period of rainfed and irrigated crops. Consequently, GSMaP data should increasingly be taken into account for index generation in Central Asia. Moreover, the obtained results demonstrate the potential of satellite-based weather data for designing and implementing index insurances focused on drought during the vegetation period of rainfed crops (March-May), on floods during the seeding of irrigated crops (May) and on floods during the harvesting of irrigated crops (September-October). Drought events from March-May (the critical period for rainfed vegetation), for instance, have a significant influence on wheat, barley and potato yields and quality. Extended wet spells in May (the beginning of the cotton vegetation period) hit and damage the cottonseeds, significantly affecting cotton yields and requiring re-seeding, which means additional technical efforts and expenses are needed. Floods during the cotton harvesting period significantly decrease the quality of the harvested cotton, which affects the price paid by buyers.

Accuracy comparisons between decadal, monthly and seasonal precipitation measurements by GSMaP and CHIRPS show that the agreement among stations and SPE improved as higher aggregation was applied. This finding shows the reasonability of using precipitation measurements in larger time intervals for better accuracy. Overall, globally available climate data could serve as a good source for establishing index insurance products in Central Asia; however, a careful selection of source and index is required.

Our study is limited to stations located in the arid and semi-arid climatic zones of Uzbekistan. It would be interesting to also investigate the accuracy of these and other satellite-based weather data at stations located in similar and other climatic zones of neighboring countries. Nevertheless, the vast majority of Central Asian countries are located in arid and semi-arid zones (Bobojonov et al., 2016). Moreover, there are limitations regarding crop quality, re-seeding and yield data. For that reason, we think it would also prove interesting to investigate the relationship between SPE/MDIs and various crop quality, re-seeding and yield data in the region.

3. The role of crop classification in detecting wheat yield variation for index-based agricultural insurance in arid and semiarid environments[6]

3.1. Introduction

Over the past two decades, the frequency of weather extremes such as floods and droughts has increased (WMO, 2021). Variable and unpredictable weather significantly limits agriculture and agricultural development (Niles et al., 2015; Rao, 2011), since farmers avoid investments when there is a high risk of weather shocks and yield losses (Benami et al., 2021). Moreover, uninsured production risk also limits access to agricultural credits for producers, substantially hindering agricultural and rural development (Hellmuth et al., 2009). Moreover, these limitations may threaten global food security, in particular in societies where wheat is the main staple (FAO, 2015). Wheat (Triticum spp.) is one of the most important and strategic food crops for the majority of the world's countries and populations, being the staple food of about 35% of the world's population and accounting for 20% of the food calories consumed globally (Breiman and Graur, 1995).

Being the main source of wheat yield reduction and climatic variability (Ray et al., 2015), rising climate risk creates need for new risk management and risk coping strategies in agriculture (FAO, 2015; Hellmuth et al., 2009; IPCC, 2022). One financial tool is agricultural insurance, which is intended to transfer agricultural production risks from farmers to insurance companies (Bobojonov et al., 2019; Giné et al., 2010). However, in developing countries, the hedging effectiveness of conventional agricultural insurance (also known as 'named-peril' and 'multi-peril' crop insurance) is challenged by high premiums, moral hazards and problems of adverse selection (Coleman et al., 2018). To overcome some of these challenges, index-based agricultural insurance (henceforth "index insurance") has been suggested (Coleman et al., 2018; Dick et al., 2011; World Bank, 2011). In index insurance, payoffs are contingent on the value of a pre-determined index (average yield of a unit, temperature, rainfall, soil moisture, vegetation, etc.), which cannot be manipulated by third parties (Barnett et al., 2008), therefore reducing adverse selection and problems of moral hazard (Miranda and Gonzalez-Vega, 2011). Moreover, index insurance does not require a ground verification of the reported crop yield losses, thus significantly lowering administrative costs (Benami et al., 2021).

The main challenge of index design is to achieve sufficient correlation between crop yields and the selected index (Norton et al., 2015). Previously, the most common and widely used form of index insurance was weather index insurance (WII). Meteorological station-based WIIs have been the subject of numerous feasibility and efficiency analysis (Bobojonov et al., 2014; Bokusheva and Breustedt, 2012; Conradt et al., 2015; Kath et al., 2019). While being a promising data source in high-income countries, meteorological stations are rarely available in developing countries (Barnett and Mahul, 2007). In Central Asia (CA) specifically, Eltazarov et al. (2021) demonstrate the low insufficiency of meteorological stations for designing index insurance, with sparsely distributed weather

[6] This chapter was published as the following open-access article: Eltazarov, S., Bobojonov, I., Kuhn, L., Glauben, T. (2023): The role of crop classification in detecting wheat yield variation for index-based agricultural insurance in arid and semiarid environments. Environmental and Sustainability Indicators, 18, 100250. https://doi.org/10.1016/j.indic.2023.100250; This chapter benefitted from the comments by the anonymous referees of Environmental and Sustainability Indicators

stations often failing at capturing wide spatial crop losses and contributing to geographical basis risk (Makaudze and Miranda, 2010). Thus, weather data from meteorological stations rarely correlates with crop yields due to high basis risk (Smith and Watts, 2009). The cost of installation and maintenance of new weather stations every 10-20 km, as suggested for instance by Hazell et al. (2010), would significantly increase the prices of the insurance products. Finally, new weather stations cannot provide historical weather records, which is necessary for index design (Norton et al., 2012).

To overcome these data limitations, scholars have proposed and tested the applicability of satellite-based weather products, especially precipitation data, for index insurance development and implementation (Coleman et al., 2018; Osgood et al., 2018; Tarnavsky et al., 2018). Satellite products are provided in near-real time and available free of charge for most locations worldwide (CHC, 2015; Didan, 2015). Numerous studies have investigated the potential and applicability of satellite-based precipitation products for WII design and implementation in developing and emerging economies (Black et al., 2016a; Brahm et al., 2019; Collier et al., 2009; M Enenkel et al., 2018; Osgood et al., 2018; Tarnavsky et al., 2018). While WII is only valid for rainfed farming systems, satellite-based land surface information, in particular the Normalized Difference Vegetation Index (NDVI), Enhanced Vegetation Index (EVI), Land Surface Temperature (LST), Actual Evapotranspiration (ETa) and Soil Moisture Index (SMI), have found to be more potential for crop loss detection and index insurance design (Coleman et al., 2018; Kölle et al., 2020; Vroege et al., 2021). Even though the sensitivity of vegetation indices significantly decreases at moderate-to-high densities of crop aboveground biomass (Li et al., 2014, 2010; Mistele and Schmidhalter, 2008), they are in fact rather suitable for insurance products that primarily focus on detecting low biomass density.

So far, only a limited number of satellite-based products such as NDVI, LST and precipitation have been tested for application in index insurance design during the last two decades in majority of continents (Benami et al., 2021; Kölle et al., 2020). The most popular index is NDVI, which was first proposed by Vicente-Serrano et al. (2006). Later, Makaudze & Miranda (2010) investigated the applicability of an NOAA Advanced Very High Resolution Radiometer (NOAA AVHRR) based on an NDVI to design index insurance using 1980-2001 rainfed maize and cotton yield data from Zimbabwe. They found that the NDVI index has higher correlation with crop yields and greater potential to protect smallholder farmers than the rainfall index.

Later research however pointed out several practical challenges: Turvey & McLaurin (2012) investigated the applicability of NOAA AVHRR for designing index insurance in the US by using yield data for rainfed corn and soybeans. Since their results were highly variable in terms of the relationship between NDVI and crop yields, they advise caution concerning the applicability and scalability of the NDVI without site-specific calibration.

The first weakness is the resolution of weather information: Bokusheva et al. (2016) examined the effectiveness of an NOAA AVHRR-based Vegetation Condition Index (VCI) (NDVI-based calculation) and Temperature Condition Index (TCI) (brightness-temperature-based calculation) to insure rainfed wheat yield losses of farmers in five counties in Kazakhstan. They conclude that finer spatial

resolution would improve the effectiveness of the insurance products as well as the significant relationship between Vegetation Heath Indices (VHI) and county-level rainfed wheat yields has the potential to substantially improve risk-sharing options. Bobojonov et al. (2014) analyzed medium-resolution satellite information (Moderate Resolution Imaging Spectroradiometer (MODIS) based on an NDVI) by comparing farm-scale rainfed wheat yield data in Syria, concluding that also an NDVI based on medium-resolution data has sufficient potential to detect yield losses and calculate insurance pay-outs.

Second, Valverde-Arias et al. (2020, 2018) urge taking the variability of agro-ecological zones into account while designing index insurance. They applied a MODIS-based NDVI, finding that rice phenology and the relationship between NDVI and rice yields significantly differs through agro-ecological zones. Using barley, wheat, sorghum and barley yield data as reported by 34 farmers, Eze et al. (2020) compared the feasibility of a MODIS-based NDVI and satellite-based precipitation products for designing index insurance in Ethiopia. Based on their findings, they contend the use of an NDVI based on area-specific crop insurance indices rather than weather parameters that are currently in use in their study area.

Thirds, as demonstrated by Turvey and McLaurin (2012), these well-known indices may yet fail to detect variation in crop yields in all environments. Therefore, there remains fundamental need for exploring additional satellite-based indices and develop specifications increasing their performance (Hazell et al., 2010; Hellmuth et al., 2009). Other, less prominent indices have not yet been taken into consideration for index insurance applications. Until just recently, a small number of studies investigated into the potential of EVI and LAI for index insurance (Báez-González et al., 2002; Cheng, 2006; Doraiswamy et al., 2002; Li et al., 2011; Wang and Lin, 2005). Dou et al. (2020), Shirsath et al. (2020) and Van Khanh Triet et al. (2018) suggest an EVI as a potential source of satellite data for the crop insurance industry. GCI has not been explored yet at all. Kölle et al. (2020) analyzed the efficiency of a MODIS-based VCI (EVI-based calculation), a TCI (land surface temperature-based calculation) and a VHI that included weather (temperature and precipitation) parameters for improving the hedging of yield risk for rainfed olives trees in Spain. They found that the VCI- and VHI-based index insurance contracts outperform index insurance contracts based on precipitation and temperature, and can serve as a potential source for index insurance development. Setiyono et al. (2018) propose a MODIS-based LAI as a possible source of data for area-yield index insurance for rainfed rice in Vietnam. Later on, Raksapatcharawong et al. (2020) suggest using a MODIS-based LAI in combination with other remote sensing and field data for index insurance design for rainfed rice in Thailand.

Finally, higher accuracy may also be reached by combining indices: Hochrainer-Stigler et al. (2014) conducted a case study with teff yield data in Ethiopia and suggest a solution of an NDVI (same source as above) integrated with land surface temperature data as a Vegetation Health Index (VHI), concluding that VHI allows for trigger points to be identified and premiums to be calculated. Moreover, one of the main requirements is that site-specific calibration of the satellite-based data to index-based insurance product design and the variability of agro-ecological zones should be taken

into account when designing index insurance (Turvey and McLaurin, 2012; Valverde-Arias et al., 2020, 2018).

Based on this literature overview, following research gaps are identified: Many wheat producing regions worldwide are not purely rainfed, but at least partially irrigated or fully irrigated. According to Wang et al. (2021), around 35% of global wheat is produced in irrigated areas. Nevertheless, in practice, these regions also suffer from high variation in water availability, as surface water used for irrigation also reacts to variability in weather conditions. As can be seen in this summary, so far there are no studies focused on testing the applicability of the satellite data sources for index insurance development for wheat producers in irrigated and mixed lands. Additionally, in all of the above-mentioned studies, the satellite data samplings are determined by administrative regions, which omits the effects of crop rotation, diversity, allocation and land cover/use change on regional index values. Meanwhile, in areas with strong spatial heterogeneities in land use/cover, estimating regional index value based on all pixels from all land cover/use types within administrative boundaries may not have good power for detection of crop yield variation and index insurance design. All in all, this literature review shows a need for a comprehensive and comparative analyses of the applicability of various satellite-based data to index insurance among various farming types and land cover/use classifications.

The study thus provides several key contributions to the literature: Firstly, to the best of the authors' knowledge, this study is the first to study the effect of using land cover classification (e.g. croplands and wheat cultivated lands, hereafter cropland and wheatland masks) in addition to administrative boundaries for index insurance design. Second, the applicability of MODIS-based vegetation indices, such as an EVI, GCI and LAI, as well as a well-known NDVI and LST (all five indices will from here on be referred to as "vegetation index" for convenience) are compared for index insurance development in rainfed, irrigated and mixed lands. To test the robustness of the findings across climatic zones, the sample includes districts across Central Asia and Mongolia. In these countries, frequent climate shocks in the past years have created particular need for financial instruments for risk sharing (Bobojonov et al., 2019).

For this analysis, district level wheat yield data is used; this choice may admittedly lead to aggregation biases that likely cause farm-level risk underestimation. Nevertheless, the presented findings are valid for district scale index insurance and area-yield insurance programs in the region.

3.2. Methods and materials

3.2.1. Study area and wheat yield data

Central Asia was selected as case region for following reasons: For once, here the effect of climate change is above the global average (de Beurs et al., 2018; Haag et al., 2019). For instance, drought events during 2000-2001 and 2007-2008 had a great effect on crop production and the socio-economy of Central Asia (Bobojonov et al., 2014; Patrick, 2017). In 2000-2001, the loss of agricultural production was evaluated at $800 million USD for the whole region and contributed to a loss of 80%

of rural households' incomes. The consequences of this were increased poverty rates and a negative impact on food security and public health (Patrick, 2017; World Bank, 2005) as well as a decline in grassland productivity and a loss of lakes, resulting in a huge migration of herders to the capital city and adverse effects on food security in Mongolia (Densambuu et al., 2015; Hessl et al., 2018).

This study covers wheat growing regions in Kazakhstan (KAZ), Kyrgyzstan (KYR), Mongolia (MON) and Uzbekistan (UZB) (Figure 3.1), where wheat is one of the most strategic crops. It is grown on irrigated land in the vast majority of Uzbekistan (Khalikulov et al., 2016) and mostly on rainfed lands in Kazakhstan and Mongolia (Fehér et al., 2017; Tuvdendorj et al., 2019), and mixed lands in Kyrgyzstan (ADB, 2013). The heterogeneity of farming systems (e.g., irrigated, rainfed, mixed), frequent weather events and high variability among harvests in this region provide a unique environment for comparing the suitability of indices across farming systems, which has not yet been tackled within the international literature yet. Three provinces from Kazakhstan were selected, particularly Akmola (Akm), Kostanay (Kos) and the North Kazakhstan (N. Kaz) provinces (oblasts), which together account for around 70% of wheat production in the country (Fehér et al., 2017). For Kyrgyzstan, the province Chuy covers the vast majority of national cropland (Dzunusova et al., 2008). The Mongolian provinces of Bulgan (Bul), Darhan Uul (Dar), Dornod (Dor), Huvsgul (Huv), Selenge (Sel) and Tuv are main steady cultivation regions of spring wheat (FAO, 2020). The Uzbek provinces of Djizzakh (Djiz), Kashakadarya (Kash), Khorezm (Khor) and Navai (Nav) were chosen as this combination of provinces covers all three varieties of farming systems that exist in the country. Overall, the analysis used annual district-level spring wheat yield data for 50 districts in Kazakhstan, and winter wheat yield data for 8 districts in Kyrgyzstan, spring wheat yield data for 43 districts in Mongolia and 41 districts in Uzbekistan. Figure A.2.1.1 exhibits the location of croplands in the study area and in vast majority of lands wheat is being cultivated continuously or in rotation with other crops (USDA, 2022). Figure 3.2 presents the cropping calendars for wheat in the three countries. While cropping calendars may locally vary by a few days according to local weather conditions and farm management strategies, unbiased results over the whole sample can be expected due to the large numbers of observations.

All wheat yield data was obtained from local state statistical organizations and is reported in tons per hectare (ton/ha). Wheat yield data was obtained for the years 2000–2015 in Kazakhstan, for 2007–2017 in Kyrgyzstan, for 2000–2018 in Mongolia, and for 2007–2017 in Uzbekistan. The data was checked for outliers by using a Grubbs's test (Grubbs, 1950)[7]. In total 2,060 yield observations from 152 districts across Central Asia and Mongolia were employed. The average record length is 15.9 years for Kazakhstan, 11 years for Kyrgyzstan, 17.7 years for Mongolia and 10.2 years for Uzbekistan. Descriptive statistics of wheat yield data can be found in Table A.2.1.2.

[7] Initially, 2,063 yield observations were obtained. After checking for outliers using a Grubbs's test (Grubbs, 1950) only three outliers (p-values = 0.0035, 0.0196, 0.025) were detected and eliminated from the Mongolian dataset.

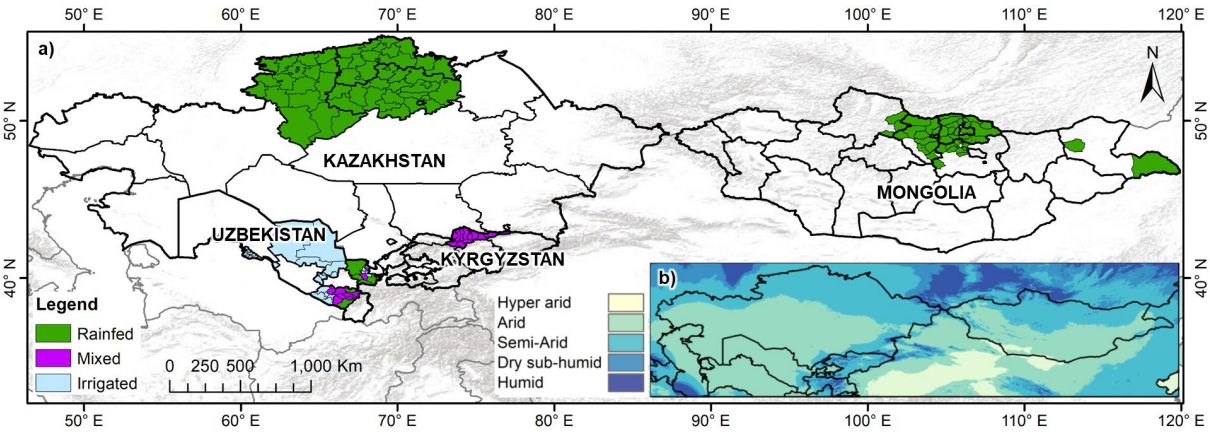

Figure 3.1: Locations of the study regions and farming systems (a) and climate classes (b)

Source: Authors' presentation based on data from Trabucco and Zomer (2019).

Retrieved from the published open-access article: Eltazarov, S., Bobojonov, I., Kuhn, L., Glauben, T. (2023): The role of crop classification in detecting wheat yield variation for index-based agricultural insurance in arid and semiarid environments. Environmental and Sustainability Indicators, 18, 100250.

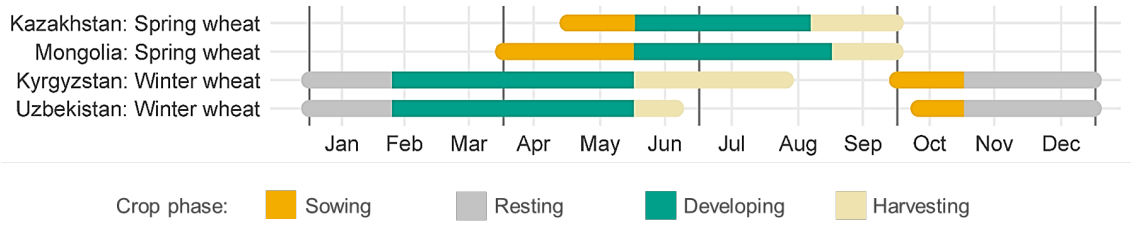

Figure 3.2: The cropping calendar of spring wheat in Kazakhstan and Mongolia and winter wheat in Uzbekistan and Kyrgyzstan

Source: Authors' illustration based on data adapted from Conrad et al. (2014), the FAO (2021, 2020) and Shamanin et al. (2016)

Retrieved from the published open-access article: Eltazarov, S., Bobojonov, I., Kuhn, L., Glauben, T. (2023): The role of crop classification in detecting wheat yield variation for index-based agricultural insurance in arid and semiarid environments. Environmental and Sustainability Indicators, 18, 100250.

3.2.2. Satellite data

This study employs data produced by a Moderate Resolution Imaging Spectroradiometer (MODIS), which is an instrument that's been installed in the board of the Terra and Aqua satellites since the 2000s for observing the earth's surface and making images on a daily basis. For the analyses, Normalized Difference Vegetation Index (NDVI) and Enhanced Vegetation Index (EVI) layers from a MOD13Q1 V6 product were used. Both vegetation indices have a 250 meter spatial resolution with a composite of 16 days (Didan, 2015). Moreover, the Leaf Area Index (LAI) product has a 500 meter spatial resolution with a 4-day composite dataset from MCD15A3H V6 (Myneni et al., 2015), while

the Land Surface Temperature (LST)[8] product from the MOD11A2 V6 dataset has a pixel size of 1 kilometer and 8-day averaged images (Wan et al., 2015). Additionally, the analysis employs the Green Chlorophyll Index (GCI), which was calculated according to Gitelson et al. (2005) who employed an NIR and GREEN bands. The underlying data was obtained from the MOD09A1 V6, which provides 500 meter resolution with an 8-day composite (Vermote, 2015). Temporal and spatial revolution as well as historical range of data availability is listed in Table 3.1.

Table 3.1: Summary of MODIS based land surface metrics

Metric	Equation	Available since	Temporal resolution	Spatial resolution	Data reference	Data
NDVI	(NIR-RED)/(NIR + Red)	2000	16 days	250 meters	Didan (2015)	MOD13Q1 V6
EVI	2.5×(NIR-RED)/(NIR+6×RED-7.5×BLUE+1)	2000	16 days	500 meters	Didan (2015)	MOD13Q1 V6
GCI	NIR/GREEN - 1	2000	8 days	500 meters	Vermote (2015)	MOD09A1 V6
LST (Day)	See reference for algorithm	2002	8 days	1,000 meters	Wan et al. (2015)	MOD11A2 V6
LAI	See reference for algorithm	2002	4 days	500 meters	Myneni et al. (2015)	MCD15A3H V6
LCU	See reference for algorithm	2001	1 year	500 meters	Friedl & Sulla-Menashe (2019)	MCD12Q1 V6

Source: compiled by the authors.

Retrieved from the published open-access article: Eltazarov, S., Bobojonov, I., Kuhn, L., Glauben, T. (2023): The role of crop classification in detecting wheat yield variation for index-based agricultural insurance in arid and semiarid environments. Environmental and Sustainability Indicators, 18, 100250.

3.2.3. Spatial scales of index value extraction

The index values for each study site were extracted in three spatial scales: 1) the entire area of the districts, 2) cropland and 3) wheatland. The area of croplands was obtained from an open access yearly Land Cover and Use (LCU) product. The location of the wheatlands in each district were identified by us based on cropping calendars and wheat phenology (Edlinger et al., 2012; Hao et al., 2016; Zhang et al., 2011); details of the cropland and wheatland masks are provided in the following sections.

3.2.3.1. Cropland classification

The croplands were masked using the land cover and -use product MODIS-MCD12Q1 V6, which provides yearly information on global land cover types since 2001 (Friedl and Sulla-Menashe, 2019). For this study, the cropland mask used is a merge of all-time series croplands generated by MCD12Q1-V6 during 2001-2019. Specifically, the "Annual International Geosphere-Biosphere Programme (IGBP) classification" sub-model was employed. In order to capture all possible croplands in the selected areas, layers 12 and 14, as well as all years since 2001 until 2019 were combined in order to produce a single mask for croplands. The used cropland mask from the MCD12Q1-V6 (500 meter

[8] Following Zhang et al. (2022), daytime LST were employed. Also according to Chen et al. (2019) daytime temperature has greater and consistent effect on wheat yield.

pixel size) product has an overall accuracy of approximately 75-80 percent (Friedl and Sulla-Menashe, 2019).

There are some alternative land cover/use products like the European Space Agency based World-Cover (Zanaga et al., 2021) and the Copernicus Global Land Service (Buchhorn et al., 2020). However, these products only provide data for the most recent years, which makes them unsuitable for this study. In the end, MOD13Q1-V6 based on NDVI images was chosen for wheatland classifications due to their large spatial coverage and the shortage of continuous cloudless images for the long-time period in Landsat images.

3.2.3.2. Wheat classification

Following the Knowledge-Based Detection method suggested by Edlinger et al. (2012), the data on wheat areas for each year and district were classified and extracted based on the cropping calendar (Figure 3.2) and the phenology of spring wheat in Kazakhstan and Mongolia, and winter wheat in Kyrgyzstan and Uzbekistan. Additionally, croplands mask from MCD12Q1-V6 product, high resolution images from Google Earth and ground truth data (38 locations) from the Bukhara province (Uzbekistan) were employed to clarify the wheatland classification parameters. For phenology detection, the MOD13Q1 V6-based NDVI was employed. For avoiding to mistakenly classifying grasslands, which have similar phenology with winter wheat, as winter wheat in Kyrgyzstan and Uzbekistan's hilly and mountainous areas, a surface slope map was calculated based on The Shuttle Radar Topography Mission (SRTM) digital elevation dataset (Jarvis et al., 2008). The 90-meter spatial resolution of SRTM dataset was considered sufficient for this study, as the spatial resolution of the tested vegetation indices varies from 250 to 1000 meters.

Equations 1-3 classify and mask the wheat cultivated lands from selected vegetation indices:

$$\text{Spring wheat lands in Kazakhstan} = (NDVI_{81\text{-}96} < 0.1) \text{ AND } ((NDVI_{193\text{-}208} > 0.35) \text{ OR } (NDVI_{209\text{-}224} > 0.35)) \text{ AND } (NDVI_{273\text{-}288} < 0.30) \quad (3.1)$$

$$\text{Spring wheat lands in Mongolia} = (NDVI_{97} < 0.25) \text{ AND } (NDVI_{129} < 0.25) \text{ AND } ((NDVI_{209} > 0.35) \text{ OR } (NDVI_{225} > 0.35)) \text{ AND } (NDVI_{289\text{-}305} < 0.35) \text{ AND } (SLOPE < 5) \quad (3.2)$$

$$\text{Winter wheat lands in Kyrgyzstan and Uzbekistan} = (NDVI_{17\text{-}32} < 0.1) \text{ AND } (NDVI_{97\text{-}128} > 0.40) \text{ AND } ((NDVI_{161\text{-}176} < 0.30) \text{ OR } (NDVI_{177\text{-}193} < 0.30)) \text{ AND } (SLOPE < 4) \quad (3.3)$$

where SLOPE is the inclination of land surface of measured in degrees and NDVI are the NDVI values within the indicated time period during which wheat has a specific phonological pattern. This definition was developed based on the respective region's cropping calendar as presented in Figure 3.2 and NDVI-based phenology dynamics of winter and spring wheat. Based on these specific phenology dynamics at specified times, it is possible to precisely distinguish spring or winter crop lands from other crops.

A similar classification method showed approximately 90 percent accuracy using Landsat images that have 30 meter spatial resolution (Edlinger et al., 2012). Conrad et al. (2011) obtained 75-96

percent accuracy for wheatland classification using the same MODIS images. The wheatland classification accuracy for this study was tested for a subsample in Bukhara province (Uzbekistan) based on ground truth data from 2019, reaching accuracy levels of 79 percent accuracy, which is within the range of above studies' accuracy.

3.2.4. Satellite data processing and acquisition platform

One of the main disadvantages of using satellite products in index insurance is the fact that the acquisition and processing of satellite products requires special technical skills. Therefore, a user-friendly web platform was established that allows users free convenient access to satellite products. For accessing above-mentioned MODIS-based products, a unique automatic web platform using the Google Earth Engine (GEE) was developed for this project (Gorelick et al., 2017). This Satellite Data Extractor can be accessed under the following link: https://www.klimalez.org/satellite-indices. All of the satellite-based data processing and extractions within this study are based on the GEE platform.

3.2.5. Correlation and regression of wheat yields with vegetation indices

One of the key requirements for applying satellite-based products for the development of agricultural index insurance is that the index should be highly correlated with crop yields (Barnett and Mahul, 2007; Siebert, 2016) in order to increase the hedging efficiency of the resulting insurance product (Breustedt et al., 2008; Kölle et al., 2021; Norton et al., 2012). In order to check the applicability and potential of the selected vegetation indices, correlation and regression analyses between wheat yield data and satellite-based indices are performed. Borrowing from Turvey and McLaurin (2012), the mean and maximum values of indices during the vegetation period are the best predictors of crop yields and the most widely used temporal aggregation method in the index insurance industry. Adapted from Markus Enenkel et al. (2018); Kogan et al. (2018) and Wang et al. (2014), time series Pearson's correlation analyses between wheat yields and each periodical record of the indices for each district were conducted. Pearson's correlation is a suitable measure for linear relationship between continuous data (vegetation indices and wheat yield data), whereas Spearman's correlation is rather used for monotonic relationships between ordinal variables. Along Pearson's correlation, the time periods with the strongest correlation between index and wheat yield data were chosen as the timespan for the mean value calculation for each index and country (Panek and Gozdowski, 2020). In cases of max index value calculation, the entire vegetation period of wheat in the respective country was used, which was 1-274 days for Kazakhstan; 1-290 days for Mongolia; 1-220 days for Kyrgyzstan; and 1-162 days for Uzbekistan. In the following, the max and mean temporal aggregations were calculated, and correlation analyses between them and wheat yields conducted.

In order to investigate the potential of the selected satellite data sources for modelling the wheat yields, linear regression analyses were applied, using the index values within the period that was

identified to exhibit the strongest correlation with wheat yields. Despite the availability of time series, panel data analysis was not an option, as this approach would assume the same marginal response to indices in every district (Turvey and McLaurin, 2012), whereas this study sought to understand how marginal effects differ by districts and the overall ability of the variables to model the actual wheat yields.

The detailed estimation model is adapted from Kogan et al. (2018) in terms of indices and the strongest correlated time periods (critical stages of crop growth). The application of a similar model was suggested for index insurance development by Xu et al. (2008), which employed time series precipitation and temperature data.

$$dY = \beta_0 + \beta_1 VI_1 + \beta_2 VI_2 + \beta_3 VI_3 + \ldots + e \quad (3.4)$$

where dY is the district-scale wheat yield data, VI is the value of the respective vegetation index in the period that has high correlation between yield and indices. β_0 is a constant, e the error term. This method has been applied for all selected indices and mask types.

Additionally, the Wilcoxon test (Bauer, 1972) was performed to compare the group of correlation coefficients and to check for improvements in the significance of the relationship between indices and wheat yields after the application of land cover and use masks.

3.2.6. Wheat yield loss detection

To evaluate the ability of the indices to capture the wheat yield losses among various correlation coefficients, two categorical metrics were applied, namely Probability of Detection (POD) and False Alarm Ration (FAR). POD measures the probability of an index to capture the yield losses, while FAR indicates the probability of falsely detecting yield losses. These metrics were estimated based on the contingency matrix shown in Table 3.2 and the equation of the selected metrics, which are exhibited in Table 3.3.

Table 3.2: Contingency table for comparing indices and crop yields

	Yield ≤ Trigger	**Yield > Trigger**
Index ≤ Trigger	a	b
Index > Trigger	c	d

Source: compiled by the authors.

Retrieved from the published open-access article: Eltazarov, S., Bobojonov, I., Kuhn, L., Glauben, T. (2023): The role of crop classification in detecting wheat yield variation for index-based agricultural insurance in arid and semiarid environments. Environmental and Sustainability Indicators, 18, 100250.

The equation for estimating the trigger value was adapted from Turvey and McLaurin (2012), which is defined as $average\ Yield - (0.25 standard\ deviation)$. Actual yield and modelled yield values

with district masks from all selected indices and locations were used for categorical metric estimations.

Table 3.3: Formulas of categorical metrics

Statistics	Formula	Range	Perfect value
Probability of detection	$POD = \frac{a}{a+c}$	0 to 1	1
False Alarm Ratio	$FAR = \frac{b}{a+b}$	0 to 1	0

Note: Where a=number of hits; b=number of false alarms; and c=number of misses.

Source: compiled by the authors.

Retrieved from the published open-access article: Eltazarov, S., Bobojonov, I., Kuhn, L., Glauben, T. (2023): The role of crop classification in detecting wheat yield variation for index-based agricultural insurance in arid and semiarid environments. Environmental and Sustainability Indicators, 18, 100250.

Based on the trigger equation, the yield loss cases were identified for each study location and index. In the next step, the data were filtered and grouped according to their correlation level with actual yield data. For each grouped dataset, the identified yield loss cases were compared with the POD and FAR matrices. In total 18,848 observations were used for calculations. All statistical calculations and figures for this study were developed using the R project (R Development Core Team, 2018).

3.3. Results

Figure 3.3 indicates the time periods of strongest correlation between vegetation indices and wheat yields (for exact coefficient values see Appendix 2.2). For the majority of indices, no large differences can be observed between district areas, cropland masks and wheatland masks.

As assumed, the periods with the strongest correlation between indices and wheat yields differ among countries. It can be observed that these differences in periods among countries and indices are caused by a variety of climate conditions and are consequently due to different cropping calendars, farming systems and types of wheat (Figure 3.2). At the same time, some similarities between the correlated periods for spring wheat in Kazakhstan and Mongolia can be observed. For all vegetation indices in Kazakhstan and Mongolia, the strongest correlation occurred at the second half of the developing crop phase, which was July and the first half of August. Meanwhile, there are remarkable differences between the correlated periods for Kyrgyzstan and Uzbekistan, even though both of them produce winter wheat. In Kyrgyzstan, the strongest correlation between vegetation indices and winter wheat yields exists for April and May, which are in the second half of the developing crop phase. In terms of Uzbekistan, apart from the vegetation period, the strongest correlation with the wheat yields was during the first half of the developing crop phase, which was the months of February and March. Figure 3.3 and Appendix 2.2 present how there is not a strong relationship between vegetation indices and wheat yields during the sowing and resting period in all

four study countries. Overall, results show that the highest correlation between the vegetation indices and wheat yields are in second half of the development period of crops, except for Uzbekistan, where this is the beginning of the crop's development period.

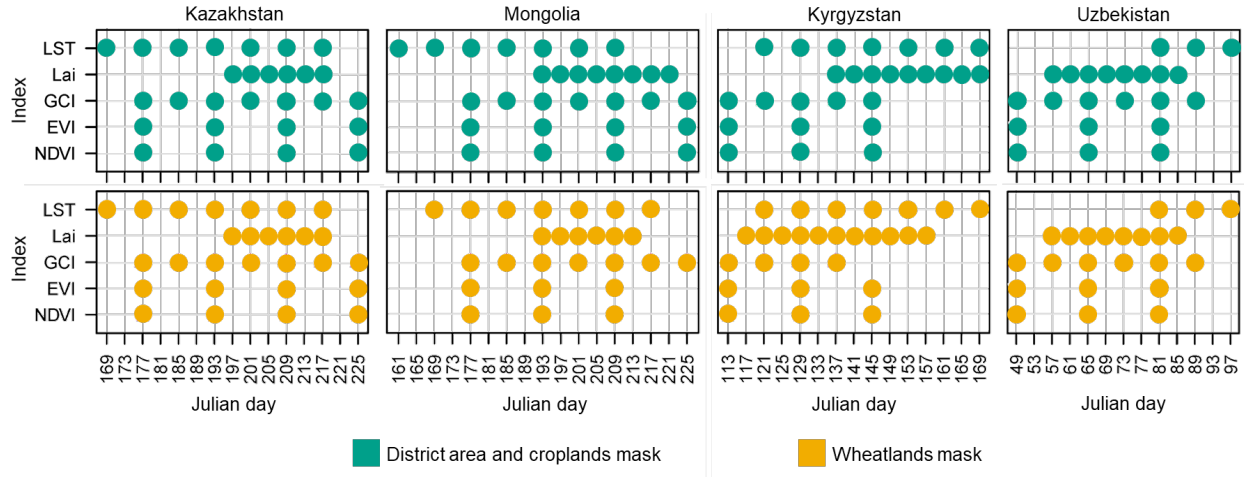

Figure 3.3: Strongest correlated time periods of satellite-based indices with wheat yields

Source: compiled by the authors.

Retrieved from the published open-access article: Eltazarov, S., Bobojonov, I., Kuhn, L., Glauben, T. (2023): The role of crop classification in detecting wheat yield variation for index-based agricultural insurance in arid and semiarid environments. Environmental and Sustainability Indicators, 18, 100250.

Figure 3.4 presents the results of correlation analyses between the mean and max values of the indices with wheat yields for individual districts. The figure demonstrates, which type of mask and index has better relationships in each country and wheat type. The figure also shows the correlation coefficients, which was used to describe the relationship between insurance index and crop yields by Eze et al. (2020). For yield estimation purposes, the positive correlation coefficient represents the ability of an index to detect wheat yield variations with the following categories: 0.0-0.2 is very weak; 0.2-0.4 is weak; 0.4-0.6 is moderate; 0.6-0.8 is strong; and 0.8-1.0 is very strong (Eze et al., 2020). Additionally, Pietola et al. (2011) found that demand for the index insurance remains strong when the correlation between index and yields is greater than 0.6, but it starts to decrease when correlation is lower than 0.5.

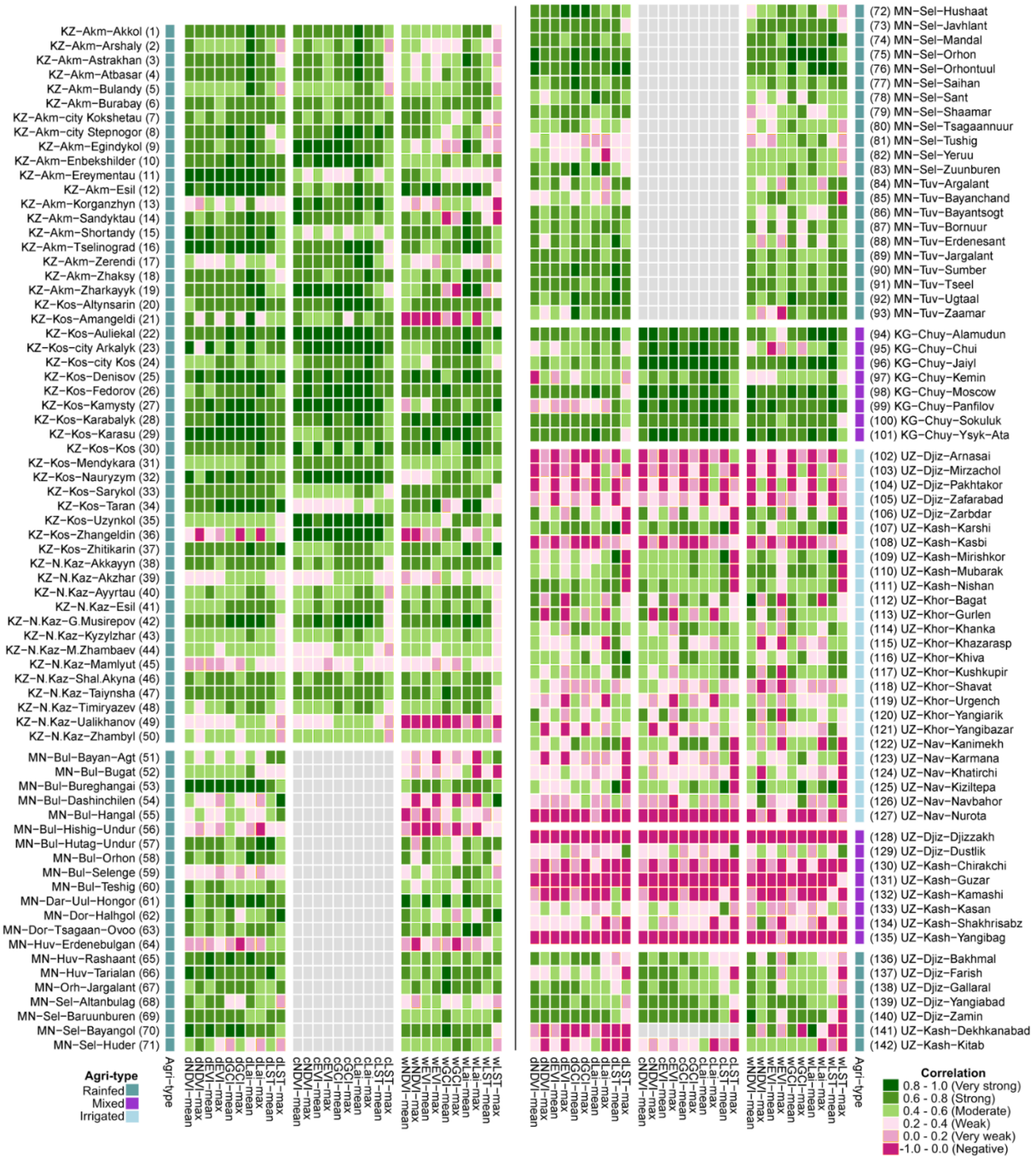

Figure 3.4: Correlation Heatmap between wheat yields and mean/max values of indices for entire district areas, croplands and wheatlands

Source: compiled by the authors.

Retrieved from the published open-access article: Eltazarov, S., Bobojonov, I., Kuhn, L., Glauben, T. (2023): The role of crop classification in detecting wheat yield variation for index-based agricultural insurance in arid and semiarid environments. Environmental and Sustainability Indicators, 18, 100250.

The results show that the strengths of indices capturing the variation in wheat yields differs among countries when various masks were applied. It can be observed that index values from entire district

areas and croplands have similarly strong correlations with wheat yields in Kazakhstan. The Wilcoxon test (Figure A.2.3.1) also showed insignificant differences between the groups of correlation coefficients. Determining which of them result in better performance is complex, as in both masks the indices in most cases are strongly correlated with wheat yields except for a few districts. For the districts under the numbers 13, 17, 21, 36 and 50 (Figure 3.3), masking croplands have improved relationships between vegetation indices and wheat yields and vice versa; the relationship increased when the value from an entire district was used in districts under the numbers 11, 15, 34 and 44. In the case of Mongolia, cropland could not be masked as MODIS-MCD12Q1 does not provide the location of croplands in this area. Moreover, cropland masks do not exist for the district under the number 141 from Uzbekistan. It can be seen that the index values for the entire district areas have higher correlation coefficients than the wheatland mask (Figure A.2.3.2). However, in the case of district numbers 59, 81, 82 and 85 (Figure 3.3), the application of wheatland masks significantly improved the correlation between index values and wheat yields. For Kyrgyzstan, using all three masks showed sufficient correlation coefficients between the vegetation indices and wheat yields. However, the strongest relationship for the vegetation indices was observed when cropland masks were applied, which improved the vast majority of the correlation values from moderate-strong to strong-very strong compared to entire district area and wheatland mask. The statistical significance of the improvement after the application of cropland and wheatland masks was confirmed by a Wilcoxon test (see Figure A.2.3.3). In the case of Uzbekistan, the performance of vegetation indices was ambiguous due to the large proportion of irrigated and mixed farming systems. Vegetation indices were mostly moderately correlated just for over half of districts in irrigated lands, while the relationship between indices and wheat yields were below weak except for a few cases of mixed agricultural lands in Uzbekistan. For rainfed lands, noticeably higher relationships between indices and wheat yields could be observed. Even though this was not proven by the Wilcoxon test, for the case of rainfed agricultural lands, the application of cropland and wheatland masks narrowed the range of correlation coefficients and slightly increased the correlation between indices and wheat yields (see Figure 3.4 and Figure A.2.3.6). In general, index means were found to correlate stronger with wheat yields than max values in the vast majority of districts. While all indices showed the potential to detect wheat yield variation in the majority of the study areas, a slightly higher performance was found for LAI and GCI in Kazakhstan and Mongolia, LAI, GCI and LST in Kyrgyzstan, as well as NDVI and EVI in Uzbekistan (seen in Appendix 2.3).

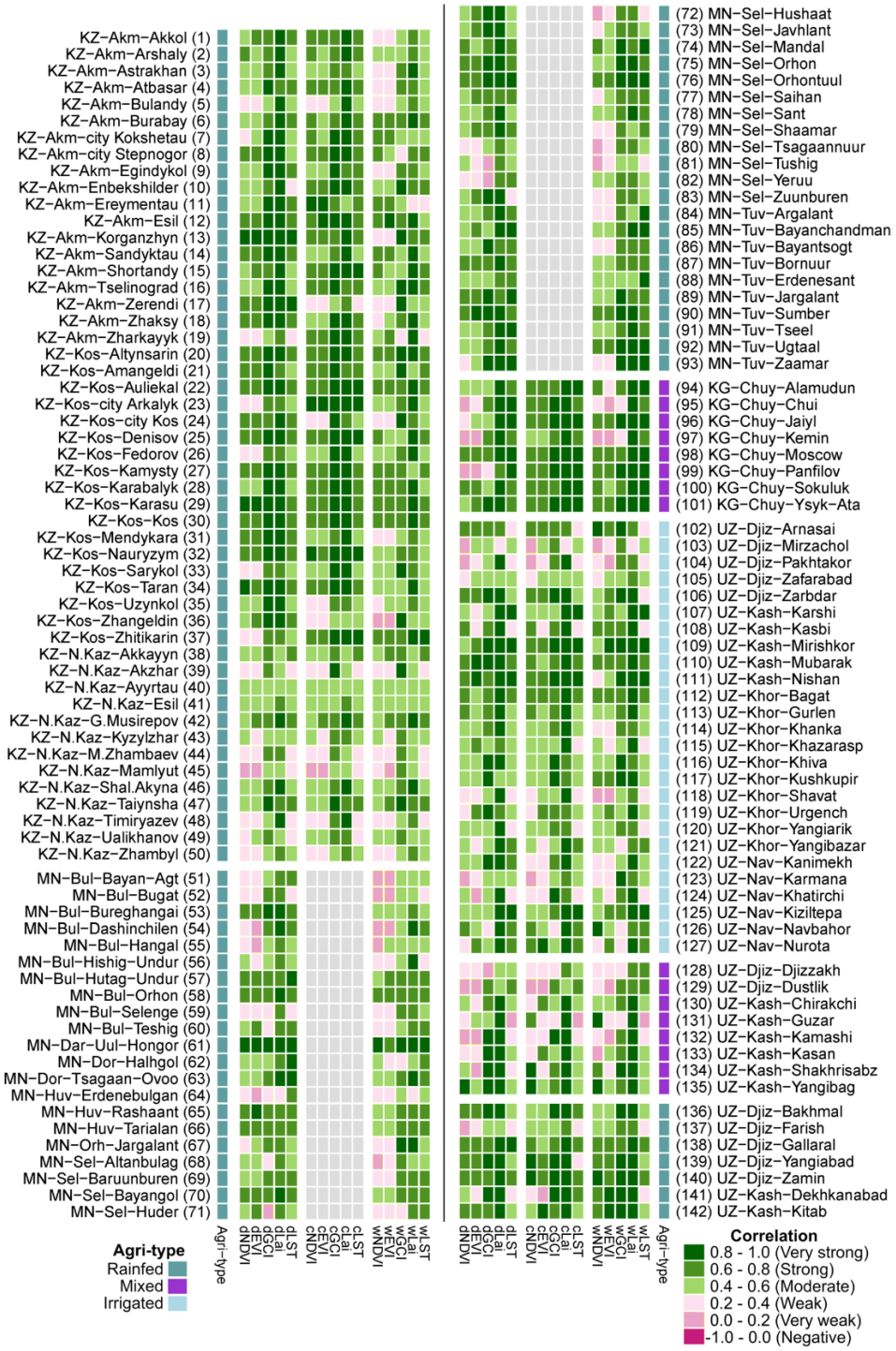

Figure 3.5: R^2 Heatmap between wheat yields and modelled yields based on indices using cropland and wheatland masks in the selected areas

Source: compiled by the authors.

Retrieved from the published open-access article: Eltazarov, S., Bobojonov, I., Kuhn, L., Glauben, T. (2023): The role of crop classification in detecting wheat yield variation for index-based agricultural insurance in arid and semiarid environments. Environmental and Sustainability Indicators, 18, 100250.

From Figure 3.5, it can be seen that the application of the modelling approach notably improved the relationship between indices and wheat yields in all countries and farming systems. Even the districts that had been weakly or negatively correlated in the mean/max approach now upgraded to be highly correlated. In addition, remarkable improvements can be seen for the case of irrigated and mixed agricultural land in Uzbekistan. Overall, among the vegetation indices, LAI and GCI showed better correlation with wheat yields once again in all countries, farming systems and masks.

Figure 3.6 provides results from the categorical accuracy assessment, which demonstrate the dynamic of POD and FAR values over the various correlation coefficients (CC). Overall, the results clearly show that the accuracy of indices to correctly detect the yield losses, represented by POD and FAR, improves with an increasing correlation coefficient indicated on the x-axis. According to both graphs shown in the Figure 3.6, the classification accuracy slowly increases until a 0.5 correlation coefficient, when it then begins to rise sharply from this point.

As demonstrated in Figure 3.7 and 3.8, the results of this study show that almost all indices have potential for index insurance design under suitable conditions. However, in majority of the cases, the LAI and GCI slightly outperforms other indices.

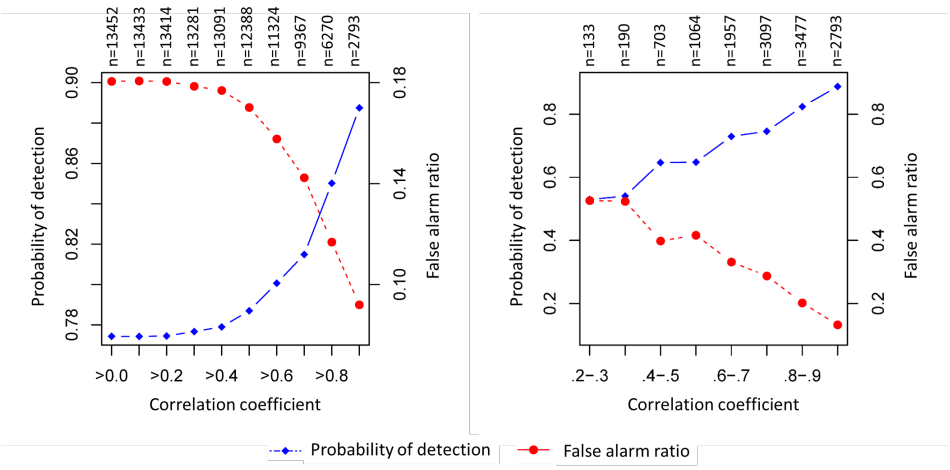

Figure 3.6: Results of the categorical accuracy assessment between yield loss events by indices and wheat yield data over the various correlation coefficients

Source: compiled by the authors.

Retrieved from the published open-access article: Eltazarov, S., Bobojonov, I., Kuhn, L., Glauben, T. (2023): The role of crop classification in detecting wheat yield variation for index-based agricultural insurance in arid and semiarid environments. Environmental and Sustainability Indicators, 18, 100250.

Country	Farming system	Correlation	dNDVI	dEVI	dGCI	dLai	dLST	cNDVI	cEVI	cGCI	cLai	cLST	wNDVI	wEVI	wGCI	wLai	wLST
Kazakhstan	rainfed	>0.5	76	80	88	92	72	80	84	84	92	76	72	72	66	88	62
		>0.6	64	66	72	84	58	64	68	78	86	64	44	48	48	76	44
Mongolia	rainfed	>0.5	74	74	79	70	79						60	58	79	72	72
		>0.6	65	65	65	60	67						37	44	58	63	56
Kyrgyzstan	mixed	>0.5	63	63	75	75	100	100	88	100	100	100	75	75	88	88	100
		>0.6	50	50	50	75	88	88	88	88	100	100	75	63	75	75	100
Uzbekistan	rainfed	>0.5	42	35	50	19	62	50	42	54	31	62	46	38	54	38	65
		>0.6	19	12	23	0	42	19	15	31	8	38	23	23	27	12	42
	irrigated	>0.5	0	0	0	0	13	0	0	0	0	13	0	0	0	0	13
		>0.6	0	0	0	0	0	0	0	0	0	13	0	0	0	0	0
	mixed	>0.5	57	57	71	57	0	83	83	67	50	17	86	86	86	71	0
		>0.6	57	57	43	29	0	83	83	50	17	0	86	86	57	29	0

Legend: 80-100% 60-80% 40-60% 20-40% 0-20%

Figure 3.7: Percentage of districts having satisfactory correlation (>0.5) and sufficient correlation (>0.6) between indices and wheat yields (Pietola et al., 2011); mean value of index approach

Source: compiled by the authors.

Retrieved from the published open-access article: Eltazarov, S., Bobojonov, I., Kuhn, L., Glauben, T. (2023): The role of crop classification in detecting wheat yield variation for index-based agricultural insurance in arid and semiarid environments. Environmental and Sustainability Indicators, 18, 100250.

Country	Farming system	Correlation	dNDVI	dEVI	dGCI	dLai	dLST	cNDVI	cEVI	cGCI	cLai	cLST	wNDVI	wEVI	wGCI	wLai	wLST
Kazakhstan	rainfed	>0.5	60	64	96	98	70	66	68	96	98	76	52	46	84	92	62
		>0.6	36	42	84	88	48	50	46	86	86	60	30	32	66	72	34
Mongolia	rainfed	>0.5	60	63	79	98	84						35	42	86	86	79
		>0.6	30	47	67	98	70						14	14	72	77	65
Kyrgyzstan	mixed	>0.5	38	38	75	100	100	88	88	100	100	100	75	50	75	100	100
		>0.6	25	38	50	100	100	88	88	100	100	100	75	50	75	100	100
Uzbekistan	rainfed	>0.5	54	65	73	92	62	54	58	85	96	62	50	58	81	96	62
		>0.6	31	31	50	85	38	38	27	69	92	35	23	42	65	96	35
	irrigated	>0.5	25	13	75	100	38	38	38	75	100	38	38	25	75	100	38
		>0.6	13	0	75	75	13	38	25	50	88	13	38	0	75	100	25
	mixed	>0.5	71	71	86	86	43	71	86	86	100	71	100	100	100	100	57
		>0.6	71	71	86	86	29	43	43	86	100	57	71	71	100	100	29

Legend: 80-100% 60-80% 40-60% 20-40% 0-20%

Figure 3.8: Percentage of districts having satisfactory correlation (>0.5) and sufficient correlation (>0.6) between indices and wheat yields (Pietola et al., 2011); regression approach

Source: compiled by the authors.

Retrieved from the published open-access article: Eltazarov, S., Bobojonov, I., Kuhn, L., Glauben, T. (2023): The role of crop classification in detecting wheat yield variation for index-based agricultural insurance in arid and semiarid environments. Environmental and Sustainability Indicators, 18, 100250.

3.4. Discussion

In the vast majority of study locations, there was a moderate to strong relationship between wheat yields and indices. However, there are differences between the individual regions in terms of those stages of vegetation periods that are most closely linked to the wheat yields. These differences are due to the wheat type and their cropping calendar, which depends on climatic conditions and farming systems. The strongest correlation between indices and wheat yields was found mainly for the second half of the developing crop phase, which is in line with Kogan et al. (2018), Panek and Gozdowski (2020) and Wang et al. (2014).

One important aim of this study was the incorporation of cropland and wheatland masks. Generally, it can be contended that the application of cropland and wheatland masks has different effects on the precision of indices for detecting wheat yield variation depending on location, climate and agricultural practice. As Figures 3.4-3.5 and Appendix 2.3 display, in all selected districts the application of cropland and wheatland masks noticeably improves the ability of indices to detect wheat yield variation for mixed lands of Kyrgyzstan and rainfed lands of Uzbekistan. These improvements might be due to high topographic variety in these regions, which contain mountains and foothills, thus significantly affecting index values. Moreover, in some cases of mixed agricultural lands in Uzbekistan, the application of cropland and wheatland masks improves the association between vegetation index and wheat yields, where there is some degree of positive correlation using index values from entire district areas. In cases of Kazakhstan, the index values from croplands and the entire district area outperform indices calculated from wheatlands only. This may be due to monotone agricultural practices, a wide breadth in the geographical location of croplands and low topological variety in these areas. However, in some areas the application of cropland and wheatland masks significantly improves the correlation between vegetation indices and wheat yields. Meanwhile, index values from the entire district area show the highest performance in Mongolia, since using wheatland mask may capture only the areas with regular phenology and a cropping calendar, which may result in missing the abnormal areas due to crop delays because of climate or human factors. However, there are some cases when wheatland mask improved the ability of indices to detect the wheat yield variety. Moreover, there is not a monotonous positive relationship between indices and the wheat yields of irrigated and mixed agricultural lands. The weak relationship of irrigated and mixed agricultural lands might be caused by a geographical situation, topographic types and crop varieties in the areas (Dick et al., 2011; Kölle et al., 2020). Further investigations should be conducted on irrigated lands by using farm and village scale wheat yield data.

It is important to mention that the mean values from indices show noticeably higher correlation with wheat yields than the max values among the vast majority of districts. Moreover, the wheat yield modelling approach using highly correlated periods of satellite data (critical stages of crop growth), as suggested by Kogan et al. (2018), demonstrates vital enhancements on the relationship between indices and wheat yields in all of the study sites and farming systems. These improvements can especially be observed for irrigated and mixed agricultural lands of Uzbekistan (see Figure 3.7 and 3.8).

Further results concern the suitability of novel indices as compared to conventional solutions like NDVI. Several prior studies found NDVI and precipitation to be most successful for capturing crop yield conditions, and as a data source for index insurance design and development (Bobojonov et al., 2014; Hochrainer-Stigler et al., 2014b; Makaudze and Miranda, 2010). However, in the presented case GCI and LAI indices slightly outperform and have higher correlation with wheat yields and a greater potential for index insurance development and implementation, even though these indices were not investigated and taken into account by other authors as a potential source for index insurance development.

Moreover, it is clear that the increase in correlation between the index and crop yields leads to a reduction in design and basis risk (Breustedt et al., 2008; Kölle et al., 2021; Norton et al., 2012), which are crucial during the index insurance design and implementation phases (Norton et al., 2015). According to the study conducted by Pietola et al. (2011), the critical threshold of index insurance from the demand side is situated at a correlation coefficient of 0.5-0.6. These findings are also in line with the results of this study, in which the precision of crop loss detection rises abruptly from a level of 0.5 correlation coefficient onwards (see Figure 3.6).

3.5. Conclusions

The main aim of the study was to explore the potential gains of using land use classification for designing and implementing an index insurance by comparing the suitability of multiple well-known and less prominent satellite-based indices in various wheat farming systems located in Central Asia and Mongolia. For this assessment, the study used 2,060 yield observations from 152 districts across Central Asia and Mongolia with irrigated, mixed and rainfed wheat farming systems.

The results of this study highlight the importance of testing cropland and wheatland masks during the process of index insurance design and development. Moreover, Lai and GCI indices was found to slightly outperform other well-known indices in detecting wheat yield variation and thus have greater potential for index insurance design. Overall, globally available MODIS-based indices could serve as a suitable source for establishing index insurance products in Central Asia and Mongolia; however, a careful selection of sources, boundaries, indices and methods is required.

Moreover, it is important to note that the usage of district level data can induce an aggregation biases, which means farm-level risks are likely underestimated. Nevertheless, the featured results are still informative for district scale index insurance and area-yield insurance programs in the region (e.g., which may be applied by industry or farmer co-operatives). It would be interesting to also analyze the relationship between indices and wheat yields at the farm and county scale, which would allow us to more deeply investigate the capacity of satellite data for index insurance development and implementation. Additionally, there are limitations regarding crop diversity, cultivated area, crop quality, fertilizers and re-seeding data, and it would also be interesting to examine the effects of these factors on the relationship between indices and wheat yields.

The lack of high-quality weather and yield data is a dominant limiting factor in developing countries for the implementation of index insurance. These findings are therefore relevant for improving insurance markets in Central Asia and Mongolia, being a potential source of data for index insurance design and operation. Moreover, the results of this study are also important for improving know-how of policymakers and farmers within the region on index insurance. There are, however, few start-up projects focused on piloting the implementation of index insurance in the region (see Eltazarov et al. (2021)). It should be also mentioned that, based on the initial results of this study, 385 farmers and 22,338 ha in Mongolia have been insured based on a MODIS-NDVI.

Future advances in satellite technology could further increase precision of crop loss prediction. For once, the correlation between vegetation indices and wheat yields obviously depends on the proportion of wheatland per pixel of the satellite images. Furthermore, data availability also limits the generation of cropland mask for each year individually. One disadvantage of MCD12Q1-V6 is that the delay of the land cover product is 1-1.5 years, which is not practical in terms of the index insurance establishment. Furthermore, MCD12Q1-V6 does not provide the areas of cropland located in Mongolia. For that reason, open source satellite data with a higher spatial resolution, such as Sentinel 2 or Landsat satellite series, could improve the accuracy of cropland and wheatland identification. Additionally, using state developed cadaster maps would lead to further improvements in correlation and reduction of basis risk of spatial resolution.

4. Improving risk reduction potential of weather index insurance by spatially downscaling gridded climate data - a machine learning approach[9]

4.1. Introduction

Extreme weather events are major drivers of volatility of agricultural production (Powell and Reinhard, 2016). Drought in particular causes low crop yields that can lead to substantial financial instability (Webber et al., 2018). Climate change is expected to increase the frequency and magnitude of extreme weather events, resulting also in increased agricultural production risks (FAO, 2015; IPCC, 2022). Therefore, coping with droughts is essential for safeguarding against volatility in agricultural production and guaranteeing farmers' income stability. Activities such as using drought-tolerant crops, crop diversification and rotation, improving irrigation systems, and minimum tillage may mitigate some drought risks. However, they may still fail during wide-spread extreme drought events (Olesen et al., 2011). Complementary to these adaptation measures, crop insurances offer the opportunity of risk-sharing and hedging against the risk of yield defaults caused by drought, hail, flood, etc. However, traditional crop insurances are challenged by a high administrative cost of crop loss assessment, adverse selection and moral hazard issues. As an alternative, weather index-based insurance (from here onwards used as "index insurance"), formally known as weather derivatives or parametric insurance (Collier et al., 2009; Vedenov and Barnett, 2004; Xu et al., 2008), has been recognized as a promising financial risk management tool (Collier et al., 2009; Giné et al., 2010; World Bank, 2011). In index insurance, the payout is based on a pre-determined index, and when the value falls below or exceeds a certain threshold value, insurers make a payment without any physical check-up. This approach is intended to reduce administrative costs, reduce the problem of information asymmetry, and promises rapid and efficient determination of payouts (Fisher et al., 2019; Greatrex et al., 2015; World Bank, 2015).

Commonly, index insurances for crops draw on climate data from weather stations for the calculation of precipitation and temperature aggregates. However, the performance of index insurance based on weather stations significantly decreases when the distance between farm and weather station is higher than 20-25 kilometers (Gommes and Göbel, 2013; Osgood et al., 2007). Thus, index insurances based on data from weather stations are, particularly in developing countries, inhibited by the low density of weather stations. Installment of new weather stations might be a solution, but installing and maintaining a new weather station every 10-20 kilometers would significantly affect the price of the insurance premium and also still not provide the historical data required for index design.

Besides data from weather stations, gridded climate data can also be used for index insurance. Its suitability for index design was confirmed for precipitation data (Black et al., 2016b; Brahm et al., 2019; Osgood et al., 2018; Tarnavsky et al., 2018), temperature data (Bokusheva et al., 2016;

[9] This chapter was published as the following open-access article: Eltazarov, S., Bobojonov, I., Kuhn, L., Glauben, T. (2023): Improving risk reduction potential of weather index insurance by spatially downscaling gridded climate data - a machine learning approach. Big Earth Data.
https://doi.org/10.1080/20964471.2023.2196830; This chapter benefitted from the comments by the anonymous referees of Big Earth Data

Hellmuth et al., 2009; Kölle et al., 2020; Möllmann et al., 2019), soil moisture data (Enenkel et al., 2017; Markus Enenkel et al., 2018; Vroege et al., 2021) and evapotranspiration indices (Coleman et al., 2018; Markus Enenkel et al., 2018; Ndegwa et al., 2022). In contrast to weather station data, gridded climate data are mostly open source and near-real time. However, the vast majority of gridded climate data with fine resolution is only available for limited land areas or time periods (Eltazarov et al., 2021), which significantly limits their applicability for index design. For instance, Climate Hazards Group InfraRed Precipitation with Station Data (CHIRPS) provides a gridded precipitation data since 1982, but it only snaps latitudes between 50°S-50°N (Funk et al., 2015). Global Satellite Mapping of Precipitation (GSMaP) and Integrated Multi-satellite Retrievals for GPM (IMERG) cover the whole earth, but have only provided data since 2000 (Mega et al., 2019). Tropical Application of Meteorology Using Satellite Data (TAMSAT) and NOAA-based African Rainfall Climatology Version 2 (ARC2) do provide gridded climate data since 1983, but only for the African continent (Maidment et al., 2014; Novella and Thiaw, 2012). Moreover, Global Land Data Assimilation System (GLDAS) provides gridded temperature data across the globe, but only since 2000 (Rodell et al., 2004). Modern-Era Retrospective analysis for Research and Applications version 2 (MERRA-2) provides long-term temperature data since 1980, but the spatial resolution is around 60 km. Furthermore, NASA-USDA Enhanced SMAP Global soil moisture data provides soil moisture information for the whole world at 10-km spatial resolution, but only since 2015.

All in all, there is a need for long historical climate records with fine spatial resolution covering the whole earth in index insurance industry, in order to assess the risk and design well-functioning crop insurances. There is some potential re-analysis based climate data for index insurance design such as ERA5-based climate data from the European Centre for Medium-Range Weather Forecasts (ECMWF) (Hersbach et al., 2020). Similarly, satellite base climate data from the European Space Agency (ESA) fed into the Climate Change Initiative (CCI)-based soil moisture data (Dorigo et al., 2017) that covers the whole earth and has available data from the 1980s onwards. Nevertheless, the spatial resolution of these datasets is very low, approximately 25-30 kilometers, which significantly decreases the potential of these data sources in their application for index design and implementation. Especially designing index insurance based on such coarse-resolution climate data may lead to an increase of basis risk.

One potential and so far under-researched method to deal with the issue of spatial resolution could be to spatially downscale gridded climate data using statistic methods. A number of studies have investigated and demonstrated the ability and accuracy of downscaling the spatial resolution of gridded climate data sources using regression and machine learning methods (Bai et al., 2019; Hu et al., 2020; Im et al., 2016; Liu et al., 2020; Zhang et al., 2021; Zhu et al., 2017). For instance, Shen and Yong (2021) and Yan et al. (2021) systematically compared the accuracy of various machine learning methods to downscale gridded precipitation data from 10 km to 1 km and were able obtain a significant agreement between downscaled and gauge observations. Meanwhile, Alexakis and Tsanis (2016) and Sharifi et al. (2019) compared multiple linear regression, machine learning models and interpolation techniques to downscale gridded precipitation data, and have concluded that ma-

chine learning methods slightly outperform other methods in downscaling precipitation data. Moreover, Bai et al. (2019) and Liu et al. (2020) compared various downscaling methods and various combination of features to find optimal setups to downscale low resolution (10 km and 35 km) soil moisture data to fine resolution (1 km). dos Santos (2020) and Zhang et al. (2021) compared machine learning and regression models to downscale temperature data and were able to create 1-km long-term daily temperature data.

In general, the existing literature mainly focuses on the accuracy of various downscaling methods and combination of features. Only a few studies have worked on real-world applications of downscaled climate data. For example, López López et al. (2018) used the downscaled gridded precipitation data for river discharge modelling and found a better agreement with ground observations when the model was run using the downscaled precipitation data. Seyyedi et al. (2014) demonstrated improvements in runoff simulations and flood modelling when downscaled precipitation data compared to the coarse precipitation product. Bastola and Misra (2014) studied the applicability of dynamically downscaled precipitation data for hydrological simulations and found that downscaled data was superior to other meteorological datasets. Ha et al. (2013) did an extensive review of downscaling methods of coarse gridded evapotranspiration (ET) data for irrigation scheduling purposes and found that downscaled ET improves the estimation of crop water requirements. Srivastava et al. (2013) found that downscaled soil moisture data improves the estimates of hydrological modelling for a local and regional scale compared to the original coarse resolution. Hrisko et al. (2021) estimated heat storage in urban areas using multispectral satellite data and found that heat storage can be stably downscaled from lower to higher spatial resolution and monitored over time. Meanwhile, the potential of downscaled climate data for index insurance design, as well as the ability to detect shortfalls and their downside risk reduction capacity, have not yet been studied. Even so, downscaling is an effective approach to convert coarse climate data to a finer spatial resolution (Abbaszadeh et al., 2019), and downscaled climate data have a better accuracy than the original coarser resolution (F. Chen et al., 2019; Chu et al., 2011; Fang et al., 2022), which is essential to improve the quality of index insurance and decrease basis risk. Moreover, based on our literature review, there are only a few number of studies (Markus Enenkel et al., 2018; Petropoulos and Islam, 2017; Vroege et al., 2021) that explore the potential of satellite-retrieved soil moisture data for index insurance design and operation.

We provide two key contributions to the literature. Firstly, we systematically evaluate and compare index insurance products with a design based on original coarse resolution and spatially downscaled climate data to reduce farmers' financial downside risk exposure. We spatially downscale long-term and spatially coarse resolution soil moisture, precipitation and temperature data using machine learning algorithms. Second, for each county we identify the best source of climate data for index insurance products to maximize the climate risk reduction capacity. We test the robustness of our findings in the case of wheat produces in Kazakhstan and Mongolia. Since systematic drought is becoming more frequent and putting agricultural production at risk (de Beurs et al., 2018; Haag et al., 2019), there is an increased demand for financial instruments and social security mechanisms in these regions (Bobojonov et al., 2019).

This paper is structured as follows: In the second chapter, we report on the study area, machine learning methods and features for downscaling the gridded climate data. Moreover, we provide details on index insurance design and measuring the risk reduction capacity of index insurance based on original coarse resolution and downscaled climate data. The third chapter provides the results from our analyses and a comprehensive discussion. Lastly, we wrap up our article with conclusions retrieved from the study.

4.2. Methods and materials

4.2.1. Study area and yield data

Wheat is one of the most strategic crops for Kazakhstan and Mongolia, and it is grown mostly on rainfed lands (Fehér et al., 2017; Tuvdendorj et al., 2019). Figure 4.1 illustrates our case study consisting of rainfed spring wheat producing counties in Kazakhstan (34 counties) and Mongolia (22 counties). Figure 4.2 shows the cropping calendar of spring wheat in the study areas. The reasons for using these regions for our analysis are: (1) In these regions, spring wheat is steadily being cultivated, and they are the main wheat producing regions (FAO, 2020; Fehér et al., 2017); (2) Frequent drought events in the regions have happened in the beginning of the century and in recent years; (3) There is a homogenous climate, crop management and cropping calendar (FAO, 2020; Shamanin et al., 2016); (4) There is a low density of weather stations (NCEI, 2019); (5) In the region, climate-oriented financial instruments and social mechanisms are in high demand (Bobojonov et al., 2019); (6) There is a lack of traditional insurance markets due to a large land area and low population density. The study counties are located in a semi-arid climatic region (Trabucco and Zomer, 2019).

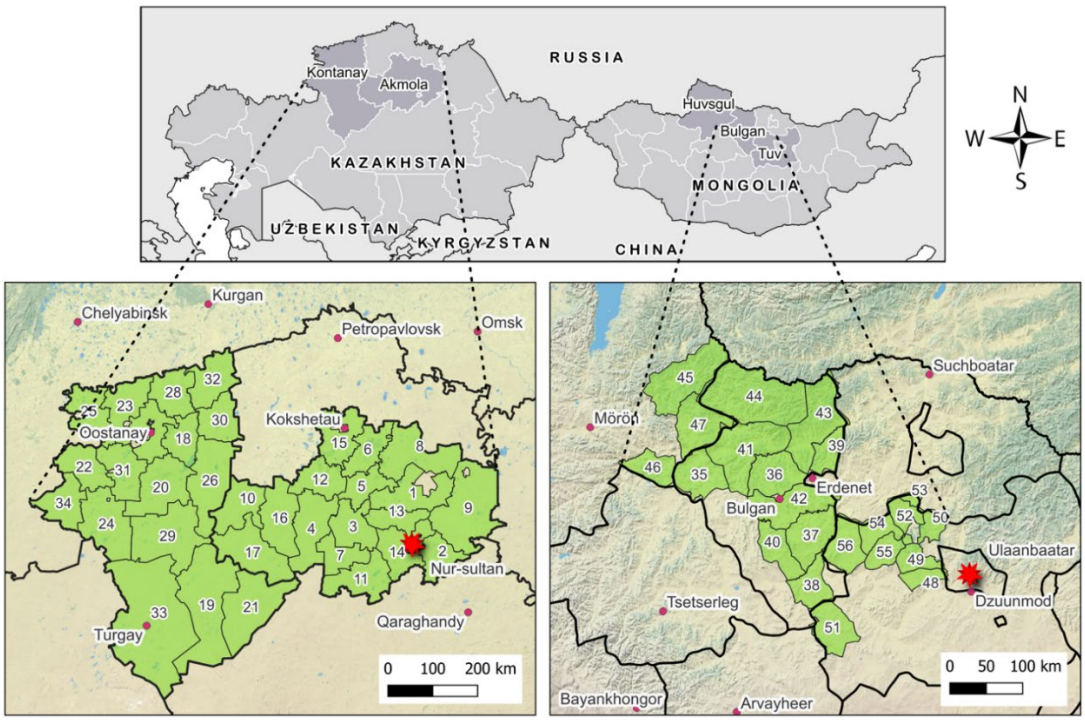

Figure 4.1: Location of study regions and counties in Kazakhstan and Mongolia

Note: Each number on the map refers to unique counties. County names are provided in Table A.3.1.

Source: compiled by the authors.

Retrieved from the published open-access article: Eltazarov, S., Bobojonov, I., Kuhn, L., Glauben, T. (2023): Improving risk reduction potential of weather index insurance by spatially downscaling gridded climate data - a machine learning approach. Big Earth Data.

It is important to note that in our study we used county-scale spring wheat yield and index data, and we considered counties as farm co-operatives who purchase an insurance contract as a group of farmers. It's true that the calibration of the index by county-scale yield data might omit farm-level management differences (Finger 2012). However, typically commercial index insurances do not take these management differences into account anyway, in order to avoid moral hazard. Moreover, a recent study by Paliwal and Jain (2020) reported that self-reported farm scale crop yield data is actually inaccurate for calibrating satellite-based remote sensing data. As a consequence, regional aggregation is practiced in particular in areas with relative spatial homogeneity (Kath et al., 2019).

In order to check the robustness of the proposed method to design index insurance, this paper uses spring wheat yield data from two countries and in total 56 counties, involving a total of 1337 yield observations (Table A.3.1). Taking into account the technological progress in the wheat production industry between 1982 and 2018, and removing the deterministic trends in historical spring wheat yields, yield observations were de-trended. Failing to do so would have led to an overestimation of yield variability and biased the strike level and risk-reduction potentials for insurance applications. To capture technological trends, country-level yield data between 1991 and 2019 was employed (FAO, 2022). Following Finger (2013) and Bucheli et al. (2021), this approach applied an M-estimator to identify linear trends, which was found to equal $\beta = 0.123$ in Kazakhstan and $\beta = 0.26$ in Mongolia. In the next step, county-individual de-trended yields were identified using the following equation by using slope coefficient for each country and $t_{end} = 2015$ for counties in Kazakhstan and $t_{end} = 2018$ for counties in Mongolia. Moreover, i refers to county and t indicates time.

$$y_{it}^{detr} = y_{it} + (t_{end} - t) * \beta \tag{4.1}$$

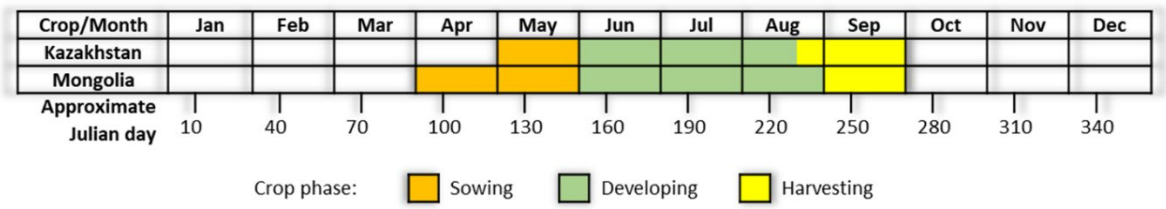

Figure 4.2: The cropping calendar of spring wheat in Kazakhstan and Mongolia

Source: Authors' presentation based on data adapted from the FAO (2021, 2020) and Shamanin et al. (2016).

Retrieved from the published open-access article: Eltazarov, S., Bobojonov, I., Kuhn, L., Glauben, T. (2023): Improving risk reduction potential of weather index insurance by spatially downscaling gridded climate data - a machine learning approach. Big Earth Data.

4.2.2. Gridded climate data

After a systematic review of available gridded climate products based on geographical coverage and availability of long-term historical weather records, we selected two gridded climate products and three climate parameters to check the robustness of proposed method: ERA5 as a source of precipitation and temperature data, and ESA-CCI as a source of soil moisture data. ERA5 is the fifth generation ECMWF atmospheric reanalysis of the global climate (Hersbach et al., 2020). Reanalysis combines model data with in-situ and satellite observations from across the world into a globally complete and consistent dataset. ERA5 provides large numbers of atmospheric, ocean-wave and land-surface quantities on an hourly, daily and monthly scale with ≈30 km spatial resolution. We only used monthly temperature and precipitation data in this study. ESA-CCI was initiated by ESA to monitor the earth surface variables corresponding to climate change (Markus Enenkel et al., 2018). Among others, the program aims at long-time monitoring soil moisture with ≈30 km spatial resolution by integrating and synthesizing both active and passive microwave remote sensing sensors. For our analyses, we used monthly aggregations and volumetric unit (m^3/m^{-3}) of the version 03.3 of ESA-CCI SM.

As discussed earlier, only very few satellite products spatially cover the whole earth with long historical records at near-real time velocity. For downscaling ERA5 and ESA-CCI data, which is of coarser resolution, this study employs optical bands and indices from the NOAA Climate Data Record (CDR) of the Advanced Very High Resolution Radiometer (AVHRR), and the digital elevation model from The Shuttle Radar Topography Mission (SRTM). NOAA CDR of AVHRR is a dataset that contains gridded surface reflectance, brightness temperatures (BT) and NDVI derived from the AVHRR sensors onboard eight NOAA polar orbiting satellites. The dataset spans from 1981 to the present on a daily temporal scale with ≈5 km spatial resolution.

4.2.3. Spatial downscaling

In general, there are two types of spatial downscaling techniques, namely dynamic and statistic. Dynamic downscaling employs a regional climate model or a numerical climate model to produce climate parameters in finer spatial resolution by simulating the physical processes of the linked land-atmosphere system (Sharifi et al., 2019). The statistic technique, on the other hand, is modelling the statistical relationship between high and low scale covariates. This technique adopts climate parameters based on auxiliary data such as vegetation index, land surface temperature, elevation, soil type, etc. (Sharifi et al., 2019).

4.2.3.1. Random forest method

During the last decade, various statistical downscaling methods have been developed. According to the literature, random forest (RF) is a very suitable machine learning algorithm in term of accuracy and simplicity for downscaling climate parameters is (Chen et al., 2021; Hu et al., 2020; Im et al., 2016; Liu et al., 2020, 2018; Yan et al., 2021). For instance, Shen and Yong (2021), Yan et al. (2021)

and C. Chen et al. (2021) investigated the accuracy of RF to downscale coarse precipitation data and came into conclusion that RF-based downscaled precipitation have high spatial correspondence with original coarse data. Yang et al. (2017), Bartkowiak et al. (2019) and Tang et al. (2021) studied the applicability of RF to downscale coarse temperature and confirmed the strong potential of RF for producing improved and high spatial resolution temperature data. Hu et al. (2020), Hongyan Zhang et al. (2022) and Q. Chen et al. (2020) examined the suitability of RF to downscale soil moisture and found that RF-based downscaling is able to capture the variation of soil moisture, even downscale soil moisture have higher correlation with in situ observations than the original coarse data.

RF is a tree-based ensemble method, meaning that data patterns are predicted according to an aggregation of the predictions of several decision trees, with each tree depending on a collection of random variables for classification and regression. Furthermore, the prediction performance is improved by bootstrap aggregation, which reduces the variance of predictions by drawing (with replacement) a fixed number of samples from the training set (Breiman, 2001). For the constructing of each tree, features are selected randomly at each decision node. For obtaining the final output, i.e. the classification or prediction output, RF uses a majority vote to aggregate the predictions of each individual tree.

4.2.3.2. Downscaling process

Initially, all satellite-based datasets used in this study were aggregated to a monthly scale[10] for comparability. In order to develop a RF based downscaling model, NOAA and SRTM products with fine spatial resolution were reaggregated to a resolution of ≈30 km. Then, following Chen et al. (2021) and Yan et al. (2021), we used NDVI and BT obtained from NOAA AVHRR as well as elevation, slope and aspect data generated from SRTM to train RF model to estimate ERA5-based precipitation data.

$$PCP = f(NDVI, BT, elevation, slope, aspect) \tag{4.2}$$

Following Zhang et al. (2021), we utilized the same features to train the RF model to estimate the ERA5-based temperature data.

$$TEMP = f(NDVI, BT, elevation, slope, aspect) \tag{4.3}$$

In addition, NDVI, BT, Red, Near-Infrared (NIR) from NOAA AVHRR as well as elevation and slope from SRTM were employed to train a RF model to estimate the ESA-CCI-based soil moisture data, as also suggested by Hu et al. (2020) and Liu et al. (2018).

$$SM = f(NDVI, BT, RED, NIR, elevation, slope, aspect) \tag{4.4}$$

[10] Earliest tests of our study showed slightly better performance of index insurance when they were designed based on monthly scale weather parameters than 10day scale. Moreover, the gridded weather parameters have a better agreement between in-situ observations when a higher temporal aggregation (monthly, seasonal, etc.) is used (Coleman et al., 2018; Eltazarov et al., 2021; Usman and Nichol, 2020).

In the following, the RF models trained to estimate climate parameters at coarse spatial resolution were applied to feature at 5 km resolution to obtain climate data at fine resolution. The same procedure was repeated for each of June and July months from 1982 to 2015 for study sites in Kazakhstan and from 2000 to 2018 for study sites in Mongolia (reasons for the selection of these months are given in the results section). The training, estimating and downscaling processes were done for each selected month, study site and climate parameter separately, as combining them would assume the same marginal response of features to climate parameters in all months and study sites. A total of 2264 and 780 samples (all pixels from study sites) were extracted from selected features for each of selected months and climate parameters for sites in Kazakhstan and Mongolia, respectively, and used to develop the RF models. In each RF model, we set the number of trees parameter to 50, as further increase in number of trees did not demonstrate significant improvement in the cross validation accuracy.

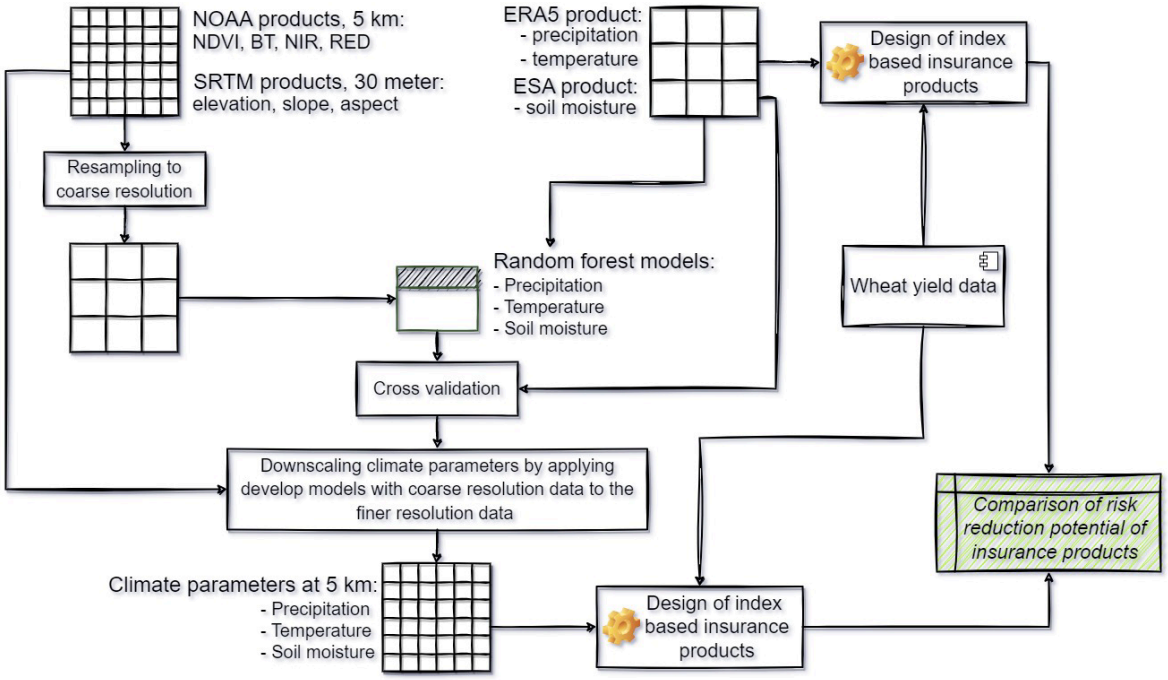

Figure 4.3: Procedure of relevant data processing and climate data downscaling

Source: compiled by the authors.

Retrieved from the published open-access article: Eltazarov, S., Bobojonov, I., Kuhn, L., Glauben, T. (2023): Improving risk reduction potential of weather index insurance by spatially downscaling gridded climate data - a machine learning approach. Big Earth Data.

4.2.3.3. Cross validation

In order to assess the performance of the RF models, a cross-validation was conducted at the coarse spatial resolution. The trained RF models obtained from the coarse spatial resolution were used to estimate climate parameters at coarse spatial resolution. To measure the performance of the RF

models in estimating the climate parameters for our sample, we used three accuracy measures, namely root mean square error (RMSE), percent bias (PBIAS) and correlation coefficient (CC) (Chen et al., 2021).

$$RMSE = \sqrt{\frac{1}{n}\sum_{i=1}^{n}(E_i - O_i)^2} \tag{4.5}$$

$$PBIAS = \frac{\sum_{i=1}^{n}(E_i - O_i)}{\sum_{i=1}^{n}(O_i)} \times 100\% \tag{4.6}$$

$$CC = \frac{\sum_{i=1}^{n}(O_i - \overline{O})(E_i - \overline{E})}{\sqrt{\sum_{i=1}^{n}(O_i - \overline{O})^2}\sqrt{\sum_{i=1}^{n}(E_i - \overline{E})^2}} \tag{4.7}$$

General stages of process flow are illustrated by Figure 4.3. All of the gridded climate and satellite-based data processing and machine learning analysis within this study was carried out using the Google Earth Engine platform. For statistical analyses and graph visualization we used R Project (R Development Core Team, 2018).

4.2.4. Design of index insurance products

Intra-seasonal climate data typically outperform season-long data in detecting crop yield variation (Ortiz-Bobea et al., 2019; Schierhorn et al., 2021). The most critical vegetation period is in this case identified along the Spearman correlation coefficient[11] between the respective climate parameter and spring wheat yield for each county (Möllmann et al., 2019). Climate parameters are then averaged over this most critical vegetation period.

For building the index, we combined indicators of original coarse resolution and downscaled precipitation, temperature and soil moisture data. Higher precipitation and soil moisture decrease the likeliness of drought events, while high temperature increases drought occurrence.

In the index insurance contract, the payout $PO_{t,i}$ is determined based on whether the index falls below a certain threshold in county i, which is called strike level S_i as shown in Equation (7). In our study, the strike level is determined by the 30 percent quantile of the index value (Bokusheva et al., 2016; Kölle et al., 2020).

$$PO_{t,i} = \max(S_i - I_{t,i}, 0) \times V_i \tag{4.8}$$

where $I_{t,i}$ corresponds to the index of climate parameter calculated for time period t for county i. The relevant time periods were identified using time-series correlation analysis for each index and county. V_i represents the tick size, which determines the indemnity payout per unit of the difference between the strike level S_i. The tick size V_i corresponds to the slope coefficient β_i from the following regression model (8).

$$y_i = c_i + \beta_i I_{t,i} + \varepsilon_i \tag{4.9}$$

[11] We employed Spearman's correlation coefficient as the relationship between weather and crop yield is non-linear (Konduri et al., 2020; Semenov and Porter, 1995).

where y_i is the wheat yield of the county i, $I_{t,i}$ stands for the index value in period t, β_i is the slope coefficient of the regression equation, c_i is a constant, and error term ε_i is the variation of wheat yield that cannot be explained by the index value. Following Bucheli et al. (2021) and Conradt et al. (2015), in order to estimate the β_i and c_i we applied quantile regression (QR). QR is typically reducing the basis risk of index insurance as compared to Ordinal Least Squares (OLS), due to its property of estimating coefficients separately for each quantile of the outcome variable rather than at the population mean. Thus, QR minimizes the sum of absolute residuals and is more robust to outliers (Koenker and Bassett, 1978). As we are focused on the lower tail of the yield distribution, we chose the 30 percent quantile, following literature (Bokusheva et al., 2016; Bucheli et al., 2021; Kölle et al., 2021, 2020; Möllmann et al., 2019). Furthermore, for this study we assume the case of an actuarily fair insurance, where premiums are calculated based on an average of payouts for each county over the time period, excluding surcharges resulting from administrative costs and business margins. Using this simplistic pricing method allows us to identify the risk-reduction potential of insurance products without being inhibited by any mis-specified insurance premiums (Bucheli et al., 2021).

4.2.5. Estimation of the hedging effectiveness

Due to this study's focus on climate-related production risk, the indemnities and fair premiums are measured in quantity units of wheat yield. To assess the risk reduction potential of each insurance product based on original coarse resolution and downscaled climate parameters, the hedging effectiveness of insurance contracts (the degree to which yield losses are offset by the hedging instrument's payouts) was estimated by comparing net incomes from uninsured vs. insured yields. According to Bokusheva (2018), we calculated the insured wheat yield $y_{t,i}^{insured}$ as follows:

$$y_{t,i}^{insured} = y_{t,i} + PO_{t,i} - FP_i \tag{4.10}$$

where $y_{t,i}$ refers to the wheat yield for producer i at time t, $PO_{t,i}$ is the indemnity payout, and FP_i indicates the fair premium.

Following Vedenov and Barnett (2004), we estimate the hedging effectiveness of insurance contracts by comparing downside risk measure semi-variance (SV) of uninsured yields with the SV of insured yields. The downside risk measure SV is calculated as follows:

$$SV_i = \frac{1}{N}\sum_{t=1}^{N}[\min(y_{t,i} - \overline{y_i}, 0)]^2 \tag{4.11}$$

where $y_{t,i}$ indicates the insured or uninsured wheat yield, $\overline{y_i}$ stands for uninsured average wheat of the respective study area, and N denotes the number of yield observations. Consequently, we identify the hedging effectiveness[12] (HE) of the index insurance product by comparing the SV of wheat yield without insurance contract with the SV of wheat yields with insurance contract, as shown in Equation (11).

$$HE = 1 - \frac{SV^{insured}}{SV^{uninsured}} \tag{4.12}$$

[12] Higher hedging effectiveness corresponds to a lower basis risk and a higher potential for risk reduction.

To test for significant differences between the hedging effectiveness of the designed index insurance based on original and downscaled climate data, we applied non-parametric Wilcoxon rank sum tests for improved cases. The Wilcoxon rank sum test examines the null hypothesis that ranks of paired two groups are not significantly different. In contrast to the t test, Wilcoxon rank sum test does not require the data to be normally distributed (Möllmann et al., 2019).

All statistical calculations have been developed using the R project (R Development Core Team, 2018). In order to support practical applications of this work, the authors developed an R package that includes calculation of hedging effectiveness and other statistical indicators to analyze the performance of index insurance. Details about the R package "climate-insurance" can be found under the following link https://github.com/klimalez/climate-insurance. Additionally, the authors developed an open-source web application based on this R package, the "Climate Risk Insurance Design and Performance Analysis" that helps to test the performance of selected index for insurance design: https://klimalez.org/climate-insurance.

4.3. Results and Discussion

4.3.1. Climate data validation

We find that RF estimated climate data at coarse spatial resolution has a good correlation with the climate data in original spatial resolution. The cross validation between original climate data and data estimated by the RF models at original spatial resolution demonstrates a good performance, with a 0.99 correlation coefficient for all climate parameters, which is in line with the performance achieved for instance by Shen & Yong (2021) and Yan et al. (2021). For study sites in Kazakhstan we find average RSME of 0.59 mm, 0.058 ^{o}C, 0.0006 m3/m3 and PBIAS 1.19%, 0.25%, 0.27% for precipitation, temperature and soil moisture, respectively, which are in line with the existing literature (Hu et al., 2020; Liu et al., 2020; Yan et al., 2021). Furthermore, we find similar results for study sites in Mongolia with average RMSE 0.72 mm, 0.059 ^{o}C, 0.0006 m^3/m^3 and PBIAS 0.71%, 0.31% and 0.27% precipitation, temperature and soil moisture, respectively.

Figure 4.4 graphically illustrates differences between original coarse data (column 1 "Original") and estimated climate data by RF model at original spatial resolution (RF Estimated) along one example region and year, as well as downscaled climate data at ~5 km spatial resolution (RF Downscaled). The column RF estimated shows the initial cross-validation of the performance of the RF models, where climate parameters are estimated at the same spatial resolution as the original coarse climate data sources.

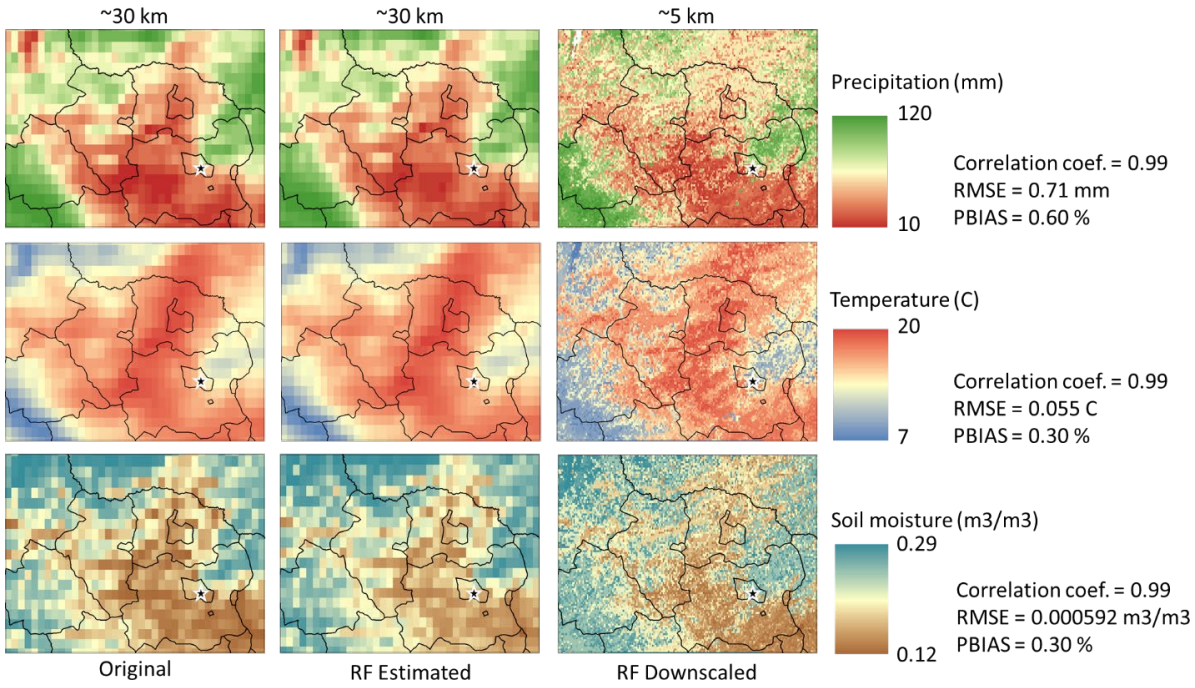

Figure 4.4: Original coarse resolution, random forest based estimated and downscaled climate parameters, Northern Mongolia in June 2015.

Source: compiled by the authors.

Retrieved from the published open-access article: Eltazarov, S., Bobojonov, I., Kuhn, L., Glauben, T. (2023): Improving risk reduction potential of weather index insurance by spatially downscaling gridded climate data - a machine learning approach. Big Earth Data.

4.3.2. Assessment of risk reduction potential of index insurance products

Moreover, primary tests of our study showed a slightly better performance of index insurance when they were designed based on monthly scale climate parameters rather than on 10-day scale (average for temperature and soil moisture, cumulative for precipitation). Figure 4.5 graphs the mean CC between wheat yield and climate parameters for each month by country. For both countries, spring wheat yields showed the highest correlation with all climate parameters in the months of June and July, which was also found by other recent studies (Möllmann et al., 2019; Schierhorn et al., 2021).

Table 4.1 summarizes the hedging effectiveness on a national level. For Kazakhstan, the hedging efficiency was 18% for soil moisture, 14% for precipitation, and 24% temperature, based on the original spatial resolution. For the same country, downscaled data increased the hedging efficiency to 18% for precipitation, and 25% for temperature-based index insurance, however, it had no notable effect on the hedging effectiveness of soil moisture. For Mongolia, indices based on original spatial resolution data delivered an average hedging effectiveness of 18% for soil moisture, 12% for precipitation, and 12% for temperature; downscaling increased these values to 22% for soil moisture, 21% for precipitation, and 14% for temperature-based index insurance. In summary, downscaled climate data improved the risk reduction capacity of index insurance for most index

products. While hedging efficiency was higher on average in Kazakhstan, the improvements of downscaling were higher in Mongolia. In particular, we observed a noticeable improvement of downscaling for precipitation data. Overall, the hedging efficiency of index insurances based on both original coarse resolution and downscaled data was higher than the results obtained by Möllmann et al. (2019).

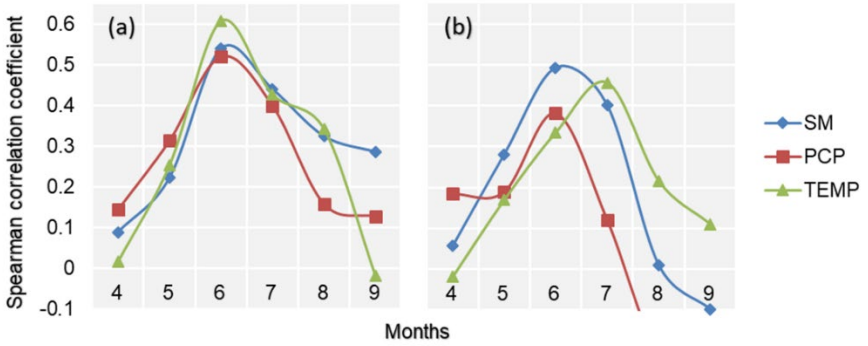

Figure 4.5: Dynamics of the Spearman correlation coefficient between spring wheat yield and monthly scale ERA5-based precipitation and temperature, and ESA-based soil moisture

Note: Counties in (a) Kazakhstan and (b) Mongolia

Source: compiled by the authors.

Retrieved from the published open-access article: Eltazarov, S., Bobojonov, I., Kuhn, L., Glauben, T. (2023): Improving risk reduction potential of weather index insurance by spatially downscaling gridded climate data - a machine learning approach. Big Earth Data.

Table 4.1: Mean hedging effectiveness of index insurance products based on original coarse resolution and downscaled climate data

Hedging effective-ness	Kazakhstan		Mongolia	
	Original	Downscaled	Original	Downscaled
Soil moisture	18%	18%	18%	22%
Precipitation	14%	18%	12%	21%
Temperature	24%	25%	12%	14%

Source: compiled by the authors.

Retrieved from the published open-access article: Eltazarov, S., Bobojonov, I., Kuhn, L., Glauben, T. (2023): Improving risk reduction potential of weather index insurance by spatially downscaling gridded climate data - a machine learning approach. Big Earth Data.

However, it should be pointed out that the hedging effectiveness fluctuates considerably among indices and regions. In particular the regional variation in the hedging effectiveness of wheat index insurance was already noted in previous studies (Bokusheva et al., 2016; Kölle et al., 2021). Figure

A.3.4 reports on the hedging effectiveness of index insurance based on the original coarse resolution and downscaled soil moisture, precipitation and temperature data across counties.

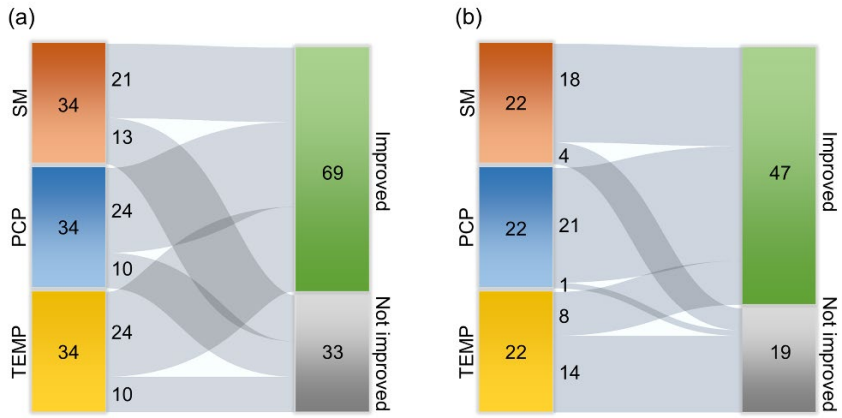

Figure 4.6: Change of hedging effectiveness of index insurances after using downscaled climate data

Note: Counties in (a) Kazakhstan and (b) Mongolia. Numbers represent the number of counties.

Source: compiled by the authors.

Retrieved from the published open-access article: Eltazarov, S., Bobojonov, I., Kuhn, L., Glauben, T. (2023): Improving risk reduction potential of weather index insurance by spatially downscaling gridded climate data - a machine learning approach. Big Earth Data.

Our previous analysis demonstrated that designing index insurance based on downscaled climate data lowers the basis risk in the majority of our cases. Figure 4.6 presents the exact number of counties where hedging effectiveness of index insurances were improved and not improved due to use of downscaled climate data. In the case of Kazakhstan, designing an index insurance based on downscaled soil moisture increased hedging effectiveness in 21 counties out of 34, downscaled precipitation improved hedging effectiveness in 24 counties out of 34, and downscaled temperature enhanced hedging effectiveness in 24 counties out of 34. Meanwhile, in Mongolia, index insurance based on downscaled soil moisture improved hedging effectiveness in 18 counties out of 22, downscaled precipitation increased hedging effectiveness in 21 counties out of 22, and downscaled temperature increased hedging effectiveness in 8 counties out of 22.

Consequently, Wilcoxon test's results and boxplot of hedging effectiveness per country and index (Figure 4.7) also demonstrate that improvements in hedging effectiveness are significant in both countries after using downscaled climate data for index insurance design.

Since a higher hedging effectiveness corresponds to a lower basis risk and a higher potential for risk reduction, it can be concluded that index insurance products based on downscaled climate data have a lower basis risk and a higher potential for risk reduction than the original coarse spatial scale climate data. With reference to these results, the first objective of our study is addressed. With an

increasing spatial resolution of gridded climate data using machine learning, the hedging effectiveness of index insurance increases. Earlier similar outcomes were assumed by Möllmann et al. (2019), and similar results were obtained in the study conducted by Kölle et al. (2021), in which hedging effectiveness of index insurance based on medium and high resolution NDVI data were compared. Due to the increased number of pixels per area, a more accurate representation of climate conditions is possible, which is important for lowering the basis risk.

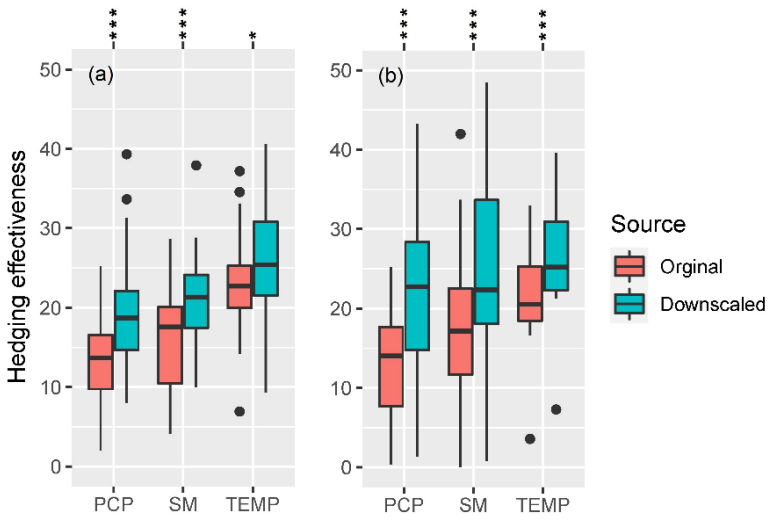

Figure 4.7: Boxplot and Wilcoxon test results for the hedging effectiveness of index insurance design based on original coarse resolution and downscaled climate data

Note: Counties in (a) Kazakhstan and (b) Mongolia. Statistical significance is indicated by the following p-values: *p≤0.05, ** p≤0.01, ***p≤0.001.

Source: compiled by the authors.

Retrieved from the published open-access article: Eltazarov, S., Bobojonov, I., Kuhn, L., Glauben, T. (2023): Improving risk reduction potential of weather index insurance by spatially downscaling gridded climate data - a machine learning approach. Big Earth Data.

As noted above, the hedging effectiveness of our three indices fluctuated considerably on a county level despite similar environmental conditions, a phenomenon that was also observed by Bucheli et al. (2021). These difference between the areas in term of most suitable index insurance can be due to variety of reasons, such as the type of farming systems, the intensity of crop management, management strategy and soil/seed quality (Kölle et al., 2021). Figure 4.8 demonstrates which source of climate data is the best for index insurance design to mitigate climate risk. According to our results, in Kazakhstan, the majority of counties have a higher hedging effectiveness when the index insurance design is based on downscaled temperature. Moreover, downscaled precipitation and original coarse resolution temperature have the highest hedging effectiveness in some cases, but the rest

only in a few cases. In the case of Mongolia, index insurance design based on downscaled precipitation and soil moisture data have the highest risk reduction potential in the majority of counties. The remaining data sources have demonstrated their potential only in rare cases.

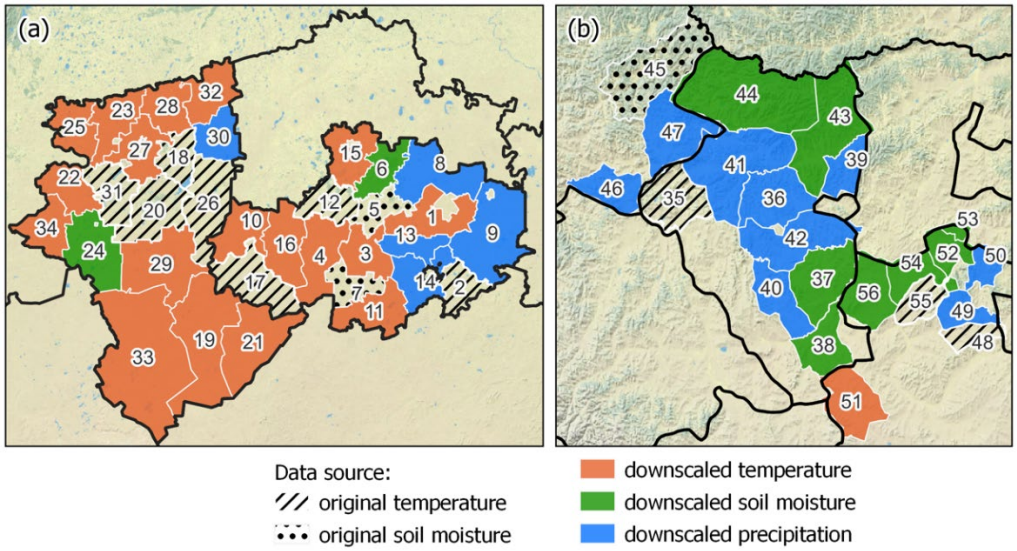

Figure 4.8: The best index insurance for each county according to hedging effectiveness

Note: Counties in (a) Kazakhstan and (b) Mongolia

Source: compiled by the authors.

Retrieved from the published open-access article: Eltazarov, S., Bobojonov, I., Kuhn, L., Glauben, T. (2023): Improving risk reduction potential of weather index insurance by spatially downscaling gridded climate data - a machine learning approach. Big Earth Data.

We see a potential to further refine the procedure of downscaling climate data for increasing hedging efficiency illustrated in this paper. For instance, including land cover/use information into index insurance design can obtain a significantly higher risk reduction capacity. However, the non-existence of long term and open source land cover/use information limits any potential benefits that might be obtained. Actually, there is a MODIS-based global scale land cover/use product. However, it has provided information since 2002 and has an accuracy of approximately 75-80 percent (Friedl and Sulla-Menashe, 2019). Moreover, our investigations showed that in the MODIS land cover/use product, the croplands identification has yet to be calibrated for Mongolia. Possible solution could be classifying land cover/use based on satellite images or requesting data from state cadaster organizations.

Furthermore, estimating agronomically suitable meteorological drought indices based on downscaled climate data and using them for index insurance design should also be considered for future studies, as they also can substantially improve the risk reduction potential of index insurance. The effectiveness of using meteorological drought indices for index insurance design have already

been confirmed by using weather station data by Bobojonov et al. (2014) and Finger (2013). Additionally, for future studies, it would also be interesting to compare the accuracy of index insurance product designs based on downscaled climate data with other climate data in fine spatial resolution with short historical records. Moreover, it would also be interesting to find at which points increases in hedging effectiveness are only marginal and not proportional in terms of findings training datasets.

It should be also noted that for our analysis we used county scale yield data. It would be also very interesting to shift the level of analysis to village or even farm level, as variation and heterogeneity of village-scale climate data increased after spatially downscaling them to finer resolution, according to our results from Local Moran's I[13] (see Table A.3.5 and A.3.6). Specifically, village and farm scale yield data could be based on ground level sensors from harvester combines. That would allow us to more deeply study the benefits of machine learning-based downscaling models for index insurance. Furthermore, having information about crop-cultivated areas, crop diversity, crop quality, fertilizers and re-seeding data would be also interesting, in order to inspect these factors on the hedging effectiveness of index insurance.

Moreover, descriptive statistics of variation of validation metrics and Wilcoxon test of county-wise validation metrics between improved and not improved insurance cases did not show significant differences (Figure A.3.7-11 and Table A.3.12-15). These results indicate that in our case the spatial accuracy of RF models do not influence the variation of improvements of hedging effectiveness. However, we believe having more detailed information about the study area, for instance on variation of topography, crop diversity, land use/cover and portion of croplands in the region would help to understand in more detail why effect of designing index insurance product based on downscaled climate parameters vary.

4.4. Conclusion

In this paper, we examined and compered the climate risk-reduction potential of index insurance design using machine learning-based spatially downscaled precipitation, temperature and soil moisture data with the original spatial resolution of gridded climate sources. We found that in the vast majority of cases, using downscaled climate data for index insurance design has increased their hedging effectiveness. These improvements are statistically significant for a case study of spring wheat in Kazakhstan and Mongolia. In general, index insurance design based on downscaled temperature in Kazakhstan and downscaled precipitation in Mongolia has the greatest risk-reduction potential. Additionally, our study demonstrates that each area has an individual most suitable underlying source of index to minimize basis risk. There is no single universal source of index that may assist well everywhere. Our results underline that an insurer should test multiple sources of indices during index insurance design and operation.

[13] Moran's I measures the spatial autocorrelation of a dataset that helps to identify how an object is similar to others surrounding it.

Moreover, within the framework of our study we have developed two R-packages, namely “climate-insurance” and web platform “Climate Insurance Design and Performance Analysis”, which help to rapidly design index insurance and to analyze the performance of index insurance using multiple statistical indicators. Since a web platform does not require any knowledge of statistics and only requires users to enter the data, we hope that it will ease further dissemination and implementation of index insurance for non-scientists who are in interested in the field of index insurance.

5. General concluding remarks and perspectives for future research

5.1. Summary of main findings

In general, weather extremes caused by climate change, which have occurred in the last decades have significantly affected the socio-economy of the region. Due to this, the governments of all countries are interested in introducing agricultural insurance schemes and have already initiated various activities towards this goal. However, the realization and dissemination of such plans are hindered by the high cost of traditional insurance and issues related to information asymmetry. Introducing index insurance in the region may assist in mitigating issues related to price and information asymmetry and secure agricultural producers against unexpected weather extremes. However, long-term and accurate weather data is required to design index insurance products and minimize the basis risk. Spatial analyses show that the density of weather stations in the region is insufficient to monitor weather variation in croplands and establish index insurance products in the vast majority of croplands in the region. Therefore, within the framework of this dissertation, the potential and feasibility of satellite-based data for index insurance development and implementation in the region have been investigated.

In the second chapter, the performance of satellite-based weather data to measure temperature and precipitation and their ability to detect extreme weather events has been studied. Our analysis indicates that selected satellite sources may provide the necessary data for an accessible and adequate climate service to develop and implement index insurance in the region. However, a considerable risk of overestimation and underestimation depending on the source of satellite data may exist, especially for precipitation data in the conditions of arid zones. Among the tested datasets, GSMaP showed a relatively better performance than CHIRPS in precipitation estimation for drought and flood detection. In order to reduce detection inaccuracy, the application of satellite weather products for index insurance is possible when temporal aggregation (e.g., monthly, seasonal) is considered.

In the third chapter, the potential accuracy gains from land-use classification that allow designing indices specifically for croplands and wheatlands have been analyzed. Moreover, the performance of less-recognized compared with well-known satellite-based indices to detect the variation of wheat yield in various farming systems was tested. The results show that the majority of selected indices are suitable for detecting wheat yield variations in rainfed and mixed agricultural lands, although they remain ambiguous for irrigated lands. Land-use classification and the design of indices based on croplands and wheatlands noticeably increase the relationship between indices and wheat yields in rainfed and mixed lands. Notably, the LAI and GCI outperform other well-known indices in detecting wheat yield variation.

In the fourth chapter, the effect of index insurance contracts based on spatially downscaled climate data for hedging crop yield has been investigated. Climate data with spatially coarse-resolution have been downscaled using finer-resolution satellite-based data and machine learning algorithms. The results show that in most cases (70%), the hedging effectiveness of index insurances increases when climate data is spatially downscaled. These improvements are statistically significant ($p \leq 0.05$).

Among other climate data, more improvements in hedging effectiveness have been observed when the insurance design is based on downscaled temperature and precipitation data.

5.2. Conclusions, policy implications and further research

Rising climate variability and unpredictability caused by climate change have been determined as key limitations for agricultural production and food security. To reduce climate-related risks for agricultural producers, index insurance could efficiently transfer risks from farmers to insurance companies. So far, in Central Asia and Mongolia, only limited research on index insurance has been conducted, which means that government policymakers and insurance companies still have a relatively low comprehension of index insurance. Moreover, farmers in the region also have a significant lack of awareness of how index insurance could assist them in mitigating and managing climate-related financial losses. This study illustrates the potential and feasibility of various index insurance products in many crop-growing regions of Central Asia and Mongolia. In general, the findings of this study are essential for improving the index insurance know-how of policymakers, insurance companies and farmers in the region.

The lack of high-quality weather and yield data is a dominant limiting factor for introducing and implementing index insurance in developing countries, which is also true for Central Asia and Mongolia. Therefore, the findings of this study are also relevant for insurance companies and international research communities, as they demonstrate the applicability of satellite-based data sources for index insurance design and operation in the region. Generally, satellite-based weather and vegetation data could serve as a good source to establish index insurance products in the region. Nevertheless, a careful assessment and selection of index, temporal aggregation, and land use classification by insurance companies remain essential. This study demonstrates that these criteria are sometimes regional specific and may differ significantly. The positive results from testing various less-known satellite-based data in the index insurance industry can encourage international research communities to discover and test other alternative satellite-based data sources to design and establish more accurate and reliable index insurance products. Moreover, this study highlights the reasonability and the benefits of downscaling climate data for insurance design and operation that needs to be taken into consideration by researchers and insurance companies in data-limited regions worldwide.

Index insurance is suggested as a solution for managing climate variability in agricultural production under climate change. However, this study highlights that there is lack of correlation between various indices and crop yield in some areas. In those areas, index insurance might not be a feasible solution to mitigate climate variability. Thus, in addition to index insurance, it would be more efficient and successful if policymakers also focused on alternative nature-based risk-management and climate adaptation solutions such as crop diversification, improving water-use efficiency, zero/reduced tillage farming, etc.

Moreover, within the framework of this dissertation, three web platforms and one R-package have been developed, which may help researchers and insurance companies to rapidly obtain satellite-

based data and design index insurance as well as analyze the performance of index insurance using multiple statistical indicators. Since web platforms do not require any knowledge of remote sensing and statistics and only require users to enter the data, there is hope that they will ease further dissemination and implementation of index insurance by insurance companies. Moreover, there is hope that the novel functions of these web platforms, such as data extraction only from croplands and analyzing the performance of index insurance products, will further disseminate the finding and outputs of this dissertation.

It is important to note that this study is limited to areas located in the arid and semi-arid climatic zones of Central Asia and Mongolia. It would also be interesting to investigate the accuracy and performance of this and other satellite-based data in similar and other climatic zones of neighboring countries. Moreover, within this study, the district/county scale crop yield data has been employed that may induce an aggregation bias, which means farm-level risks are likely underestimated. It would also be interesting to analyze the relationship between indices and crop yields at village or farm scale. Specifically, village and farm-scale yield data could be based on ground-level sensors from combine harvesters. This would allow for a deeper investigation of the capacity of satellite data for index insurance development and implementation. Furthermore, with sufficient information about crop-cultivated areas, crop diversity, crop quality, fertilizers and re-seeding data, it would also be interesting to examine the effects of these factors on the performance of satellite-based index insurance for climate risk reduction in the region.

References

Abbaszadeh, P., Moradkhani, H., Zhan, X., 2019. Downscaling SMAP Radiometer Soil Moisture Over the CONUS Using an Ensemble Learning Method. Water Resour. Res. 55, 324–344. https://doi.org/https://doi.org/10.1029/2018WR023354

ADB, 2013. Developing Water Resources Sector Strategies in Central and West Asia (Kyrgyz Republic): Final Report.

Alexakis, D.D., Tsanis, I.K., 2016. Comparison of multiple linear regression and artificial neural network models for downscaling TRMM precipitation products using MODIS data. Environ. Earth Sci. 75, 1077. https://doi.org/10.1007/s12665-016-5883-z

Allinsurance, 2018. Soil moisture deficit index insurance introduced in Kazakhstan [WWW Document]. URL https://allinsurance.kz/news/market-kaz/6533-v-kazakhstane-vnedreno-indeksnoe-agrostrakhovanie-defitsita-vlagi-v-pochve (accessed 10.3.19).

Ashouri, H., Hsu, K.-L., Sorooshian, S., Braithwaite, D.K., Knapp, K.R., Cecil, L.D., Nelson, B.R., Prat, O.P., 2014. PERSIANN-CDR: Daily Precipitation Climate Data Record from Multisatellite Observations for Hydrological and Climate Studies. Bull. Am. Meteorol. Soc. 96, 69–83. https://doi.org/10.1175/BAMS-D-13-00068.1

Báez-González, A.D., Chen, P.-Y., Tiscareño-López, M., Srinivasan, R., 2002. Using satellite and field data with crop growth modeling to monitor and estimate corn yield in Mexico. Crop Sci. 42, 1943–1949. https://doi.org/10.2135/cropsci2002.1943

Bai, J., Cui, Q., Zhang, W., Meng, L., 2019. An Approach for Downscaling SMAP Soil Moisture by Combining Sentinel-1 SAR and MODIS Data. Remote Sens. . https://doi.org/10.3390/rs11232736

Barnett, B.J., Barrett, C.B., Skees, J.R., 2008. Poverty Traps and Index-Based Risk Transfer Products. World Dev. 36, 1766–1785. https://doi.org/10.1016/J.WORLDDEV.2007.10.016

Barnett, B.J., Mahul, O., 2007. Weather index insurance for agriculture and rural areas in lower-income countries. Am. J. Agric. Econ. 89, 1241–1247. https://doi.org/10.1111/j.1467-8276.2007.01091.x

Bartkowiak, P., Castelli, M., Notarnicola, C., 2019. Downscaling Land Surface Temperature from MODIS Dataset with Random Forest Approach over Alpine Vegetated Areas. Remote Sens. 11. https://doi.org/10.3390/rs11111319

Bastola, S., Misra, V., 2014. Evaluation of dynamically downscaled reanalysis precipitation data for hydrological application. Hydrol. Process. 28, 1989–2002. https://doi.org/https://doi.org/10.1002/hyp.9734

Bauer, D.F., 1972. Constructing Confidence Sets Using Rank Statistics. J. Am. Stat. Assoc. 67, 687–690. https://doi.org/10.1080/01621459.1972.10481279

Beguería, S., Maintainer, S.M.V.-S., 2017. SPEI: Calculation of the Standardised Precipitation-Evapotranspiration Index. R Packag. version 1.17.

Benami, E., Jin, Z., Carter, M.R., Ghosh, A., Hijmans, R.J., Hobbs, A., Kenduiywo, B., Lobell, D.B., 2021. Uniting remote sensing, crop modelling and economics for agricultural risk management. Nat. Rev. Earth Environ. 2, 140–159. https://doi.org/10.1038/s43017-020-00122-y

Bezdan, J., Bezdan, A., Blagojević, B., Mesaroš, M., Pejič, B., Vraneševič, M., Pavič, D., Nikolič-Dorić, E., 2019. SPEI-based approach to agricultural drought monitoring in Vojvodina region. Water (Switzerland) 11. https://doi.org/10.3390/w11071481

Black, E., Greatrex, H., Young, M., Maidment, R., 2016a. Incorporating Satellite Data Into Weather

Index Insurance. Bull. Am. Meteorol. Soc. 97, ES203–ES206. https://doi.org/10.1175/BAMS-D-16-0148.1

Black, E., Tarnavsky, E., Maidment, R., Greatrex, H., Mookerjee, A., Quaife, T., Brown, M., 2016b. The Use of Remotely Sensed Rainfall for Managing Drought Risk: A Case Study of Weather Index Insurance in Zambia. Remote Sens. 8, 342. https://doi.org/10.3390/rs8040342

Bobojonov, I., Aw-Hassan, A., 2014. Impacts of climate change on farm income security in Central Asia: An integrated modeling approach. Agric. Ecosyst. Environ. 188, 245–255. https://doi.org/https://doi.org/10.1016/j.agee.2014.02.033

Bobojonov, I., Aw-Hassan, A., Sommer, R., 2014. Index-based insurance for climate risk management and rural development in Syria. Clim. Dev. 6, 166–178. https://doi.org/10.1080/17565529.2013.844676

Bobojonov, I., Berg, E., Franz-Vasdeki, J., Martius, C., Lamers, J.P.A., 2016. Income and irrigation water use efficiency under climate change: An application of spatial stochastic crop and water allocation model to Western Uzbekistan. Clim. Risk Manag. 13, 19–30. https://doi.org/https://doi.org/10.1016/j.crm.2016.05.004

Bobojonov, I., Kuhn, L., Moritz, L., Eltazarov, S., Glauben, T., 2019. Risk management tested in realistic simulation. Improving climate resilience through agricultural insurance - the KlimALEZ project, IAMO Annual 2019. Halle, Germany.

Bokusheva, R., 2018. Using copulas for rating weather index insurance contracts. J. Appl. Stat. 45, 2328–2356. https://doi.org/10.1080/02664763.2017.1420146

Bokusheva, R., Breustedt, G., 2012. The effectiveness of weather-based index insurance and area-yield crop insurance: How reliable are ex post predictions for yield risk reduction? Q. J. Int. Agric. 51, 135–156.

Bokusheva, R., Kogan, F., Vitkovskaya, I., Conradt, S., Batyrbayeva, M., 2016. Satellite-based vegetation health indices as a criteria for insuring against drought-related yield losses. Agric. For. Meteorol. 220, 200–206. https://doi.org/10.1016/J.AGRFORMET.2015.12.066

Brahm, M., Vila, D., Martinez Saenz, S., Osgood, D., 2019. Can disaster events reporting be used to drive remote sensing applications? A Latin America weather index insurance case study. Meteorol. Appl. 26, 632–641. https://doi.org/10.1002/met.1790

Breiman, A., Graur, D., 1995. WHEAT EVOLUTION. Isr. J. Plant Sci. 43, 85–98. https://doi.org/10.1080/07929978.1995.10676595

Breiman, L., 2001. Random Forests. Mach. Learn. 45, 5–32. https://doi.org/10.1023/A:1010933404324

Breustedt, G., Bokusheva, R., Heidelbach, O., 2008. Evaluating the Potential of Index Insurance Schemes to Reduce Crop Yield Risk in an Arid Region. J. Agric. Econ. 59, 312–328. https://doi.org/https://doi.org/10.1111/j.1477-9552.2007.00152.x

Broka, S., Giertz, Å., Christensen, G.N., Hanif, C.W., Rasmussen, D.L., 2016a. Tajikistan - Agricultural sector risk assessment (English). Washington DC, USA.

Broka, S., Giertz, Å., Christensen, G.N., Hanif, C.W., Rasmussen, D.L., Rubaiza, R., 2016b. Kyrgyz Republic - Agricultural sector risk assessment (English). Washington DC, USA.

Broka, S., Giertz, Å., Christensen, G.N., Rasmussen, D.L., Morgounov, A., Fileccia, T., Rubaiza, R., 2016c. Kazakhstan - Agricultural sector risk assessment (English). Washington DC, USA.

Bucheli, J., Dalhaus, T., Finger, R., 2021. The optimal drought index for designing weather index insurance. Eur. Rev. Agric. Econ. 48, 573–597. https://doi.org/10.1093/erae/jbaa014

Buchhorn, M., Lesiv, M., Tsendbazar, N.-E., Herold, M., Bertels, L., Smets, B., 2020. Copernicus

Global Land Cover Layers-Collection 2. Remote Sens. https://doi.org/10.3390/rs12061044

Cade, B.S., Noon, B.R., 2003. A Gentle Introduction to Quantile Regression for Ecologists. Front. Ecol. Environ. 1, 412–420. https://doi.org/10.2307/3868138

Chantarat, S., Barrett, C.B., Mude, A.G., Turvey, C.G., 2007. Using Weather Index Insurance to Improve Drought Response for Famine Prevention. Am. J. Agric. Econ. 89, 1262–1268. https://doi.org/10.1111/j.1467-8276.2007.01094.x

CHC, C.H.C., 2021. List of stations used [WWW Document]. Univ. California, St. Barbar. URL https://data.chc.ucsb.edu/products/CHIRPS-2.0/diagnostics/list_of_stations_used/monthly/ (accessed 7.31.21).

CHC, C.H.C., 2015. CHIRPS: Rainfall Estimates from Rain Gauge and Satellite Observations [WWW Document]. Univ. California, St. Barbar. URL https://www.chc.ucsb.edu/data/chirps (accessed 8.13.19).

Chen, C., Hu, B., Li, Y., 2021. Easy-to-use spatial random-forest-based downscaling-calibration method for producing precipitation data with high resolution and high accuracy. Hydrol. Earth Syst. Sci. 25, 5667–5682. https://doi.org/10.5194/hess-25-5667-2021

Chen, F., Gao, Y., Wang, Y., Qin, F., Li, X., 2019. Downscaling satellite-derived daily precipitation products with an integrated framework. Int. J. Climatol. 39, 1287–1304. https://doi.org/https://doi.org/10.1002/joc.5879

Chen, Q., Miao, F., Wang, H., Xu, Z.-X., Tang, Z., Yang, L., Qi, S., 2020. Downscaling of Satellite Remote Sensing Soil Moisture Products Over the Tibetan Plateau Based on the Random Forest Algorithm: Preliminary Results. Earth Sp. Sci. 7, e2020EA001265. https://doi.org/https://doi.org/10.1029/2020EA001265

Chen, X., Tian, G., Qin, Z., Bi, X., 2019. High Daytime and Nighttime Temperatures Exert Large and Opposing Impacts on Winter Wheat Yield in China. Weather. Clim. Soc. 11, 777–790. https://doi.org/10.1175/WCAS-D-19-0026.1

Chen, Y., Yang, K., Qin, J., Zhao, L., Tang, W., Han, M., 2013. Evaluation of AMSR-E retrievals and GLDAS simulations against observations of a soil moisture network on the central Tibetan Plateau. J. Geophys. Res. Atmos. 118, 4466–4475. https://doi.org/10.1002/jgrd.50301

Cheng, Q., 2006. Models for rice yield estimation using remote sensing data of MOD13. Nongye Gongcheng Xuebao/Transactions Chinese Soc. Agric. Eng. 22, 79–83.

Christmann, S., Martius, C., Bedoshvili, D., Bobojonov, I., Carli, C., Devkota, K., Ibragimov, Z., Khalikulov, Z., Kienzler, K.M., Manthrithilake, H., Mavlyanova, R., Mirzabaev, A., Nishanov, N., Sharma, R., Tashpulatova, B., Toderich, K., Turdieva, M., 2009. Food security and climate change in Central Asia and the Caucasus. Beirut, Lebanon.

Chu, W., Gao, X., Phillips, T.J., Sorooshian, S., 2011. Consistency of spatial patterns of the daily precipitation field in the western United States and its application to precipitation disaggregation. Geophys. Res. Lett. 38. https://doi.org/https://doi.org/10.1029/2010GL046473

Coleman, E., Dick, W., Gilliams, S., Piccard, I., Rispoli, F., Stoppa, A., 2018. Remote sensing for index insurance: Findings and lessons learned for smallholder agriculture.

Collier, B., Skees, J., Barnett, B., 2009. Weather index insurance and climate change: Opportunities and challenges in lower income countries. Geneva Pap. Risk Insur. Issues Pract. 401–424. https://doi.org/10.1057/gpp.2009.11

Conrad, C., Colditz, R.R., Dech, S., Klein, D., Vlek, P.L.G., 2011. Temporal segmentation of MODIS time series for improving crop classification in Central Asian irrigation systems. Int. J. Remote Sens. 32, 8763–8778. https://doi.org/10.1080/01431161.2010.550647

Conrad, C., Dech, S., Dubovyk, O., Fritsch, S., Klein, D., Löw, F., Schorcht, G., Zeidler, J., 2014. Derivation of temporal windows for accurate crop discrimination in heterogeneous croplands of Uzbekistan using multitemporal RapidEye images. Comput. Electron. Agric. 103, 63–74. https://doi.org/https://doi.org/10.1016/j.compag.2014.02.003

Conradt, S., Finger, R., Bokusheva, R., 2015. Tailored to the extremes: Quantile regression for index-based insurance contract design. Agric. Econ. (United Kingdom) 46, 537–547. https://doi.org/10.1111/agec.12180

Darand, M., Khandu, K., 2020. Statistical evaluation of gridded precipitation datasets using rain gauge observations over Iran. J. Arid Environ. 178, 104172. https://doi.org/https://doi.org/10.1016/j.jaridenv.2020.104172

de Beurs, K.M., Henebry, G.M., Owsley, B.C., Sokolik, I.N., 2018. Large scale climate oscillation impacts on temperature, precipitation and land surface phenology in Central Asia. Environ. Res. Lett. 13, 065018. https://doi.org/10.1088/1748-9326/aac4d0

De Leeuw, J., Vrieling, A., Shee, A., Atzberger, C., Hadgu, K.M., Biradar, C.M., Keah, H., Turvey, C., 2014. The Potential and Uptake of Remote Sensing in Insurance: A Review. Remote Sens. 6, 10888–10912.

De Pauw, E., 2008. ICARDA regional GIS datasets for Central Asia: Explanatory notes. GIS unit technical bulletin. Int. Cent. Agric. Res. Dry Areas.

Densambuu, B., Sainnemekh, S., Bestelmeyer, B., Ulambayar, B., 2015. National report on the rangeland health of Mongolia. Ulaanbaatar, Mongolia.

Dick, W., Stoppa, A., Anderson, J., Coleman, E., Rispoli, F., 2011. Weather index-based insurance in agricultural development: A technical guide. Int. Fund Agric. Dev. 18.

Didan, K., 2015. MOD13Q1 MODIS/Terra Vegetation Indices 16-Day L3 Global 250m SIN Grid V006 [Data set]. NASA EOSDIS Land Processes DAAC. [WWW Document]. https://doi.org/https://doi.org/10.5067/MODIS/MOD13Q1.006

Dinku, T., Funk, C., Peterson, P., Maidment, R., Tadesse, T., Gadain, H., Ceccato, P., 2018. Validation of the CHIRPS satellite rainfall estimates over eastern Africa. Q. J. R. Meteorol. Soc. 144, 292–312. https://doi.org/10.1002/qj.3244

Doraiswamy, P., Hollinger, S., Sinclair, T.R., Stern, A., Akhmedov, B., Prueger, J., 2002. Application of MODIS derived parameters for regional yield assessment. Proc. SPIE - Int. Soc. Opt. Eng. 4542, 1–8. https://doi.org/10.1117/12.454181

Dorigo, W., Wagner, W., Albergel, C., Albrecht, F., Balsamo, G., Brocca, L., Chung, D., Ertl, M., Forkel, M., Gruber, A., Haas, E., Hamer, P.D., Hirschi, M., Ikonen, J., de Jeu, R., Kidd, R., Lahoz, W., Liu, Y.Y., Miralles, D., Mistelbauer, T., Nicolai-Shaw, N., Parinussa, R., Pratola, C., Reimer, C., van der Schalie, R., Seneviratne, S.I., Smolander, T., Lecomte, P., 2017. ESA CCI Soil Moisture for improved Earth system understanding: State-of-the art and future directions. Remote Sens. Environ. 203, 185–215. https://doi.org/https://doi.org/10.1016/j.rse.2017.07.001

dos Santos, R.S., 2020. Estimating spatio-temporal air temperature in London (UK) using machine learning and earth observation satellite data. Int. J. Appl. Earth Obs. Geoinf. 88, 102066. https://doi.org/https://doi.org/10.1016/j.jag.2020.102066

Dou, Y., Huang, R., Mansaray, L.R., Huang, J., 2020. Mapping high temperature damaged area of paddy rice along the Yangtze River using Moderate Resolution Imaging Spectroradiometer data. Int. J. Remote Sens. 41, 471–486. https://doi.org/10.1080/01431161.2019.1643936

Dubovyk, O., Ghazaryan, G., González, J., Graw, V., Löw, F., Schreier, J., 2019. Drought hazard in Kazakhstan in 2000–2016: a remote sensing perspective. Environ. Monit. Assess. 191, 510. https://doi.org/10.1007/s10661-019-7620-z

Dzunusova, M., Apasov, R., Mammadov, A., 2008. The state of plant genetic resources for food and agriculture in Kyrgyzstan.

Edlinger, J., Conrad, C., Lamers, J., Khasankhanova, G., Koellner, T., 2012. Reconstructing the Spatio-Temporal Development of Irrigation Systems in Uzbekistan Using Landsat Time Series. Remote Sens. 4, 3972–3994. https://doi.org/10.3390/rs4123972

Elhag, K.M., Zhang, W., 2018. Monitoring and Assessment of Drought Focused on Its Impact on Sorghum Yield over Sudan by Using Meteorological Drought Indices for the Period 2001–2011. Remote Sens. 10, 1231.

Eltazarov, S., Bobojonov, I., Kuhn, L., Glauben, T., 2021. Mapping weather risk – A multi-indicator analysis of satellite-based weather data for agricultural index insurance development in semi-arid and arid zones of Central Asia. Clim. Serv. 23, 100251. https://doi.org/https://doi.org/10.1016/j.cliser.2021.100251

Enenkel, M, Farah, C., Hain, C., White, A., Anderson, M., You, L., Wagner, W., Osgood, D., 2018. What rainfall does not tell us-enhancing financial instruments with satellite-derived soil moisture and evaporative stress. Remote Sens. 10. https://doi.org/10.3390/rs10111819

Enenkel, Markus, Osgood, D., Anderson, M., Powell, B., McCarty, J., Neigh, C., Carroll, M., Wooten, M., Husak, G., Hain, C., Brown, M., 2018. Exploiting the Convergence of Evidence in Satellite Data for Advanced Weather Index Insurance Design. Weather. Clim. Soc. 11, 65–93. https://doi.org/10.1175/WCAS-D-17-0111.1

Enenkel, M., Osgood, D., Powell, B., 2017. The Added Value of Satellite Soil Moisture for Agricultural Index Insurance, in: Remote Sensing of Hydrometeorological Hazards. pp. 69–83. https://doi.org/10.1201/9781315154947-4

Eze, E., Girma, A., Zenebe, A.A., Zenebe, G., 2020. Feasible crop insurance indexes for drought risk management in Northern Ethiopia. Int. J. Disaster Risk Reduct. 47, 101544. https://doi.org/10.1016/J.IJDRR.2020.101544

Fang, B., Lakshmi, V., Cosh, M., Liu, P.-W., Bindlish, R., Jackson, T.J., 2022. A global 1-km downscaled SMAP soil moisture product based on thermal inertia theory. Vadose Zo. J. 21, e20182. https://doi.org/https://doi.org/10.1002/vzj2.20182

FAO, 2022. FAOSTAT [WWW Document]. URL https://www.fao.org/faostat/ (accessed 1.15.22).

FAO, 2021. Global Information and Early Warning System (Kyrgyzstan) [WWW Document]. URL http://www.fao.org/giews/countrybrief/country.jsp?code=KGZ&lang=en (accessed 6.10.21).

FAO, 2020. Global Information and Early Warning System (Mongolia) [WWW Document]. URL http://www.fao.org/giews/countrybrief/country.jsp?code=MNG&lang=en (accessed 6.10.21).

FAO, 2015. Climate change and food security: risks and responses. Rome, Italy.

FAO, UNICEF, 2023. Climate change and nutrition in Mongolia: a risk profile. Ulaanbaatar, Mongolia.

Fatkhuroyan, TrinahWati, 2018. Accuracy Assessment of Global Satellite Mapping of Precipitation (GSMaP) Product Over Indonesian Maritime Continent. IOP Conf. Ser. Earth Environ. Sci. 187, 12060. https://doi.org/10.1088/1755-1315/187/1/012060

Fehér, I., Lehota, J., Lakner, Z., Kende, Z., Bálint, C., Vinogradov, S., Fieldsend, A., 2017. Kazakhstan's Wheat Production Potential BT - The Eurasian Wheat Belt and Food Security: Global and Regional Aspects, in: Gomez y Paloma, S., Mary, S., Langrell, S., Ciaian, P. (Eds.), . Springer International Publishing, Cham, pp. 177–194. https://doi.org/10.1007/978-3-319-33239-0_11

Finger, R., 2013. Investigating the performance of different estimation techniques for crop yield

data analysis in crop insurance applications. Agric. Econ. 44, 217–230. https://doi.org/https://doi.org/10.1111/agec.12005

Fisher, E., Hellin, J., Greatrex, H., Jensen, N., 2019. Index insurance and climate risk management: Addressing social equity. Dev. Policy Rev. 37, 581–602. https://doi.org/10.1111/dpr.12387

Flatnes, J.E., Carter, M.R., 2016. Fail-safe index insurance without the cost: a satellite based conditional audit approach. Department of Agricultural and Resource Economics, University of California.

Friedl, M., Sulla-Menashe, D., 2019. MCD12Q1 MODIS/Terra+Aqua Land Cover Type Yearly L3 Global 500m SIN Grid V006 [Data set]. NASA EOSDIS Land Processes DAAC. [WWW Document]. https://doi.org/https://doi.org/10.5067/MODIS/MCD12Q1.006

Fu, Q., Ruan, R., Liu, Y., 2011. Accuracy Assessment of Global Satellite Mapping of Precipitation (GSMaP) Product over Poyang Lake Basin, China. Procedia Environ. Sci. 10, 2265–2271. https://doi.org/https://doi.org/10.1016/j.proenv.2011.09.354

Funk, C., Peterson, P., Landsfeld, M., Pedreros, D., Verdin, J., Shukla, S., Husak, G., Rowland, J., Harrison, L., Hoell, A., Michaelsen, J., 2015. The climate hazards infrared precipitation with stations—a new environmental record for monitoring extremes. Sci. Data 2, 150066. https://doi.org/10.1038/sdata.2015.66

Gerapetritis, H., Pelissier, J.M., 2004. The critical success index and warning strategy, in: 17th Conference on Probablity and Statistics in the Atmospheric Sciences, Seattle.

Ghamghami, M., Hejabi, S., Rahimi, J., Bazrafshan, J., Olya, H., 2017. Modeling a drought index using a nonparametric approach. Glob. Nest J. 19, 58–68.

Giné, X., Menand, L., Townsend, R., Vickery, J., 2010. Microinsurance: a case study of the Indian rainfall index insurance market, Policy Research Working Papers. The World Bank. https://doi.org/doi:10.1596/1813-9450-5459

Gitelson, A.A., Viña, A., Ciganda, V., Rundquist, D.C., Arkebauer, T.J., 2005. Remote estimation of canopy chlorophyll content in crops. Geophys. Res. Lett. 32. https://doi.org/10.1029/2005GL022688

Gommes, R., Göbel, W., 2013. Beyond simple, one-station rainfall indices, in: EC Joint Research Centre (JRC) (Ed.), The Challenges of Index-Based Insurance for Food Security in Developing Countries. International Research Institute for Climate and Society (IRI, Earth Institute, Columbia University), Milan, Italy, pp. 205–221.

Gorelick, N., Hancher, M., Dixon, M., Ilyushchenko, S., Thau, D., Moore, R., 2017. Google Earth Engine: Planetary-scale geospatial analysis for everyone. Remote Sens. Environ. 202, 18–27. https://doi.org/https://doi.org/10.1016/j.rse.2017.06.031

Greatrex, H., Hansen, J., Garvin, S., Diro, R., Blakeley, S., Le Guen, M., Rao, K., Osgood, D., 2015. Scaling up index insurance for smallholder farmers: Recent evidence and insights. Copenhagen, Denmark.

Grubbs, F.E., 1950. Sample Criteria for Testing Outlying Observations. Ann. Math. Stat. 21, 27–58.

GSFC DISC, G.E.S.D. and I.S.C., 2019. Atmospheric Composition, Water & Energy Cycles and Climate Variability [WWW Document]. Goddard Earth Sci. Data Inf. Serv. Cent. URL https://disc.gsfc.nasa.gov/ (accessed 8.20.20).

Gunst, L., Rego, F., Dias, S., Bifulco, C., Sttage, Rocha, M., Van Lanen, H., 2015. Links between meteorological drought indices and yields (1979-2009) of the main European crops. Wageningen University, Wageningen, The Nederlands.

Ha, W., Gowda, P.H., Howell, T.A., 2013. A review of downscaling methods for remote sensing-based irrigation management: part I. Irrig. Sci. 31, 831–850. https://doi.org/10.1007/s00271-

012-0331-7

Haag, I., Jones, P.D., Samimi, C., 2019. Central Asia's Changing Climate: How Temperature and Precipitation Have Changed across Time, Space, and Altitude. Climate 7. https://doi.org/10.3390/cli7100123

Hamidov, A., Helming, K., Balla, D., 2016. Impact of agricultural land use in Central Asia: a review. Agron. Sustain. Dev. 36, 6. https://doi.org/10.1007/s13593-015-0337-7

Hao, P., Wang, L., Zhan, Y., Wang, C., Niu, Z., Wu, M., 2016. Crop classification using crop knowledge of the previous-year: Case study in Southwest Kansas, USA. Eur. J. Remote Sens. 49, 1061–1077. https://doi.org/10.5721/EuJRS20164954

Hargreaves, G.H., Samani, Z.A., 1982. Estimating potential evapotranspiration. J. Irrig. Drain. Div. 108, 225–230.

Hazell, P., Anderson, J., Balzer, N., Hastrup Clemmensen, A., Hess, U., Rispoli, F., 2010. The potential for scale and sustainability in weather index insurance for agriculture and rural livelihoods. World Food Programme (WFP), Rome, Italy.

Hellmuth, M.E., Osgood, D.E., Hess, U., Moorhead, A., Bhojwani, H., 2009. Index insurance and climate risk: Prospects for development and disaster management. International Research Institute for Climate and Society (IRI), Columbia University, New York, USA.

Hersbach, H., Bell, B., Berrisford, P., Hirahara, S., Horányi, A., Muñoz-Sabater, J., Nicolas, J., Peubey, C., Radu, R., Schepers, D., Simmons, A., Soci, C., Abdalla, S., Abellan, X., Balsamo, G., Bechtold, P., Biavati, G., Bidlot, J., Bonavita, M., De Chiara, G., Dahlgren, P., Dee, D., Diamantakis, M., Dragani, R., Flemming, J., Forbes, R., Fuentes, M., Geer, A., Haimberger, L., Healy, S., Hogan, R.J., Hólm, E., Janisková, M., Keeley, S., Laloyaux, P., Lopez, P., Lupu, C., Radnoti, G., de Rosnay, P., Rozum, I., Vamborg, F., Villaume, S., Thépaut, J.-N., 2020. The ERA5 global reanalysis. Q. J. R. Meteorol. Soc. 146, 1999–2049. https://doi.org/https://doi.org/10.1002/qj.3803

Hessl, A.E., Anchukaitis, K.J., Jelsema, C., Cook, B., Byambasuren, O., Leland, C., Nachin, B., Pederson, N., Tian, H., Hayles, L.A., 2018. Past and future drought in Mongolia. Sci. Adv. 4, e1701832. https://doi.org/10.1126/sciadv.1701832

Hochrainer-Stigler, S., van der Velde, M., Fritz, S., Pflug, G., 2014a. Remote sensing data for managing climate risks: Index-based insurance and growth related applications for smallhold-farmers in Ethiopia. Clim. Risk Manag. 6, 27–38. https://doi.org/https://doi.org/10.1016/j.crm.2014.09.002

Hochrainer-Stigler, S., van der Velde, M., Fritz, S., Pflug, G., 2014b. Remote sensing data for managing climate risks: Index-based insurance and growth related applications for smallhold-farmers in Ethiopia. Clim. Risk Manag. 6, 27–38. https://doi.org/https://doi.org/10.1016/j.crm.2014.09.002

Hrisko, J., Ramamurthy, P., Gonzalez, J.E., 2021. Estimating heat storage in urban areas using multispectral satellite data and machine learning. Remote Sens. Environ. 252, 112125. https://doi.org/https://doi.org/10.1016/j.rse.2020.112125

Hu, F., Wei, Z., Zhang, W., Dorjee, D., Meng, L., 2020. A spatial downscaling method for SMAP soil moisture through visible and shortwave-infrared remote sensing data. J. Hydrol. 590, 125360. https://doi.org/https://doi.org/10.1016/j.jhydrol.2020.125360

Hu, Q., Yang, D., Wang, Y., Yang, H., 2013. Accuracy and spatio-temporal variation of high resolution satellite rainfall estimate over the Ganjiang River Basin. Sci. China Technol. Sci. 56, 853–865. https://doi.org/10.1007/s11431-013-5176-7

Huffman, G.J., Adler, R.F., Arkin, P., Chang, A., Ferraro, R., Gruber, A., Janowiak, J., McNab, A., Rudolf, B., Schneider, U., 1997. The Global Precipitation Climatology Project (GPCP)

Combined Precipitation Dataset. Bull. Am. Meteorol. Soc. 78, 5–20. https://doi.org/10.1175/1520-0477(1997)078<0005:TGPCPG>2.0.CO;2

Iliasov, S., Yakimov, V., 2009. The Kyrgyz Republic's Second National Communication to the United Nations Framework Convention on Climate Change. Bishkek, Kyrg. Repub. United Nations Dev. Program.

ILO, I.L.O., 2022. Mongolia: The Employment, Environment, Climate Nexus [Fact sheet].

Im, J., Park, S., Rhee, J., Baik, J., Choi, M., 2016. Downscaling of AMSR-E soil moisture with MODIS products using machine learning approaches. Environ. Earth Sci. 75, 1120. https://doi.org/10.1007/s12665-016-5917-6

IPCC, 2022. Climate Change 2022: Impacts, Adaptation and Vulnerability. Contribution of Working Group II to the Sixth Assessment Report of the Intergovernmental Panel on Climate Change. Cambridge, UK and New York, NY, USA. https://doi.org/doi:10.1017/9781009325844

Jarvis, A., Guevara, E., Reuter, H.I., Nelson, A.D., 2008. Hole-filled SRTM for the globe : version 4 : data grid [WWW Document]. CGIAR Consort. Spat. Inf. URL http://srtm.csi.cgiar.org/ (accessed 6.25.19).

JAXA G-Portal, 2019. Globe Portal System [WWW Document]. Japan Aerosp. Explor. Agency. URL http://www.gportal.jaxa.jp/ (accessed 8.15.19).

Ji, L., Senay, G.B., Verdin, J.P., 2015. Evaluation of the Global Land Data Assimilation System (GLDAS) Air Temperature Data Products. J. Hydrometeorol. 16, 2463–2480. https://doi.org/10.1175/JHM-D-14-0230.1

Jiang, J., Zhou, T., 2023. Agricultural drought over water-scarce Central Asia aggravated by internal climate variability. Nat. Geosci. 16, 154–161. https://doi.org/10.1038/s41561-022-01111-0

Kath, J., Mushtaq, S., Henry, R., Adeyinka, A.A., Stone, R., Marcussen, T., Kouadio, L., 2019. Spatial variability in regional scale drought index insurance viability across Australia's wheat growing regions. Clim. Risk Manag. 24, 13–29. https://doi.org/10.1016/j.crm.2019.04.002

Khalikulov, Z., Amanov, A., Sharma, R., Morgounov, A., 2016. The history of wheat breeding in Uzbekistan, in: The World Wheat Book: A History of Wheat Breeding. Paris, France, pp. 249–282.

Kimani, M.W., Hoedjes, J.C.B., Su, Z., 2018. Bayesian Bias Correction of Satellite Rainfall Estimates for Climate Studies. Remote Sens. . https://doi.org/10.3390/rs10071074

Koenker, R., Bassett, G., 1978. Regression Quantiles. Econometrica 46, 33–50. https://doi.org/10.2307/1913643

Kogan, F., Guo, W., Yang, W., Shannon, H., 2018. Space-based vegetation health for wheat yield modeling and prediction in Australia. J. Appl. Remote Sens. 12. https://doi.org/10.1117/1.JRS.12.026002

Kölle, W., Buchholz, M., Musshoff, O., 2021. Do high-resolution satellite indices at field level reduce basis risk of satellite-based weather index insurance? Agric. Financ. Rev. ahead-of-p. https://doi.org/10.1108/AFR-12-2020-0177

Kölle, W., Martínez Salgueiro, A., Buchholz, M., Musshoff, O., 2020. Can satellite-based weather index insurance improve the hedging of yield risk of perennial non-irrigated olive trees in Spain?*. Aust. J. Agric. Resour. Econ. n/a. https://doi.org/10.1111/1467-8489.12403

Konduri, V.S., Vandal, T.J., Ganguly, S., Ganguly, A.R., 2020. Data Science for Weather Impacts on Crop Yield . Front. Sustain. Food Syst. .

Kummerow, C., Simpson, J., Thiele, O., Barnes, W., Chang, A.T.C., Stocker, E., Adler, R.F., Hou, A., Kakar, R., Wentz, F., Ashcroft, P., Kozu, T., Hong, Y., Okamoto, K., Iguchi, T., Kuroiwa, H., Im,

E., Haddad, Z., Huffman, G., Ferrier, B., Olson, W.S., Zipser, E., Smith, E.A., Wilheit, T.T., North, G., Krishnamurti, T., Nakamura, K., 2000. The Status of the Tropical Rainfall Measuring Mission (TRMM) after Two Years in Orbit. J. Appl. Meteorol. 39, 1965–1982. https://doi.org/10.1175/1520-0450(2001)040<1965:TSOTTR>2.0.CO;2

Li, F., Miao, Y., Feng, G., Yuan, F., Yue, S., Gao, X., Liu, Y., Liu, B., Ustin, S.L., Chen, X., 2014. Improving estimation of summer maize nitrogen status with red edge-based spectral vegetation indices. F. Crop. Res. 157, 111–123. https://doi.org/https://doi.org/10.1016/j.fcr.2013.12.018

Li, F., Zhang, H., Jia, L., Bareth, G., Miao, Y., Chen, X., 2010. Estimating winter wheat biomass and nitrogen status using an active crop sensor. Intell. Autom. Soft Comput. 16, 1221–1230.

Li, H., Luo, Y., Xue, X., Zhao, Y., Zhao, H., Li, F., 2011. Estimating harvest index of winter wheat from canopy spectral reflectance information. J. Food, Agric. Environ. 9, 420–425.

Li, M., 2014. Moving Beyond the Linear Regression Model: Advantages of the Quantile Regression Model. J. Manage. 41, 71–98. https://doi.org/10.1177/0149206314551963

Liu, Y., Jing, W., Wang, Q., Xia, X., 2020. Generating high-resolution daily soil moisture by using spatial downscaling techniques: a comparison of six machine learning algorithms. Adv. Water Resour. 141, 103601. https://doi.org/https://doi.org/10.1016/j.advwatres.2020.103601

Liu, Y., Yang, Y., Jing, W., Yue, X., 2018. Comparison of Different Machine Learning Approaches for Monthly Satellite-Based Soil Moisture Downscaling over Northeast China. Remote Sens. . https://doi.org/10.3390/rs10010031

Logistics Cluster, 2021. Kyrgyzstan Humanitarian Background [WWW Document]. URL https://dlca.logcluster.org/display/public/DLCA/1.1+Kyrgyzstan+Humanitarian+Background (accessed 3.5.23).

López López, P., Immerzeel, W.W., Rodríguez Sandoval, E.A., Sterk, G., Schellekens, J., 2018. Spatial Downscaling of Satellite-Based Precipitation and Its Impact on Discharge Simulations in the Magdalena River Basin in Colombia. Front. Earth Sci. 6.

Maidment, R.I., Grimes, D., Allan, R.P., Tarnavsky, E., Stringer, M., Hewison, T., Roebeling, R., Black, E., 2014. The 30 year TAMSAT African Rainfall Climatology And Time series (TARCAT) data set. J. Geophys. Res. Atmos. 119, 10,610-619,644. https://doi.org/10.1002/2014JD021927

Makaudze, E.M., Miranda, M.J., 2010. Catastrophic drought insurance based on the remotely sensed normalised difference vegetation index for smallholder farmers in Zimbabwe. Agrekon 49, 418–432. https://doi.org/10.1080/03031853.2010.526690

McKee, T.B., Doesken, N.J., Kleist, J., 1993. The relationship of drought frequency and duration to time scales, in: Proceedings of the 8th Conference on Applied Climatology. Boston, pp. 179–183.

Mega, T., Ushio, T., Takahiro, M., Kubota, T., Kachi, M., Oki, R., 2019. Gauge-Adjusted Global Satellite Mapping of Precipitation. IEEE Trans. Geosci. Remote Sens. 57, 1928–1935. https://doi.org/10.1109/TGRS.2018.2870199

Miranda, M.J., Gonzalez-Vega, C., 2011. Systemic Risk, Index Insurance, and Optimal Management of Agricultural Loan Portfolios in Developing Countries. Am. J. Agric. Econ. 93, 399–406.

Mistele, B., Schmidhalter, U., 2008. Spectral measurements of the total aerial N and biomass dry weight in maize using a quadrilateral-view optic. F. Crop. Res. 106, 94–103. https://doi.org/https://doi.org/10.1016/j.fcr.2007.11.002

Möllmann, J., Buchholz, M., Musshoff, O., 2019. Comparing the Hedging Effectiveness of Weather Derivatives Based on Remotely Sensed Vegetation Health Indices and Meteorological Indices. Weather. Clim. Soc. 11, 33–48. https://doi.org/10.1175/WCAS-D-17-0127.1

Muradullayev, N., Bobojonov, I., Mustafaqulov, S., 2015. Current state and future prospects of crop insurance in Uzbekistan, in: Regional Economic Cooperation in Central Asia: Agricultural Production and Trade (ReCCA). Leibniz Institute of Agricultural Development in Transition Economies, Halle, Germany.

Musshoff, O., Odening, M., Xu, W., 2011. Management of climate risks in agriculture - will weather derivatives permeate? Appl. Econ. https://doi.org/10.1080/00036840802600210

Myneni, R., Knyazikhin, Y., Park, T., 2015. MCD15A3H MODIS/Terra+Aqua Leaf Area Index/FPAR 4-day L4 Global 500m SIN Grid V006 [Data set]. NASA EOSDIS Land Processes DAAC. [WWW Document]. https://doi.org/https://doi.org/10.5067/MODIS/MCD15A3H.006

Nash, J.E., Sutcliffe, J. V, 1970. River flow forecasting through conceptual models part I — A discussion of principles. J. Hydrol. 10, 282–290. https://doi.org/https://doi.org/10.1016/0022-1694(70)90255-6

NCEI, N.C. for E.I., 2019. Observational data map of daily weather stations networks from around the world [WWW Document]. URL https://gis.ncdc.noaa.gov/maps/ncei/cdo/daily (accessed 8.1.19).

Ndegwa, M.K., Shee, A., Turvey, C., You, L., 2022. Sequenced Crop Evapotranspiration and Water Requirement in Developing a Multitrigger Rainfall Index Insurance and Risk-Contingent Credit. Weather. Clim. Soc. 14, 19–38. https://doi.org/10.1175/WCAS-D-21-0071.1

Niles, M.T., Lubell, M., Brown, M., 2015. How limiting factors drive agricultural adaptation to climate change. Agric. Ecosyst. Environ. 200, 178–185. https://doi.org/https://doi.org/10.1016/j.agee.2014.11.010

Norton, M., Boucher, S., Verteramo Chiu, L., 2015. Geostatistics, Basis Risk, and Index Insurance. https://doi.org/10.22004/ag.econ.205755

Norton, M.T., Turvey, C., Osgood, D., 2012. Quantifying spatial basis risk for weather index insurance. J. Risk Financ. 14, 20–34. https://doi.org/10.1108/15265941311288086

Novella, N.S., Thiaw, W.M., 2012. African Rainfall Climatology Version 2 for Famine Early Warning Systems. J. Appl. Meteorol. Climatol. 52, 588–606. https://doi.org/10.1175/JAMC-D-11-0238.1

Odening, M., Mußhoff, O., Xu, W., 2007. Analysis of rainfall derivatives using daily precipitation models: Opportunities and pitfalls. Agric. Financ. Rev. 67, 135. https://doi.org/10.1108/00214660780001202

Okpara, J.N., Afiesimama, E.A., Anuforom, A.C., Owino, A., Ogunjobi, K.O., 2017. The applicability of Standardized Precipitation Index: drought characterization for early warning system and weather index insurance in West Africa. Nat. Hazards 89, 555–583. https://doi.org/10.1007/s11069-017-2980-6

Olesen, J.E., Trnka, M., Kersebaum, K.C., Skjelvåg, A.O., Seguin, B., Peltonen-Sainio, P., Rossi, F., Kozyra, J., Micale, F., 2011. Impacts and adaptation of European crop production systems to climate change. Eur. J. Agron. 34, 96–112. https://doi.org/https://doi.org/10.1016/j.eja.2010.11.003

Ortiz-Bobea, A., Wang, H., Carrillo, C.M., Ault, T.R., 2019. Unpacking the climatic drivers of US agricultural yields. Environ. Res. Lett. 14, 064003. https://doi.org/10.1088/1748-9326/ab1e75

Osgood, D., McLaurin, M., Carriquiry, M., Mishra, A., Fiondella, F., Hansen, J.W., Peterson, N., Ward, M.N., 2007. Designing Weather Insurance Contracts for Farmers in Malawi, Tanzania and Kenya: Final Report to the Commodity Risk Management Group, ARD, World Bank. New York, USA. https://doi.org/10.7916/D88P66DJ

Osgood, D., Powell, B., Diro, R., Farah, C., Enenkel, M., Brown, M., Husak, G., Blakeley, S., Hoffman, L., McCarty, J., 2018. Farmer Perception, Recollection, and Remote Sensing in Weather Index Insurance: An Ethiopia Case Study. Remote Sens. 10, 1887. https://doi.org/10.3390/rs10121887

Paliwal, A., Jain, M., 2020. The Accuracy of Self-Reported Crop Yield Estimates and Their Ability to Train Remote Sensing Algorithms. Front. Sustain. Food Syst. 4.

Panek, E., Gozdowski, D., 2020. Analysis of relationship between cereal yield and NDVI for selected regions of Central Europe based on MODIS satellite data. Remote Sens. Appl. Soc. Environ. 17, 100286. https://doi.org/10.1016/j.rsase.2019.100286

Patrick, E., 2017. Drought characteristics and management in Central Asia and Turkey, FAO Water Reports. Food and Agriculture Organization of the United Nations, Rome, Italy.

Peng, F., Zhao, S., Chen, C., Cong, D., Wang, Y., Ouyang, H., 2020. Evaluation and comparison of the precipitation detection ability of multiple satellite products in a typical agriculture area of China. Atmos. Res. 236, 104814. https://doi.org/https://doi.org/10.1016/j.atmosres.2019.104814

Petropoulos, G.P., Islam, T., 2017. Remote Sensing of Hydrometeorological Hazards. CRC Press. https://doi.org/https://doi.org/10.1201/9781315154947

Pietola, K., Myyra, S., Niemi, J.K., Van Asseldonk, M.A.P.M., 2011. Insure or Invest in Green Technologies to Protect Against Adverse Weather Events?, MTT Discussion Papers. https://doi.org/ISNN 1795-5300

Potts, J.M., Folland, C.K., Jolliffe, I.T., Sexton, D., 1996. Revised "LEPS" Scores for Assessing Climate Model Simulations and Long-Range Forecasts. J. Clim. 9, 34–53. https://doi.org/10.1175/1520-0442(1996)009<0034:RSFACM>2.0.CO;2

Powell, J.P., Reinhard, S., 2016. Measuring the effects of extreme weather events on yields. Weather Clim. Extrem. 12, 69–79. https://doi.org/https://doi.org/10.1016/j.wace.2016.02.003

R Development Core Team, 2018. R: a Language and Environment for Statistical Computing. R Foundation for Statistical Computing.

Rakhmatova, N., Arushanov, M., Shardakova, L., Nishonov, B., Taryannikova, R., Rakhmatova, V., Belikov, D.A., 2021. Evaluation of the Perspective of ERA-Interim and ERA5 Reanalyses for Calculation of Drought Indicators for Uzbekistan. Atmosphere (Basel). https://doi.org/10.3390/atmos12050527

Raksapatcharawong, M., Veerakachen, W., Homma, K., Maki, M., Oki, K., 2020. Satellite-based drought impact assessment on rice yield in Thailand with SIMRIW-RS. Remote Sens. 12. https://doi.org/10.3390/rs12132099

Rao, G.P., 2011. Climate Change Adaptation Strategies in Agriculture and Allied Sectors. Scientific Publishers, Valencia, CA, USA.

Ray, D.K., Gerber, J.S., MacDonald, G.K., West, P.C., 2015. Climate variation explains a third of global crop yield variability. Nat. Commun. 6, 5989. https://doi.org/10.1038/ncomms6989

Reddy, M.V., Mitra, Ashis K, Momin, I.M., Mitra, Ashim K, Pai, D.S., 2019. Evaluation and inter-comparison of high-resolution multi-satellite rainfall products over India for the southwest monsoon period. Int. J. Remote Sens. 40, 4577–4603. https://doi.org/10.1080/01431161.2019.1569786

Rivera, J.A., Marianetti, G., Hinrichs, S., 2018. Validation of CHIRPS precipitation dataset along the Central Andes of Argentina. Atmos. Res. 213, 437–449. https://doi.org/https://doi.org/10.1016/j.atmosres.2018.06.023

Rodell, M., Houser, P.R., Jambor, U., Gottschalck, J., Mitchell, K., Meng, C.-J., Arsenault, K., Cosgrove, B., Radakovich, J., Bosilovich, M., Entin, J.K., Walker, J.P., Lohmann, D., Toll, D., 2004. The Global Land Data Assimilation System. Bull. Am. Meteorol. Soc. 85, 381–394. https://doi.org/10.1175/bams-85-3-381

Salehnia, N., Zare, H., Kolsoumi, S., Bannayan, M., 2018. Predictive value of Keetch-Byram Drought Index for cereal yields in a semi-arid environment. Theor. Appl. Climatol. 134, 1005–1014. https://doi.org/10.1007/s00704-017-2315-2

Schaefer, J.T., 1990. The Critical Success Index as an Indicator of Warning Skill. Weather Forecast. 5, 570–575. https://doi.org/10.1175/1520-0434(1990)005<0570:TCSIAA>2.0.CO;2

Schierhorn, F., Hofmann, M., Gagalyuk, T., Ostapchuk, I., Müller, D., 2021. Machine learning reveals complex effects of climatic means and weather extremes on wheat yields during different plant developmental stages. Clim. Change 169, 39. https://doi.org/10.1007/s10584-021-03272-0

Semenov, M.A., Porter, J.R., 1995. Climatic variability and the modelling of crop yields. Agric. For. Meteorol. 73, 265–283. https://doi.org/https://doi.org/10.1016/0168-1923(94)05078-K

Setiyono, T.D., Quicho, E.D., Gatti, L., Campos-Taberner, M., Busetto, L., Collivignarelli, F., García-Haro, F.J., Boschetti, M., Khan, N.I., Holecz, F., 2018. Spatial rice yield estimation based on MODIS and Sentinel-1 SAR data and ORYZA crop growth model. Remote Sens. 10. https://doi.org/10.3390/rs10020293

Seyyedi, H., Anagnostou, E.N., Beighley, E., McCollum, J., 2014. Satellite-driven downscaling of global reanalysis precipitation products for hydrological applications. Hydrol. Earth Syst. Sci. 18, 5077–5091. https://doi.org/10.5194/hess-18-5077-2014

Shamanin, V., Salina, E., Wanyera, R., Zelenskiy, Y., Olivera, P., Morgounov, A., 2016. Genetic diversity of spring wheat from Kazakhstan and Russia for resistance to stem rust Ug99. Euphytica 212, 287–296. https://doi.org/10.1007/s10681-016-1769-0

Sharifi, E., Saghafian, B., Steinacker, R., 2019. Downscaling Satellite Precipitation Estimates With Multiple Linear Regression, Artificial Neural Networks, and Spline Interpolation Techniques. J. Geophys. Res. Atmos. 124, 789–805. https://doi.org/https://doi.org/10.1029/2018JD028795

Shen, Z., Yong, B., 2021. Downscaling the GPM-based satellite precipitation retrievals using gradient boosting decision tree approach over Mainland China. J. Hydrol. 602. https://doi.org/https://doi.org/10.1016/j.jhydrol.2021.126803

Shen, Z., Yong, B., Gourley, J.J., Qi, W., Lu, D., Liu, J., Ren, L., Hong, Y., Zhang, J., 2020. Recent global performance of the Climate Hazards group Infrared Precipitation (CHIRP) with Stations (CHIRPS). J. Hydrol. 591, 125284. https://doi.org/https://doi.org/10.1016/j.jhydrol.2020.125284

Shirsath, P.B., Sehgal, V.K., Aggarwal, P.K., 2020. Downscaling regional crop yields to local scale using remote sensing. Agric. 10. https://doi.org/10.3390/agriculture10030058

Siebert, A., 2016. Analysis of Index Insurance Potential for Adaptation to Hydroclimatic Risks in the West African Sahel. Weather. Clim. Soc. 8, 265–283. https://doi.org/10.1175/WCAS-D-15-0040.1

Sinha, S., Tripathi, N.K., 2016. Hybrid satellite agriculture drought indices: A multi criteria approach to improve crop insurance, in: 2016 Fifth International Conference on Agro-Geoinformatics (Agro-Geoinformatics). pp. 1–5. https://doi.org/10.1109/Agro-Geoinformatics.2016.7577664

Smith, V., Watts, M., 2009. Index based agricultural insurance in developing countries: Feasibility, scalability and sustainability. Gates Found. 1–40.

Sorooshian, S., Hsu, K.-L., Gao, X., Gupta, H. V, Imam, B., Braithwaite, D., 2000. Evaluation of

PERSIANN System Satellite-Based Estimates of Tropical Rainfall. Bull. Am. Meteorol. Soc. 81, 2035–2046. https://doi.org/10.1175/1520-0477(2000)081<2035:EOPSSE>2.3.CO;2

Srivastava, P.K., Han, D., Ramirez, M.R., Islam, T., 2013. Machine Learning Techniques for Downscaling SMOS Satellite Soil Moisture Using MODIS Land Surface Temperature for Hydrological Application. Water Resour. Manag. 27, 3127–3144. https://doi.org/10.1007/s11269-013-0337-9

StataCorp, 2019. Stata Statistical Software: Release 16.

Stephenson, D.B., 2000. Use of the "Odds Ratio" for Diagnosing Forecast Skill. Weather Forecast. 15, 221–232. https://doi.org/10.1175/1520-0434(2000)015<0221:UOTORF>2.0.CO;2

Sutton, W.R., Srivastava, J.P., Neumann, J.E., Droogers, P., Boehlert, B.B., 2013. Reducing the vulnerability of Uzbekistan's agricultural systems to climate change : impact assessment and adaptation options (English). Washington DC, USA.

Tadesse, M.A., Shiferaw, B.A., Erenstein, O., 2015. Weather index insurance for managing drought risk in smallholder agriculture: lessons and policy implications for sub-Saharan Africa. Agric. Food Econ. 3. https://doi.org/10.1186/s40100-015-0044-3

Tang, K., Zhu, H., Ni, P., 2021. Spatial Downscaling of Land Surface Temperature over Heterogeneous Regions Using Random Forest Regression Considering Spatial Features. Remote Sens. 13. https://doi.org/10.3390/rs13183645

Tarnavsky, E., Chavez, E., Boogaard, H., 2018. Agro-meteorological risks to maize production in Tanzania: Sensitivity of an adapted Water Requirements Satisfaction Index (WRSI) model to rainfall. Int. J. Appl. Earth Obs. Geoinf. 73, 77–87. https://doi.org/10.1016/J.JAG.2018.04.008

Tarnavsky, E., Grimes, D., Maidment, R., Black, E., Allan, R.P., Stringer, M., Chadwick, R., Kayitakire, F., 2014. Extension of the TAMSAT Satellite-Based Rainfall Monitoring over Africa and from 1983 to Present. J. Appl. Meteorol. Climatol. 53, 2805–2822. https://doi.org/10.1175/JAMC-D-14-0016.1

Teluguntla, P.G., Thenkabail, P.S., Xiong, J., Gumma, M.K., Giri, C., Milesi, C., Ozdogan, M., Congalton, R., Tilton, J., Sankey, T.T., 2015. Global cropland area database (GCAD) derived from remote sensing in support of food security in the twenty-first century: current achievements and future possibilities, in: Land Resources: Monitoring, Modelling, and Mapping, Remote Sensing Handbook. CRC Press.

Thiemig, V., Rojas, R., Zambrano-Bigiarini, M., Levizzani, V., De Roo, A., 2012. Validation of Satellite-Based Precipitation Products over Sparsely Gauged African River Basins. J. Hydrometeorol. 13, 1760–1783. https://doi.org/10.1175/JHM-D-12-032.1

Todisco, F., Vergni, L., Mannocchi, F., 2008. An evaluation of some drought indices in the monitoring and prediction of agricultural drought impact in central Italy. Irrig. Mediterr. Agric. challenges Innov. next Decad.

Tolipov, H., Solokov, V., 2022. Uzbekistan Country Survey Report: Draft concept for revision the national action program to combat drought and land degradation in republic of Uzbekistan. Tashkent.

Trabucco, A., Zomer, R., 2019. Global Aridity Index and Potential Evapotranspiration (ET0) Climate Database v2. https://doi.org/10.6084/m9.figshare.7504448.v3

Trinh-Tuan, L., Matsumoto, J., Ngo-Duc, T., Nodzu, M.I., Inoue, T., 2019. Evaluation of satellite precipitation products over Central Vietnam. Prog. Earth Planet. Sci. 6, 54. https://doi.org/10.1186/s40645-019-0297-7

Turvey, C.G., McLaurin, M.K., 2012. Applicability of the normalized difference vegetation index (NDVI) In index-based crop insurance design. Weather. Clim. Soc. 4, 271–284.

https://doi.org/10.1175/WCAS-D-11-00059.1

Tuvdendorj, B., Wu, B., Zeng, H., Batdelger, G., Nanzad, L., 2019. Determination of Appropriate Remote Sensing Indices for Spring Wheat Yield Estimation in Mongolia. Remote Sens. 11. https://doi.org/10.3390/rs11212568

UNDP, U.N.D.P., 2016. UNDP moves on to pursue indemnity and index insurance to secure Kazakh farmers [WWW Document]. URL http://www.kz.undp.org/content/kazakhstan/en/home/presscenter/pressreleases/2016/05/03/undp-moves-on-to-pursue-indemnity-and-index-insurance-to-secure-kazakh-farmers.html (accessed 10.3.19).

USDA, U.S.D. of A., 2022. Wheat Explorer [WWW Document]. URL https://ipad.fas.usda.gov/cropexplorer/cropview/commodityView.aspx?cropid=0410000 (accessed 11.15.22).

USGCRP, U.S.G.C.R.P., 2017. Climate Science Special Report: Fourth National Climate Assessment, Volume I. Washington, DC, USA. https://doi.org/10.7930/J0J964J6

Usman, M., Nichol, J.E., 2020. A Spatio-Temporal Analysis of Rainfall and Drought Monitoring in the Tharparkar Region of Pakistan. Remote Sens. 12, 580. https://doi.org/10.3390/rs12030580

Uzhydromet, C. of H.S. of U., 2008. Center of Hydrometeorological Service of Uzbekistan (Uzhydromet) [WWW Document]. URL https://www.meteo.uz/#/en/about (accessed 5.2.19).

Valverde-Arias, O., Esteve, P., María Tarquis, A., Garrido, A., 2020. Remote sensing in an index-based insurance design for hedging economic impacts on rice cultivation. Nat. Hazards Earth Syst. Sci. 20, 345–362. https://doi.org/10.5194/nhess-20-345-2020

Valverde-Arias, O., Garrido, A., Saa-Requejo, A., Carreño, F., Tarquis, A.M., 2018. Agro-ecological variability effects on an index-based insurance design for extreme events. Geoderma 337, 1341–1350. https://doi.org/10.1016/j.geoderma.2018.10.043

Van Khanh Triet, N., Viet Dung, N., Merz, B., Apel, H., 2018. Towards risk-based flood management in highly productive paddy rice cultivation-concept development and application to the Mekong Delta. Nat. Hazards Earth Syst. Sci. 18, 2859–2876. https://doi.org/10.5194/nhess-18-2859-2018

Vedenov, D. V, Barnett, B.J., 2004. Efficiency of Weather Derivatives as Primary Crop Insurance Instruments. J. Agric. Resour. Econ. 29, 387–403.

Vermote, E., 2015. MOD09A1 MODIS/Terra Surface Reflectance 8-Day L3 Global 500m SIN Grid V006 [Data set]. NASA EOSDIS Land Processes DAAC. [WWW Document]. https://doi.org/https://doi.org/10.5067/MODIS/MOD09A1.006

Vicente-Serrano, S., Cuadrat-Prats, J.M., Romo, A., 2006. Early prediction of crop production using drought indices at different time-scales and remote sensing data: Application in the Ebro Valley (north-east Spain). Int. J. Remote Sens. 27, 511–518. https://doi.org/10.1080/01431160500296032

Vicente-Serrano, S.M., Beguería, S., López-Moreno, J.I., 2010. A Multiscalar Drought Index Sensitive to Global Warming: The Standardized Precipitation Evapotranspiration Index. J. Clim. 23, 1696–1718. https://doi.org/10.1175/2009jcli2909.1

Vicente-Serrano, S.M., Beguería, S., Lorenzo-Lacruz, J., Camarero, J.J., López-Moreno, J.I., Azorin-Molina, C., Revuelto, J., Morán-Tejeda, E., Sanchez-Lorenzo, A., 2012. Performance of Drought Indices for Ecological, Agricultural, and Hydrological Applications. Earth Interact. 16, 1–27. https://doi.org/10.1175/2012ei000434.1

Vila, D.A., de Goncalves, L.G.G., Toll, D.L., Rozante, J.R., 2009. Statistical Evaluation of Combined

Daily Gauge Observations and Rainfall Satellite Estimates over Continental South America. J. Hydrometeorol. 10, 533–543. https://doi.org/10.1175/2008JHM1048.1

Vroege, W., Bucheli, J., Dalhaus, T., Hirschi, M., Finger, R., 2021. Insuring crops from space: the potential of satellite-retrieved soil moisture to reduce farmers' drought risk exposure. Eur. Rev. Agric. Econ. 48, 266–314. https://doi.org/10.1093/erae/jbab010

Wan, Z., Hook, S., Hulley, G., 2015. MOD11A2 MODIS/Terra Land Surface Temperature/Emissivity 8-Day L3 Global 1km SIN Grid V006 [Data set]. NASA EOSDIS Land Processes DAAC. [WWW Document]. https://doi.org/https://doi.org/10.5067/MODIS/MOD11A2.006

Wanders, N., Van Loon, A.F., Van Lanen, H.A.J., 2017. Frequently used drought indices reflect different drought conditions on global scale. Hydrol. Earth Syst. Sci. Discuss. 2017, 1–16. https://doi.org/10.5194/hess-2017-512

Wang, C., Lin, W., 2005. Winter wheat yield estimation based on MODIS EVI. Nongye Gongcheng Xuebao/Transactions Chinese Soc. Agric. Eng. 21, 90–94.

Wang, M., Tao, F.-L., Shi, W.-J., 2014. Corn yield forecasting in northeast china using remotely sensed spectral indices and crop phenology metrics. J. Integr. Agric. 13, 1538–1545. https://doi.org/10.1016/S2095-3119(14)60817-0

Wang, W., Cui, W., Wang, X., Chen, X., 2016. Evaluation of GLDAS-1 and GLDAS-2 Forcing Data and Noah Model Simulations over China at the Monthly Scale. J. Hydrometeorol. 17, 2815–2833. https://doi.org/10.1175/JHM-D-15-0191.1

Wang, X., Müller, C., Elliot, J., Mueller, N.D., Ciais, P., Jägermeyr, J., Gerber, J., Dumas, P., Wang, C., Yang, H., Li, L., Deryng, D., Folberth, C., Liu, W., Makowski, D., Olin, S., Pugh, T.A.M., Reddy, A., Schmid, E., Jeong, S., Zhou, F., Piao, S., 2021. Global irrigation contribution to wheat and maize yield. Nat. Commun. 12, 1235. https://doi.org/10.1038/s41467-021-21498-5

Webber, H., Ewert, F., Olesen, J.E., Müller, C., Fronzek, S., Ruane, A.C., Bourgault, M., Martre, P., Ababaei, B., Bindi, M., Ferrise, R., Finger, R., Fodor, N., Gabaldón-Leal, C., Gaiser, T., Jabloun, M., Kersebaum, K.-C., Lizaso, J.I., Lorite, I.J., Manceau, L., Moriondo, M., Nendel, C., Rodríguez, A., Ruiz-Ramos, M., Semenov, M.A., Siebert, S., Stella, T., Stratonovitch, P., Trombi, G., Wallach, D., 2018. Diverging importance of drought stress for maize and winter wheat in Europe. Nat. Commun. 9, 4249. https://doi.org/10.1038/s41467-018-06525-2

Westerhold, A., Walters, C., Brooks, K., Vandeveer, M., Volesky, J., Schacht, W., 2018. Risk implications from the selection of rainfall index insurance intervals. Agric. Financ. Rev. 78, 514–531. https://doi.org/10.1108/AFR-10-2017-0097

Willmott, C.J., 1981. On the validation of models. Phys. Geogr. 2, 184–194. https://doi.org/10.1080/02723646.1981.10642213

WMO, W.M.O., 2021. Weather-related disasters increase over past 50 years, causing more damage but fewer deaths [WWW Document]. URL https://public.wmo.int/en/media/press-release/weather-related-disasters-increase-over-past-50-years-causing-more-damage-fewer (accessed 11.18.22).

World Bank, 2023. Tajikistan - Vulnerability [WWW Document]. URL https://climateknowledgeportal.worldbank.org/country/tajikistan/vulnerability (accessed 2.5.23).

World Bank, 2015. Achievements in ACP Countries by Global Index Insurance Facility (GIIF) Program : Phase 1 (2010–2015) (English). World Bank Group, Washington DC, USA.

World Bank, 2011. Weather index insurance for agriculture : guidance for development practitioners (English). World Bank Group, Washington DC, USA.

World Bank, 2005. Drought: Management and Mitigation Assessment for Central Asia and the

Caucasus: Regional and Country Profiles and Strategies.

Xie, P., Arkin, P.A., 1997. Global Precipitation: A 17-Year Monthly Analysis Based on Gauge Observations, Satellite Estimates, and Numerical Model Outputs. Bull. Am. Meteorol. Soc. 78, 2539–2558. https://doi.org/10.1175/1520-0477(1997)078<2539:GPAYMA>2.0.CO;2

Xu, W., Odening, M., Musshoff, O., 2008. Indifference Pricing of Weather Derivatives. Am. J. Agric. Econ. 90, 979–993.

Yan, X., Chen, H., Tian, B., Sheng, S., Wang, J., Kim, J.-S., 2021. A Downscaling–Merging Scheme for Improving Daily Spatial Precipitation Estimates Based on Random Forest and Cokriging. Remote Sens. 13. https://doi.org/10.3390/rs13112040

Yang, Y., Cao, C., Pan, X., Li, X., Zhu, X., 2017. Downscaling Land Surface Temperature in an Arid Area by Using Multiple Remote Sensing Indices with Random Forest Regression. Remote Sens. 9. https://doi.org/10.3390/rs9080789

Yeh, N.-C., Chuang, Y.-C., Peng, H.-S., Hsu, K.-L., 2020. Bias Adjustment of Satellite Precipitation Estimation Using Ground-Based Observation: Mei-Yu Front Case Studies in Taiwan. Asia-Pacific J. Atmos. Sci. 56, 485–492. https://doi.org/10.1007/s13143-019-00152-7

Yu, C., Hu, D., Liu, M., Wang, S., Di, Y., 2020. Spatio-temporal accuracy evaluation of three high-resolution satellite precipitation products in China area. Atmos. Res. 241, 104952. https://doi.org/https://doi.org/10.1016/j.atmosres.2020.104952

Yu, Q., You, L., Wood-Sichra, U., Ru, Y., Joglekar, A.K.B., Fritz, S., Xiong, W., Lu, M., Wu, W., Yang, P., 2020. A cultivated planet in 2010 – Part 2: The global gridded agricultural-production maps. Earth Syst. Sci. Data 12, 3545–3572. https://doi.org/10.5194/essd-12-3545-2020

Zanaga, D., Van De Kerchove, R., De Keersmaecker, W., Souverijns, N., Brockmann, C., Quast, R., Wevers, J., Grosu, A., Paccini, A., Vergnaud, S., Cartus, O., Santoro, M., Fritz, S., Georgieva, I., Lesiv, M., Carter, S., Herold, M., Li, L., Tsendbazar, N.-E., Ramoino, F., Arino, O., 2021. ESA WorldCover 10 m 2020 v100. https://doi.org/10.5281/ZENODO.5571936

Zhang, H., Immerzeel, W.W., Zhang, F., de Kok, R.J., Gorrie, S.J., Ye, M., 2021. Creating 1-km long-term (1980–2014) daily average air temperatures over the Tibetan Plateau by integrating eight types of reanalysis and land data assimilation products downscaled with MODIS-estimated temperature lapse rates based on machine learning. Int. J. Appl. Earth Obs. Geoinf. 97, 102295. https://doi.org/https://doi.org/10.1016/j.jag.2021.102295

Zhang, H., Wang, S., Liu, K., Li, X., Li, Z., Zhang, X., Liu, B., 2022. Downscaling of AMSR-E Soil Moisture over North China Using Random Forest Regression. ISPRS Int. J. Geo-Information 11. https://doi.org/10.3390/ijgi11020101

Zhang, J., Tian, H., Wang, P., Tansey, K., Zhang, S., Li, H., 2022. Improving wheat yield estimates using data augmentation models and remotely sensed biophysical indices within deep neural networks in the Guanzhong Plain, PR China. Comput. Electron. Agric. 192, 106616. https://doi.org/https://doi.org/10.1016/j.compag.2021.106616

Zhang, M., Chen, Y., Shen, Y., Li, B., 2019. Tracking climate change in Central Asia through temperature and precipitation extremes. J. Geogr. Sci. 29, 3–28. https://doi.org/10.1007/s11442-019-1581-6

Zhang, S., Lei, Y., Wang, L., Li, H., Zhao, H., 2011. Crop classification using MODIS NDVI data denoised by wavelet: A case study in Hebei Plain, China. Chinese Geogr. Sci. 21, 322. https://doi.org/10.1007/s11769-011-0472-2

Zhu, W., Lű, A., Jia, S., Yan, J., Mahmood, R., 2017. Retrievals of all-weather daytime air temperature from MODIS products. Remote Sens. Environ. 189, 152–163. https://doi.org/https://doi.org/10.1016/j.rse.2016.11.011

Appendix

Appendix 1: Mapping weather risk: A multi-indicator analysis of satellite-based weather data for agricultural index insurance development in semi-arid and arid zones of Central Asia[14]

Appendix 1.1: Distance from meteorological station to crop fields

The figure also demonstrates the distance from the cropland to the station where non-active stations were removed from the dataset. There are 252 active stations with various historical records in Central Asia, and the majority of the active stations are located in croplands. Nevertheless, as it is demonstrated in Figure A.1.1.1, the diversity of stations is very low: only 0.4% of croplands are located within a 5-kilometer distance to a station, 1.1% of croplands are located within a 5- to 10-kilometre distance, 1.7% of croplands are located within a 1- to 15-kilometre distance, and 2.2% of croplands are located within a 15-to 20-kilometre distance to stations.

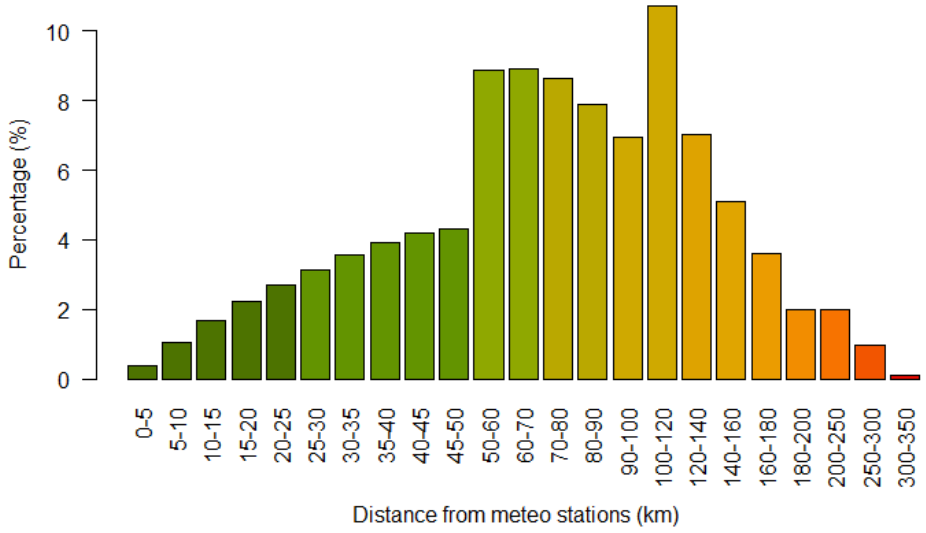

Figure A.1.1.1. Percentage of cropland located at different distances from meteorological stations. Source: author's calculation

Appendix 1.2: Literature review on application of satellite-based land cover data

Hochrainer-Stigler et al. (2014) have explored the applicability and usefulness of index insurance for smallholder farmers in North Shewa, Ethiopia. They found a satisfactory relationship between NOAA Advanced Very High Resolution Radiometer (NOAA AVHRR)-based Vegetation Health Index (VHI) and crop yield that allows for the identification of trigger points for claim payments and premium

[14] This appendix was published as part of the following open-access article: Eltazarov, S., Bobojonov, I., Kuhn, L., Glauben, T. (2021): Mapping weather risk – A multi-indicator analysis of satellite-based weather data for agricultural index insurance development in semi-arid and arid zones of Central Asia. Climate Service, 23, 100251. https://doi.org/10.1016/j.cliser.2021.100251

calculation on a promotion and protection-level. Bokusheva et al. (2016) have analyzed the applicability of NOAA AVHRR-based Vegetation Condition Index (VCI) and Temperature Condition Index (TCI) to insure yield losses of wheat-producing farms in Kazakhstan; they employed different capula approaches and concluded that VH indices can be a solid basis for detecting drought-related yield losses and implementing index insurance on a district scale. Sinha & Tripathi (2016) have investigated the usefulness of hybrid satellite agriculture drought indices to improve rice index insurance in Thailand; they combined LANDSAT-based Normalized Difference Vegetation Index (NDVI), Land Surface Temperature (LST) and Temperature Vegetation Index (TVI) to produce a unique hybrid index and identified significant potential to assess drought impact on a district scale when there is a shortage of long-term historical data. Flatnes & Carter (2016) have used plot-level rice yields in Tanzania to analyze the efficiency contract, by using a Moderate Resolution Imaging Spectroradiometer (MODIS)-based NDVI-based index insurance as a primary index which also contains the possibility for famers to request an audit if the primary index fails to predict yields; according to the results, by using this method it is possible to eliminate design risk at a very modest cost, which is useful for the future of index-based insurance in developing countries. Coleman et al. (2018) have used village-scale groundnut, millet and maize yield data in Senegal to review and examine the applicability and ways of using European Remote Sensing (ERS)-based Soil Moisture, METOP Advanced Scatterometer (ASCAT)-based Soil Water Index (SWI), MODIS-based Actual Evapotranspiration (ETa), METEOSAT-based Relative Evapotranspiration (ETr), SPOT/PROBA-based NDVI and SPOT/PROBA-based Fraction of Absorbed Photosynthetically Active Radiation (fAPAR) in designing index insurance; they concluded that satellites are operationally feasible for agricultural index insurance and developed several recommendations to deal with challenges and improve the quality of the index insurance. Osgood et al. (2018) have tested the cross-consistency of community-level farmers-reported drought years in Ethiopia against independent satellite data sources such as MODIS-NDVI, MODIS-based Enhanced Vegetation Index (EVI), The Atmosphere Land Exchange Inverse (ALEXI)-based Evapotranspiration (ET), and European Space Agency (ESA)-based Soil Moisture; they found evidence that events reported by farmer are independently reflected in satellite datasets. Eze et al. (2020) have examined MODIS-NDVI to design area-specific yield index insurance in Ethiopia; their results demonstrated that designed indexes performed very well when payout conditions were evaluated in recent drought years.

Appendix 1.3: Need for satellite weather data usage

Introducing low-cost insurance schemes like index insurance or other types of agricultural index-based insurances in the region would help to make small farmers more resilient to climate variabilities and uncertainties. A variable and unpredictable climate significantly restricts the options of farmers and so limits their development (Rao, 2011). As farmers avoid taking risks, there is a possibility of weather shocks. Moreover, creditors are also uneasy to lend if droughts or floods could cause widespread defaults, and when farmers are not insured. For farmers, not having access to credits critically limits their use of agricultural inputs and technologies. Even if a drought or flood happens only once in five or six years, the threat of the phenomenon is sufficient to slow down the

economic development and wealth growth in all those years. Therefore, based on our study, we recommend the implementation of satellite-based index insurance in the regions, which might solve some of the existing issues for farmers regarding credits and investment into improved seeds and fertilizers. Using satellite products for design and implementation will significantly lower the price of the insurance and decrease the issues related to weather data, as weather data is an essential component of index insurance design and its sustainability. Moreover, satellite-based index insurance will improve the information asymmetry between the insurance company and the insured farmer, as none of them can influence the pre-defined index. This minimizes adverse selection and problems of moral peril frequently encountered in traditional agricultural insurances (Fisher et al., 2019; World Bank, 2015). In addition, there is a great basis risk when the density of stations is very low, as is the case in Central Asia. Using satellite-based weather data for index insurance design will minimize the basis risk. Employing satellite-based weather data will also significantly reduce product and administrative costs, which offers the potential for lower premiums, as satellite-based weather data is free of charge, and index insurance does not require field visits to assess losses reported by farmers.

Appendix 1.4: Location of selected meteo stations

The agro-climatic class of the locations was identified according to De Pauw (2008); accordingly, stations are located either in arid or semi-arid agro-climatic zones. All data has been received in paper form and manually digitized.

Table A.1.4.1: List and details of meteorological stations

Name	Province	Country	Latitude	Longitude	Elevation	Agro-climatic Zone
Djizzakh	Djizzakh	Uzbekistan	40.117	67.833	345	SA-C-W[15]
Gallaral	Djizzakh	Uzbekistan	40	67.6	571	SA-K-W[16]
Lalmikor	Djizzakh	Uzbekistan	39.9	67.5	744	SA-K-W[16]
Samarkand	Samarkand	Uzbekistan	39.57	66.95	485	SA-C-W[15]
Karshi	Kashkadarya	Uzbekistan	38.8	65.717	376	A-K-VW[17]
Takhtakupir	Karakalpakstan Republic	Uzbekistan	43.01	60.27	59	A-K-W[18]

Appendix 1.5: Review of existing globally available precipitation data

Every satellite-based precipitation estimate (SPE) product has its own advantages and disadvantages in terms of accuracy, near-real time data availability, spatial resolution, temporal resolution, historical time coverage, land surface coverage, complexity of acquisition and processing of the satellite data. For the most part, weather data from satellite products is freely available in 5 to 50 kilometre

[15] SA-C-W: Semi-arid, cool winter, warm summer

[16] SA-K-W: Semi-arid, cold winter, warm summer

[17] A-K-VW: Arid, cool winter, very warm summer

[18] A-K-W: Arid, cool winter, warm summer

spatial resolution and in daily, decadal, monthly, seasonal and annual scales. For example, the Tropical Application of Meteorology Using Satellite Data (TAMSAT) produces daily rainfall estimates for the entire African continent at 4 km spatial resolution, and its archive spans a period from 1983 to the delayed present (Maidment et al., 2014; Tarnavsky et al., 2014). The NOAA-based African Rainfall Climatology Version 2 (ARC2) consist of daily rainfall estimates from 1983 to nearly real time at 0.1° spatial resolution for the whole African continent (Novella and Thiaw, 2012). The Historical Database for Gridded Daily Precipitation Dataset over Latin America (LatAmPrec) provides daily rainfall estimates for the entire South American continent at 0.25° spatial resolution, and has a temporal coverage from 2000 to the near present (Vila et al., 2009). The Tropical Rainfall Measuring Mission (TRMM) generates 3-hourly rainfall estimates from 2000 to the near present at 0.25° spatial resolution for the latitudes 60S - 60N (Kummerow et al., 2000). The Precipitation Estimation from Remotely Sensed Information using Artificial Neural Networks - Cloud Classification System (PERSIANN-CCS) contains daily rainfall estimates from 1983 until the near present at 0.25° spatial resolution for the latitudes 60S - 60N (Ashouri et al., 2014; Sorooshian et al., 2000). The NOAA CDR Climate Prediction Center morphing technique (CMORPH) produces daily rainfall estimates for the latitudes 60S - 60N from 2002 to the present at a 30-minute temporal resolution and 0.07° spatial resolution. The Global Precipitation Climatology Project (GPCP) provides monthly rainfall estimates from 1979 to the delayed present for the whole world, at 2.5° spatial resolution (Huffman et al., 1997). The CPC Merged Analysis of Precipitation (CMAP) produces monthly and pentadal rainfall estimates at 2.5° spatial resolution from 1978 to the delayed present for the whole world (Xie and Arkin, 1997) . The Climate Hazards Group InfraRed Precipitation with Station (CHIRPS) provides semi-global daily, pentadal, decadal and monthly rainfall estimates, covering the 50°S-50°N latitudes at 0.05° spatial resolution from 1981 to the near present (Funk et al., 2015). The Global Satellite Mapping of Precipitation (GSMaP) generates global 1-hourly precipitation estimates at 0.1° spatial resolution from 2000 to near real time (Ushio et al., 2009).

Appendix 1.6: Satellite Remote Sensing data acquisition, online free platform

One of the main disadvantages of using satellite products in index insurance is the fact that acquisition and processing of satellite products require special technical skills that are highly problematic for the insurance market. In this study, we therefore aimed to develop a user-friendly web platform which allows obtaining data from satellite products for everyone who has an access to the internet. In order to obtain CHIRPS, GSMaP and GLDAS data on a daily scale, we developed an algorithm and programmed one unique automatic web platform using the Google Earth Engine (GEE). GEE is an open source platform for satellite imagery analysis and geospatial datasets on a planetary scale. GEE aims to increase quality and time efficiency of spatial analyses for research, business and government users (Gorelick et al., 2017). This platform allows for satellite image analysis in the cloud system of the server, which in turn allows for the minimalization of several steps in satellite image analyses and the production of final outputs.

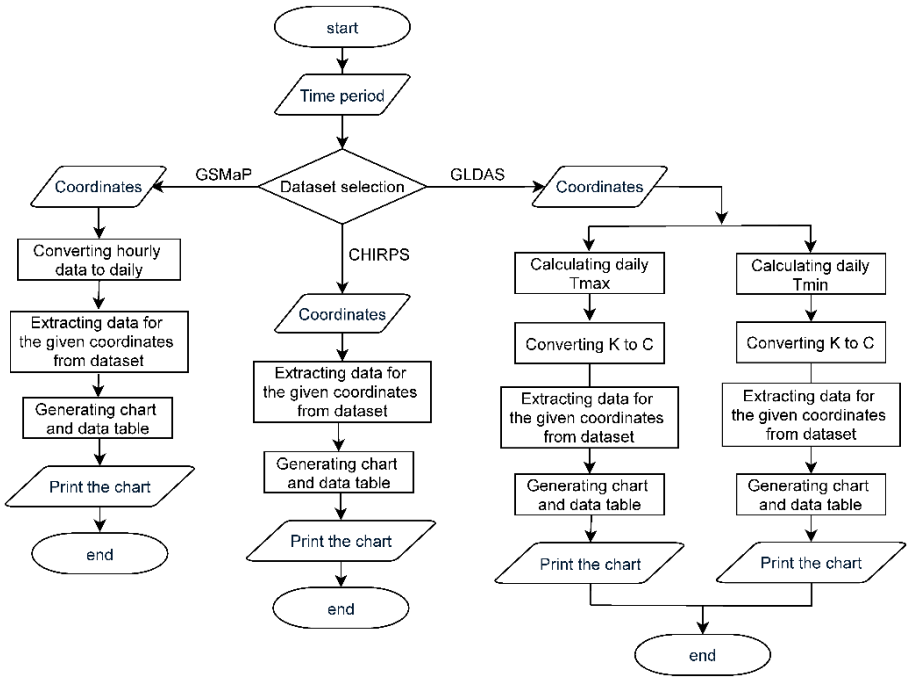

Figure A.1.6.1: Flowchart of the developed automatic web platforms for extracting daily remote sensing data from (a) CHIRPS, (b) GSMaP and (c) GLDAS. Source: Authors' own presentations

Figure demonstrates the algorithm for how data is obtained from existing daily GSMaP precipitation data from original hourly data, daily GLDAS maximum temperature (Tmax) and minimum temperature (Tmin) data from original 3-hourly data, and CHIRPS data originally in daily scale.

A web platform was developed for an automatic point scale daily data acquisition process and to be made available for interested parties in open access, as it does not require any knowledge of remote sensing data acquisition and processing. The web platform requires the user to enter a time period and the desired coordinates. The coordinates can be inserted by entering them manually or by clicking the area of interest on the map. The web platform produces the daily GSMaP precipitation data from the original hourly data, daily GLDAS maximum temperature (Tmax) and minimum temperature (Tmin) data from the original 3-hourly data, and CHIRPS data originally in daily scale. The GLDAS air temperature data are originally in Kelvin units. The unit was converted to Celsius to be in line with the meteorological data. Decadal and monthly data were produced from daily data.

Appendix 1.7: Visualization of monthly precipitation and temperature data for remaining 5 stations.

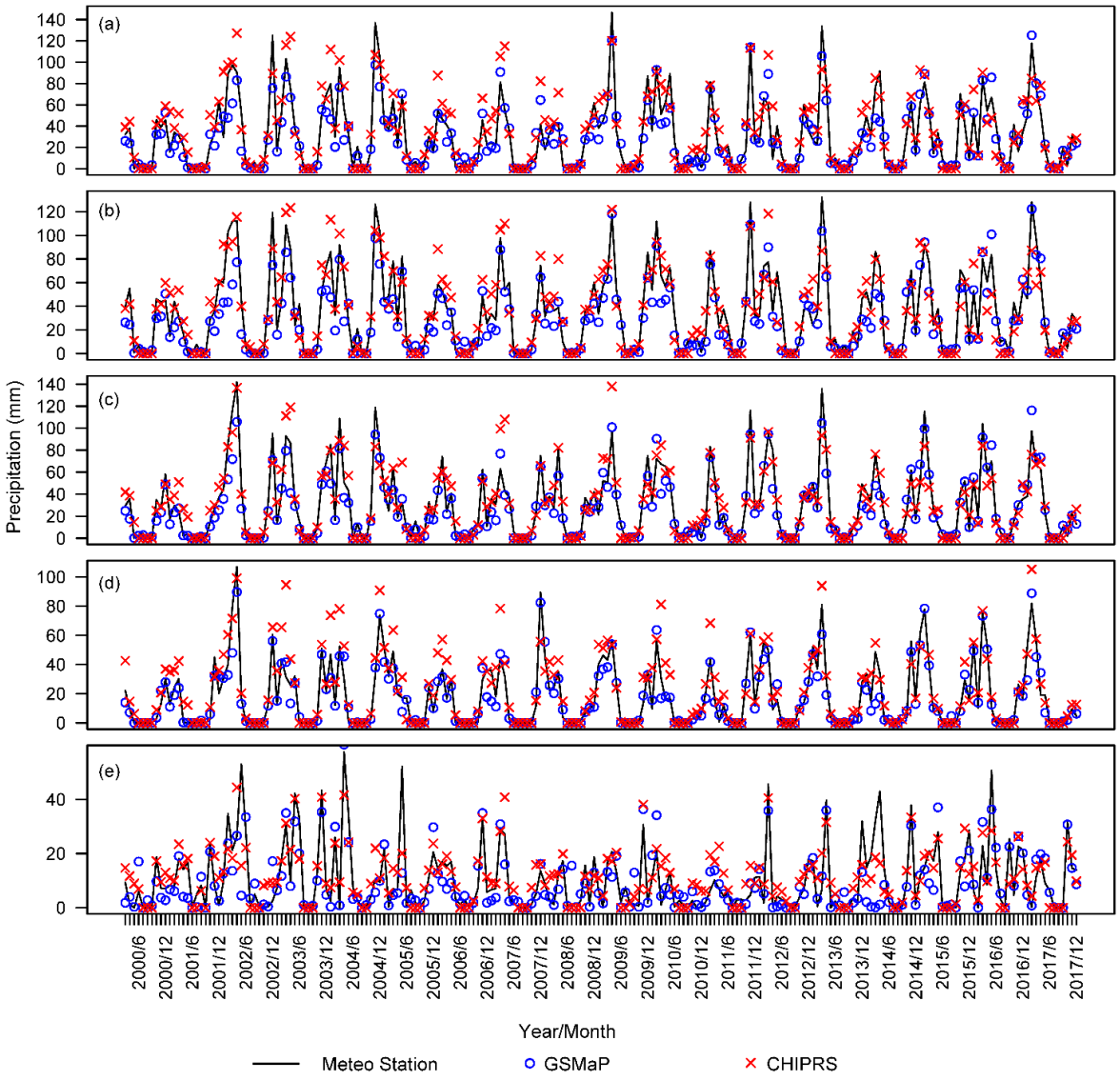

Figure A.1.7.1: Monthly precipitation by stations, GSMaP and CHIRPS in selected locations (a) Gallaral, (b) Lalmikor, (c) Samarkand, (d) Karshi and (e) Takhtakupir

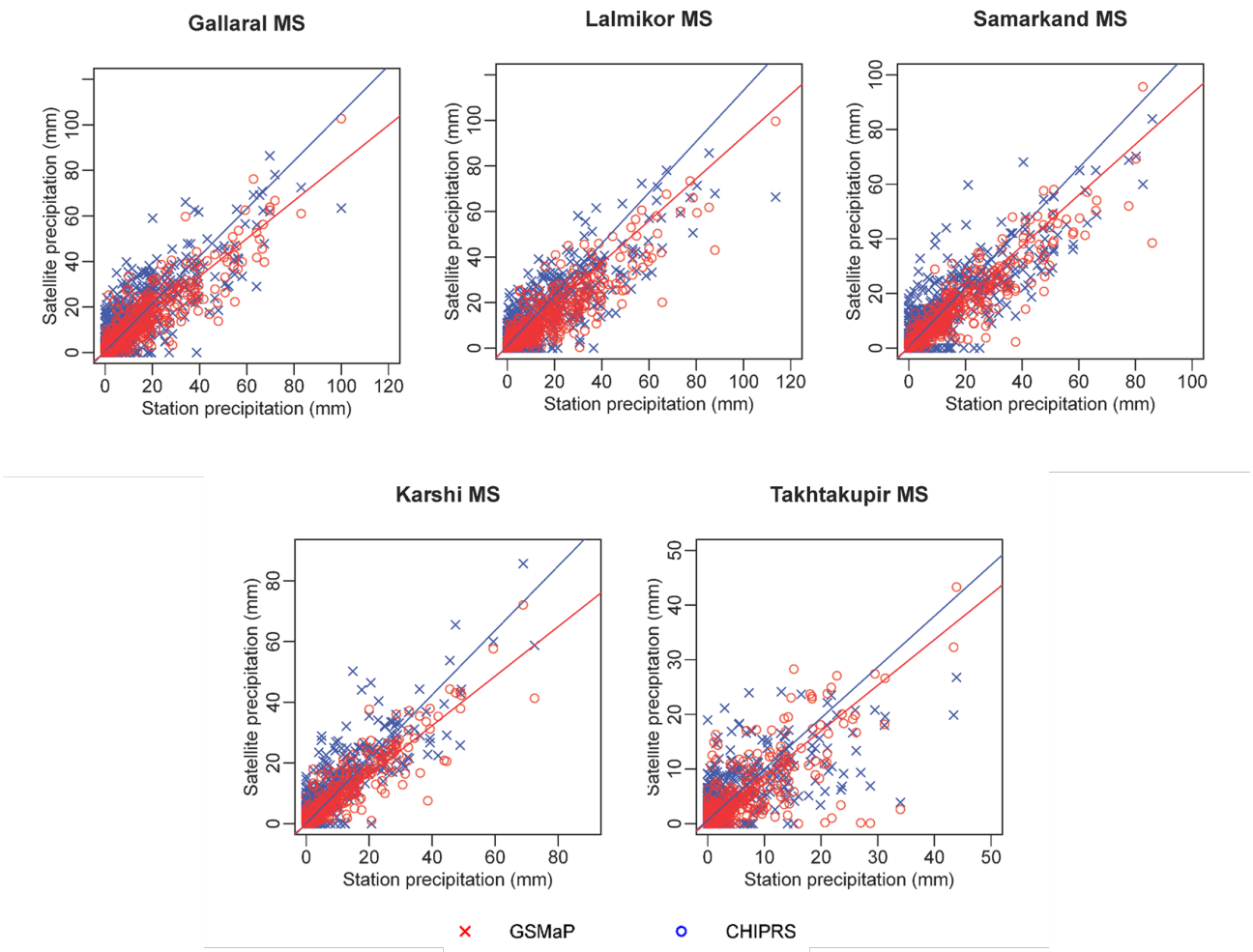

Figure A.1.7.2: Decadal precipitation by stations vs GSMaP and CHIRPS in selected locations

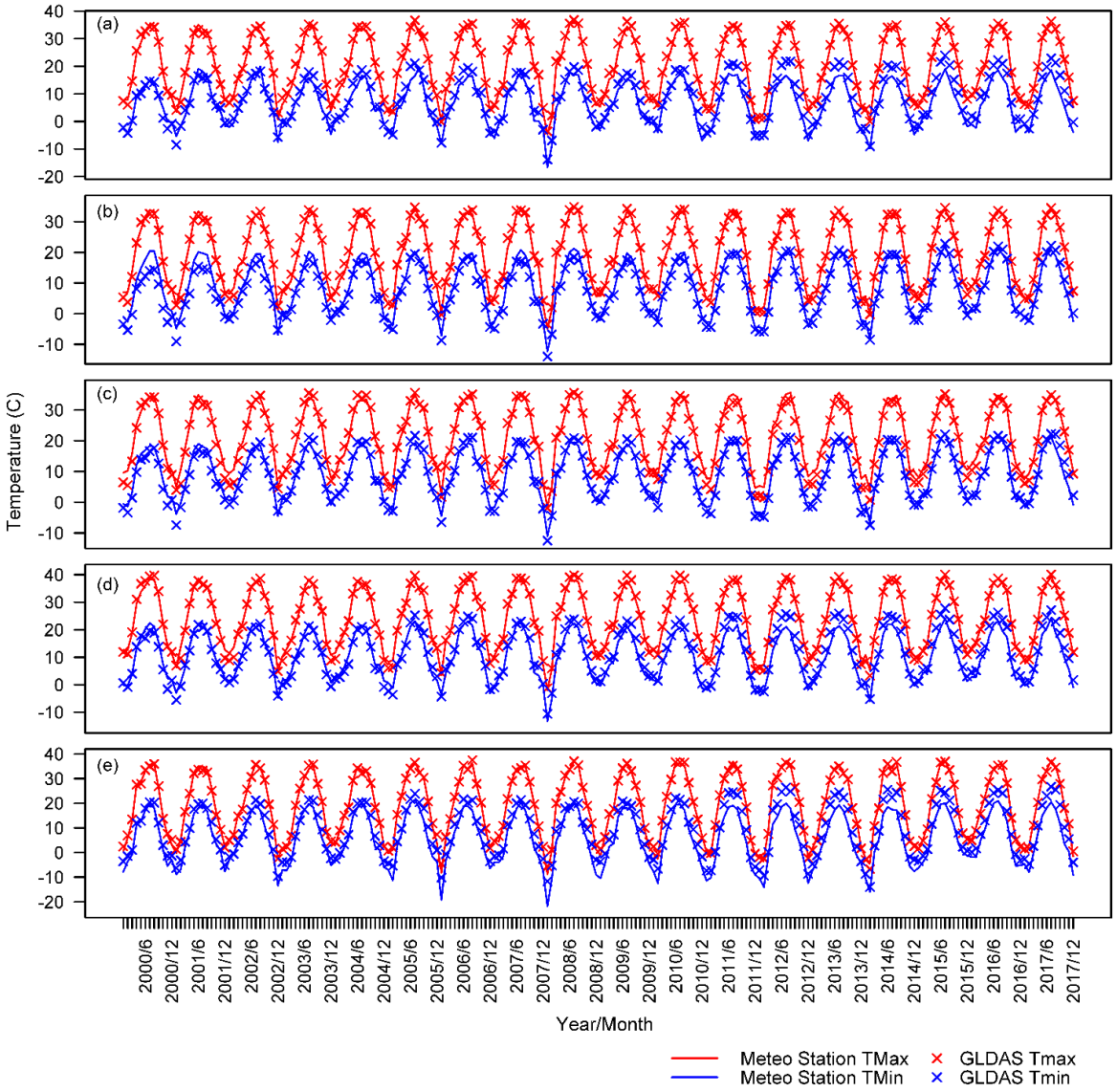

Figure A.1.7.3: Monthly average Tmax and Tmin by stations and GLDAS in selected locations (a) Gallaral, (b) Lalmikor, (c) Samarkand, (d) Karshi and (e) Takhtakupir

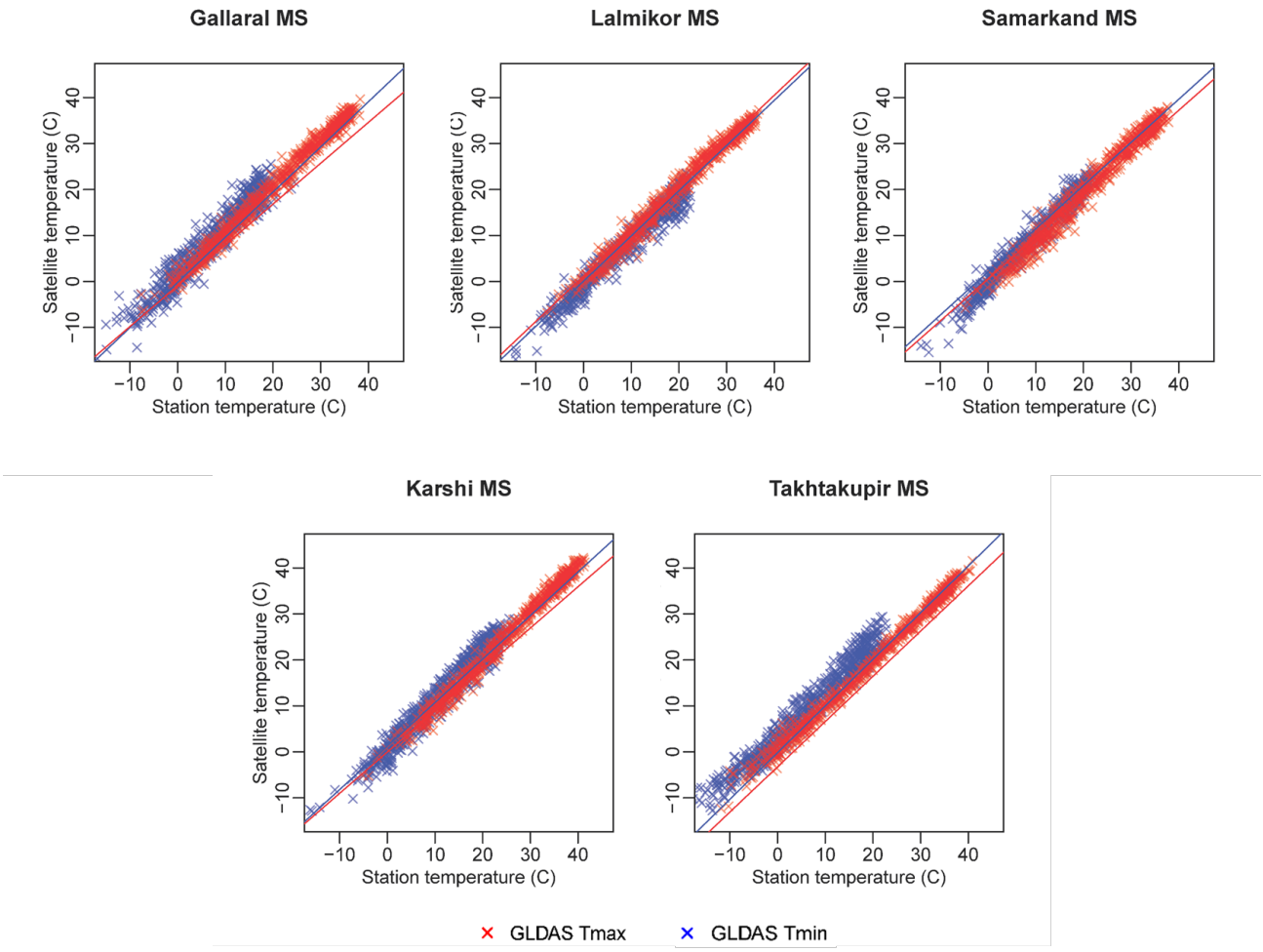

Figure A.1.7.4: Decadal precipitation by stations vs GLDAS Tmax and Tmin in selected locations

Appendix 1.8: Results of accuracy assessment for decadal precipitation measurements

Table A.1.8.1: Accuracy assessment of continuous decadal precipitation in selected locations (March 2000-December 2017)

	Djizzakh		Gallaral		Lalmikor		Samarkand		Karshi		Takhtakupir		Average	
	GSMaP	CHIPRS	GSMaP	CHIPRS	GSMaP	CHIPRS	GSMaP	CHIRPS	GSMaP	CHIPRS	GSMaP	CHIPRS	GSMaP	CHIRPS
BIAS	1.17	0.89	1.19	0.90	1.16	0.88	1.24	0.87	1.40	1.02	1.26	0.91	1.24	0.91
CSI	0.84	0.89	0.83	0.86	0.86	0.86	0.81	0.86	0.71	0.91	0.72	0.82	0.80	0.87
POD	1.00	0.89	1.00	0.88	1.00	0.87	1.00	0.87	1.00	0.97	0.95	0.86	0.99	0.89
FAR	0.15	0.00	0.16	0.02	0.14	0.01	0.19	0.01	0.29	0.05	0.25	0.05	0.20	0.02
PBIAS	-14.2	10.60	-9.10	18.00	-18.9	4.00	-12.90	4.90	-6.80	28.5	-13.9	9.50	-12.63	12.58
MBE	-4.68	3.50	-2.79	5.52	-6.48	1.37	-3.81	1.46	-1.22	5.11	-1.41	0.96	-3.40	2.99
MAE	6.45	10.37	7.77	11.74	9.25	10.93	6.27	8.33	3.69	6.97	4.15	4.86	6.26	8.87
RMSE	11.13	15.76	12.37	16.98	14.11	15.71	10.64	12.77	6.59	11.6	7.58	7.26	10.41	13.34
SC	0.97	0.92	0.94	0.91	0.95	0.91	0.98	0.94	0.96	0.95	0.84	0.84	0.94	0.91
PC	0.96	0.90	0.93	0.88	0.93	0.89	0.95	0.92	0.96	0.91	0.79	0.80	0.92	0.88
R^2	0.93	0.81	0.86	0.78	0.87	0.79	0.91	0.84	0.92	0.84	0.63	0.65	0.85	0.78
p	0.00	0.00	0.00	0.00	0.00	0.00	0.00	0.00	0.00	0.00	0.00	0.00	0.00	0.00
d	0.97	0.94	0.96	0.93	0.95	0.94	0.97	0.96	0.97	0.94	0.88	0.88	0.95	0.93
LEPS	0.05	0.08	0.06	0.09	0.07	0.09	0.04	0.07	0.04	0.06	0.10	0.13	0.06	0.09

Table A.1.8.2: Accuracy assessment of continues decadal average temperature in selected locations (January 2000 – December 2017)

	Djizzakh		Gallaral		Lalmikor		Samarkand		Karshi		Takhtakupir		Average	
	Tmax	Tmin	Tmax	Tmin	Tmax	Tmin	Tmax	Tmin	Tmax	Tmin	Tmax	Tmin	Tmax	Tmin
BIAS	1.00	1.00	1.00	1.00	1.00	1.00	1.00	1.00	1.00	1.00	1.00	1.00	1.00	1.00
CSI	1.00	1.00	1.00	1.00	1.00	1.00	1.00	1.00	1.00	1.00	1.00	1.00	1.00	1.00
POD	1.00	1.00	1.00	1.00	1.00	1.00	1.00	1.00	1.00	1.00	1.00	1.00	1.00	1.00
FAR	0.00	0.00	0.00	0.00	0.00	0.00	0.00	0.00	0.00	0.00	0.00	0.00	0.00	0.00
PBIAS	3.40	4.60	2.80	28.60	1.30	-11.6	-3.70	2.20	0.20	11.6	-0.70	58.7	0.55	15.68
MBE	0.73	0.43	0.58	1.86	0.26	-1.03	-0.81	0.20	0.04	1.21	-0.13	3.39	0.11	1.01
MAE	1.26	1.41	1.12	2.40	1.09	1.53	1.46	1.18	1.02	2.07	0.92	3.44	1.14	2.00
RMSE	1.57	1.76	1.43	3.03	1.41	2.02	1.89	1.58	1.31	2.46	1.22	4.02	1.47	2.48
SC	0.99	0.98	0.99	0.96	0.99	0.98	0.99	0.98	0.99	0.97	1.00	0.98	0.99	0.98
PC	0.99	0.98	0.99	0.96	0.99	0.98	0.99	0.98	0.99	0.97	1.00	0.98	0.99	0.98
R^2	0.99	0.97	0.99	0.93	0.98	0.96	0.98	0.97	0.99	0.95	0.99	0.96	0.99	0.95
p	0.00	0.00	0.00	0.00	0.00	0.00	0.00	0.00	0.00	0.00	0.00	0.00	0.00	0.00
d	1.00	0.99	1.00	0.97	1.00	0.99	0.99	0.99	1.00	0.98	1.00	0.96	1.00	0.98
LEPS	0.04	0.05	0.03	0.08	0.03	0.05	0.04	0.04	0.03	0.07	0.02	0.09	0.03	0.06
NSE	0.98	0.95	0.98	0.86	0.98	0.94	0.97	0.96	0.99	0.92	0.99	0.86	0.98	0.91

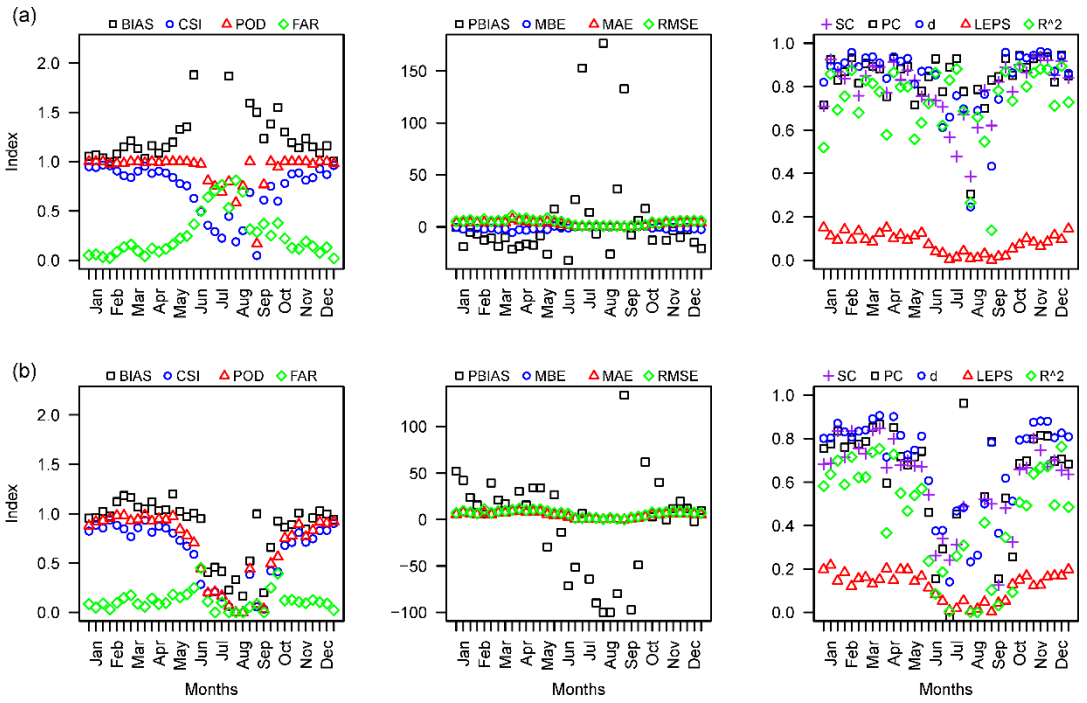

Figure A.1.8.3: Average results of classification, quantitative and agreement accuracy metrics of decadal precipitation for all stations, by (a) GSMaP and (b) CHIRPS

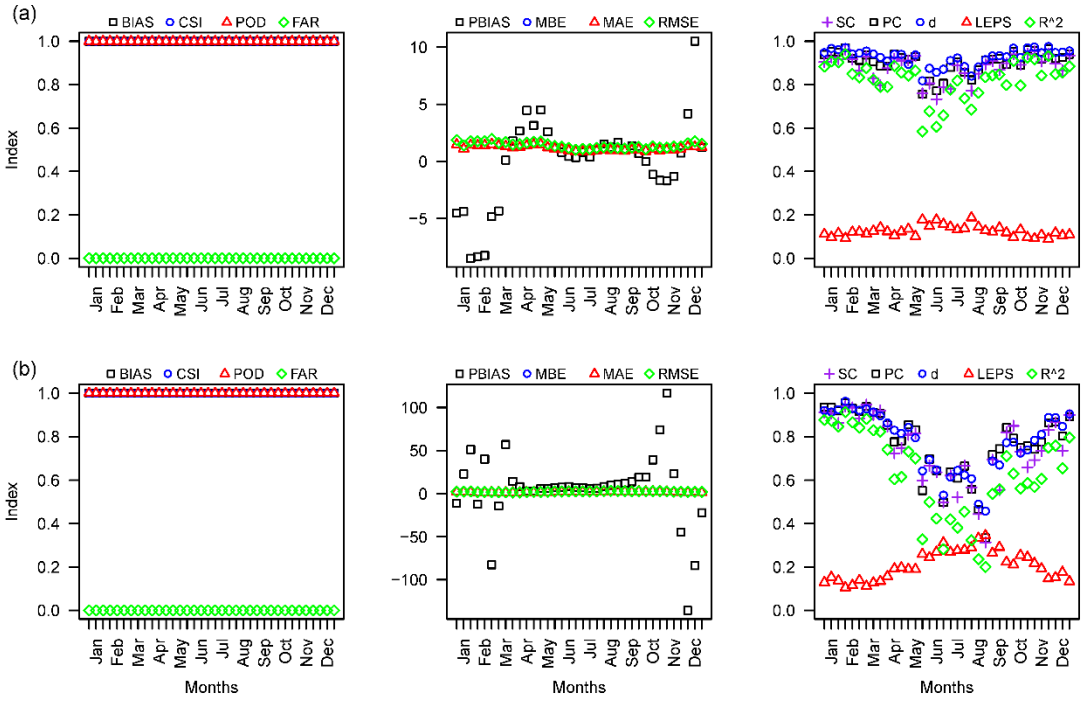

Figure A.1.8.4: Average results of classification, quantitative and agreement accuracy metrics of decadal temperature for all stations, for (a) GLDAS Tmax and (b) GLDAS Tmin

Appendix 1.9: Visualization of quantile regressions results for GSMaP, CHIRPS and GLDAS in selected locations

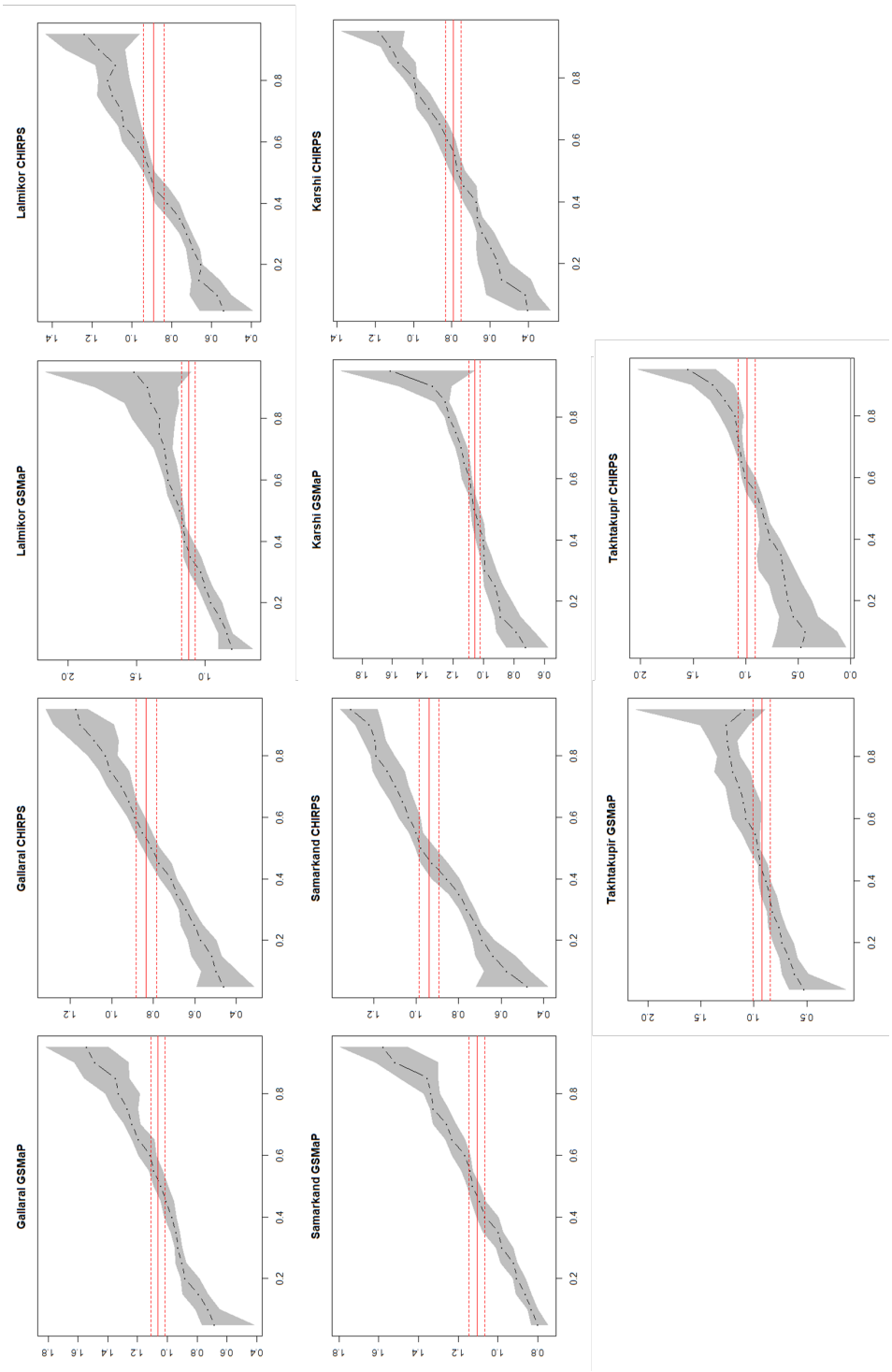

Figure A.1.9.1: Estimated results of quantile regressions for GSMaP and CHIRPS for remaining 5 stations (monthly scale)

Table A.1.9.2: Quantile regression results of satellite-based precipitation estimates for remaining 5 stations (monthly scale) (n = 214)

		OLS	0.5	0.1	0.25	0.5	0.75	0.9	0.95
Gallaral-GSMaP	Coef.	1.063***	0.684***	0.728***	0.902***	1.044***	1.268***	1.488***	1.541***
	SE	-0.029	-0.077	-0.037	-0.024	-0.029	-0.041	-0.053	-0.088
	R^2/pR^2	0.861	0.359	0.474	0.621	0.690	0.702	0.712	0.713
Gallaral-CHIRPS	Coef.	0.833***	0.461***	0.499***	0.602***	0.808***	1.007***	1.153***	1.171***
	SE	-0.03	-0.043	-0.03	-0.03	-0.03	-0.046	-0.071	-0.072
	R^2/pR^2	0.779	0.280	0.371	0.507	0.594	0.615	0.634	0.651
Lalmikor-GSMaP	Coef.	1.120***	0.805***	0.839***	0.998***	1.181***	1.333***	1.420***	1.516***
	SE	-0.030	-0.048	-0.045	-0.035	-0.025	-0.037	-0.073	-0.159
	R^2/pR^2	0.871	0.436	0.528	0.646	0.711	0.701	0.666	0.641
Lalmikor-CHIRPS	Coef.	0.891***	0.539***	0.570***	0.695***	0.912***	1.098***	1.166***	1.237***
	SE	-0.031	-0.042	-0.043	-0.025	-0.034	-0.046	-0.1	-0.103
	R^2/pR^2	0.795	0.350	0.410	0.548	0.611	0.607	0.590	0.584
Samarkand-GSMaP	Coef.	1.105***	0.801***	0.831***	0.920***	1.127***	1.327***	1.519***	1.579***
	SE	-0.024	-0.033	-0.018	-0.022	-0.023	-0.022	-0.066	-0.06
	R^2/pR^2	0.909	0.607	0.647	0.711	0.766	0.785	0.776	0.777
Samarkand-CHIRPS	Coef.	0.940***	0.478***	0.573***	0.718***	0.979***	1.137***	1.220***	1.307***
	SE	-0.028	-0.047	-0.042	-0.029	-0.031	-0.03	-0.041	-0.061
	R^2/pR^2	0.842	0.306	0.392	0.555	0.660	0.718	0.746	0.749
Karshi-GSMaP	Coef.	1.059***	0.723***	0.785***	0.924***	1.062***	1.181***	1.335***	1.614***
	SE	-0.022	-0.038	-0.043	-0.025	-0.014	-0.019	-0.085	-0.122
	R^2/pR^2	0.916	0.459	0.532	0.674	0.786	0.799	0.755	0.720
Karshi-CHIRPS	Coef.	0.792***	0.404***	0.416***	0.594***	0.771***	0.984***	1.122***	1.186***
	SE	-0.024	-0.031	-0.038	-0.026	-0.021	-0.026	-0.041	-0.054
	R^2/pR^2	0.835	0.287	0.356	0.530	0.682	0.727	0.733	0.729
Takhtakupir-GSMaP	Coef.	0.926***	0.524***	0.614***	0.761***	0.956***	1.197***	1.260***	1.088
	SE	-0.049	-0.074	-0.042	-0.03	-0.033	-0.056	-0.126	-0.553
	R^2/pR^2	0.626	0.166	0.288	0.435	0.521	0.522	0.460	0.358
Takhtakupir-CHIRPS	Coef.	0.990***	0.470***	0.431***	0.621***	0.849***	1.083***	1.312***	1.550***
	SE	-0.05	-0.047	-0.048	-0.062	-0.046	-0.054	-0.157	-0.296
	R^2/pR^2	0.647	0.079	0.154	0.301	0.458	0.523	0.502	0.468

Coef. = Coefficient; SE = standard error; R^2 = R-square for OLS; pR^2 = pseudo R-square for quantiles; * p<0.05, ** p<0.01, *** p<0.001

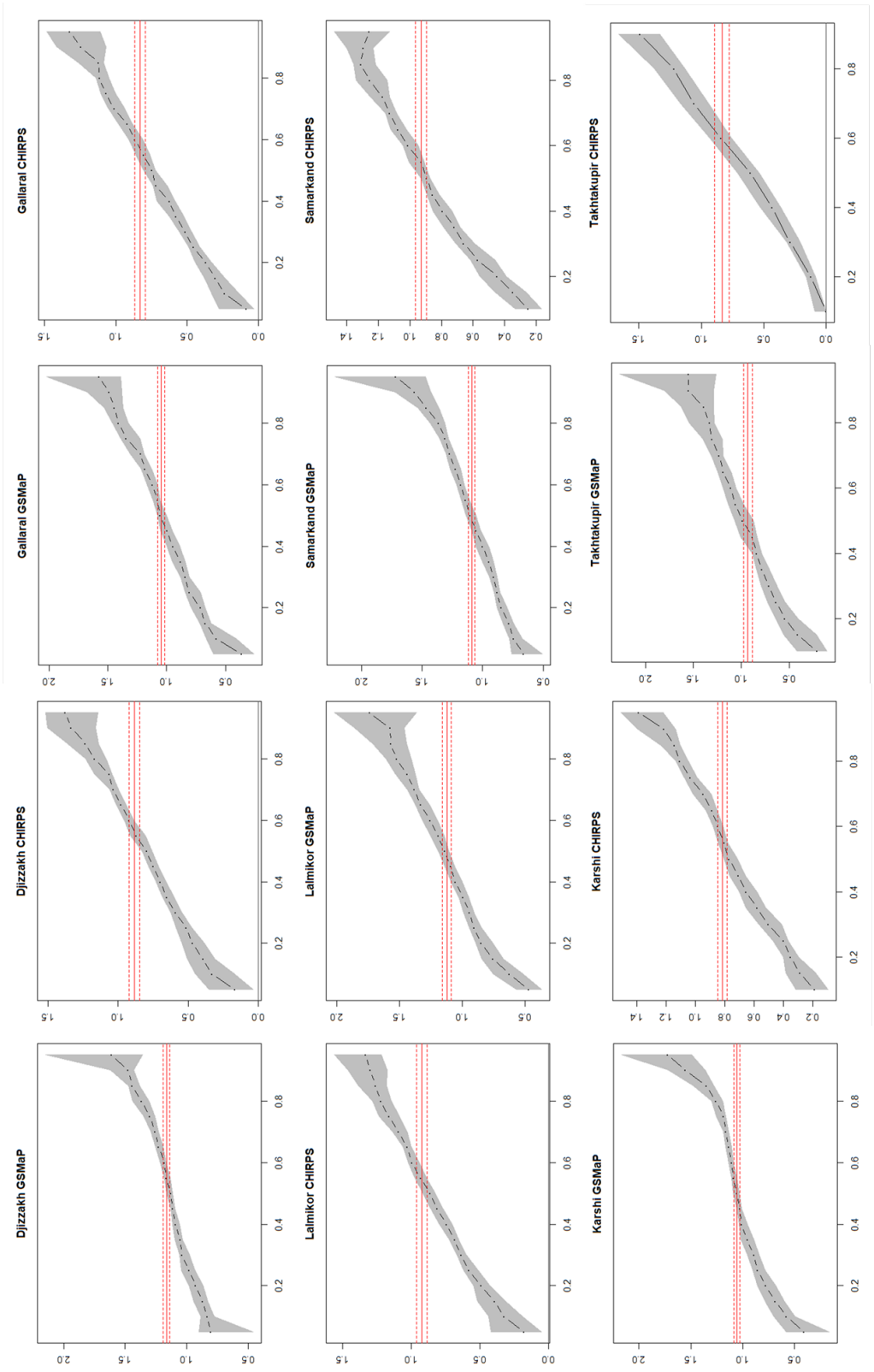

Figure A.1.9.3: Estimated results of quantile regressions for GSMaP and CHIRPS in selected locations (decadal scale)

Table A.1.9.4: Quantile regression results of satellite-based precipitation estimates for the selected stations (decadal scale) (n = 642)

		OLS	0.5	0.1	0.25	0.5	0.75	0.9	0.95
Djizzakh-GSMaP	Coef.	1.165***	0.805***	0.835***	0.980***	1.13***	1.299***	1.478***	1.612***
	SE	0.014	0.064	0.028	0.040	0.026	0.029	0.035	0.189
	R^2/pR^2	0.906	0.335	0.467	0.627	0.761	0.799	0.787	0.760
Djizzakh-CHIRPS	Coef.	0.885***	0.166**	0.333***	0.515***	0.798***	1.065***	1.335***	1.376***
	SE	0.023	0.060	0.069	0.039	0.028	0.046	0.128	0.115
	R^2/pR^2	0.693	0.043	0.111	0.305	0.504	0.568	0.542	0.539
Gallaral-GSMaP	Coef.	1.0458***	0.365***	0.578***	0.807***	1.054***	1.343***	1.489***	1.577***
	SE	0.019	0.083	0.056	0.045	0.036	0.043	0.071	0.124
	R^2/pR^2	0.827	0.175	0.282	0.474	0.638	0.694	0.705	0.700
Gallaral-CHIRPS	Coef.	0.831***	0.088*	0.241***	0.458***	0.747***	1.068***	1.246***	1.322***
	SE	0.022	0.052	0.056	0.037	0.031	0.033	0.076	0.125
	R^2/pR^2	0.682	0.026	0.092	0.272	0.473	0.547	0.550	0.554
Lalmikor-GSMaP	Coef.	1.122***	0.47***	0.624***	0.906***	1.14***	1.439***	1.572***	1.738***
	SE	0.02	0.059	0.075	0.041	0.032	0.049	0.118	0.184
	R^2/pR^2	0.826	0.218	0.309	0.494	0.643	0.687	0.680	0.674
Lalmikor-CHIRPS	Coef.	0.925***	0.182***	0.324***	0.581***	***0.864	1.164***	1.300***	1.334***
	SE	0.023	0.050	0.043	0.039	0.034	0.052	0.099	0.127
	R^2/pR^2	0.719	0.056	0.133	0.319	0.511	0.569	0.553	0.573
Samarkand-GSMaP	Coef.	1.092***	0.661***	0.746***	0.881***	1.104***	1.311***	1.564***	1.719***
	SE	0.017	0.075	0.035	0.025	0.033	0.022	0.063	0.088
	R^2/pR^2	0.868	0.338	0.447	0.593	0.712	0.763	0.752	0.722
Samarkand-CHIRPS	Coef.	0.930***	0.135**	0.253***	0.573***	0.894***	1.174***	1.297***	1.259***
	SE	0.022	0.052	0.038	0.054	0.031	0.038	0.050	0.091
	R^2/pR^2	0.738	0.028	0.097	0.288	0.522	0.608	0.620	0.617
Karshi-GSMaP	Coef.	1.059***	0.413***	0.58***	0.857***	1.058***	1.186***	1.554***	1.726***
	SE	0.017	0.117	0.057	0.048	0.019	0.024	0.094	0.168
	R^2/pR^2	0.857	0.143	0.286	0.503	0.701	0.772	0.757	0.730
Karshi-CHIRPS	Coef.	0.815***	0.085*	0.187***	0.399***	0.771***	1.034***	1.216***	1.387***
	SE	0.018	0.042	0.048	0.040	0.038	0.036	0.093	0.088
	R^2/pR^2	0.752	0.003	0.064	0.252	0.515	0.651	0.674	0.672
Takhtakupir-GSMaP	Coef.	0.933***	0.077*	0.215*	0.64***	0.987***	1.309***	1.554***	1.551***
	SE	0.029	0.034	0.090	0.057	0.070	0.058	0.077	0.078
	R^2/pR^2	0.624	0.023	0.064	0.260	0.470	0.573	0.551	0.489
Takhtakupir-CHIRPS	Coef.	0.834***			0.18***	0.608***	1.175***	1.49***	1.678***
	SE	0.036			0.043	0.076	0.067	0.084	0.180
	R^2/pR^2	0.451			0.056	0.234	0.383	0.426	0.425

Coef. = Coefficient; SE = standard error; R^2 = R-square for OLS; pR^2 = pseudo R-square for quantiles; * p<0.05, ** p<0.01, *** p<0.001

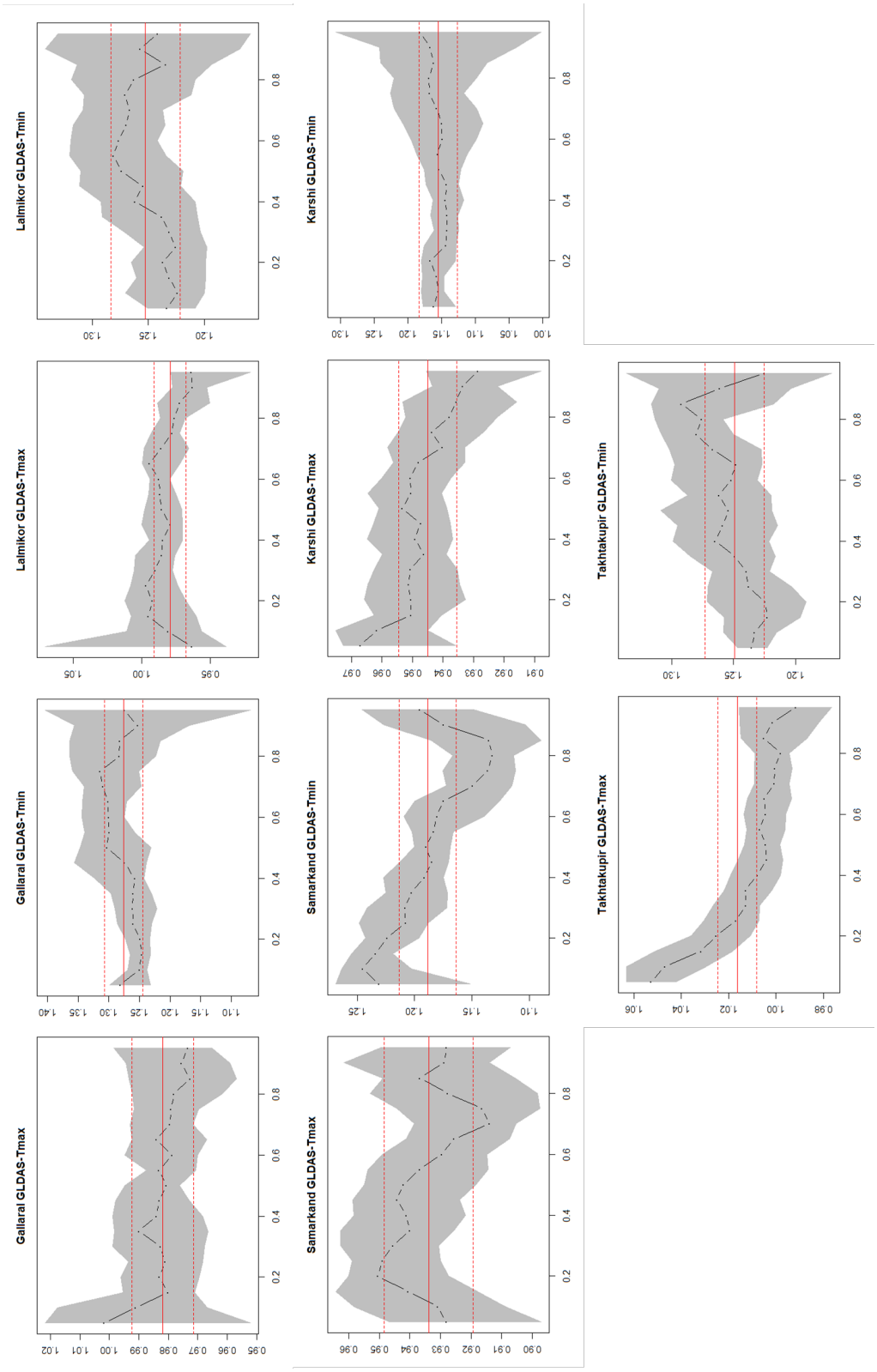

Figure A.1.9.5: Estimated results of quantile regressions for GLDAS Tmax and Tmin in selected locations (monthly scale)

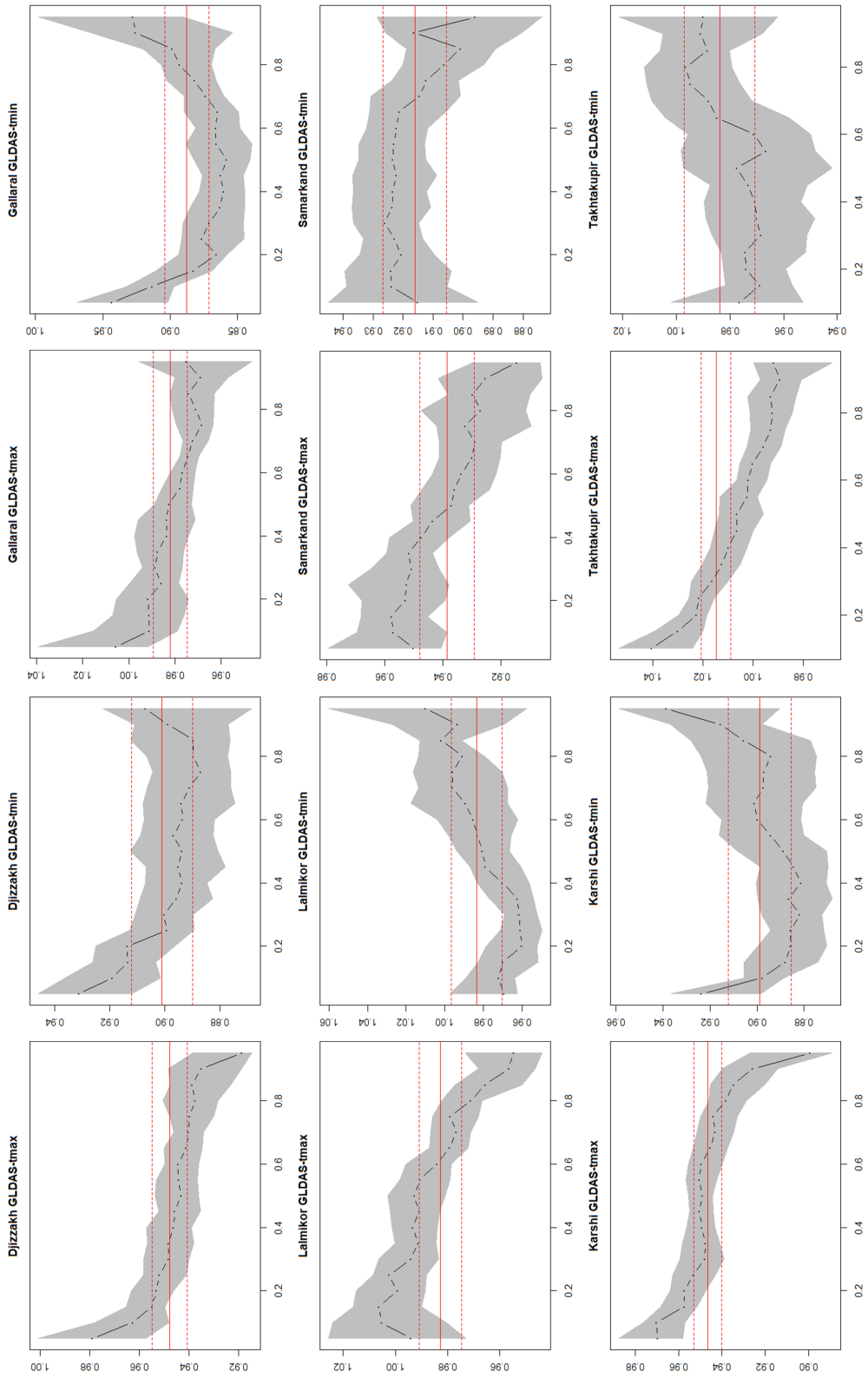

Figure A.1.9.6: Estimated results of quantile regressions for GLDAS Tmax and Tmin in selected locations (decadal scale)

Table A.1.9.7: Estimated results of OLS regressions for GLDAS Tmax and GLDAS Tmin in all locations (decadal scale)

	Djizzakh		Gallaral		Lalmikor		Samarkand		Karshi		Takhtakupir	
	GLDAS Tmax	GLDAS Tmin	GLDAS Tmax	GLDAS Tmin	GLDAS Tmax	GLDAS Tmin	GLDAS Tmax	GLDAS Tmin	GLDAS Tmax	GLDAS Tmin	GLDAS Tmax	GLDAS Tmin
Coef.	0.948***	0.901***	0.982***	0.888***	0.983***	0.983***	0.938***	0.916***	0.946***	0.898***	1.015***	0.984***
SE	0.004	0.007	0.004	0.009	0.005	0.008	0.006	0.006	0.004	0.008	0.004	0.008
R^2	0.987	0.965	0.987	0.926	0.984	0.959	0.977	0.969	0.989	0.95	0.992	0.959

Coef. = Coefficient; SE = standard error; R^2 = R-square for OLS; pR^2 = pseudo R-square for quantiles; * p<0.05, ** p<0.01, *** p<0.001

Appendix 1.10: Results of accuracy assessment for seasonal precipitation measurements

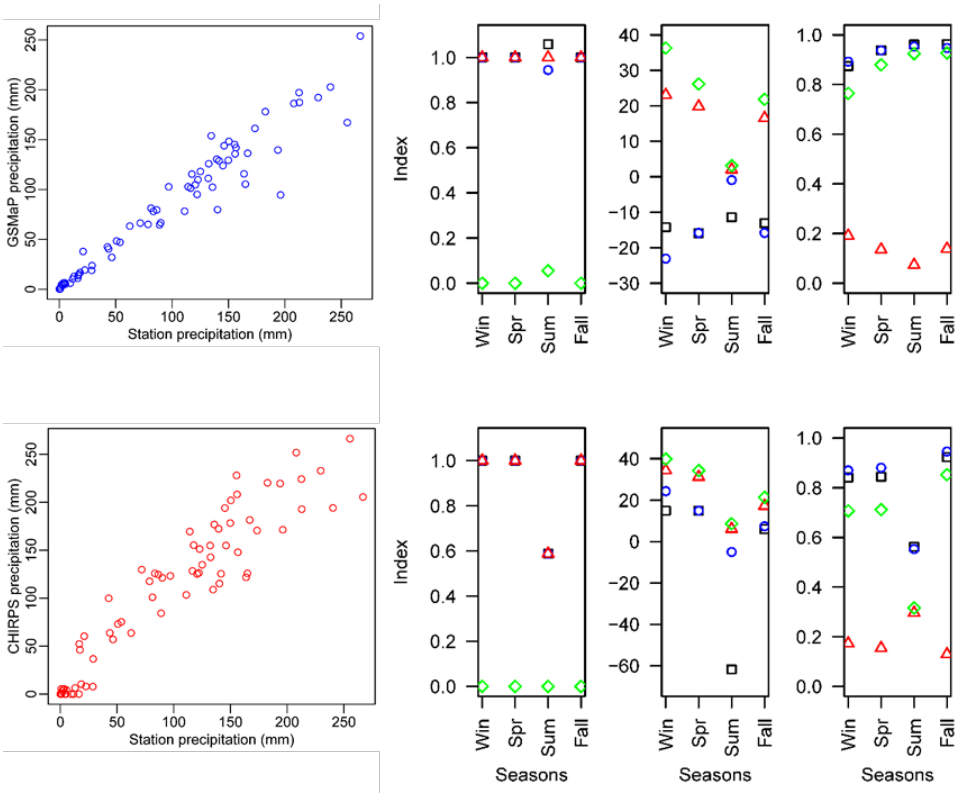

Figure A.1.10.1: Results of classification, quantitative and agreement accuracy metrics of seasonal precipitation for the Djizzakh station, first row is GSMaP and second row is CHIRPS (legends are same as in above Figure A.1.7.1)

Table A.1.10.2: Accuracy assessment of continuous decadal and seasonal precipitation at the Djizzakh station

	BIAS	CSI	POD	FAR	PBIAS	MBE	MAE	RMSE	SC	PC	R^2	p	*d*	LEPS
GSMaP	1.01	0.99	1	0.01	-14.2	-13.91	622.1	24.94	0.98	0.97	0.93	0.000	0.97	0.07
CHIRPS	0.9	0.9	0.9	0	10.6	10.41	822.1	28.67	0.96	0.94	0.88	0.000	0.96	0.09

Appendix 1.11: Visualization of MDIs and classification accuracy assessment of anomaly detection for remaining 5 stations

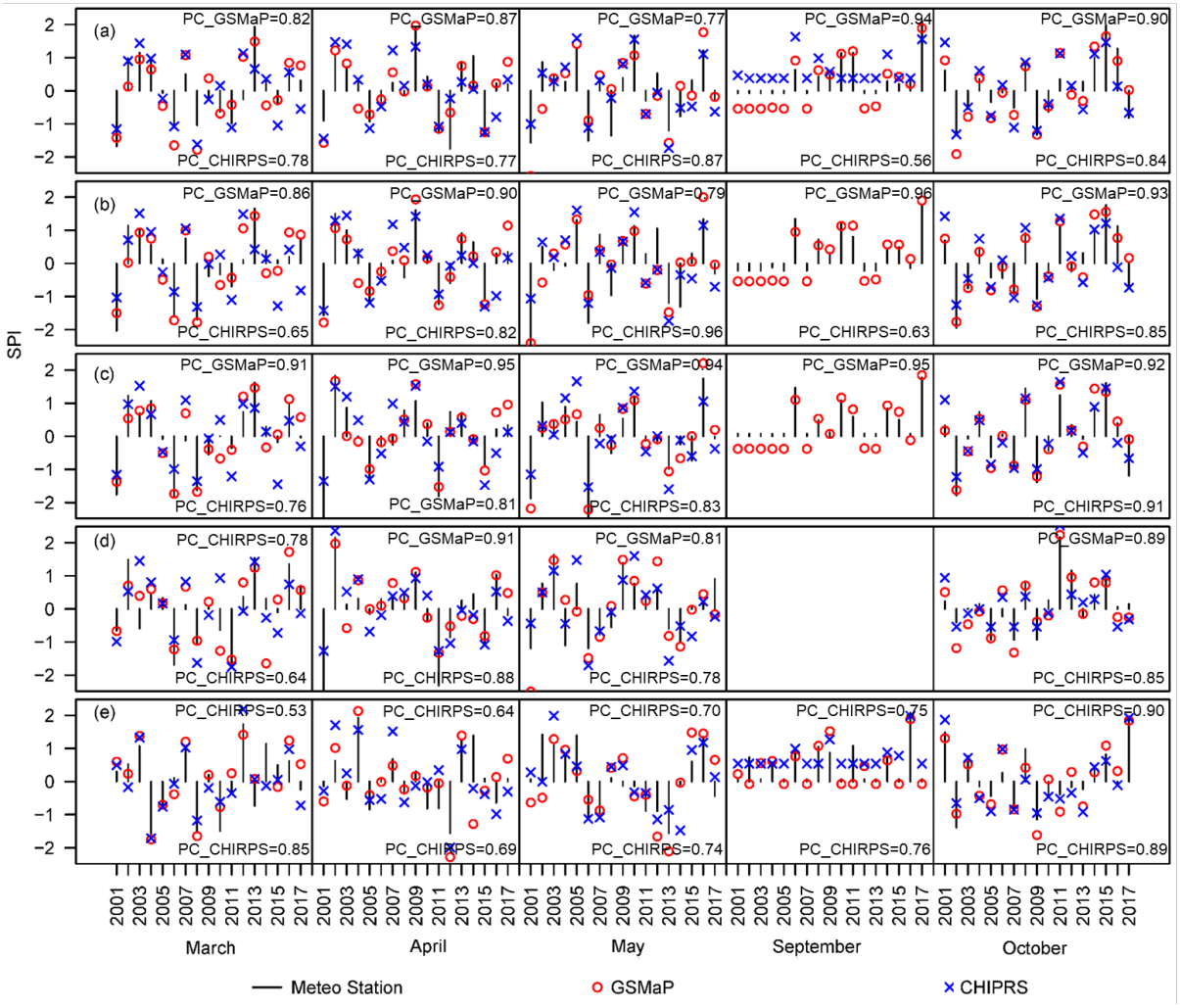

Figure A.1.11.1: Monthly values of Standardized Precipitation Index by stations, GSMaP and CHIRPS in selected locations (a) Gallaral, (b) Lalmikor, (c) Samarkand, (d) Karshi and (e) Takhtakupir

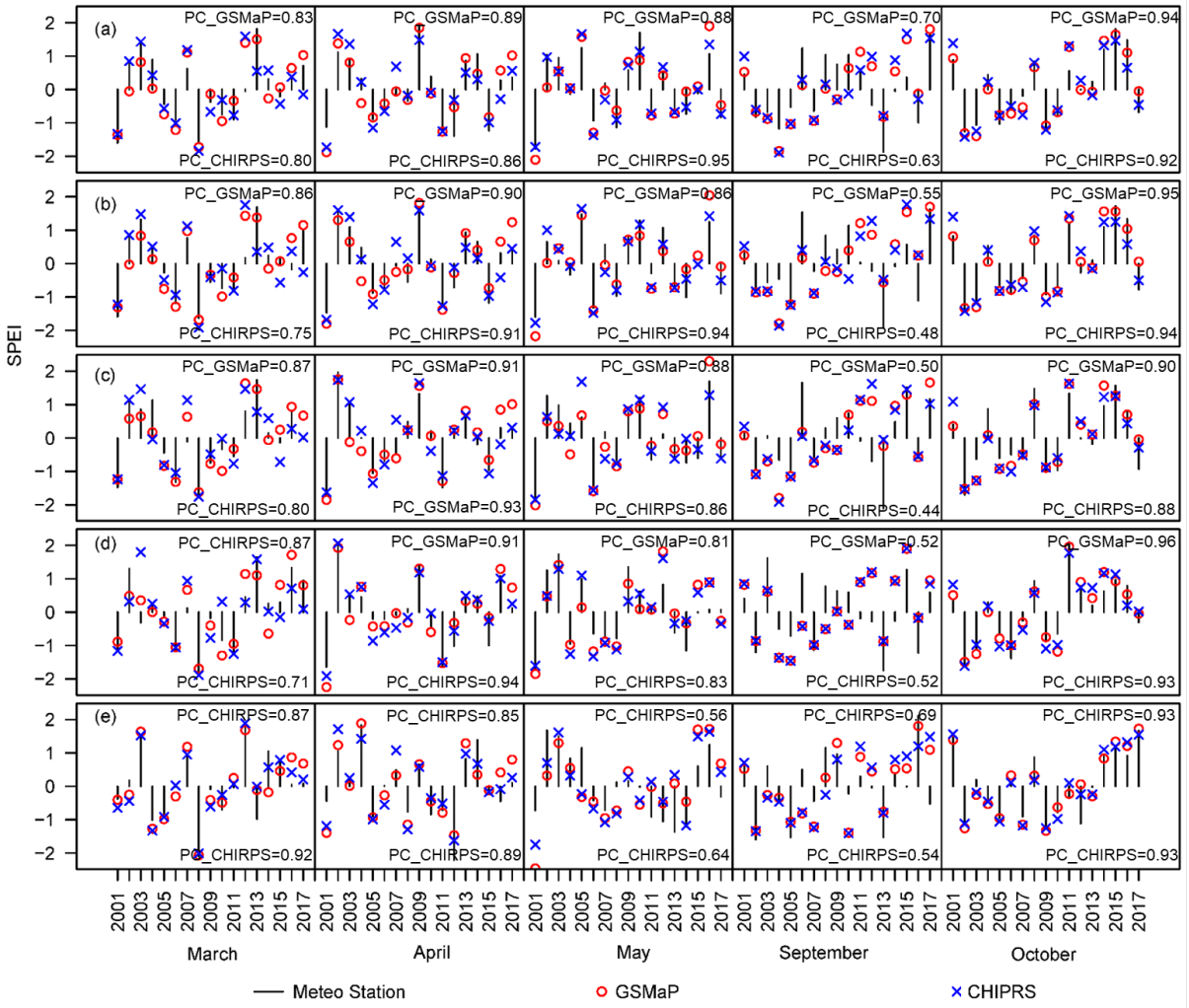

Figure A.1.11.2: Monthly values of Standardized Precipitation-Evapotranspiration Index by the combinations of MS & MS, GSMaP & GLDAS and CHIRPS & GLDAS in selected locations (a) Gallaral, (b) Lalmikor, (c) Samarkand, (d) Karshi and (e) Takhtakupir

Table A.1.11.3: Detailed classification accuracy assessment of anomaly detection at <10th and <20th (March, April and May) percentiles for drought and >80th and >90th (May, September, October) percentiles for flood by GSMaP and CHIRPS at the Djizzakh station.

Percentile:		<10th								<20th								>80th								>90th			
	Metrics	GSMaP-Overall	CHIRPS-Overall	GSMaP-March	CHIRPS-March	GSMaP-April	CHIRPS-April	GSMaP-May	CHIRPS-May	GSMaP-Overall	CHIRPS-Overall	GSMaP-March	CHIRPS-March	GSMaP-April	CHIRPS-April	GSMaP-May	CHIRPS-May	GSMaP-Overall	CHIRPS-Overall	GSMaP-May	CHIRPS-May	GSMaP-September	CHIRPS-September	GSMaP-October	CHIRPS-October	GSMaP-Overall	CHIRPS-Overall	GSMaP-May	CHIRPS-May	GSMaP-September	CHIRPS-September	GSMaP-October	CHIRPS-October
Monthly	BIAS	1.2	0.8	1.3	0.7	1.7	1.3	0.8	0.5	1	0.8	0.8	0.6	1.3	0.9	0.9	0.6	1.3	2.7	2	3	1	2	1	3	1.3	1.7	2	2	1	2	1	1
	CSI	0.7	0.5	0.8	0.7	0.6	0.4	0.8	0.5	0.7	0.6	0.8	0.3	0.6	0.6	0.6	0.9	0.8	0.4	0.5	0.3	1	0.5	1	0.3	0.8	0.6	0.5	0.5	1	0.5	1	1
	POD	0.9	0.6	1	0.7	1	0.7	0.8	0.5	0.8	0.7	0.8	0.4	0.9	0.7	0.7	0.9	1	1	1	1	1	1	1	1	1	1	1	1	1	1	1	1	1
	FAR	0.3	0.3	0.3	0	0.4	0.5	0	0	0.2	0.1	0	0.3	0.3	0.2	0.2	0	0.3	0.6	0.5	0.7	0	0.5	0	0.7	0.3	0.4	0.5	0.5	0	0.5	0	0.7	0
Decadal	BIAS	0.9	0.6	1.2	0.5	0.9	0.6	0.9	0.5	1	0.7	1.1	0.7	0.9	0.7	0.9	0.6	0.8	0.9	0.6	0.6	0.7	0.2	0.7	1.2	0.8	0.8	0.7	0.7	1	1.5	1	0.8
	CSI	0.8	0.4	0.9	0.3	0.8	0.5	0.8	0.4	0.8	0.6	0.8	0.5	0.8	0.5	0.8	0.6	0.8	0.3	0.4	0.2	0.7	0.3	0.8	0.5	0.6	0.2	0.4	0.3	1	0.3	0.6	0.2
	POD	0.9	0.4	1	0.3	0.8	0.5	0.8	0.4	0.9	0.6	0.9	0.6	0.8	0.6	0.9	0.6	0.6	0.4	0.4	0.3	0.7	0.3	0.8	0.5	0.7	0.3	0.5	0.3	1	0.5	0.8	0.3
	FAR	0.1	0.3	0.1	0.4	0.1	0.2	0	0.2	0.1	0.1	0.2	0.1	0.1	0.2	0	0	0.2	0.6	0.3	0.5	0	0.7	0.2	0.6	0.2	0.6	0.3	0.5	0	0.7	0.3	0.7

Table A.1.11.4: Overall classification accuracy assessment of anomaly detection at <10th and <20th (March, April and May) percentiles for drought and >80th and >90th (May, September, October) percentiles for flood by GSMaP and CHIRPS for remaining 5 stations

	Monthly								Decadal							
	<10		<20		<80		<90		<10		<20		>80		>90	
	GSMaP	CHIRPS	GSMaP	CHIRPS	GSMaP	CHIRPS	GSMaP	CHIRPS	GSMaP	CHIRPS	GSMaP	CHIRPS	GSMaP	CHIRPS	GSMaP	CHIRPS
Gallaral	0.8	0.6	0.9	0.9	1.3	2.7	1.0	2.0	1.0	0.6	1.0	0.7	1.2	1.4	1.1	1.0
	0.6	0.5	0.6	0.6	0.4	0.4	0.5	0.5	0.6	0.4	0.7	0.6	0.6	0.3	0.5	0.3
	0.7	0.5	0.7	0.7	0.7	1.0	0.7	1.0	0.8	0.4	0.9	0.6	0.8	0.5	0.7	0.4
	0.1	0.1	0.2	0.2	0.5	0.6	0.3	0.5	0.2	0.3	0.2	0.1	0.3	0.6	0.4	0.6
Lalmikor	0.8	0.6	1.1	1.0	0.7	1.5	1.0	1.3	1.2	0.5	1.1	0.7	0.8	1.0	0.8	0.8
	0.8	0.5	0.7	0.5	0.4	0.4	0.6	0.1	0.6	0.4	0.7	0.6	0.5	0.4	0.5	0.3
	0.8	0.5	0.8	0.7	0.5	0.7	0.8	0.3	0.8	0.4	0.9	0.6	0.6	0.5	0.6	0.4
	0.0	0.1	0.2	0.3	0.3	0.6	0.3	0.8	0.3	0.2	0.2	0.1	0.2	0.5	0.3	0.5
Samarkand	1.0	1.1	1.1	1.2	1.0	1.0	1.3	-	1.0	0.5	1.0	0.7	1.0	1.0	1.3	1.1
	1.0	0.5	0.8	0.8	0.4	0.1	0.4	-	0.8	0.4	0.8	0.5	0.5	0.2	0.4	0.1
	1.0	0.7	0.9	0.9	0.6	0.2	0.5	-	0.9	0.4	0.9	0.5	0.6	0.3	0.6	0.3
	0.0	0.4	0.1	0.2	0.4	0.8	0.7	-	0.1	0.2	0.1	0.2	0.4	0.7	0.5	0.8
Karshi	0.9	0.8	1.1	1.0	1.3	1.0	1.7	1.3	0.9	0.6	1.0	0.6	1.5	1.5	1.4	1.3
	0.6	0.5	0.6	0.6	0.8	0.3	0.6	0.4	0.8	0.4	0.8	0.6	0.7	0.4	0.7	0.3
	0.7	0.6	0.8	0.8	1.0	0.5	1.0	0.7	0.8	0.5	0.9	0.6	1.0	0.8	1.0	0.6
	0.2	0.3	0.2	0.2	0.2	0.5	0.4	0.5	0.1	0.2	0.1	0.0	0.3	0.5	0.3	0.6
Takhtakupir	1.3	0.8	1.5	0.8	1.0	0.8	0.8	0.8	1.1	0.4	1.1	0.7	1.0	0.9	0.9	1.1
	0.5	0.7	0.5	0.6	0.4	0.3	0.5	0.3	0.8	0.4	0.8	0.6	0.3	0.2	0.3	0.2
	0.7	0.7	0.9	0.7	0.6	0.4	0.6	0.4	0.9	0.4	0.9	0.6	0.5	0.3	0.4	0.4
	0.4	0.1	0.4	0.2	0.4	0.5	0.3	0.5	0.2	0.1	0.2	0.1	0.5	0.7	0.6	0.6

Appendix 2: The role of crop classification in detecting wheat yield variation for index-based agricultural insurance in arid and semiarid environments[19]

Appendix 2.1: Location of croplands and descriptive stations of wheat yield data

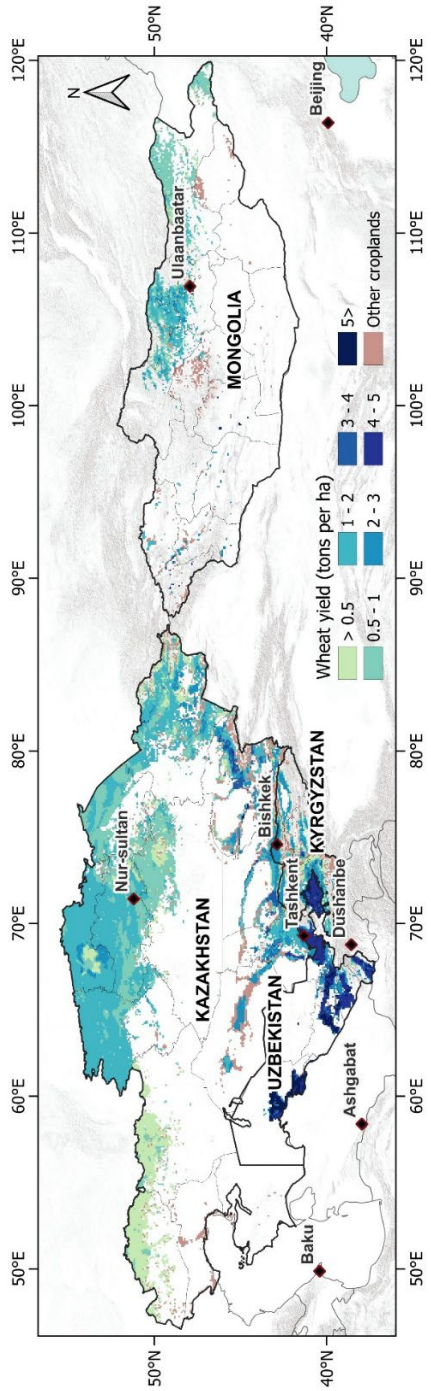

Figure A.2.1.1: Location of croplands, wheat cultivated areas and average wheat yield in Central Asia and Mongolia. Source: Authors' presentation based on data from Yu et al. (2020)

[19] This appendix was published as part of the following open-access article: Eltazarov, S., Bobojonov, I., Kuhn, L., Glauben, T. (2021): The role of crop classification in detecting wheat yield variation for index-based agricultural insurance in arid and semiarid environments. Environmental and Sustainability Indicators, 18, 100250. https://doi.org/10.1016/j.indic.2023.100250

Table A.2.1.2: Descriptive statistics of wheat yield data (ton/ha)

Num-ber	Country	Province	District	Farming system	Period of yield data	MAX	MEAN	MIN	SD	RSD (%)
1	Kazakhstan	Akmola	Akkol	rainfed	2000-2015	1.27	0.85	0.40	0.26	30.5
2	Kazakhstan	Akmola	Arshaly	rainfed	2000-2015	1.26	0.93	0.63	0.20	21.3
3	Kazakhstan	Akmola	Astrakhan	rainfed	2000-2015	1.26	0.84	0.39	0.22	26.7
4	Kazakhstan	Akmola	Atbasar	rainfed	2000-2015	1.50	0.91	0.51	0.26	28.6
5	Kazakhstan	Akmola	Bulandy	rainfed	2000-2015	1.58	0.96	0.63	0.28	28.9
6	Kazakhstan	Akmola	Burabay	rainfed	2000-2015	1.79	1.13	0.66	0.29	25.9
7	Kazakhstan	Akmola	Egindykol	rainfed	2000-2015	1.20	0.78	0.43	0.22	28.6
8	Kazakhstan	Akmola	Enbekshilder	rainfed	2000-2015	1.58	1.09	0.41	0.38	34.6
9	Kazakhstan	Akmola	Ereymentau	rainfed	2000-2015	1.14	0.67	0.37	0.22	33.2
10	Kazakhstan	Akmola	Esil	rainfed	2000-2015	1.94	0.85	0.31	0.37	43.3
11	Kazakhstan	Akmola	Korganzhyn	rainfed	2000-2015	1.04	0.63	0.37	0.21	33.0
12	Kazakhstan	Akmola	Sandyktau	rainfed	2000-2015	1.81	1.15	0.75	0.27	23.5
13	Kazakhstan	Akmola	Shortandy	rainfed	2000-2015	1.25	0.95	0.42	0.23	24.3
14	Kazakhstan	Akmola	Tselinograd	rainfed	2000-2015	1.11	0.83	0.42	0.20	23.7
15	Kazakhstan	Akmola	Zerendi	rainfed	2000-2015	2.22	1.20	0.51	0.37	31.1
16	Kazakhstan	Akmola	Zhaksy	rainfed	2000-2015	2.04	1.08	0.51	0.39	36.1
17	Kazakhstan	Akmola	Zharkayyk	rainfed	2000-2015	1.69	0.88	0.44	0.30	33.9
18	Kazakhstan	Akmola	Kokshetau city	rainfed	2000-2015	1.68	0.63	0.16	0.37	59.0
19	Kazakhstan	Akmola	Stepnogor city	rainfed	2000-2015	1.16	0.52	0.00	0.36	69.8
20	Kazakhstan	Kostanay	Altynsarin	rainfed	2000-2015	1.91	1.15	0.55	0.36	31.4
21	Kazakhstan	Kostanay	Amangeldi	rainfed	2000-2015	1.39	0.80	0.35	0.27	33.7
22	Kazakhstan	Kostanay	Auliekal	rainfed	2000-2015	1.64	0.88	0.35	0.31	35.2
23	Kazakhstan	Kostanay	Denisov	rainfed	2000-2015	1.92	1.08	0.48	0.38	35.6
24	Kazakhstan	Kostanay	Fedorov	rainfed	2000-2015	2.29	1.46	1.00	0.34	23.4
25	Kazakhstan	Kostanay	Kamysty	rainfed	2000-2015	1.31	0.88	0.34	0.27	31.1
26	Kazakhstan	Kostanay	Karabalyk	rainfed	2000-2015	2.01	1.31	0.82	0.32	24.6
27	Kazakhstan	Kostanay	Karasu	rainfed	2000-2015	1.97	1.06	0.55	0.35	33.0
28	Kazakhstan	Kostanay	Kostanay	rainfed	2000-2015	2.21	1.33	0.82	0.39	29.0
29	Kazakhstan	Kostanay	Mendykara	rainfed	2000-2015	1.98	1.29	0.81	0.29	22.7
30	Kazakhstan	Kostanay	Nauryzym	rainfed	2000-2015	1.29	0.80	0.29	0.27	34.2
31	Kazakhstan	Kostanay	Sarykol	rainfed	2000-2015	2.16	1.28	0.64	0.39	30.6
32	Kazakhstan	Kostanay	Taran	rainfed	2000-2015	1.90	1.03	0.52	0.35	33.6
33	Kazakhstan	Kostanay	Uzynkol	rainfed	2000-2015	2.06	1.27	0.79	0.35	27.6
34	Kazakhstan	Kostanay	Zhangeldin	rainfed	2000-2015	1.25	0.65	0.20	0.24	36.4
35	Kazakhstan	Kostanay	Zhitikarin	rainfed	2000-2015	1.18	0.76	0.28	0.23	30.2
36	Kazakhstan	Kostanay	Arkalyk city	rainfed	2000-2015	1.60	0.89	0.35	0.31	34.6
37	Kazakhstan	Kostanay	Kostanay city	rainfed	2000-2015	1.98	0.75	0.00	0.56	74.5
38	Kazakhstan	N. Kazakhstan	Akkayyn	rainfed	2000-2015	2.17	1.46	0.94	0.34	23.6
39	Kazakhstan	N. Kazakhstan	Akzhar	rainfed	2000-2015	1.58	1.05	0.57	0.33	31.3
40	Kazakhstan	N. Kazakhstan	Ayyrtau	rainfed	2000-2015	2.30	1.26	0.77	0.38	30.2
41	Kazakhstan	N. Kazakhstan	Esil	rainfed	2000-2015	2.34	1.44	1.00	0.35	24.0
42	Kazakhstan	N. Kazakhstan	Gabil Musirepov	rainfed	2000-2015	2.25	1.25	0.72	0.39	31.0
43	Kazakhstan	N. Kazakhstan	Kyzylzhar	rainfed	2000-2015	2.37	1.58	1.21	0.34	21.6
44	Kazakhstan	N. Kazakhstan	M. Zhambaev	rainfed	2000-2015	2.19	1.44	0.99	0.34	23.6
45	Kazakhstan	N. Kazakhstan	Mamlyut	rainfed	2000-2015	2.10	1.43	1.08	0.28	19.8
46	Kazakhstan	N. Kazakhstan	Shal.Akyna	rainfed	2000-2015	1.91	1.18	0.78	0.30	25.5
47	Kazakhstan	N. Kazakhstan	Taiynsha	rainfed	2000-2015	1.91	1.20	0.57	0.30	25.4
48	Kazakhstan	N. Kazakhstan	Timiryazev	rainfed	2000-2015	2.55	1.22	0.76	0.45	36.9
49	Kazakhstan	N. Kazakhstan	Ualikhanov	rainfed	2000-2015	1.51	1.01	0.58	0.32	31.5
50	Kazakhstan	N. Kazakhstan	Zhambyl	rainfed	2000-2015	1.94	1.23	0.76	0.33	27.2
51	Kyrgyzstan	Chuy	Alamudun	mixed	2007-2017	2.95	2.48	1.77	0.46	18.5
52	Kyrgyzstan	Chuy	Chui	mixed	2007-2017	2.87	2.46	1.93	0.36	14.5
53	Kyrgyzstan	Chuy	Jaiyl	mixed	2007-2017	2.76	2.09	1.09	0.58	27.7
54	Kyrgyzstan	Chuy	Kemin	mixed	2007-2017	2.93	2.23	1.42	0.46	20.8
55	Kyrgyzstan	Chuy	Moscow	mixed	2007-2017	2.70	2.11	1.18	0.52	24.5
56	Kyrgyzstan	Chuy	Panfilov	mixed	2007-2017	2.36	1.92	1.11	0.45	23.4
57	Kyrgyzstan	Chuy	Sokuluk	mixed	2007-2017	2.97	2.38	1.48	0.50	21.1
58	Kyrgyzstan	Chuy	Ysyk.Ata	mixed	2007-2017	3.30	2.67	1.88	0.42	15.8

Table A.2.1.2 *(continued)*

59	Mongolia	Bulgan	Bayan.Agt	rainfed	2000-2018	3.07	1.14	0.08	0.71	62.0
60	Mongolia	Bulgan	Bugat	rainfed	2000-2018	2.00	1.25	0.75	0.41	33.0
61	Mongolia	Bulgan	Bureghangai	rainfed	2000-2018	1.84	0.94	0.18	0.49	52.4
62	Mongolia	Bulgan	Dashinchilen	rainfed	2006-2018	2.72	1.32	0.00	0.89	66.9
63	Mongolia	Bulgan	Hangal	rainfed	2000-2018	2.57	1.51	0.72	0.46	30.3
64	Mongolia	Bulgan	Hishig.Undur	rainfed	2000-2018	2.67	1.14	0.14	0.68	59.6
65	Mongolia	Bulgan	Hutag.Undur	rainfed	2000-2018	1.83	1.16	0.61	0.39	33.6
66	Mongolia	Bulgan	Orhon	rainfed	2000-2018	1.91	1.09	0.45	0.37	34.3
67	Mongolia	Bulgan	Selenge	rainfed	2000-2018	1.88	1.15	0.80	0.29	24.9
68	Mongolia	Bulgan	Teshig	rainfed	2000-2018	1.85	1.26	0.57	0.43	34.0
69	Mongolia	Darhan Uul	Hongor	rainfed	2009-2018	1.76	1.14	0.26	0.44	38.8
70	Mongolia	Dornod	Halhgol	rainfed	2000-2018	1.86	1.01	0.35	0.49	48.8
71	Mongolia	Dornod	Tsagaan Ovoo	rainfed	2000-2018	2.80	1.09	0.00	0.82	74.9
72	Mongolia	Huvsgul	Erdenebulgan	rainfed	2000-2018	1.52	0.99	0.29	0.37	37.2
73	Mongolia	Huvsgul	Rashaant	rainfed	2000-2018	2.39	1.30	0.31	0.61	47.2
74	Mongolia	Huvsgul	Tarialan	rainfed	2000-2018	1.98	1.24	0.52	0.45	36.1
75	Mongolia	Orhon	Jargalant	rainfed	2000-2018	3.11	1.55	0.51	0.77	49.4
76	Mongolia	Selenge	Altanbulag	rainfed	2000-2018	1.80	1.10	0.39	0.44	40.1
77	Mongolia	Selenge	Baruunburen	rainfed	2000-2018	1.60	0.83	0.02	0.48	58.1
78	Mongolia	Selenge	Bayangol	rainfed	2000-2018	1.68	0.95	0.12	0.45	46.8
79	Mongolia	Selenge	Huder	rainfed	2000-2018	1.72	1.05	0.20	0.38	36.3
80	Mongolia	Selenge	Hushaat	rainfed	2000-2018	2.40	1.18	0.15	0.62	52.2
81	Mongolia	Selenge	Javhlant	rainfed	2000-2018	1.81	0.99	0.17	0.46	46.5
82	Mongolia	Selenge	Mandal	rainfed	2000-2018	1.82	1.08	0.22	0.46	42.5
83	Mongolia	Selenge	Orhon	rainfed	2000-2018	1.56	0.89	0.14	0.44	49.8
84	Mongolia	Selenge	Orhontuul	rainfed	2000-2018	2.12	1.02	0.19	0.55	54.0
85	Mongolia	Selenge	Saihan	rainfed	2000-2018	1.90	1.20	0.20	0.54	44.7
86	Mongolia	Selenge	Sant	rainfed	2000-2018	2.15	0.97	0.15	0.64	66.2
87	Mongolia	Selenge	Shaamar	rainfed	2000-2018	1.98	0.87	0.27	0.44	51.0
88	Mongolia	Selenge	Tsagaannuur	rainfed	2000-2018	2.09	1.27	0.54	0.48	37.6
89	Mongolia	Selenge	Tushig	rainfed	2000-2018	2.66	1.42	0.37	0.70	49.1
90	Mongolia	Selenge	Yeruu	rainfed	2000-2018	2.11	1.20	0.36	0.49	40.7
91	Mongolia	Selenge	Zuunburen	rainfed	2000-2018	1.95	1.23	0.32	0.49	39.9
92	Mongolia	Tuv	Argalant	rainfed	2000-2018	2.05	0.91	0.01	0.71	78.2
93	Mongolia	Tuv	Bay-anchandmani	rainfed	2001-2016	2.00	1.05	0.65	0.39	37.0
94	Mongolia	Tuv	Bayantsogt	rainfed	2000-2018	1.60	0.76	0.10	0.50	66.5
95	Mongolia	Tuv	Bornuur	rainfed	2000-2018	1.70	0.95	0.01	0.45	47.5
96	Mongolia	Tuv	Erdenesant	rainfed	2000-2018	2.12	0.95	0.03	0.61	64.3
97	Mongolia	Tuv	Jargalant	rainfed	2000-2018	1.96	0.94	0.20	0.48	51.4
98	Mongolia	Tuv	Sumber	rainfed	2000-2018	1.78	1.01	0.09	0.53	52.7
99	Mongolia	Tuv	Tseel	rainfed	2000-2018	2.67	1.27	0.08	0.70	55.3
100	Mongolia	Tuv	Ugtaal	rainfed	2000-2018	2.16	1.07	0.06	0.76	70.7
101	Mongolia	Tuv	Zaamar	rainfed	2000-2018	1.46	0.64	0.07	0.45	69.7
102	Uzbekistan	Djizzakh	Arnasai	irrigated	2007-2018	4.55	3.71	2.92	0.53	14.3
103	Uzbekistan	Djizzakh	Mirzachol	irrigated	2007-2018	1.85	1.42	0.94	0.33	23.4
104	Uzbekistan	Djizzakh	Pakhtakor	irrigated	2007-2018	5.74	3.85	3.10	0.92	23.8
105	Uzbekistan	Djizzakh	Zafarabad	irrigated	2007-2018	6.49	5.38	2.75	1.19	22.2
106	Uzbekistan	Djizzakh	Zarbdar	irrigated	2007-2018	0.82	0.59	0.09	0.21	36.1
107	Uzbekistan	Kashkadarya	Karshi	irrigated	2007-2018	1.35	0.90	0.41	0.27	30.0
108	Uzbekistan	Kashkadarya	Kasbi	irrigated	2007-2018	5.76	4.68	4.23	0.48	10.2
109	Uzbekistan	Kashkadarya	Mirishkor	irrigated	2007-2018	6.15	5.08	4.64	0.44	8.7
110	Uzbekistan	Kashkadarya	Mubarak	irrigated	2007-2018	1.43	0.86	0.14	0.33	38.2
111	Uzbekistan	Kashkadarya	Nishan	irrigated	2007-2018	5.26	3.98	2.64	0.65	16.2
112	Uzbekistan	Khorezm	Bagat	irrigated	2007-2018	2.76	2.28	1.79	0.30	13.4
113	Uzbekistan	Khorezm	Gurlen	irrigated	2007-2018	4.56	3.76	2.73	0.56	14.8
114	Uzbekistan	Khorezm	Khanka	irrigated	2008-2016	5.41	2.93	1.98	1.04	35.6
115	Uzbekistan	Khorezm	Khazarasp	irrigated	2009-2016	6.10	1.85	1.00	1.89	101.7
116	Uzbekistan	Khorezm	Khiva	irrigated	2008-2016	5.70	4.79	4.05	0.58	12.2

Table A.2.1.2 *(continued)*

117	Uzbekistan	Khorezm	Kushkupir	irrigated	2008-2016	5.70	4.44	3.78	0.66	14.8
118	Uzbekistan	Khorezm	Shavat	irrigated	2008-2016	6.20	5.91	5.23	0.31	5.3
119	Uzbekistan	Khorezm	Urgench	irrigated	2008-2016	6.29	5.48	4.23	0.72	13.2
120	Uzbekistan	Khorezm	Yangiarik	irrigated	2008-2016	6.50	5.78	2.97	1.11	19.3
121	Uzbekistan	Khorezm	Yangibazar	irrigated	2008-2016	8.06	5.09	3.74	1.42	27.9
122	Uzbekistan	Navai	Kanimekh	irrigated	2008-2016	6.16	5.17	4.25	0.61	11.9
123	Uzbekistan	Navai	Karmana	irrigated	2008-2016	6.02	5.24	4.59	0.47	8.9
124	Uzbekistan	Navai	Khatirchi	irrigated	2008-2016	6.20	5.30	4.60	0.54	10.3
125	Uzbekistan	Navai	Kiziltepa	irrigated	2008-2016	8.78	6.12	4.94	1.17	19.0
126	Uzbekistan	Navai	Navbahor	irrigated	2008-2016	6.84	5.14	4.00	1.01	19.7
127	Uzbekistan	Navai	Nurota	irrigated	2007-2017	4.83	4.41	3.73	0.32	7.4
128	Uzbekistan	Djizzakh	Djizzakh	mixed	2007-2017	4.95	4.47	3.35	0.44	9.8
129	Uzbekistan	Djizzakh	Dustlik	mixed	2007-2017	5.05	4.46	3.65	0.46	10.3
130	Uzbekistan	Kashkadarya	Chirakchi	mixed	2007-2017	5.32	4.45	3.78	0.46	10.4
131	Uzbekistan	Kashkadarya	Guzar	mixed	2007-2017	4.79	4.42	3.99	0.28	6.3
132	Uzbekistan	Kashkadarya	Kamashi	mixed	2007-2017	4.87	4.14	2.88	0.62	15.0
133	Uzbekistan	Kashkadarya	Kasan	mixed	2007-2017	4.79	3.99	2.44	0.72	17.9
134	Uzbekistan	Kashkadarya	Shakhrisabz	mixed	2007-2017	5.03	4.46	3.63	0.39	8.8
135	Uzbekistan	Kashkadarya	Yangibag	mixed	2007-2017	4.80	4.20	2.95	0.52	12.5
136	Uzbekistan	Djizzakh	Bakhmal	rainfed	2007-2017	4.81	4.49	3.59	0.36	8.0
137	Uzbekistan	Djizzakh	Farish	rainfed	2008-2017	4.65	4.13	3.69	0.28	6.8
138	Uzbekistan	Djizzakh	Gallaral	rainfed	2008-2017	6.25	5.01	4.44	0.60	12.0
139	Uzbekistan	Djizzakh	Yangiabad	rainfed	2008-2017	5.61	5.34	4.98	0.22	4.1
140	Uzbekistan	Djizzakh	Zamin	rainfed	2008-2017	5.62	4.70	3.63	0.58	12.3
141	Uzbekistan	Kashkadarya	Dekhkanabad	rainfed	2008-2017	5.70	4.78	1.64	1.25	26.2
142	Uzbekistan	Kashkadarya	Kitab	rainfed	2008-2017	4.43	2.09	1.01	0.98	47.0

Appendix 2.2: Correlation time series between indices and wheat yield

Table A.2.2.1: Correlation time series between NDVI and wheat yield per country and mask type

	District borders								Croplands								Wheatlands							
	MON		KAZ		KGZ		UZB		MON		KAZ		KGZ		UZB		MON		KAZ		KGZ		UZB	
Day of year	mean	median	mean	median	mean	median	mean	median	mean	median	mean	median	mean	median	mean	median	mean	median	mean	median	mean	median	mean	median
17	0.16	0.20	-0.05	-0.06	0.03	0.10	0.18	0.27	0.16	0.20	-0.04	0.01	0.05	0.05	0.23	0.29	0.19	0.22	-0.08	-0.03	0.10	0.10	0.16	0.26
33	0.19	0.22	-0.06	-0.06	0.10	0.18	0.19	0.22	0.19	0.22	-0.09	-0.05	0.19	0.24	0.21	0.24	0.20	0.19	-0.12	-0.10	0.26	0.23	0.22	0.22
49	0.13	0.16	-0.02	-0.02	0.55	0.61	0.29	0.45	0.13	0.16	0.00	0.02	0.59	0.62	0.32	0.40	0.17	0.18	-0.05	-0.03	0.66	0.64	0.32	0.39
65	0.12	0.14	-0.09	-0.08	0.32	0.39	0.25	0.33	0.12	0.14	-0.12	-0.09	0.43	0.52	0.30	0.36	0.13	0.17	-0.14	-0.12	0.50	0.50	0.32	0.40
81	0.05	0.09	-0.14	-0.16	0.31	0.40	0.29	0.34	0.05	0.09	-0.13	-0.15	0.49	0.54	0.33	0.37	-0.03	0.00	-0.09	-0.08	0.50	0.50	0.34	0.41
97	0.14	0.16	-0.06	-0.06	0.20	0.24	0.23	0.23	0.14	0.16	-0.01	-0.04	0.40	0.42	0.25	0.23	-0.06	-0.01	-0.02	-0.04	0.17	0.09	0.25	0.25
113	0.21	0.19	0.06	0.04	0.35	0.44	0.22	0.26	0.21	0.19	-0.03	-0.02	0.65	0.71	0.23	0.23	0.04	0.07	0.07	0.04	0.63	0.67	0.19	0.21
129	0.12	0.14	0.11	0.08	0.45	0.54	0.13	0.18	0.12	0.14	-0.01	-0.05	0.68	0.75	0.11	0.10	-0.03	-0.01	0.06	0.01	0.59	0.65	-0.06	-0.11
145	0.09	0.05	0.32	0.34	0.49	0.59	0.09	0.13	0.09	0.05	0.14	0.16	0.78	0.79	0.06	0.04	-0.03	-0.05	0.16	0.14	0.44	0.55	-0.06	-0.12
161	0.23	0.29	0.31	0.31	0.63	0.73	0.11	0.13	0.23	0.29	0.10	0.13	0.75	0.74	0.04	0.09	0.15	0.18	0.11	0.11	0.19	0.15	-0.12	-0.14
177	0.52	0.58	0.47	0.50	0.57	0.61	0.14	0.21	0.52	0.58	0.40	0.46	0.76	0.77	0.15	0.17	0.40	0.36	0.29	0.32	-0.14	-0.20	-0.03	-0.01
193	0.59	0.65	0.62	0.65	0.49	0.50	0.13	0.20	0.59	0.65	0.59	0.65	0.52	0.49	0.12	0.12	0.52	0.57	0.53	0.60	-0.49	-0.51	-0.04	0.00
209	0.56	0.57	0.59	0.60	0.61	0.67	0.20	0.27	0.56	0.57	0.54	0.55	0.49	0.46	0.21	0.20	0.40	0.47	0.49	0.53	-0.41	-0.40	0.02	0.02
225	0.41	0.45	0.49	0.51	0.72	0.76	0.18	0.23	0.41	0.45	0.46	0.51	0.61	0.59	0.19	0.17	0.18	0.21	0.41	0.47	-0.32	-0.26	-0.03	-0.06
241	0.15	0.18	0.22	0.27	0.64	0.65	0.19	0.24	0.15	0.18	0.18	0.28	0.72	0.73	0.16	0.13	-0.10	-0.09	0.09	0.17	-0.37	-0.37	-0.03	-0.06
257	-0.01	-0.01	0.08	0.10	0.70	0.74	0.09	0.16	-0.01	-0.01	-0.01	0.06	0.72	0.74	0.04	0.02	-0.20	-0.23	-0.07	-0.06	-0.25	-0.30	-0.12	-0.15

Table A.2.2.2: Correlation time series between EVI and wheat yield per country and mask type

Day of year	District borders								Croplands								Wheatlands							
	MON		KAZ		KGZ		UZB		MON		KAZ		KGZ		UZB		MON		KAZ		KGZ		UZB	
	mean	median	mean	median	mean	median	mean	median	mean	median	mean	median	mean	median	mean	median	mean	median	mean	median	mean	median	mean	median
17	0.18	0.20	-0.03	-0.03	-0.03	0.02	0.19	0.26	0.18	0.20	-0.02	0.04	0.03	0.07	0.19	0.29	0.20	0.22	-0.06	0.02	0.10	0.07	0.17	0.26
33	0.22	0.23	-0.06	-0.05	0.09	0.20	0.19	0.21	0.22	0.23	-0.09	-0.05	0.22	0.29	0.22	0.21	0.22	0.22	-0.12	-0.11	0.30	0.25	0.20	0.21
49	0.18	0.21	-0.03	-0.03	0.53	0.65	0.31	0.45	0.18	0.21	-0.01	0.00	0.59	0.64	0.31	0.42	0.21	0.20	-0.06	-0.03	0.65	0.64	0.34	0.41
65	0.16	0.18	-0.13	-0.10	0.25	0.33	0.21	0.27	0.16	0.18	-0.15	-0.13	0.39	0.51	0.24	0.32	0.17	0.20	-0.16	-0.17	0.49	0.50	0.29	0.37
81	0.05	0.07	-0.14	-0.16	0.25	0.37	0.26	0.33	0.05	0.07	-0.13	-0.13	0.44	0.51	0.25	0.33	0.01	0.07	-0.10	-0.11	0.46	0.41	0.31	0.37
97	0.26	0.26	-0.06	-0.06	0.16	0.20	0.21	0.24	0.26	0.26	-0.01	-0.04	0.33	0.34	0.21	0.23	0.17	0.14	0.00	-0.04	0.15	0.06	0.26	0.28
113	0.22	0.25	0.05	0.02	0.29	0.37	0.22	0.26	0.22	0.25	-0.03	-0.08	0.56	0.60	0.23	0.20	0.12	0.12	0.09	0.07	0.42	0.48	0.15	0.14
129	0.16	0.21	0.10	0.06	0.47	0.57	0.12	0.13	0.16	0.21	-0.05	-0.07	0.69	0.76	0.08	0.05	0.17	0.15	0.08	0.03	0.52	0.63	-0.08	-0.10
145	0.12	0.11	0.34	0.37	0.50	0.60	0.09	0.11	0.12	0.11	0.15	0.16	0.77	0.78	0.02	0.01	0.03	0.01	0.18	0.17	0.37	0.48	-0.08	-0.12
161	0.26	0.31	0.33	0.36	0.61	0.70	0.04	0.09	0.26	0.31	0.14	0.13	0.72	0.71	-0.04	-0.04	0.20	0.22	0.15	0.15	-0.02	-0.03	-0.16	-0.19
177	0.48	0.57	0.50	0.54	0.57	0.60	0.11	0.17	0.48	0.57	0.44	0.49	0.74	0.76	0.07	0.15	0.40	0.40	0.34	0.40	-0.57	-0.59	-0.07	-0.05
193	0.61	0.67	0.61	0.63	0.41	0.46	0.08	0.15	0.61	0.67	0.57	0.64	0.50	0.47	0.06	0.08	0.53	0.57	0.51	0.55	-0.63	-0.68	-0.07	-0.05
209	0.53	0.55	0.60	0.63	0.60	0.64	0.15	0.19	0.53	0.55	0.56	0.59	0.53	0.52	0.14	0.13	0.38	0.43	0.50	0.54	-0.64	-0.62	-0.03	-0.05
225	0.41	0.45	0.49	0.49	0.70	0.74	0.14	0.19	0.41	0.45	0.47	0.52	0.50	0.47	0.14	0.15	0.23	0.29	0.41	0.47	-0.56	-0.56	-0.07	-0.09
241	0.21	0.25	0.22	0.24	0.62	0.63	0.14	0.19	0.21	0.25	0.20	0.27	0.61	0.61	0.10	0.12	-0.02	-0.06	0.11	0.21	-0.56	-0.60	-0.07	-0.09
257	-0.01	-0.01	0.07	0.08	0.59	0.66	0.04	0.05	-0.01	-0.01	0.05	0.04	0.49	0.50	-0.04	-0.07	-0.15	-0.15	-0.03	-0.02	-0.58	-0.68	-0.16	-0.18

Table A.2.2.3: Correlation time series between GCI and wheat yield per country and mask type

Day of year	District borders								Croplands								Wheatlands							
	MON		KAZ		KGZ		UZB		MON		KAZ		KGZ		UZB		MON		KAZ		KGZ		UZB	
	mean	median	mean	median	mean	median	mean	median	mean	median	mean	median	mean	median	mean	median	mean	median	mean	median	mean	median	mean	median
33	0.20	0.25	-0.07	-0.06	-0.02	0.01	0.21	0.23	0.20	0.25	-0.07	-0.06	0.04	0.02	0.23	0.29	0.20	0.20	-0.03	-0.05	0.07	0.02	0.23	0.29
41	0.16	0.15	-0.12	-0.10	0.05	0.10	0.13	0.09	0.16	0.15	-0.18	-0.18	0.19	0.19	0.12	0.10	0.19	0.20	-0.15	-0.13	0.27	0.19	0.16	0.15
49	0.08	0.09	-0.05	-0.02	0.44	0.52	0.21	0.27	0.08	0.09	-0.02	0.00	0.51	0.54	0.19	0.24	0.11	0.13	-0.06	-0.03	0.52	0.50	0.19	0.23
57	0.12	0.14	-0.11	-0.09	0.55	0.62	0.25	0.35	0.11	0.16	-0.09	-0.10	0.61	0.65	0.25	0.34	0.13	0.17	-0.11	-0.07	0.68	0.67	0.28	0.37
65	0.09	0.09	-0.14	-0.12	0.32	0.40	0.23	0.24	0.09	0.09	-0.14	-0.13	0.45	0.54	0.21	0.24	0.11	0.11	-0.16	-0.14	0.52	0.55	0.21	0.23
73	0.15	0.14	-0.10	-0.10	0.28	0.36	0.17	0.19	0.15	0.14	-0.14	-0.14	0.40	0.49	0.18	0.27	0.18	0.21	-0.17	-0.19	0.43	0.46	0.25	0.30
81	0.20	0.19	-0.05	-0.08	0.34	0.38	0.26	0.29	0.20	0.19	-0.11	-0.13	0.51	0.56	0.24	0.31	0.14	0.20	-0.09	-0.08	0.30	0.26	0.27	0.32
89	0.06	0.11	-0.15	-0.15	0.32	0.42	0.27	0.32	0.06	0.11	-0.18	-0.19	0.54	0.58	0.27	0.36	0.01	0.05	-0.11	-0.11	0.43	0.46	0.32	0.39
97	0.20	0.21	-0.03	-0.03	0.25	0.27	0.24	0.26	0.20	0.21	-0.08	-0.06	0.40	0.44	0.21	0.23	0.09	0.08	0.00	0.00	0.30	0.35	0.25	0.28
105	0.13	0.17	-0.12	-0.13	0.10	0.13	0.26	0.27	0.13	0.17	-0.13	-0.12	0.40	0.40	0.28	0.26	0.07	0.03	-0.08	-0.09	0.06	0.01	0.30	0.35
113	0.14	0.15	-0.05	-0.03	0.35	0.41	0.20	0.29	0.14	0.15	-0.01	-0.02	0.64	0.69	0.20	0.23	0.09	0.11	-0.04	-0.04	0.57	0.61	0.19	0.24
121	0.11	0.09	0.01	0.03	0.38	0.47	0.23	0.23	0.11	0.09	-0.01	0.02	0.63	0.65	0.22	0.17	0.01	0.01	0.02	0.01	0.62	0.68	0.23	0.27
129	0.18	0.20	-0.01	-0.03	0.38	0.45	0.24	0.22	0.18	0.20	-0.05	-0.06	0.69	0.71	0.26	0.20	0.14	0.13	-0.04	0.00	0.62	0.69	0.18	0.18
137	0.14	0.11	0.11	0.12	0.61	0.64	0.12	0.20	0.14	0.11	0.04	0.04	0.74	0.76	0.08	0.12	0.10	0.10	0.04	0.01	0.65	0.76	0.01	0.02
145	0.05	0.04	0.16	0.18	0.52	0.59	0.10	0.12	0.05	0.04	0.07	0.04	0.77	0.77	0.03	0.05	-0.01	-0.03	0.04	0.05	0.39	0.50	-0.04	-0.05
153	0.12	0.11	0.35	0.37	0.49	0.56	0.08	0.16	0.12	0.11	0.21	0.26	0.69	0.69	0.03	0.02	0.04	0.06	0.17	0.15	0.19	0.34	-0.03	0.00
161	0.24	0.26	0.39	0.38	0.52	0.61	0.11	0.14	0.24	0.26	0.20	0.23	0.73	0.75	0.04	0.08	0.16	0.17	0.23	0.22	0.30	0.33	-0.01	-0.02
169	0.23	0.30	0.08	0.06	0.49	0.58	0.14	0.19	0.23	0.30	-0.02	-0.02	0.75	0.76	0.13	0.25	0.30	0.32	-0.10	-0.07	0.13	0.09	0.03	0.05
177	0.49	0.53	0.51	0.55	0.48	0.53	0.10	0.17	0.49	0.53	0.34	0.38	0.79	0.77	0.05	0.03	0.43	0.45	0.32	0.35	0.08	0.11	-0.01	-0.02
185	0.51	0.58	0.47	0.52	0.55	0.57	0.15	0.19	0.51	0.58	0.28	0.35	0.68	0.67	0.15	0.18	0.49	0.54	0.26	0.29	-0.05	-0.05	0.06	0.02
193	0.52	0.58	0.58	0.61	0.55	0.63	0.13	0.19	0.52	0.58	0.39	0.42	0.65	0.64	0.08	0.12	0.53	0.53	0.42	0.43	-0.21	-0.12	-0.01	-0.01
201	0.56	0.62	0.61	0.64	0.63	0.64	0.13	0.24	0.56	0.62	0.45	0.50	0.59	0.56	0.10	0.12	0.54	0.57	0.47	0.48	-0.34	-0.31	0.00	0.00
209	0.55	0.59	0.58	0.61	0.49	0.50	0.19	0.26	0.55	0.59	0.43	0.45	0.52	0.48	0.18	0.26	0.47	0.52	0.46	0.47	-0.30	-0.30	0.05	0.03
217	0.49	0.54	0.61	0.63	0.64	0.67	0.18	0.26	0.49	0.54	0.46	0.51	0.52	0.50	0.18	0.25	0.44	0.51	0.50	0.49	-0.36	-0.31	0.06	0.06
225	0.41	0.45	0.52	0.55	0.64	0.63	0.17	0.22	0.41	0.45	0.40	0.42	0.55	0.54	0.15	0.21	0.35	0.44	0.44	0.46	-0.16	-0.07	0.01	0.02
233	0.38	0.37	0.27	0.25	0.67	0.70	0.19	0.22	0.38	0.37	0.17	0.13	0.61	0.60	0.19	0.21	0.21	0.24	0.21	0.20	-0.18	-0.04	0.04	0.00
241	0.27	0.31	0.27	0.29	0.57	0.55	0.18	0.21	0.27	0.31	0.18	0.18	0.71	0.69	0.12	0.13	0.02	0.09	0.18	0.18	-0.27	-0.23	-0.02	-0.07

Table A.2.2.4: Correlation time series between Lai and wheat yield per country and mask type

Day of year	District borders								Croplands								Wheatlands							
	MON		KAZ		KGZ		UZB		MON		KAZ		KGZ		UZB		MON		KAZ		KGZ		UZB	
	mean	median	mean	median	mean	median	mean	median	mean	median	mean	median	mean	median	mean	median	mean	median	mean	median	mean	median	mean	median
41	0.12	0.11	-0.27	-0.27	-0.02	-0.02	0.00	-0.01	0.12	0.11	-0.16	-0.24	0.18	0.15	-0.01	-0.03	0.13	0.17	-0.31	-0.31	0.31	0.24	0.01	-0.03
45	0.21	0.20	-0.05	-0.05	0.12	0.12	0.14	0.15	0.21	0.20	-0.04	-0.07	0.33	0.37	0.07	0.13	0.24	0.25	-0.18	-0.24	0.40	0.34	0.13	0.14
49	0.18	0.19	-0.10	-0.10	0.24	0.24	0.18	0.21	0.18	0.19	-0.07	-0.12	0.28	0.31	0.19	0.21	0.19	0.19	-0.25	-0.24	0.39	0.43	0.16	0.16
53	0.10	0.09	-0.15	-0.15	0.12	0.12	-0.04	0.01	0.10	0.09	-0.14	-0.22	0.30	0.36	-0.14	-0.15	0.19	0.22	-0.30	-0.32	0.38	0.39	-0.01	0.04
57	0.22	0.28	-0.12	-0.12	0.60	0.60	0.20	0.24	0.22	0.28	-0.11	-0.12	0.70	0.71	0.21	0.27	0.22	0.24	-0.30	-0.28	0.75	0.72	0.18	0.19
61	0.19	0.19	-0.17	-0.17	0.36	0.36	0.28	0.33	0.19	0.19	-0.13	-0.10	0.54	0.61	0.29	0.39	0.21	0.22	-0.24	-0.23	0.61	0.63	0.34	0.38
65	0.21	0.26	-0.13	-0.13	0.40	0.40	0.27	0.26	0.21	0.26	-0.17	-0.20	0.51	0.59	0.26	0.32	0.22	0.22	-0.19	-0.20	0.59	0.61	0.28	0.29
69	0.25	0.28	-0.14	-0.14	0.35	0.35	0.22	0.27	0.25	0.28	-0.10	-0.13	0.45	0.57	0.21	0.28	0.29	0.31	-0.14	-0.18	0.55	0.66	0.25	0.27
73	0.26	0.31	-0.07	-0.07	0.40	0.40	0.15	0.20	0.26	0.31	-0.06	-0.05	0.48	0.55	0.11	0.17	0.33	0.33	-0.11	-0.14	0.55	0.58	0.17	0.21
77	0.21	0.21	0.04	0.04	0.32	0.32	0.21	0.26	0.21	0.21	0.06	0.09	0.36	0.42	0.19	0.26	0.27	0.28	0.00	0.01	0.45	0.47	0.23	0.29
81	0.22	0.26	-0.07	-0.07	0.22	0.22	0.10	0.12	0.22	0.26	-0.06	-0.06	0.31	0.33	0.07	0.09	0.20	0.19	-0.07	-0.09	0.32	0.34	0.15	0.12
85	0.10	0.09	-0.04	-0.04	0.48	0.48	0.14	0.14	0.10	0.09	-0.03	0.00	0.54	0.59	0.16	0.19	0.07	0.12	-0.04	-0.04	0.58	0.57	0.16	0.18
89	0.03	0.07	-0.09	-0.09	0.33	0.33	-0.03	-0.04	0.03	0.07	-0.08	-0.04	0.43	0.42	-0.03	-0.03	0.04	0.08	-0.09	-0.08	0.32	0.31	-0.04	-0.02
93	0.22	0.24	-0.23	-0.23	0.38	0.38	0.25	0.26	0.22	0.24	-0.22	-0.20	0.49	0.51	0.23	0.27	0.21	0.21	-0.23	-0.21	0.48	0.42	0.29	0.29
97	0.13	0.13	-0.14	-0.14	0.44	0.44	0.21	0.23	0.13	0.13	-0.07	-0.09	0.45	0.50	0.20	0.22	0.02	0.02	-0.13	-0.14	0.35	0.32	0.23	0.21
101	0.13	0.14	-0.08	-0.08	0.24	0.24	0.31	0.32	0.13	0.14	-0.01	0.00	0.30	0.30	0.29	0.27	0.01	-0.03	-0.06	-0.07	0.26	0.27	0.34	0.31
105	-0.10	-0.13	-0.15	-0.15	0.04	0.04	0.18	0.19	-0.10	-0.13	-0.12	-0.11	0.07	0.07	0.23	0.22	-0.16	-0.25	-0.14	-0.12	-0.06	-0.10	0.20	0.23
109	0.19	0.22	-0.28	-0.28	0.14	0.14	0.34	0.37	0.19	0.22	-0.24	-0.27	0.26	0.25	0.34	0.36	0.16	0.12	-0.25	-0.27	0.08	0.09	0.36	0.40
113	-0.02	-0.03	-0.20	-0.20	0.28	0.28	0.21	0.22	-0.02	-0.03	-0.19	-0.18	0.40	0.41	0.25	0.23	-0.08	-0.14	-0.16	-0.13	0.33	0.34	0.19	0.17
117	-0.04	-0.07	-0.03	-0.03	0.64	0.64	0.16	0.19	-0.04	-0.07	-0.03	0.01	0.75	0.82	0.16	0.16	-0.08	-0.14	0.00	0.00	0.76	0.85	0.14	0.14
121	0.31	0.31	0.07	0.07	0.05	0.05	0.16	0.24	0.31	0.31	0.04	0.02	0.16	0.16	0.18	0.22	0.30	0.34	0.12	0.15	0.06	0.08	0.14	0.13
125	-0.02	-0.02	0.09	0.09	0.46	0.46	0.12	0.11	-0.02	-0.02	0.04	0.08	0.61	0.67	0.11	0.05	-0.09	-0.07	0.09	0.10	0.66	0.79	0.02	0.01
129	0.19	0.23	0.00	0.00	0.26	0.26	0.05	0.04	0.19	0.23	-0.05	-0.09	0.53	0.55	0.06	0.07	0.17	0.17	-0.01	-0.05	0.49	0.54	-0.03	-0.09
133	0.20	0.22	0.00	0.00	0.41	0.41	0.20	0.17	0.20	0.22	-0.10	-0.15	0.57	0.65	0.26	0.23	0.24	0.27	-0.04	-0.04	0.54	0.58	0.17	0.20
137	0.17	0.18	0.07	0.07	0.59	0.59	0.19	0.26	0.17	0.18	-0.01	-0.01	0.72	0.73	0.17	0.18	0.19	0.15	0.04	0.03	0.65	0.65	0.04	0.07
141	0.08	0.06	0.04	0.04	0.55	0.55	0.12	0.18	0.08	0.06	-0.08	-0.08	0.63	0.67	0.10	0.11	0.12	0.12	0.00	-0.04	0.54	0.60	-0.04	0.02
145	0.09	0.09	0.16	0.16	0.67	0.67	0.14	0.20	0.09	0.09	0.02	0.05	0.77	0.80	0.11	0.05	0.12	0.17	0.10	0.11	0.64	0.74	-0.02	0.01
149	0.14	0.13	0.13	0.13	0.69	0.69	0.15	0.11	0.14	0.13	-0.01	0.05	0.83	0.82	0.11	0.07	0.16	0.12	0.05	0.05	0.66	0.77	0.02	0.04
153	0.18	0.18	0.25	0.25	0.48	0.48	0.02	0.03	0.18	0.18	0.09	0.12	0.74	0.79	-0.06	-0.06	0.22	0.21	0.13	0.16	0.50	0.62	-0.10	-0.11
157	0.14	0.12	0.44	0.44	0.64	0.64	0.09	0.12	0.14	0.12	0.27	0.35	0.79	0.81	0.02	0.04	0.15	0.12	0.31	0.33	0.55	0.61	-0.05	-0.06
161	0.23	0.22	0.46	0.46	0.34	0.34	0.05	0.03	0.23	0.22	0.28	0.29	0.63	0.63	0.00	0.01	0.20	0.16	0.34	0.35	0.24	0.25	-0.07	-0.09
165	0.16	0.20	0.50	0.50	0.50	0.50	0.12	0.16	0.16	0.20	0.33	0.36	0.71	0.72	0.15	0.13	0.19	0.22	0.35	0.34	0.45	0.50	0.05	0.00
169	0.07	0.13	0.26	0.26	0.51	0.51	0.13	0.17	0.07	0.13	0.13	0.14	0.70	0.70	0.13	0.15	0.16	0.22	0.13	0.11	0.17	0.15	-0.02	0.01
173	0.09	0.11	0.12	0.12	0.35	0.35	0.08	0.14	0.09	0.11	-0.03	-0.09	0.56	0.57	0.01	0.02	0.22	0.22	-0.04	-0.06	0.12	0.08	-0.10	-0.09
177	0.40	0.46	0.51	0.51	0.48	0.48	0.09	0.12	0.40	0.46	0.42	0.44	0.69	0.67	0.09	0.18	0.49	0.50	0.38	0.45	0.09	0.06	-0.07	-0.06
181	0.53	0.56	0.45	0.45	0.41	0.41	0.13	0.22	0.53	0.56	0.39	0.45	0.65	0.65	0.07	0.02	0.52	0.53	0.32	0.36	-0.12	-0.10	-0.04	-0.05

Table A.2.2.4 *(continued)*

185	0.36	0.44	0.53	0.53	0.54	0.54	0.15	0.25	0.36	0.44	0.47	0.49	0.65	0.67	0.11	0.17	0.41	0.44	0.40	0.47	0.08	0.05	0.01	-0.05
189	0.44	0.57	0.45	0.45	0.52	0.52	0.13	0.23	0.44	0.57	0.41	0.44	0.60	0.58	0.04	0.13	0.53	0.59	0.34	0.36	0.11	0.13	-0.07	-0.08
193	0.60	0.68	0.49	0.49	0.54	0.54	0.14	0.15	0.60	0.68	0.46	0.50	0.58	0.56	0.15	0.20	0.60	0.64	0.39	0.45	-0.22	-0.14	0.03	0.02
197	0.37	0.47	0.65	0.65	0.35	0.35	0.15	0.21	0.37	0.47	0.61	0.68	0.42	0.39	0.06	0.04	0.40	0.44	0.53	0.62	-0.16	-0.15	-0.04	-0.09
201	0.49	0.61	0.66	0.66	0.41	0.41	0.13	0.24	0.49	0.61	0.62	0.65	0.45	0.45	0.13	0.15	0.54	0.58	0.53	0.56	-0.16	-0.14	0.00	0.01
205	0.52	0.58	0.61	0.61	0.68	0.68	0.08	0.15	0.52	0.58	0.55	0.61	0.54	0.54	-0.02	0.03	0.54	0.56	0.52	0.53	-0.12	-0.09	-0.14	-0.13
209	0.62	0.64	0.63	0.63	0.44	0.44	0.16	0.21	0.62	0.66	0.56	0.61	0.45	0.45	0.15	0.25	0.58	0.64	0.55	0.58	-0.32	-0.32	-0.03	-0.05
213	0.35	0.39	0.60	0.60	0.32	0.32	0.25	0.33	0.35	0.39	0.58	0.64	0.37	0.37	0.13	0.21	0.37	0.41	0.53	0.59	-0.18	-0.17	0.04	0.03
217	0.35	0.43	0.60	0.60	0.58	0.58	0.20	0.31	0.35	0.43	0.53	0.58	0.49	0.43	0.17	0.22	0.37	0.43	0.51	0.51	-0.14	-0.08	0.03	0.09
221	0.48	0.54	0.56	0.56	0.50	0.50	0.16	0.20	0.48	0.54	0.50	0.52	0.46	0.45	0.07	0.05	0.43	0.49	0.47	0.48	-0.10	-0.05	-0.06	-0.09
225	0.43	0.46	0.52	0.52	0.74	0.74	0.19	0.24	0.43	0.46	0.53	0.56	0.65	0.61	0.17	0.25	0.42	0.41	0.45	0.47	-0.09	-0.03	0.02	0.02
229	0.38	0.36	0.38	0.38	0.60	0.60	0.23	0.29	0.38	0.36	0.36	0.37	0.46	0.41	0.20	0.22	0.28	0.30	0.31	0.33	-0.23	-0.17	0.04	0.01

Table A.2.2.5: Correlation time series between LST and wheat yield per country and mask type

Day of year	District borders								Croplands								Wheatlands							
	MON		KAZ		KGZ		UZB		MON		KAZ		KGZ		UZB		MON		KAZ		KGZ		UZB	
	mean	median	mean	median	mean	median	mean	median	mean	median	mean	median	mean	median	mean	median	mean	median	mean	median	mean	median	mean	median
65	0.01	0.01	-0.02	0.04	0.25	0.31	0.19	0.18	0.19	0.23	0.00	0.03	0.37	0.44	0.19	0.16	0.05	0.05	-0.01	0.02	0.42	0.46	0.18	0.14
73	0.09	0.10	0.17	0.15	0.12	0.09	-0.11	-0.14	0.18	0.18	0.20	0.18	0.19	0.17	-0.09	-0.09	0.14	0.15	0.17	0.19	0.22	0.17	-0.09	-0.11
81	0.13	0.15	0.02	0.04	0.17	0.20	-0.16	-0.20	0.20	0.22	0.04	0.04	0.10	0.10	-0.21	-0.21	0.17	0.17	0.01	0.02	0.13	0.13	-0.17	-0.19
89	0.12	0.14	-0.12	-0.13	-0.37	-0.39	-0.28	-0.28	0.26	0.30	-0.11	-0.14	-0.41	-0.44	-0.30	-0.34	0.15	0.16	-0.13	-0.14	-0.40	-0.38	-0.27	-0.28
97	0.21	0.28	-0.01	-0.02	-0.11	-0.11	-0.10	-0.08	0.28	0.33	-0.04	-0.04	-0.24	-0.28	-0.11	-0.15	0.23	0.25	0.00	-0.01	-0.24	-0.27	-0.11	-0.13
105	0.20	0.23	-0.13	-0.14	-0.35	-0.36	-0.05	-0.05	0.09	0.15	-0.10	-0.14	-0.40	-0.41	-0.08	-0.08	0.22	0.21	-0.09	-0.11	-0.40	-0.41	-0.06	-0.07
113	-0.04	-0.03	-0.22	-0.28	-0.49	-0.48	-0.07	-0.11	0.20	0.22	-0.19	-0.17	-0.52	-0.54	-0.03	-0.10	0.01	0.03	-0.16	-0.16	-0.52	-0.51	-0.05	-0.11
121	0.13	0.14	0.02	0.01	-0.61	-0.58	-0.11	-0.13	0.01	0.03	0.05	0.01	-0.75	-0.76	-0.14	-0.16	0.16	0.17	0.07	0.01	-0.73	-0.74	-0.13	-0.14
129	-0.11	-0.15	-0.10	-0.08	-0.66	-0.68	-0.13	-0.15	-0.24	-0.26	-0.07	-0.06	-0.66	-0.67	-0.10	-0.15	-0.08	-0.08	-0.06	-0.03	-0.68	-0.70	-0.10	-0.16
137	-0.31	-0.31	-0.14	-0.13	-0.59	-0.65	-0.10	-0.14	-0.13	-0.15	-0.09	-0.11	-0.68	-0.69	-0.10	-0.12	-0.28	-0.31	-0.10	-0.09	-0.64	-0.64	-0.03	-0.10
145	-0.16	-0.21	-0.23	-0.24	-0.68	-0.74	0.00	-0.05	0.05	0.04	-0.19	-0.22	-0.78	-0.82	0.04	0.03	-0.16	-0.21	-0.19	-0.20	-0.77	-0.81	0.07	0.10
153	-0.07	-0.06	-0.34	-0.33	-0.27	-0.29	-0.02	0.01	-0.16	-0.19	-0.27	-0.29	-0.47	-0.43	0.03	0.11	-0.06	-0.03	-0.29	-0.30	-0.39	-0.35	0.05	0.11
161	-0.20	-0.26	-0.21	-0.20	-0.47	-0.48	0.02	0.01	-0.52	-0.53	-0.16	-0.16	-0.71	-0.73	0.06	0.11	-0.15	-0.22	-0.14	-0.15	-0.64	-0.66	0.08	0.09
169	-0.52	-0.53	-0.39	-0.44	-0.54	-0.53	-0.17	-0.21	-0.41	-0.46	-0.35	-0.39	-0.70	-0.71	-0.17	-0.23	-0.48	-0.47	-0.30	-0.33	-0.60	-0.61	-0.12	-0.13
177	-0.41	-0.46	-0.40	-0.43	-0.67	-0.67	0.07	0.01	-0.50	-0.51	-0.41	-0.44	-0.67	-0.66	0.08	0.06	-0.41	-0.44	-0.32	-0.37	-0.49	-0.45	0.11	0.08
185	-0.47	-0.46	-0.36	-0.38	-0.52	-0.50	0.01	0.00	-0.41	-0.47	-0.38	-0.40	-0.65	-0.66	0.01	-0.04	-0.42	-0.42	-0.28	-0.30	-0.40	-0.41	0.03	-0.03
193	-0.39	-0.45	-0.44	-0.45	-0.43	-0.42	0.00	-0.04	-0.47	-0.52	-0.43	-0.44	-0.67	-0.66	0.00	-0.07	-0.34	-0.38	-0.39	-0.42	-0.53	-0.51	0.01	-0.07
201	-0.46	-0.49	-0.43	-0.47	-0.40	-0.42	0.03	0.04	-0.36	-0.38	-0.44	-0.49	-0.52	-0.51	0.03	0.02	-0.46	-0.47	-0.40	-0.40	-0.32	-0.32	0.06	0.09
209	-0.30	-0.32	-0.39	-0.41	-0.24	-0.27	-0.18	-0.24	-0.49	-0.53	-0.46	-0.47	-0.29	-0.33	-0.14	-0.17	-0.28	-0.29	-0.35	-0.38	-0.14	-0.19	-0.08	-0.10
217	-0.46	-0.50	-0.43	-0.44	-0.58	-0.62	0.04	0.08	-0.25	-0.25	-0.49	-0.51	-0.57	-0.57	0.08	0.10	-0.43	-0.48	-0.38	-0.40	-0.33	-0.31	0.15	0.22
225	-0.26	-0.27	-0.30	-0.29	-0.55	-0.58	-0.13	-0.19	-0.27	-0.29	-0.36	-0.35	-0.60	-0.64	-0.09	-0.12	-0.20	-0.22	-0.27	-0.26	-0.46	-0.46	-0.05	-0.05
233	-0.28	-0.31	-0.34	-0.34	-0.82	-0.85	-0.03	-0.01	-0.16	-0.20	-0.39	-0.41	-0.81	-0.84	-0.04	-0.03	-0.21	-0.23	-0.32	-0.30	-0.70	-0.70	0.06	0.12
241	-0.13	-0.14	-0.11	-0.07	-0.70	-0.71	-0.02	-0.02	-0.16	-0.16	-0.13	-0.13	-0.69	-0.69	0.00	0.06	-0.08	-0.09	-0.10	-0.09	-0.55	-0.55	0.05	0.10

Appendix 2.3: Statistical significance of Wilcoxon test and boxplots

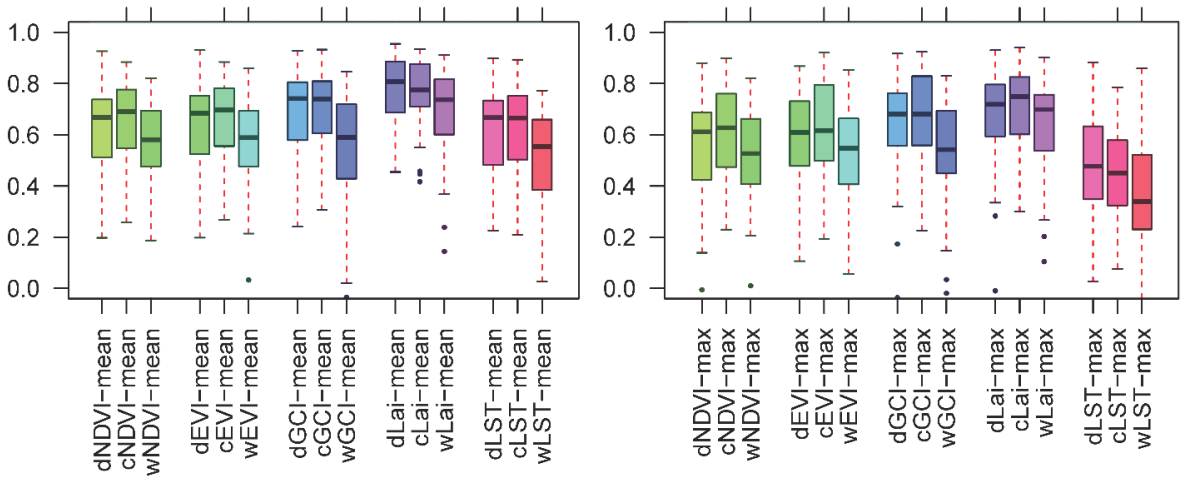

Figure A.2.3.1: Boxplot of correlation coefficients between rainfed wheat yields in Kazakhstan and mean/max values of satellite vegetation indices for the entire district area, croplands and wheatlands; Note: Statistical significance of Wilcoxon test is indicated by following p-values: **p≤0.05, ** p≤0.01, ***p≤0.001*

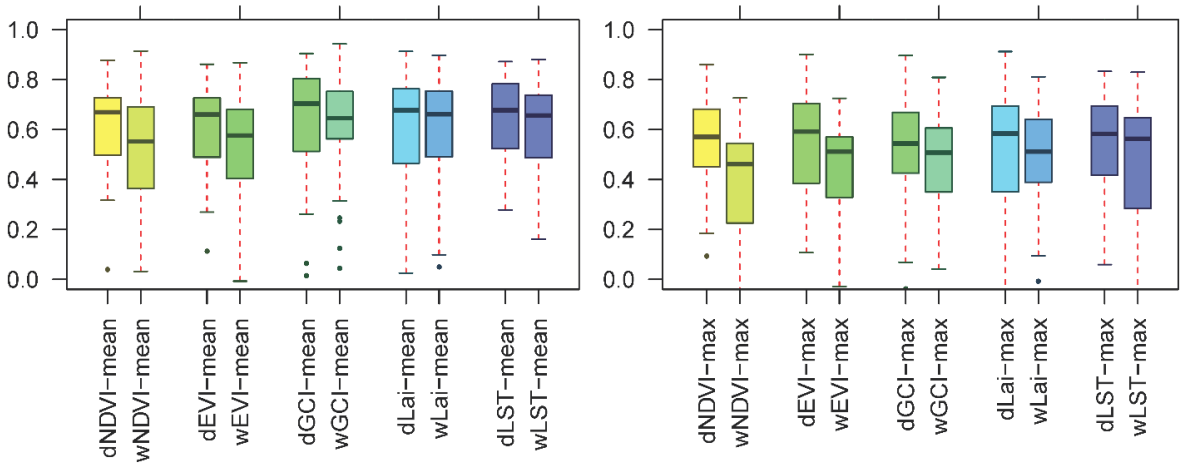

Figure A.2.3.2: Boxplot of correlation coefficients between rainfed wheat yields in Mongolia and mean/max values of indices for the entire district area, croplands and wheatlands; Note: Statistical significance of Wilcoxon test is indicated by following p-values: **p≤0.05, ** p≤0.01, ***p≤0.001*

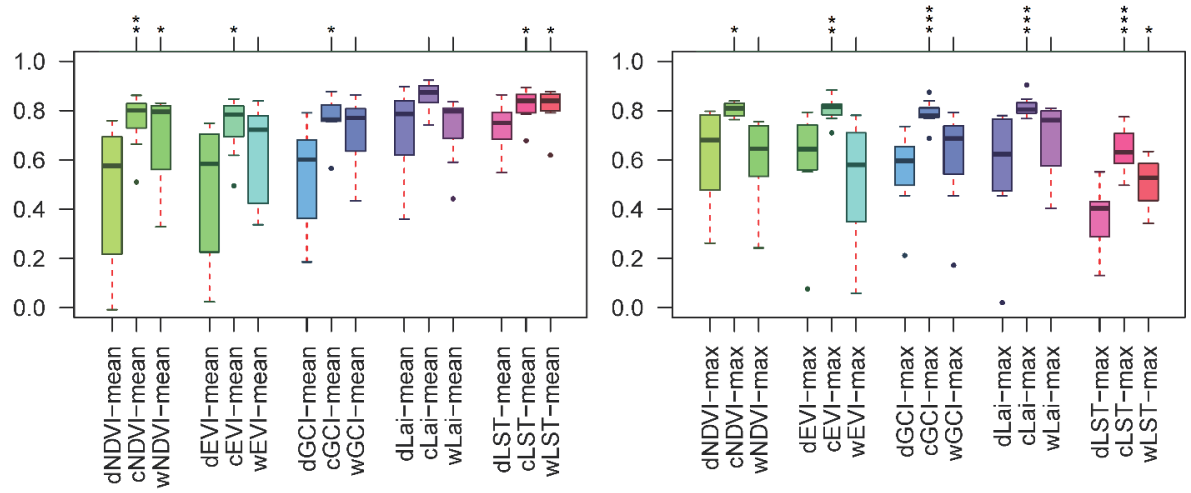

Figure A.2.3.3: Boxplot of correlation coefficients between mixed wheat yields in Kyrgyzstan and mean/max values of indices for the entire district area, croplands and wheatlands; Note: Statistical significance of Wilcoxon test is indicated by following p-values: **p≤0.05, ** p≤0.01, ***p≤0.001*.

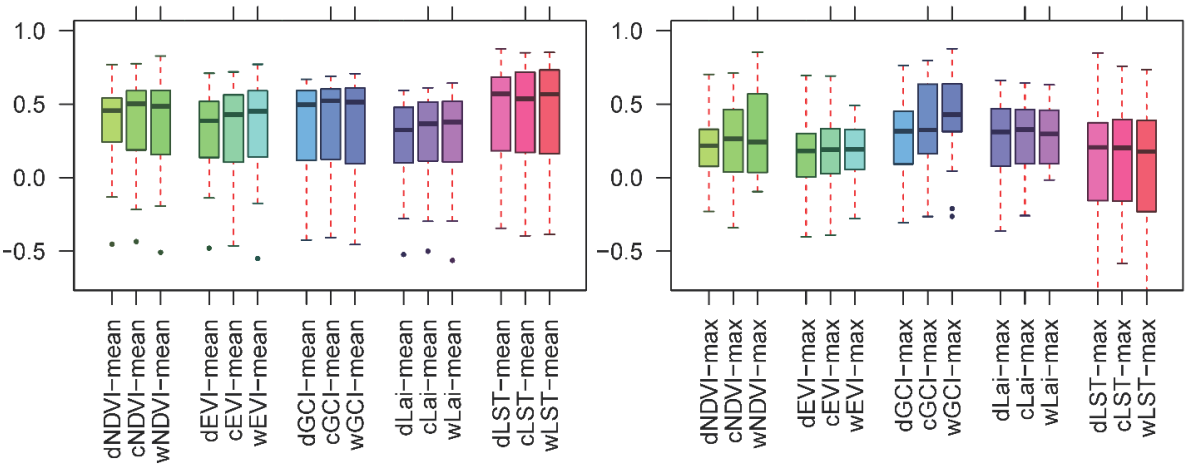

Figure A.2.3.4: Boxplot of correlation coefficients between irrigated wheat yields in Uzbekistan and mean/max values of indices for the entire district area, croplands and wheatlands; Note: Statistical significance of Wilcoxon test is indicated by following p-values: **p≤0.05, ** p≤0.01, ***p≤0.001*

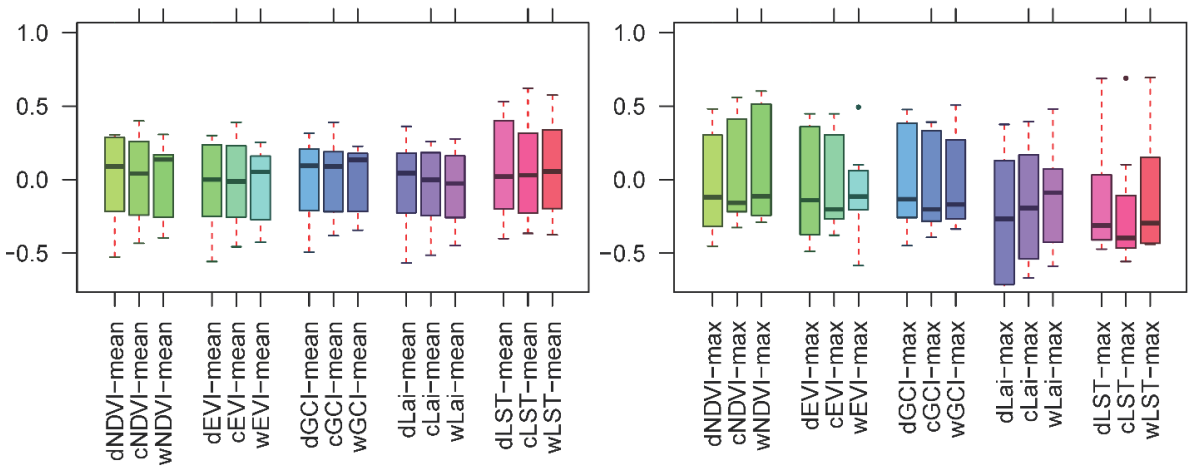

Figure A.2.3.5: Boxplot of correlation coefficients between mixed wheat yield in Uzbekistan and mean/max values of indices for entire district area, croplands and wheatlands; Note: Statistical significance of Wilcoxon test is indicated by following p-values: **p≤0.05, ** p≤0.01, ***p≤0.001*

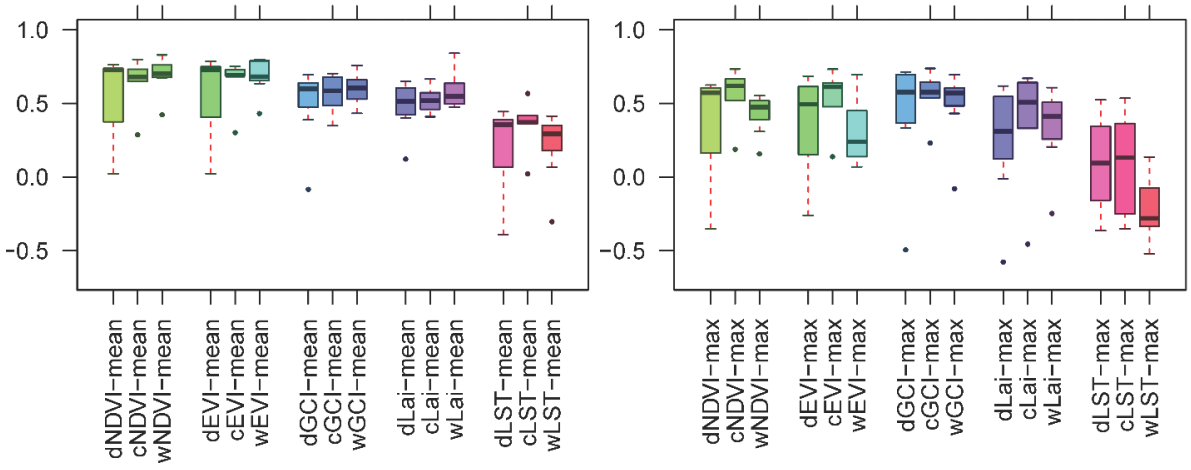

Figure A.2.3.6: Boxplot of correlation coefficients between rainfed wheat yield in Uzbekistan and mean/max values of indices for entire district area, croplands and wheatlands; Note: Statistical significance of Wilcoxon test is indicated by following p-values: **p≤0.05, ** p≤0.01, ***p≤0.001*

Appendix 3: Improving risk reduction potential of weather index insurance by spatially downscaling gridded climate data - a machine learning approach[20]

Table A.3.1: Descriptive statistics of spring wheat yield data

№	Country	Province	County	Period of yield observation	MAX	MEAN	MIN	STD
1	Kazakhstan	Akmola	Akkol	1991-2015	1.47	0.77	0.33	0.33
2	Kazakhstan	Akmola	Arshaly	1991-2015	1.43	0.90	0.48	2.33
3	Kazakhstan	Akmola	Astrakhan	1991-2015	1.45	0.80	0.36	2.89
4	Kazakhstan	Akmola	Atbasar	1991-2015	1.50	0.85	0.27	3.18
5	Kazakhstan	Akmola	Bulandy	1991-2015	1.72	0.93	0.44	3.21
6	Kazakhstan	Akmola	Burabay	1991-2015	1.79	1.12	0.49	3.18
7	Kazakhstan	Akmola	Egindykol	1991-2015	1.72	0.76	0.32	3.17
8	Kazakhstan	Akmola	Enbekshilder	1991-2015	1.58	0.91	0.17	4.46
9	Kazakhstan	Akmola	Ereymentau	1991-2015	1.56	0.68	0.32	2.89
10	Kazakhstan	Akmola	Esil	1991-2015	1.94	0.77	0.29	3.45
11	Kazakhstan	Akmola	Korganzhyn	1991-2015	1.60	0.62	0.27	2.97
12	Kazakhstan	Akmola	Sandyktau	1991-2015	1.81	1.08	0.59	3.41
13	Kazakhstan	Akmola	Shortandy	1991-2015	1.95	0.96	0.41	3.40
14	Kazakhstan	Akmola	Tselinograd	1991-2015	1.75	0.85	0.42	2.80
15	Kazakhstan	Akmola	Zerendi	1991-2015	2.22	1.12	0.48	3.95
16	Kazakhstan	Akmola	Zhaksy	1991-2015	2.04	0.94	0.31	4.10
17	Kazakhstan	Akmola	Zharkayyk	1991-2015	1.69	0.81	0.22	3.80
18	Kazakhstan	Kostanay	Altynsarin	1985-2015	1.91	1.02	0.37	4.02
19	Kazakhstan	Kostanay	Amangeldi	1997-2015	1.39	0.74	0.18	3.08
20	Kazakhstan	Kostanay	Auliekal	1982-2015	1.64	0.84	0.16	3.63
21	Kazakhstan	Kostanay	Denisov	1982-2015	1.92	0.96	0.13	4.21
22	Kazakhstan	Kostanay	Fedorov	1982-2015	2.29	1.32	0.50	4.30
23	Kazakhstan	Kostanay	Kamysty	1982-2015	1.65	0.85	0.10	3.70
24	Kazakhstan	Kostanay	Karabalyk	1982-2015	2.01	1.22	0.29	4.13
25	Kazakhstan	Kostanay	Karasu	1982-2015	1.97	0.97	0.26	3.96
26	Kazakhstan	Kostanay	Kostanay	1982-2015	2.21	1.23	0.46	4.60
27	Kazakhstan	Kostanay	Mendykara	1982-2015	1.98	1.16	0.35	4.20
28	Kazakhstan	Kostanay	Nauryzym	1982-2015	1.36	0.74	0.15	3.06
29	Kazakhstan	Kostanay	Sarykol	1982-2015	2.16	1.16	0.45	4.17
30	Kazakhstan	Kostanay	Taran	1982-2015	1.90	0.90	0.18	4.00
31	Kazakhstan	Kostanay	Uzynkol	1982-2015	2.06	1.09	0.48	3.74
32	Kazakhstan	Kostanay	Zhangeldin	1982-2015	1.25	0.62	0.11	2.49
33	Kazakhstan	Kostanay	Zhitikarin	1982-2015	1.55	0.75	0.06	3.32
34	Kazakhstan	Kostanay	city.Arkalyk	1982-2015	1.60	0.85	0.33	3.37
35	Mongolia	Bulgan	Bayan.Agt	2000-2018	3.07	1.14	0.08	7.05
36	Mongolia	Bulgan	Bugat	2000-2018	2.00	1.25	0.75	4.12
37	Mongolia	Bulgan	Bureghangai	2000-2018	1.84	0.94	0.18	4.90
38	Mongolia	Bulgan	Dashinchilen	2006-2018	2.72	1.44	0.11	8.19
39	Mongolia	Bulgan	Hangal	2000-2018	2.57	1.51	0.72	4.57
40	Mongolia	Bulgan	Hishig.Undur	2000-2018	2.67	1.14	0.14	6.80
41	Mongolia	Bulgan	Hutag.Undur	2000-2018	1.83	1.16	0.61	3.91
42	Mongolia	Bulgan	Orhon	2000-2018	1.91	1.09	0.45	3.73
43	Mongolia	Bulgan	Selenge	2000-2018	1.88	1.15	0.80	2.86
44	Mongolia	Bulgan	Teshig	2000-2018	1.85	1.26	0.57	4.29
45	Mongolia	Huvsgul	Erdenebulgan	2000-2018	1.52	0.99	0.29	3.68
46	Mongolia	Huvsgul	Rashaant	2000-2018	2.39	1.30	0.31	6.11
47	Mongolia	Huvsgul	Tarialan	2000-2018	1.98	1.24	0.52	4.46
48	Mongolia	Tuv	Argalant	2000-2017	2.05	0.91	0.01	7.13
49	Mongolia	Tuv	Bayantsogt	2000-2017	1.60	0.76	0.10	5.03

[20] This appendix was published as part of the following open-access article: Eltazarov, S., Bobojonov, I., Kuhn, L., Glauben, T. (2023): Improving risk reduction potential of weather index insurance by spatially downscaling gridded climate data - a machine learning approach. Big Earth Data. https://doi.org/10.1080/20964471.2023.2196830

Table A.3.1 *(continued)*

50	**Mongolia**	**Tuv**	**Bornuur**	**2000-2017**	**1.70**	**0.95**	**0.01**	**4.52**
51	Mongolia	Tuv	Erdenesant	2000-2018	2.12	0.95	0.03	6.11
52	Mongolia	Tuv	Jargalant	2000-2017	1.96	0.94	0.20	4.81
53	Mongolia	Tuv	Sumber	2000-2017	1.78	1.01	0.09	5.34
54	Mongolia	Tuv	Tseel	2000-2017	2.67	1.27	0.08	7.04
55	Mongolia	Tuv	Ugtaal	2000-2017	2.16	1.07	0.06	7.55
56	Mongolia	Tuv	Zaamar	2000-2017	1.46	0.64	0.07	4.45

Table A3.2: Cross validation of RF estimated climate data for each month for study site in Kazakhstan

Date	Precipitation			Temperature			Soil moisture		
	cor	**rmse**	**pbias**	**cor**	**rmse**	**pbias**	**cor**	**rmse**	**pbias**
June, 1982	0.99	0.58	1.40	0.99	0.058	0.20	0.99	0.000569	0.30
July, 1982	0.99	0.58	1.10	0.99	0.057	0.20	0.99	0.000582	0.30
June, 1983	0.99	0.58	1.20	0.99	0.059	0.30	0.99	0.000575	0.30
July, 1983	0.99	0.57	1.30	0.99	0.057	0.20	0.99	0.000577	0.30
June, 1984	0.99	0.59	1.10	0.99	0.057	0.30	0.99	0.000575	0.30
July, 1984	0.99	0.57	1.60	0.99	0.057	0.20	0.99	0.000583	0.30
June, 1985	0.99	0.58	1.50	0.99	0.058	0.30	0.99	0.000577	0.30
July, 1985	0.99	0.58	0.70	0.99	0.058	0.20	0.99	0.000577	0.30
June, 1986	0.99	0.58	1.20	0.99	0.058	0.30	0.99	0.000571	0.20
July, 1986	0.99	0.58	1.00	0.99	0.058	0.20	0.99	0.000587	0.30
June, 1987	0.99	0.58	1.90	0.99	0.058	0.30	0.99	0.000579	0.30
July, 1987	0.99	0.57	0.80	0.99	0.057	0.20	0.99	0.000577	0.30
June, 1988	0.99	0.57	2.50	0.99	0.057	0.20	0.99	0.000586	0.30
July, 1988	0.99	0.60	0.70	0.99	0.057	0.20	0.99	0.000583	0.30
June, 1989	0.99	0.58	1.60	0.99	0.057	0.30	0.99	0.000582	0.30
July, 1989	0.99	0.58	2.30	0.99	0.058	0.20	0.99	0.000574	0.30
June, 1990	0.99	0.58	1.30	0.99	0.058	0.20	0.99	0.000583	0.30
July, 1990	0.99	0.58	0.50	0.99	0.059	0.30	0.99	0.000573	0.20
June, 1991	0.99	0.57	2.40	0.99	0.058	0.20	0.99	0.000577	0.30
July, 1991	0.99	0.57	1.00	0.99	0.058	0.20	0.99	0.000573	0.30
June, 1992	0.99	0.58	0.90	0.99	0.058	0.30	0.99	0.000581	0.20
July, 1992	0.99	0.58	0.70	0.99	0.059	0.30	0.99	0.000572	0.20
June, 1993	0.99	0.59	0.80	0.99	0.058	0.30	0.99	0.000573	0.20
July, 1993	0.99	0.58	0.60	0.99	0.059	0.30	0.99	0.000582	0.20
June, 1994	0.99	0.58	1.70	0.99	0.057	0.20	0.99	0.000576	0.30
July, 1994	0.99	0.57	0.60	0.99	0.059	0.30	0.99	0.000586	0.20
June, 1995	0.99	0.58	1.80	0.99	0.058	0.30	0.99	0.000582	0.30
July, 1995	0.99	0.57	0.80	0.99	0.058	0.20	0.99	0.000567	0.30
June, 1996	0.99	0.58	1.40	0.99	0.058	0.20	0.99	0.000581	0.30
July, 1996	0.99	0.58	0.80	0.99	0.060	0.20	0.99	0.000587	0.30
June, 1997	0.99	0.57	2.00	0.99	0.057	0.30	0.99	0.000583	0.30
July, 1997	0.99	0.58	1.20	0.99	0.062	0.30	0.99	0.000583	0.30
June, 1998	0.99	0.58	1.50	0.99	0.058	0.20	0.99	0.000576	0.30
July, 1998	0.99	0.57	1.30	0.99	0.057	0.20	0.99	0.000583	0.30
June, 1999	0.99	0.58	0.80	0.99	0.058	0.30	0.99	0.000568	0.20
July, 1999	0.99	0.60	0.80	0.99	0.058	0.20	0.99	0.000568	0.30
June, 2000	0.99	0.57	0.90	0.99	0.057	0.30	0.99	0.000585	0.30
July, 2000	0.99	0.58	1.40	0.99	0.058	0.20	0.99	0.000569	0.30
June, 2001	0.99	0.58	0.80	0.99	0.059	0.30	0.99	0.000582	0.30
July, 2001	0.99	0.58	0.80	0.99	0.059	0.30	0.99	0.000573	0.30
June, 2002	0.99	0.58	0.70	0.99	0.059	0.30	0.99	0.000584	0.20
July, 2002	0.99	0.59	1.20	0.99	0.058	0.30	0.99	0.000581	0.20

Table A.3.1 *(continued)*

June, 2003	0.99	0.65	0.90	0.99	0.058	0.30	0.99	0.000577	0.20
July, 2003	0.99	0.58	0.80	0.99	0.058	0.30	0.99	0.000589	0.20
June, 2004	0.99	0.59	1.30	0.99	0.060	0.20	0.99	0.000566	0.30
July, 2004	0.99	0.58	1.10	0.99	0.058	0.20	0.99	0.000570	0.30
June, 2005	0.99	0.61	1.10	0.99	0.057	0.20	0.99	0.000579	0.30
July, 2005	0.99	0.58	1.00	0.99	0.057	0.20	0.99	0.000583	0.30
June, 2006	0.99	0.58	0.90	0.99	0.058	0.20	0.99	0.000574	0.30
July, 2006	0.99	0.59	1.00	0.99	0.057	0.30	0.99	0.000577	0.30
June, 2007	0.99	0.57	1.20	0.99	0.058	0.30	0.99	0.000578	0.20
July, 2007	0.99	0.58	0.70	0.99	0.059	0.20	0.99	0.000582	0.20
June, 2008	0.99	0.88	1.30	0.99	0.057	0.30	0.99	0.000578	0.30
July, 2008	0.99	0.58	1.00	0.99	0.057	0.20	0.99	0.000575	0.30
June, 2009	0.99	0.59	1.50	0.99	0.058	0.30	0.99	0.000580	0.30
July, 2009	0.99	0.57	0.80	0.99	0.058	0.30	0.99	0.000569	0.30
June, 2010	0.99	0.58	2.30	0.99	0.058	0.20	0.99	0.000580	0.30
July, 2010	0.99	0.58	1.20	0.99	0.057	0.20	0.99	0.000576	0.30
June, 2011	0.99	0.58	0.80	0.99	0.060	0.30	0.99	0.001443	0.20
July, 2011	0.99	0.63	0.80	0.99	0.058	0.20	0.99	0.000618	0.30
June, 2012	0.99	0.58	1.10	0.99	0.058	0.20	0.99	0.000575	0.30
July, 2012	0.99	0.57	1.10	0.99	0.057	0.20	0.99	0.000573	0.30
June, 2013	0.99	0.57	2.40	0.99	0.058	0.30	0.99	0.000577	0.30
July, 2013	0.99	0.58	0.60	0.99	0.060	0.30	0.99	0.000584	0.20
June, 2014	0.99	0.58	2.10	0.99	0.057	0.20	0.99	0.000581	0.30
July, 2014	0.99	0.58	0.70	0.99	0.058	0.30	0.99	0.000581	0.20
June, 2015	0.99	0.58	1.50	0.99	0.057	0.20	0.99	0.000567	0.20
July, 2015	0.99	0.57	1.00	0.99	0.057	0.20	0.99	0.000572	0.30
average	0.99	0.59	1.19	0.99	0.058	0.25	0.99	0.000591	0.27

Table A3.3: Cross validation of RF estimated climate data for each month for study site in Mongolia

Date	Precipitation			Temperature			Soil moisture		
	cor	rmse	pbias	cor	rmse	pbias	cor	rmse	pbias
June, 2000	0.99	0.72	0.80	0.99	0.056	0.30	0.99	0.000587	0.30
July, 2000	0.99	0.70	0.50	0.99	0.057	0.30	0.99	0.000557	0.20
June, 2001	0.99	0.70	0.70	0.99	0.059	0.30	0.99	0.000575	0.30
July, 2001	0.99	0.72	0.70	0.99	0.057	0.30	0.99	0.000597	0.30
June, 2002	0.99	0.71	0.90	0.99	0.058	0.30	0.99	0.00058	0.30
July, 2002	0.99	0.72	0.70	0.99	0.058	0.30	0.99	0.000578	0.30
June, 2003	0.99	0.69	1.00	0.99	0.057	0.30	0.99	0.000579	0.30
July, 2003	0.99	0.69	0.40	0.99	0.059	0.30	0.99	0.00059	0.30
June, 2004	0.99	0.71	0.70	0.99	0.059	0.30	0.99	0.000571	0.30
July, 2004	0.99	0.70	0.50	0.99	0.058	0.30	0.99	0.000586	0.30
June, 2005	0.99	1.29	0.70	0.99	0.057	0.30	0.99	0.000568	0.30
July, 2005	0.99	0.69	0.70	0.99	0.056	0.30	0.99	0.00059	0.30
June, 2006	0.99	0.71	0.90	0.99	0.058	0.30	0.99	0.000596	0.30
July, 2006	0.99	0.68	0.40	0.99	0.058	0.30	0.99	0.000572	0.20
June, 2007	0.99	0.71	0.70	0.99	0.057	0.30	0.99	0.000585	0.30
July, 2007	0.99	0.70	0.70	0.99	0.057	0.30	0.99	0.000562	0.30
June, 2008	0.99	0.69	0.40	0.99	0.057	0.30	0.99	0.000577	0.30
July, 2008	0.99	0.72	0.60	0.99	0.116	0.30	0.99	0.000575	0.20
June, 2009	0.99	0.71	0.60	0.99	0.059	0.40	0.99	0.00057	0.30
July, 2009	0.99	0.71	0.60	0.99	0.058	0.30	0.99	0.000594	0.30
June, 2010	0.99	0.70	0.80	0.99	0.058	0.30	0.99	0.000581	0.30
July, 2010	0.99	0.71	0.70	0.99	0.058	0.30	0.99	0.000592	0.30
June, 2011	0.99	0.71	0.70	0.99	0.057	0.30	0.99	0.000577	0.30
July, 2011	0.99	0.69	0.60	0.99	0.058	0.30	0.99	0.000571	0.20
June, 2012	0.99	0.69	0.60	0.99	0.057	0.30	0.99	0.000577	0.20
July, 2012	0.99	0.69	0.40	0.99	0.057	0.30	0.99	0.000589	0.20
June, 2013	0.99	0.71	0.80	0.99	0.058	0.40	0.99	0.000577	0.30
July, 2013	0.99	0.71	0.60	0.99	0.059	0.30	0.99	0.000572	0.20
June, 2014	0.99	0.73	0.80	0.99	0.057	0.40	0.99	0.000581	0.30
July, 2014	0.99	0.70	0.80	0.99	0.058	0.30	0.99	0.000584	0.20
June, 2015	0.99	0.71	1.50	0.99	0.055	0.30	0.99	0.000592	0.30
July, 2015	0.99	0.72	0.60	0.99	0.058	0.30	0.99	0.000595	0.30
June, 2016	0.99	0.68	0.60	0.99	0.057	0.30	0.99	0.000588	0.20
July, 2016	0.99	0.71	0.60	0.99	0.057	0.30	0.99	0.00057	0.20
June, 2017	0.99	0.70	1.40	0.99	0.057	0.30	0.99	0.000589	0.30
July, 2017	0.99	0.71	0.90	0.99	0.057	0.30	0.99	0.000588	0.30
June, 2018	0.99	0.70	0.80	0.99	0.057	0.30	0.99	0.000576	0.30
July, 2018	0.99	0.73	0.40	0.99	0.059	0.30	0.99	0.000571	0.20
average	0.99	0.72	0.71	0.99	0.059	0.308	0.99	0.000581	0.27

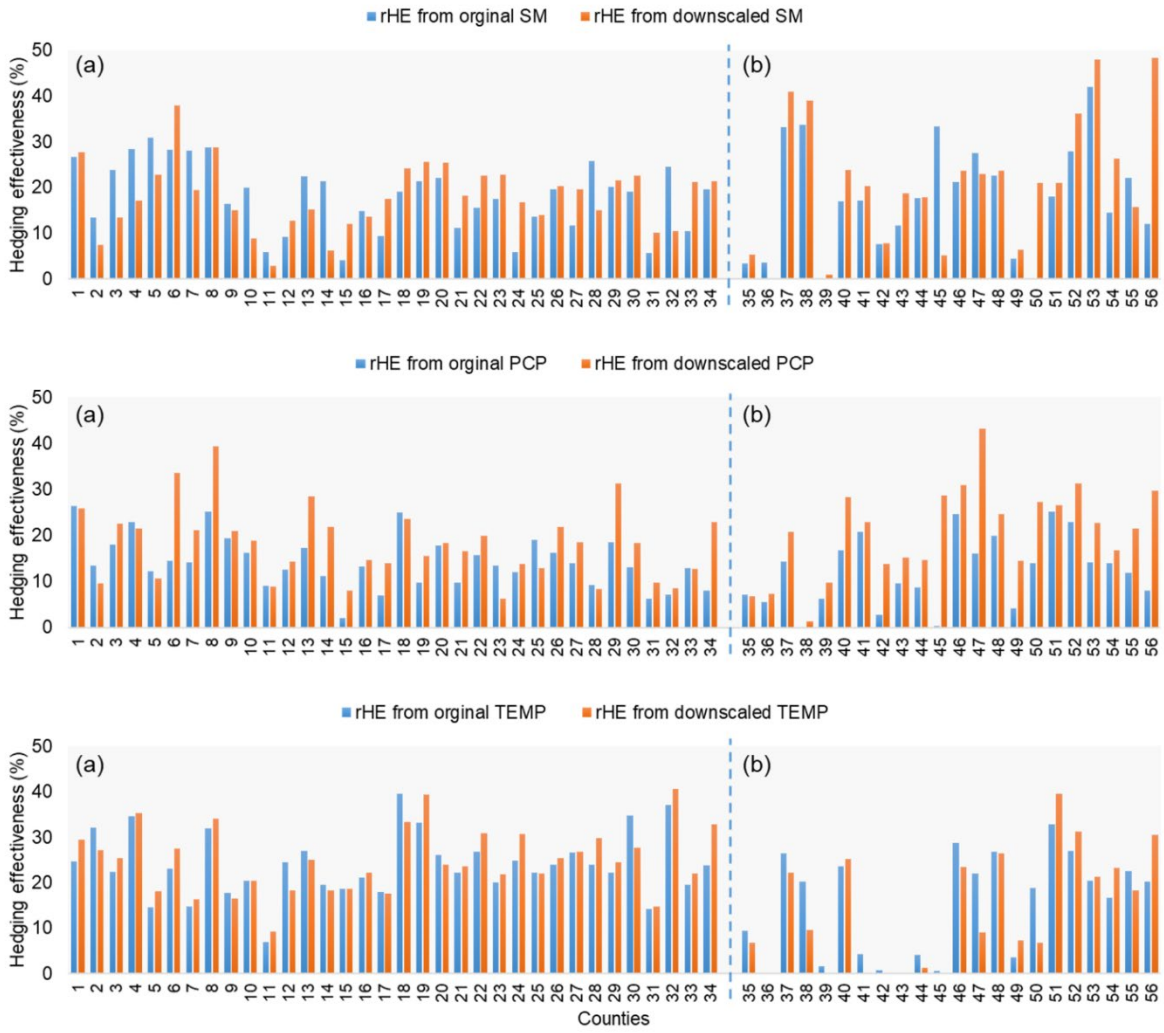

Figure A.3.4: Hedging effectiveness of index insurance products for each county based on original and downscaled climate parameters, counties in (a) Kazakhstan and (b) Mongolia

Table A.3.5: Results of Local Moran's I statistic for original climate data

Year	PCP (June)	PCP (July)	TEMP (June)	TEMP (July)	SM (June)	SM (July)
1982	0.41	0.70	0.60	0.61	0.55	0.66
1983	0.30	0.64	0.53	0.67	0.25	0.13
1984	0.46	0.80	0.52	0.63	0.73	0.14
1985	0.67	0.68	0.68	0.67	0.10	0.16
1986	0.30	0.39	0.60	0.48	0.07	0.49
1987	0.11	0.76	0.60	0.46	0.59	0.57
1988	0.79	0.63	0.71	0.72	-	-
1989	0.74	0.73	0.65	0.69	-	-
1990	0.75	0.72	0.57	0.62	-	-
1991	0.54	0.68	0.67	0.70	-	-
1992	0.37	0.62	0.68	0.60	0.78	0.13
1993	0.51	0.25	0.58	0.47	0.15	0.05
1994	0.61	0.60	0.64	0.56	0.15	0.10
1995	0.69	0.22	0.54	0.51	0.24	0.29
1996	0.70	0.75	0.67	0.70	0.48	0.25
1997	0.79	0.71	0.63	0.74	0.52	0.38
1998	0.64	0.43	0.72	0.63	0.20	0.23
1999	0.16	0.77	0.67	0.70	0.18	0.24
2000	0.60	0.67	0.68	0.74	0.66	0.22
2001	0.53	0.75	0.64	0.72	0.35	0.27
2002	0.73	0.39	0.73	0.69	0.72	0.76
2003	0.57	0.67	0.70	0.69	-0.04	0.03
2004	0.67	0.70	0.68	0.71	-0.04	0.06
2005	0.65	0.71	0.64	0.63	0.77	0.54
2006	0.72	0.73	0.65	0.72	0.64	0.01
2007	0.70	0.34	0.74	0.72	0.72	0.70
2008	0.38	0.57	0.64	0.71	0.69	0.56
2009	0.28	0.76	0.61	0.70	0.60	0.59
2010	0.06	0.02	0.63	0.68	0.68	0.56
2011	0.68	0.63	0.70	0.73	0.63	0.65
2012	0.26	0.33	0.64	0.61	0.52	0.12
2013	0.73	0.70	0.72	0.69	0.01	0.11
2014	0.53	0.66	0.62	0.69	0.20	0.28
2015	0.80	0.59	0.64	0.65	0.19	0.08
2016	0.49	0.75	0.61	0.72	0.01	0.33
2017	0.60	0.57	0.68	0.72	0.37	0.45
2018	0.17	0.35	0.66	0.65	0.19	0.02
2019	0.67	0.66	0.68	0.71	0.33	0.25
average	0.54	0.60	0.65	0.66	0.39	0.31

Table A.3.6: Results of Local Moran's I statistic for downscaled climate data

Year	PCP (June)	PCP (July)	TEMP (June)	TEMP (July)	SM (June)	SM (July)
1982	0.60	-0.03	0.37	0.17	0.03	0.53
1983	0.11	0.64	0.52	0.68	0.50	0.74
1984	0.09	0.17	0.47	0.24	0.51	0.41
1985	0.19	0.32	0.43	0.04	0.19	0.34
1986	0.39	0.37	0.11	0.37	0.01	-0.10
1987	0.66	0.44	0.30	0.22	0.28	0.35
1988	0.62	0.64	0.66	0.67	0.72	0.73
1989	-0.05	0.62	0.43	0.42	0.04	0.48
1990	0.23	0.45	0.48	0.21	0.10	0.50
1991	0.66	0.28	0.53	0.36	0.43	0.06
1992	0.41	0.08	0.33	0.41	0.61	0.06
1993	-0.06	0.15	0.14	0.50	-0.02	0.42
1994	0.64	0.22	0.43	0.18	0.49	0.36
1995	0.35	0.31	0.32	0.56	0.52	0.53
1996	0.17	0.05	0.36	0.35	0.51	0.33
1997	0.56	0.12	0.29	0.48	0.35	0.36
1998	0.59	0.27	0.42	0.55	0.39	0.49
1999	0.47	0.28	0.38	0.44	0.25	0.22
2000	0.07	0.20	0.43	0.18	0.36	0.43
2001	-0.04	0.24	0.42	0.12	0.30	0.50
2002	0.56	0.55	0.70	0.35	0.35	0.74
2003	0.21	0.08	0.29	0.33	0.32	0.39
2004	0.59	-0.01	0.31	0.17	0.48	0.17
2005	0.39	0.36	0.45	0.40	0.60	0.63
2006	0.19	0.25	0.54	-0.01	0.18	0.19
2007	0.68	0.31	0.23	0.43	0.66	0.58
2008	0.09	0.70	0.11	0.31	0.30	0.47
2009	0.46	0.48	0.48	0.32	0.79	0.67
2010	0.09	0.46	0.31	0.29	0.51	0.47
2011	0.09	0.24	0.11	0.32	0.18	0.61
2012	0.13	0.31	0.57	0.22	0.40	0.16
2013	0.57	0.32	0.27	0.41	0.22	0.13
2014	0.49	0.46	0.55	0.34	0.43	0.64
2015	0.52	-0.01	0.43	0.07	0.31	0.69
2016	0.37	0.33	0.54	0.00	0.44	0.51
2017	0.69	0.55	0.43	0.65	0.55	0.70
2018	0.57	0.18	0.63	0.14	0.43	-0.02
2019	-0.08	0.23	0.61	-0.07	0.43	-0.01
average	0.35	0.31	0.40	0.31	0.37	0.41

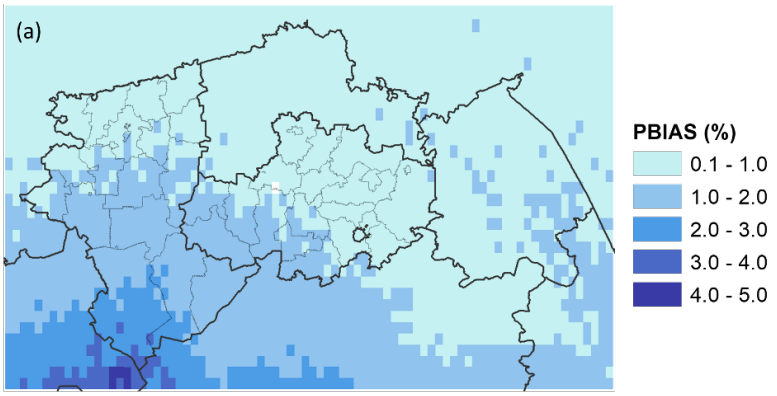

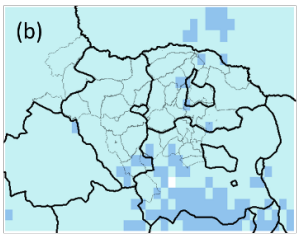

	Kazakhstan	Mongolia
min	0.60	0.20
max	3.30	1.20
range	2.70	1.00
mean	1.24	0.67
median	1.10	0.70
stddev	0.52	0.20

Figure A.3.7: Time-series cross validation (PBIAS) of RF models to estimate the precipitation in coarse resolution. June-July months of 1985-2015 and 2000-2019 for (a) Kazakhstan and (b) Mongolia, respectively

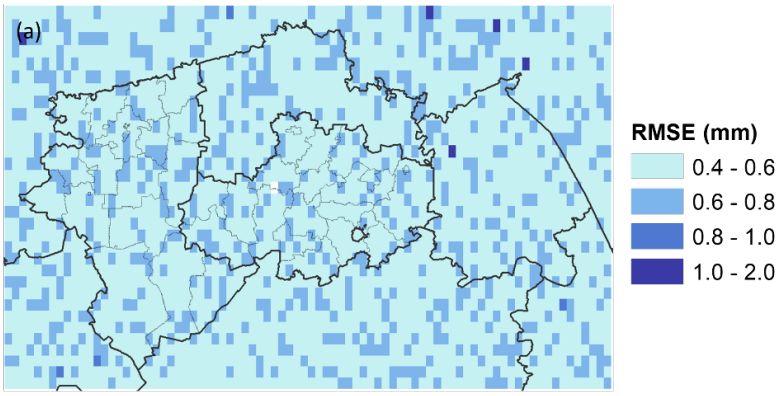

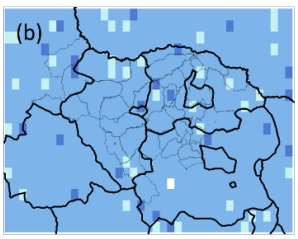

	Kazakhstan	Mongolia
min	0.477	0.538
max	0.725	0.843
range	0.247	0.305
mean	0.576	0.701
median	0.575	0.707
stddev	0.032	0.056

Figure A.3.8: Time-series cross validation (RMSE) of RF models to estimate the precipitation in coarse resolution. June-July months of 1985-2015 and 2000-2018 for (a) Kazakhstan and (b) Mongolia, respectively

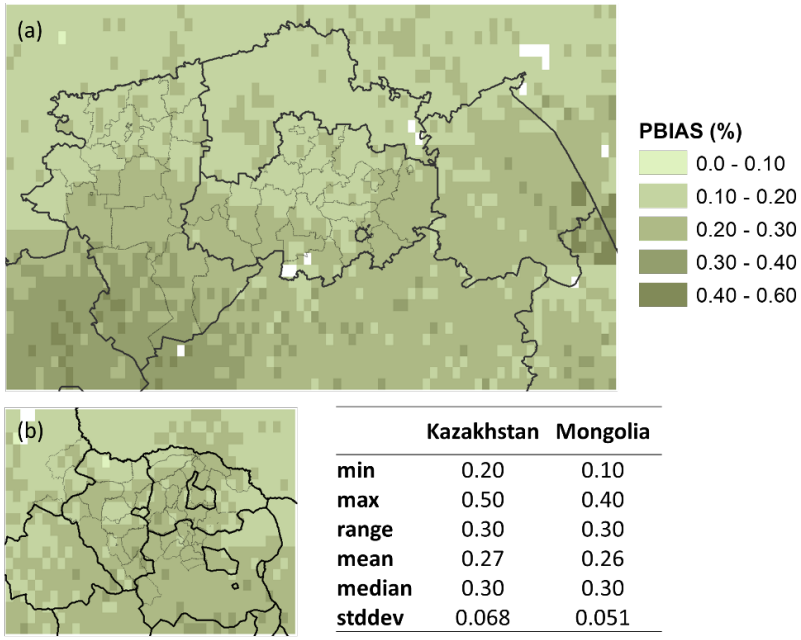

	Kazakhstan	Mongolia
min	0.20	0.10
max	0.50	0.40
range	0.30	0.30
mean	0.27	0.26
median	0.30	0.30
stddev	0.068	0.051

Figure A.3.9: Time-series cross validation (PBIAS) of RF models to estimate the soil moisture in coarse resolution. June-July months of 1985-2015 and 2000-2018 for (a) Kazakhstan and (b) Mongolia, respectively

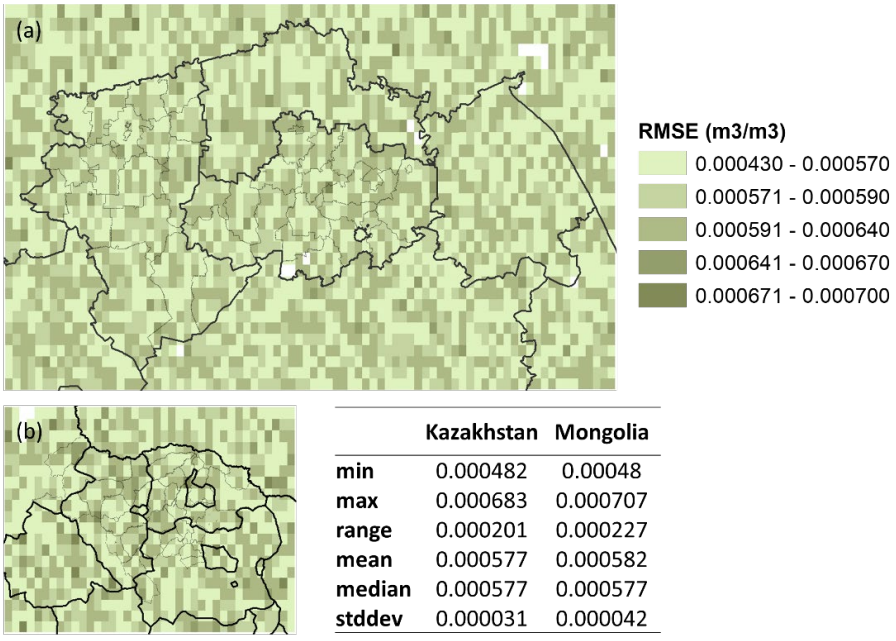

	Kazakhstan	Mongolia
min	0.000482	0.00048
max	0.000683	0.000707
range	0.000201	0.000227
mean	0.000577	0.000582
median	0.000577	0.000577
stddev	0.000031	0.000042

Figure A.3.10: Time-series cross validation (RMSE) of RF models to estimate the soil moisture in coarse resolution. June-July months of 1985-2015 and 2000-2018 for (a) Kazakhstan and (b) Mongolia, respectively

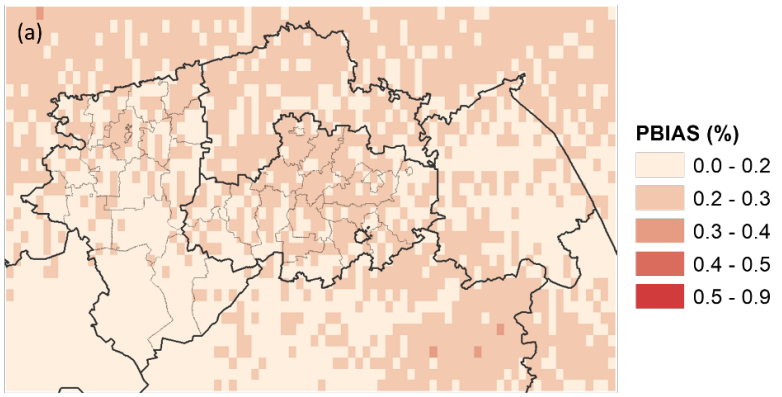

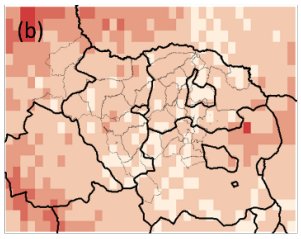

	Kazakhstan	Mongolia
min	0.20	0.20
max	0.30	0.40
range	0.10	0.20
mean	0.24	0.29
median	0.20	0.30
stddev	0.05	0.05

Figure A.3.11: Time-series cross validation (PBIAS) of RF models to estimate the temperature in coarse resolution. June-July months of 1985-2015 and 2000-2018 for (a) Kazakhstan and (b) Mongolia, respectively

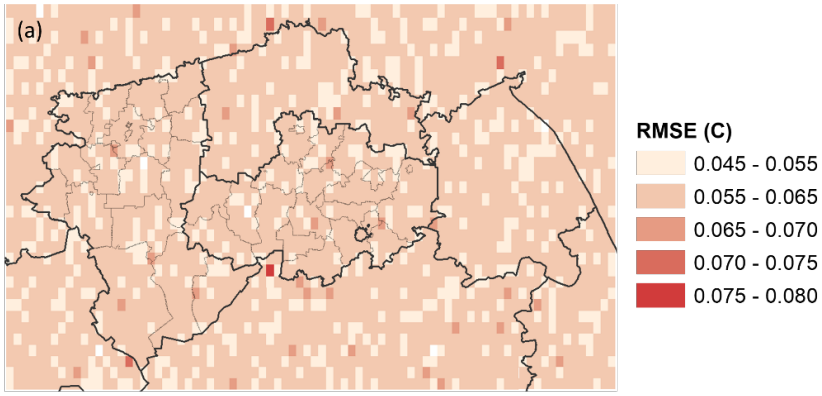

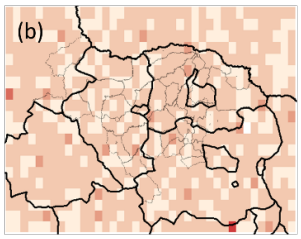

	Kazakhstan	Mongolia
min	0.049	0.049
max	0.151	0.066
range	0.102	0.016
mean	0.058	0.057
median	0.058	0.057
stddev	0.005	0.004

Figure A.3.12: Time-series cross validation (RMSE) of RF models to estimate the temperature in coarse resolution. June-July months of 1985-2015 and 2000-2018 for (a) Kazakhstan and (b) Mongolia, respectively

Table A.3.13: Wilcoxon test between county-wise RMSE of improved and not improved cases in Kazakhstan

	Climate variable	Improved HE	Number of cases	p-value
1	**Precipitation**	No	10	0.5895
		Yes	24	
2	**Temperature**	No	10	0.8091
		Yes	24	
3	**Soil moisture**	No	13	0.8871
		Yes	21	

Table A.3.14: Wilcoxon test between county-wise PBIAS of improved and not improved cases in Kazakhstan

	Climate variable	Improved HE	Number of cases	p-value
1	**Precipitation**	No	10	0.2866
		Yes	24	
2	**Temperature**	No	10	0.650
		Yes	24	
3	**Soil moisture**	No	13	0.06007
		Yes	21	

Table A.3.15: Wilcoxon test between county-wise RMSE of improved and not improved cases in Mongolia

	Climate variable	Improved HE	Number of cases	p-value
1	**Precipitation**	No	1	0.6364
		Yes	21	
2	**Temperature**	No	14	0.1653
		Yes	8	
3	**Soil moisture**	No	4	0.6094
		Yes	18	

Table A.3.16: Wilcoxon test between county-wise PBIAS of improved and not improved cases in Mongolia

	Climate variable	Improved HE	Number of cases	p-value
1	**Precipitation**	No	1	0.5278
		Yes	21	
2	**Temperature**	No	14	0.863
		Yes	8	
3	**Soil moisture**	No	4	0.0738
		Yes	18	